7-10-2017

Copper-Binding Antimicrobial and Host-Defense Peptides: Microbial Elimination through Lipid and DNA Oxidation

Mark Daben J. Libardo
University of Connecticut - Storrs, mark.libardo@uconn.edu

Copper-Binding Antimicrobial and Host-Defense Peptides:

Microbial Elimination through Lipid and DNA Oxidation

Mark Daben J. Libardo

University of Connecticut, 2017

The immune system utilizes a plethora of antimicrobial effectors to ensure efficient microbial eradication. This dissertation focuses on two of these effectors: antimicrobial peptides (AMPs) and copper ions. The work described here examines both fundamental and translational aspects of AMPs that contain the amino terminal copper and nickel (ATCUN) binding unit. The first section details our efforts to define the contribution of the ATCUN motif to the biological activity of peptides that are expressed in nature containing the metal binding sequence. In chapter 2, we show how the metal is utilized by an ATCUN-containing AMP to bring about copper-mediated membrane lipid oxidation. This activity, in turn is utilized by a homologous peptide to achieve synergistic interactions that involve oxidized lipid targeting. In chapter 3, we show the first example of an AMP that can oxidatively cleave microbial DNA in a copper-dependent fashion. This nuclease activity is intimately linked to its expression profile and to that of a homologous, yet mechanistically distinct peptide. These two AMPs show complementary effects associated with oxidation of varying targets in bacteria. The oxidative stress generated by ATCUN-AMPs lead us to speculate that a similar mode of attack can be imparted to other therapeutically relevant peptides. Therefore, our goal in the second section was to generate novel ATCUN-based antibiotics. In chapter 4, we appended the ATCUN motif

to membrane-targeting AMPs and in chapter 5, added it to an oligonucleotide-binding peptide. We observed that for both instances, a gain-of-function phenotype resulted from the exogenous addition of the metal-binding sequence, and that microbial killing was directly related to the oxidative activity of the conjugates. Finally, in chapter 6, we developed an ATCUN-based peptidomimetic that can target intracellular *Mycobacterium tuberculosis*. We reasoned that antibiotics of this nature can exploit the differential trafficking of transition metals during infection, be activated *in situ* by copper in the cellular milieu and target pathogenic bacteria that evolved to evade the metal's toxic effects. Overall, this work highlights the biological importance of ATCUN-containing AMPs and expands the catalog by which these peptides utilize transition metals for their activity.

Copper-Binding Antimicrobial and Host-Defense Peptides:

Microbial Elimination through Lipid and DNA Oxidation

Mark Daben J. Libardo

B.S., University of the Philippines – Diliman, 2011

A Dissertation

Submitted in Partial Fulfilment

of the Requirements for the Degree of

Doctor of Philosophy

at the

University of Connecticut

2017

APPROVAL PAGE

Doctor of Philosophy Dissertation

Copper-Binding Antimicrobial and Host-Defense Peptides:
Microbial Elimination through Lipid and DNA Oxidation

Presented by

Mark Daben J. Libardo

Major Advisor _____
Alfredo M. Angeles-Boza

Associate Advisor _____
Mark W. Peczuh

Associate Advisor _____
Ashis K. Basu

University of Connecticut
2017

Acknowledgements

The late Flavia Weedn once wrote: “Some people come into our lives and quickly go. Some people move our souls to dance. They awaken us to a new understanding with the passing whisper of their wisdom. Some people make the sky more beautiful to gaze upon. They stay in our lives for a while, leave footprints on our hearts, and we are never, ever the same.” This could not be a more accurate description of the people I have met during my time in graduate school. The successes I celebrated and the failures I struggled with are due in part to the amazing people who have touched my life for the past five years in UConn. I would like to express my sincerest gratitude to all the people, who, in one way or another, influenced my decisions and encouraged me to always aim beyond the reaches of the sky. Specifically, I would like to extend my heartfelt appreciation:

To **Alfredo**, the best advisor one could ever hope for. Thank you for allowing me to work in your lab and for willingly giving me the intellectual freedom I desired to complete my work. While there are very few things we disagree on scientifically, you were always very receptive of my ideas and you never failed to encourage me to pursue my goals. You have been the single most instrumental person in my success in grad school and for that I am eternally indebted. There is so much more to thank you for, but I would let words from the song *For Good* speak my heart’s sentiments: *I’ve heard it said that people come into our lives for a reason* / *Bringing something we must learn* / *And we are led to those who help us most to grow* / *If we let them and we help them in return* / *So much of me is made of what I learned from you* / *You’ll be with me like a handprint on my heart* / *And now whatever way our stories end* / *I know you have re-written mine, by being my friend* / *Who can say if I’ve been changed for the better?* / *I do believe I have been changed for the better* / *And because I knew you, I have been changed for good.*

To the members of my advisory committee, **Dr. Mark Peczuh**, **Dr. Ashish Basu**, thank you very much for the feedback and revisions on both my general exam and final thesis defense. Thank you for the great learning opportunity both in and out of the classroom.

To **Dr. Christian Brückner**, thank you for being so supportive of my endeavors in graduate school, specially for allowing me to go to the Max Planck Institute to finish part of my work. Special thanks for tirelessly writing recommendation letters in my behalf for travel and employment purposes, even going as far as sending a personal note to Prof Christopher Chang. The future of the Chemistry department looks really bright with you leading the way.

To **Dr. Kenneth Campellone**, I can’t thank you enough for introducing me to the wondrous world of infection biology. You really sparked my interest in cellular microbiology and influenced so much of my decisions in grad school and where to do a postdoc. Three semesters of classes with you was both necessary and sufficient to have a smooth “transition” into a more biological focus of research. It has been a pleasure working with you throughout the years and I will forever be grateful for everything you taught me.

To **Dr. Myriam Cotten**, thank you for acting almost as my “adjunct advisor” and for the positive reinforcements and constant encouragements throughout the years. I never would have expected that a simple visit to our department would pave the way for an amazing collaboration between our labs. I would also like to thank you for imparting some of your wisdom in writing manuscripts, my writing style and technique is largely because of examples from your papers and endless conversations over email. Like Alfredo, you never failed to push me further and reach my full potential – and for that I am eternally grateful. Finally, thank you for writing such strong recommendation letters on my behalf, part of my success in the postdoc hunt is due to your written support.

To **Prof. Dr. Stefan H.E. Kaufmann**, thank you for your generosity and warmly accommodating me in your lab in Berlin to finish my last project. Although my time in your lab was short, I learned so much of what I will be needing for the next stage of my career. Special thanks to **Gopi** and **Peggy** who worked with me closely during my stay at MPI-IB. I hope our paths will cross again in the future!

To the Chemistry department research support staff, the unseen heroes of my research – **Dr. You-Jun Fu**, **Dr. Vitaliy Gorbatyuk**, and **Ms. Charlene Fuller**. My work would have been a hundred-fold more difficult without your patience and support. For that, I thank you very much.

To **Dr. Edward Neth**, and the Teaching Stockroom staff – **Adam**, **Ben**, **Eric**, **Leah**, and **Noreen** – Thank you for lessening the burden of being a TA in the department and for giving us some academic freedom when it comes to handling our respective classes. Dr. Neth, it has been a great pleasure working with and teaching for you throughout the years.

To my labmates **Taylor**, **Sam**, **John**, **Jasmin**, and **Kankana**. Thank you for taking some of the stress of grad school off my back. Going to the lab everyday feels much less of an errand and more of an enjoyable experience because of you guys. Thank you for the support and discussions about science and all the random stuff we talked and laughed about. These moments will be forever missed, and I look forward to seeing you all again in the future. Good luck with the rest of your stay in grad school!

To the students I mentored throughout the years **Scott**, **Sai**, **Andrea**, **Stephanie**, **Jonas**, **Marie**, **Jefferson**, **Tim**, and **Evan**. Thank you for your hard work and for giving me the opportunity to mentor great minds such as yours. If I fell short as a mentor, I apologize, but I thank you for teaching me what to watch out for when teaching in the lab.

To my Fall 2012 classmates and other UConn Chem friends, thank you for keeping up with my crazy. It’s always nice when you drop by the lab and share a funny moment with us. Special thanks to **Shannon**, **Melissa**, and **Alyssa** for taking so much of my crap throughout the years. You guys will be missed!

To the amazing people I have met in Gordon conferences (AMPs: **Ariane**, **Victoria**, **Simon**, **Stefie**, **Bibi**; Metals in Medicine: **Tiffany**, **Cheryl**, **Will**, **Erin**, **Antonio**, **Allegra**, and **Marie**) and to my Max Planck friends (**Andreas**, **Lisa**, **Helen**, **Teresa**, **Ana**, and

Frida). The time we shared together is short yet sweet. I want to thank all of you for sharing your ideas and brushing off some of your smarts to me! It's nice to know that I made so many lasting friendships from short visits. Keep in touch!

To my Filipino friends also in grad school here in the US, specially to Methane (**Marco**, **Jenny**, **Ian**, and **Joe**) and to **Digs** and **Maxx**. Thank you for being the strongest support system one could ever hope for. Five years ago, we started this journey together and today, our friendship still remains strong despite being separated by hundreds of miles and state lines. I will always treasure all the trips we made and all the laughter and conversations we shared through the years. I wish that everything remains the same in terms of how frequent we see and talk to each other despite the fact that our schedules are about to change drastically. See you all on the next holiday, don't forget to bring food and booze!

To my Filipino friends in Storrs – **Christian**, **Joan**, **Annie**, **Gillian**, **Homer**, **Raven**, **Kendricks**, **Angelo**, **Donna**, **Charity**, **IC**, **MN**, and **Mia**. Thank you for adding color to my life at UConn, and for making life away from home a lot easier. I will never forget all the moments we shared – the laughter, the tears, and everything in between will be missed. We may have gone our separate ways but my success in grad school is in large part due to your constant encouragements. Maraming salamat mga beks!

Finally, to my family back home. To my mom **Imelda**, my dad **Joeben**, my sisters **Iza** and **Joemhel**, my nephew **DJ**, and my niece **Meriza**. It's always very consoling to know that a supportive family waits for you back home. Thank you for all your love and support not just in grad school but for my entire academic life. While leaving home was one of the hardest decision I ever made, it was reassuring to know that you always have my back. I love you all, and I hope I made you extremely proud.

This work is dedicated to

all the people who,

like me,

never stopped believing

in the power of dreams.

Table of Contents

List of Figures

List of Tables

Chapter 1

General Introductions

On Antimicrobial Host-Defense Peptides, Transition Metal Ions and the Innate Immune Response that bring them together

Antimicrobial and Host-Defense Peptides

Considered as one of nature's oldest forms of antibiotics, antimicrobial peptides (AMPs) play a major role in the innate immune response of virtually all forms of life.[1] AMPs are usually short, cationic and amphipathic molecules (enriched with Arg, Lys and hydrophobic residues) that provide a first line of defense against invading microbes either via membrane disruption or intracellular targeting.[2, 3] To reflect their emerging roles in regulating the immune response of multicellular organisms, some AMPs have been characterized as host-defense peptides (HDPs) – a description that highlights the immunomodulatory, anti-inflammatory, and chemotactic properties observed under physiological conditions.[4, 5] These peptides are classified based on their secondary and tertiary structural elements forming four major groups (Figure 1.1): α-helical peptides (constituting the majority of AMPs), β-sheet peptides (stabilized by two or more disulfide bridges), extended peptides (usually enriched with Gly, Pro, and Trp), and loop peptides (containing one disulfide bond).[6]

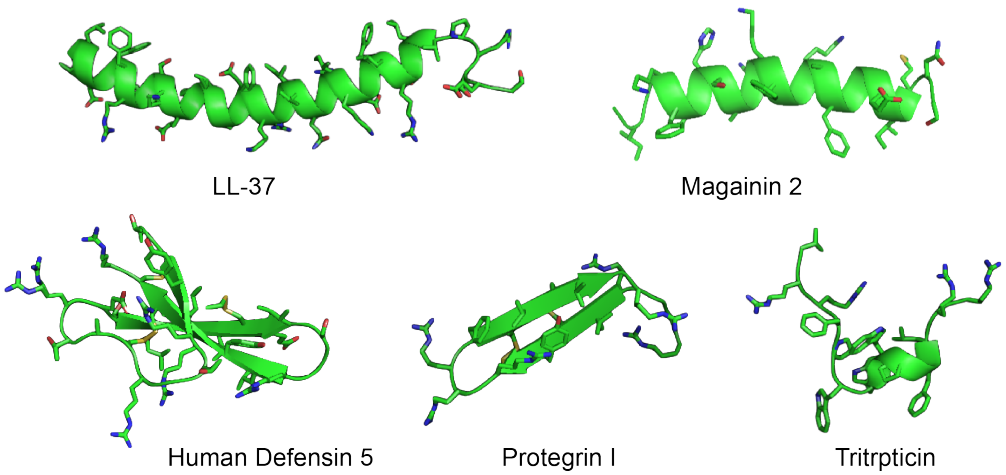

Figure 1.1 Diversity in Antimicrobial Peptide Structure. Most AMPs are α-helical, while a small fraction are β-sheets and disordered loops. Helical and sheet AMPs adopt an amphipathic structure known to be important for membranolytic activity.

A significant number of AMPs exhibit a broad-spectrum activity in the low micromolar to the nanomolar range against bacteria in axenic cultures. While largely not fully understood, AMPs' direct cytotoxic ability relies on electrostatic interaction between cationic residues in its backbone with the anionic bacterial cell surface (lipopolysaccharides in Gram-negative bacteria and the wall teichoic acid in Gram-positive bacteria).[6] It is also believed that this electrostatic complementarity explains the preference of AMPs to target bacterial over eukaryotic cells, which contain more zwitterionic components in their membrane.[7] After initial attraction to the cell surface, these peptides relocate to the interfacial region of the bilayer – a process promoted by their amphipathic nature[8] – and disrupt its structural integrity either via transmembrane pore formation or micellarization of the membrane (Figure 1.2).[3] This membranolytic effect causes leakage of cellular contents (ions, metabolites and even large proteins) and collapse of transmembrane potential ultimately leading to cell death.

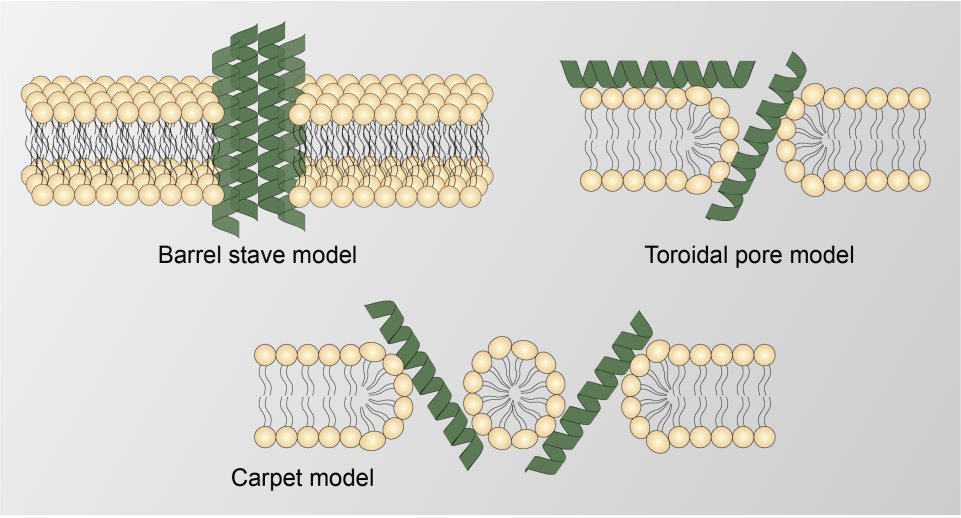

Figure 1.2. Membranolytic Activity of AMPs. Membrane poration occurs via multiple mechanisms, most notable of which are depicted in this figure. Transmembrane channel, toroidal pore, or complete micellarization of membranes lead to leakage of cellular contents to the extracellular environment.

An expanding body of evidence show that some peptides are non-membranolytic and are able to effect intracellular inhibitory mechanisms as the primary mode of bacterial killing (Figure 1.3).[9, 10] These mechanisms include binding to macromolecules like DNA[11, 12] and ribosome,[13] inhibition of macromolecular synthesis,[14, 15] inhibition of enzymatic activity,[16, 17] and perturbation of septum formation.[18] These studies challenged the paradigm that AMPs act solely on the bacterial membrane and highlight the target promiscuity of this class of antimicrobials. Indeed, it seems like natural selection favored the evolution of "dirty" antibiotics that target multiple pathways with modest potency rather than a single high-affinity target for use in the immune response,[6, 19] a concept ought to be adopted by the pharmaceutical industry. Moreover, because AMPs exhibit multiple levels of inhibition, it requires bacteria to mutate several genes in a concerted fashion before resistance is acquired. AMPs therefore pose a seemingly logical solution to the problem of antibiotics being rendered inactive by acquisition of resistance in the field. Even though resistance is less likely in this class of molecules, reports have shown bacteria that can tolerate these peptides mostly through expression of non-specific efflux pumps and/or proteases.[20, 21]

While largely regarded as antimicrobials that directly kill bacteria, AMP concentrations *in vivo* are usually very low (in the ng/mL range) and their cytotoxicity is usually inhibited by physiological concentrations of salt, and serum components.[4] Recent evidence suggests that the immunomodulatory activity of these peptides might be more relevant in a physiological setting forging many to use the term HDPs to describe these peptides (Figure 1.4). HDPs have been shown to (*i*) modulate the expression of cytokines,[22, 23] (*ii*) have anti-inflammatory properties by reducing levels of proinflammatory

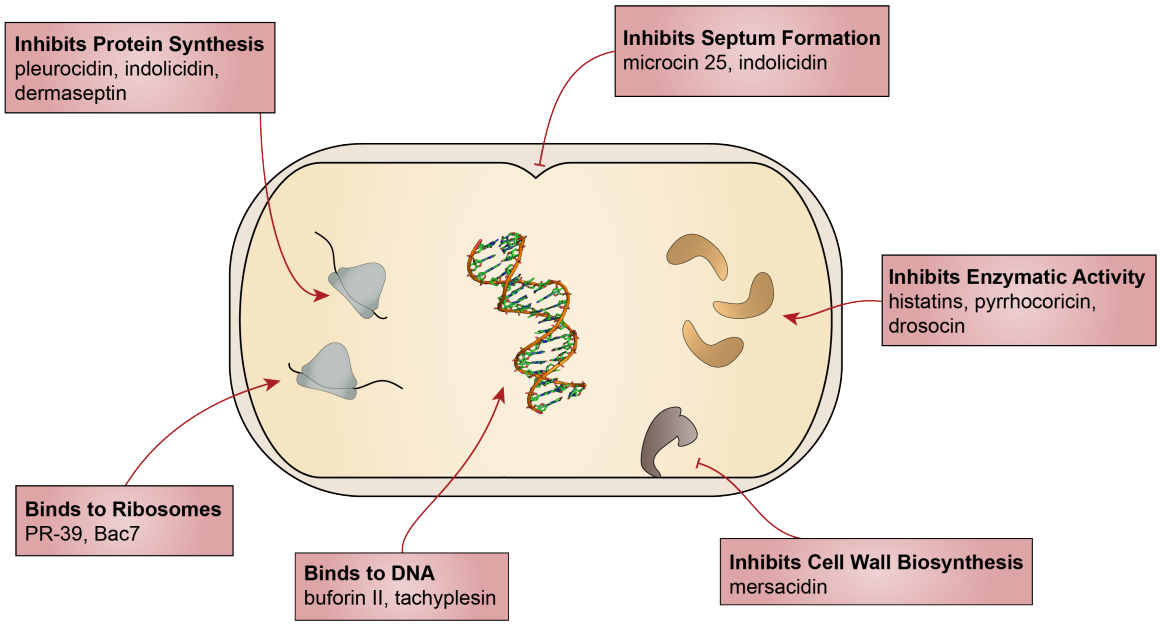

Figure 1.3. Intracellular Targeting of AMPs. Mechanisms not involving membrane disruption by AMPs are widely studied, the most notable examples are depicted above. Peptide translocates across the membrane through unknown mechanisms and binds to targets in the cytoplasm to interfere with key metabolic pathways.

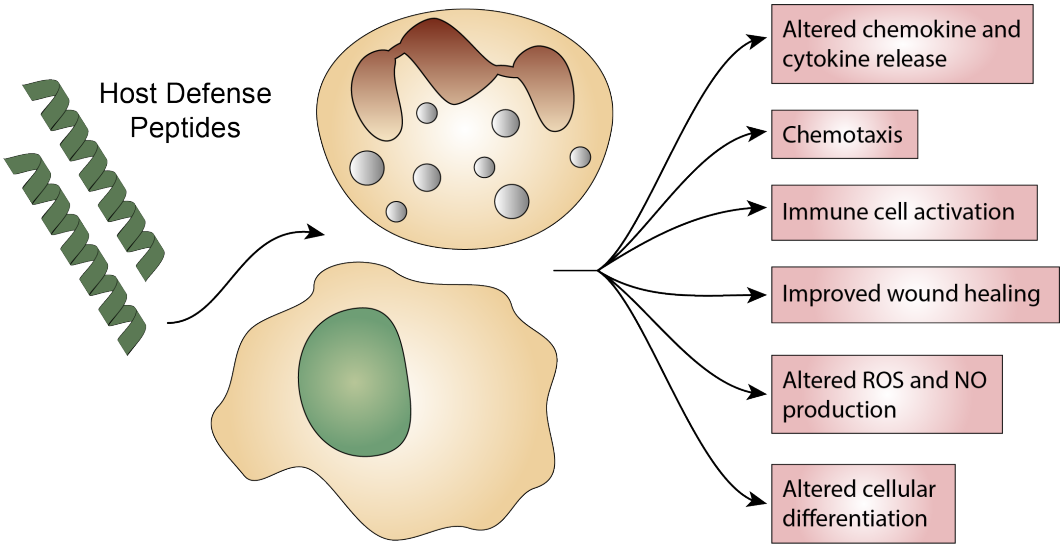

Figure 1.4. Immunomodulatory Activity of Host-Defense Peptides. Some peptides have other activities besides direct microbial killing. HDPs activate several signaling pathways in immune cells to modulate the immune response.

cytokines,[24, 25] (*iii*) have chemotactic properties and induce immune cell migration,[26] and (*iv*) promote macrophage and dendritic cell differentiation.[27, 28] Furthermore, dysregulation of HDP expression in certain tissues result in certain pathologies including autoimmune disease,[29] inflammatory bowel disease[30] and even cancer.[31, 32] Most of these immunomodulatory properties of HDPs result from interactions with high-affinity and specific cell receptors which then activate an intracellular signaling cascade.

Even though any given HDP can be polyfunctional, multicellular organisms likely rely on a plethora of HDPs to mount a quick, effective and amplified immune response – a paradigm that is becoming more apparent in recent literature. HDPs exhibit synergy amongst other peptides within their family,[33, 34] with other HDPs,[35-37] and even with endogenous or exogenous antimicrobials.[38, 39] It seems reasonable to posit that the success of the immune system against a wide array of microbes arises not only from the variety of antimicrobial effectors induced during infection, but also the countless possibility of functional synergy that exist among them.

Transition Metal Ions in the Host-Pathogen Interface

Transition metals are essential micronutrients required for many cellular processes, but their concentration must be tightly regulated because they are toxic in excess. To every organism in the biosphere, they represent a double-edged sword – requiring robust sensing, acquisition and detoxification mechanisms. In biological systems, the most common transition metals are Fe, Cu, Zn, Ni and Mn. These metals are frequently found in metalloproteins that function either in redox- and non-redox catalysis, storage and/or transport, transcriptional regulation, and signal transduction.[40-42] Because of the essentiality of transition metals, pathogenic microbes have evolved

elegant (and sometimes redundant) mechanisms to acquire metals from their host.[43, 44] Indeed, this tug-of-war for metals in the host-pathogen interface highlights the host's effort to limit microbial growth and the pathogen's need for survival in a hostile environment.

To prevent infection, the host relies on two major and contrasting strategies involving distinct groups of metals (Figure 1.5). First, the host limits the availability of iron, manganese and zinc in regions containing bacteria by expressing high-affinity metal-binding proteins.[41, 43, 44] Termed nutritional immunity, this withholding mechanism effectively starves pathogens of these essential micronutrients.[41] In response, bacteria secrete siderophores – small molecules that bind these metals with high affinity – which are then subsequently imported and degraded intracellularly to liberate the free metal.[45, 46] Second, the host leverages the inherent toxicity of copper and zinc, and deliberately traffics these metals into sites of infection.[47, 48] The sudden increase in concentration of these toxic metals causes pleiotropic effects (*vide infra*) that result in microbial killing.[47, 49, 50] To counteract this, bacteria express efflux pumps and metal-scavenging proteins to minimize direct and secondary damage by copper and zinc.[47, 51]

In vivo, bacteria encounter physiological changes in transition metal concentrations due to the aforementioned host response to infection. Transcriptional changes in the bacteria showing induction of metal detoxification pathways and siderophore biosynthesis suggests that perturbation in transition metal trafficking play a role in microbial death.[52] Similarly, bacteria that have defects in iron uptake and copper detoxification showed decreased host colonization, indicating that these metal-responsive elements are essential to their pathogenicity.[53-55]

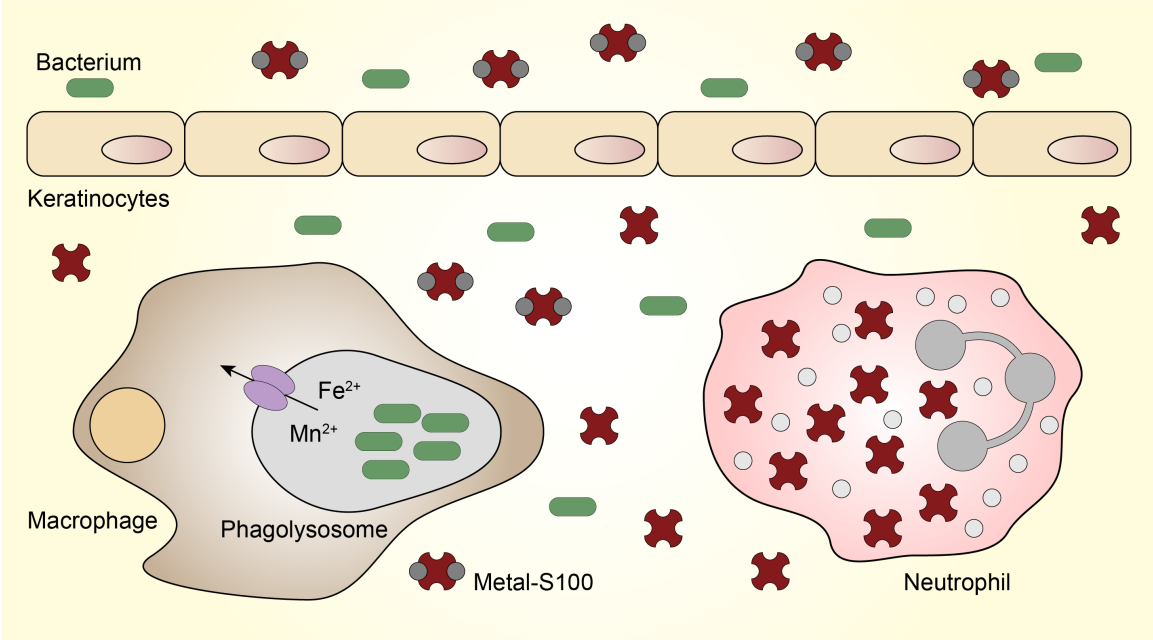

Figure 1.5. Nutritional Immunity in the Host-Pathogen Interface. Transition metal concentrations during infections are tightly regulated by the host to starve the invading microbe of these essential micronutrients. Nutritional immunity involves several host-derived effectors, most notable of which are the S100 proteins which bind to Zn^{2+}, Mn^{2+} and Fe^{2+} ions with high affinity.

A Focus on Copper in the Host-Pathogen Interface: Trafficking, Toxicity and Bacterial Resistance Mechanisms

All organisms require copper for various biological processes but despite its crucial role, excess copper can become toxic. The antimicrobial effects of copper have been observed since antiquity, where as early as 2400 B.C., the metal was used to sterilize water and wounds. In addition, during a cholera outbreak in the early 1800s, workers in a copper plant in Paris were observed to be less susceptible to the disease.[50] Today, there is a renewed interest in the antimicrobial activity of copper and research into mechanisms of copper intoxication in biological systems remains a dynamic field. Copper exists in biological systems either in the Cu^{+} (reduced) or Cu^{2+} (oxidized) state. The

Cu^{2+}/Cu^{+} couple has a reduction potential of +150 mV which guarantees that the copper speciation in the cytosol (E^0 ~ -220 mV) is tipped towards Cu^{+}.[51] While Cu(II) is a borderline Lewis acid, Cu(I) is a soft acid with a strong preference for thiol-based ligands. Indeed, the coordination chemistry of copper in biological systems is dominated by cysteine, methionine, and histidine ligands in the metal's first coordination sphere.[56]

Given the anthropologic use of copper as an antibiotic, it's not surprising that the immune system utilizes this metal for its bactericidal action as well. Multiple trafficking mechanisms involving a variety of immune effectors ensure that copper levels in sites of infection is enriched (Figure 1.6). In phagocytic cells like macrophages, infection triggers overexpression of copper transporters (Ctr1 and ATP7A) and chaperones (Atox1) resulting in increased copper uptake.[50, 53] ATP7A, a Golgi-resident transporter gets trafficked into phagosomes and delivers copper into the lumen of bacteria-containing vesicles. In fact, during *Mycobacterium tuberculosis* infections, phagosomal copper concentration was measured to be 25 – 400 μM.[57] Extracellular levels of copper increase during infections as well. Serum copper levels progressively rise during infection, irrespective of the agent (viral, bacterial, fungal), mainly due to the upregulation of the cuproprotein ceruloplasmin.[58, 59] While the exact reason why this happens is still unknown, it's reasonable to assume that ceruloplasmin – which can bind up to six copper atoms – helps to deliver copper into sites of infection.[49] Indeed, granulomas from *M. tuberculosis*-infected guinea pigs were found to contain markedly higher copper concentrations.[60] Furthermore, a significant accumulation of copper in the urine of patients infected with uropathogenic *E. coli* was also observed.[61] Its apparent that

boosting copper concentration at sites of infections is advantageous due to the metal's inherent antimicrobial activity.

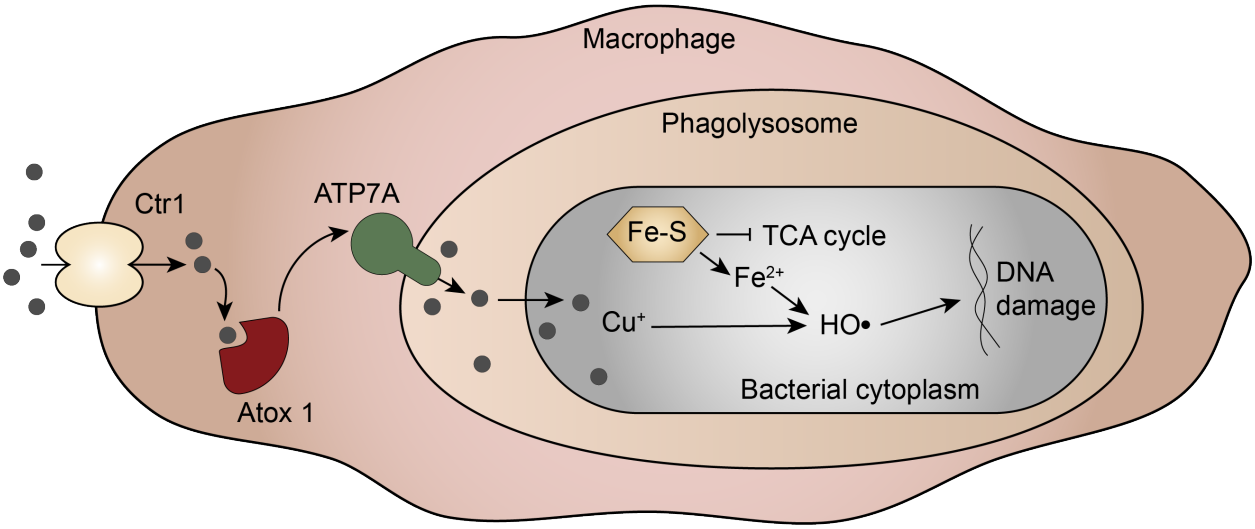

Figure 1.6. Copper Trafficking in response to Macrophage Infection. During infection, macrophages overexpress copper importers (Ctr1 and ATP7A) and chaperones (Atox1) to increase intraphagosomal copper concentration. The sudden surge of copper ions in the bacteria cytoplasm elicits multiple toxic effects like inhibition of aerobic respiration and oxidative DNA damage.

The classical view to the antimicrobial activity of copper is based on its ability to form deleterious hydroxyl radicals via a Fenton-like mechanism.[51] This direct production of reactive oxygen species (ROS) not only covalently damages multiple biomolecules but also depletes bacterial antioxidants. Recent evidence show that low molecular weight thiols (LMWTs) like glutathione (GSH) can bind to and inactivate the cycling of copper between its +1 and +2 states.[62] This makes copper intoxication via direct ROS formation less likely. Nevertheless, induction of ROS detoxifying genes occurs upon exposure of bacteria to lethal levels of copper. Recent work shows that bacterial susceptibility to copper arises from one or any combination of the following mechanisms. First, copper

can replace cofactors in metalloproteins leading to inactivation of enzymatic activity (for the case of catalytic metals) or significant structural perturbation (for the case of structural metals).[48] Next, iron-sulfur clusters of metalloproteins collapse following exposure to copper due to Cu(I) displacement of Fe(II). This liberates free ferrous ions which can then catalyze the Fenton reaction.[63] The first two routes of copper toxicity can largely be explained by the metal's position in the Irving-Williams series: Mn(II) < Fe(II) < Co(II) < Ni(II) < Cu(II) > Zn(II). From a chemical standpoint, donor atoms from proteins preferentially bind Cu(II) because it yields the highest complex stability.[64] Copper can therefore easily replace less competitive metals in the series. Finally, copper impairs membrane function by peroxidizing lipids in the bilayer.[65, 66]

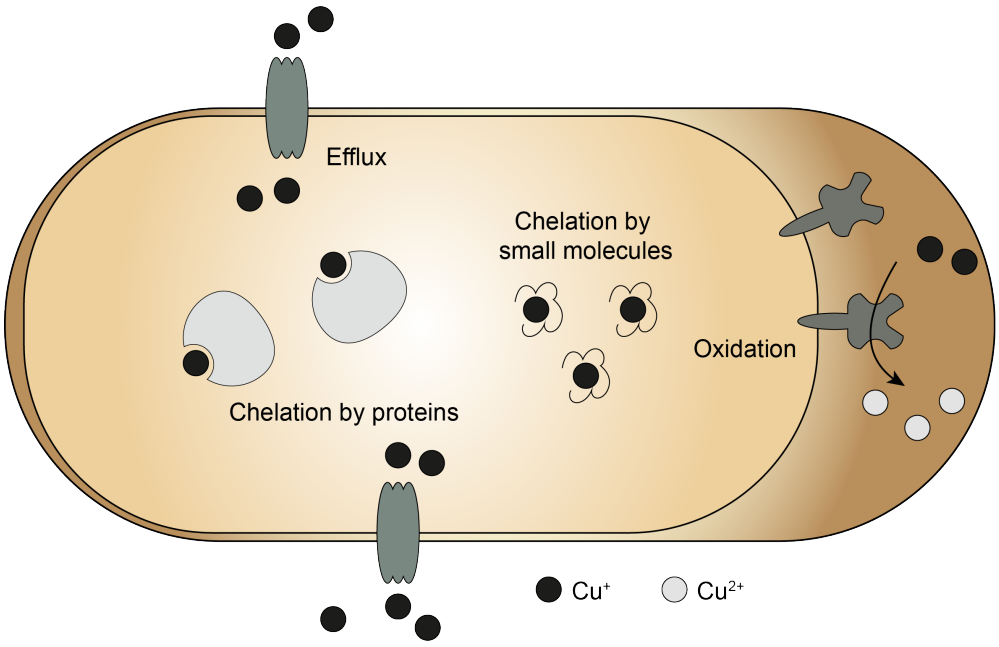

Figure 1.7. Bacterial Evasion Strategies against Copper Intoxication. In response to the increased copper concentration that the host imposes, bacteria induce multiple resistance mechanisms. Bacteria express efflux pumps, copper oxidases, and cytosolic chaperones all acting in concert to detoxify copper.

Invading bacteria often mount multiple modes of detoxification in response to the influx of copper ions to sites containing pathogens (Figure 1.7). Copper-responsive transcription factors in bacteria detect minute changes in cytosolic copper concentration and activate the expression of genes that function in copper detoxification.[67] Membrane-bound exporters in *E. coli*, *Salmonella*, *Streptococcus*, and *M. tuberculosis* have been widely studied (Figure 1.8).[51] These efflux pumps utilize energy from ATP hydrolysis or electrochemical gradients to pump copper from the bacterial cytosol back to the phagosomal lumen. Bacteria also express protein- or small molecule-based copper chelators that bind to cytosolic or periplasmic copper.[68, 69] In addition, some small molecules bind to copper and act as enzyme mimics (superoxide dismutase) to minimize secondary toxic effects of copper.[70, 71] Finally, expression of multicopper oxidases that convert the more toxic Cu(I) to the less toxic Cu(II) act to prevent the Fenton reaction.[72, 73] All of these mechanisms work in concert to ensure that concentration of "free" copper in the cytosol is maintained below picomolar levels.[74] While some of these bacterial defenses are redundant within any single pathogen, some detoxification modes are more dominant than others. Indeed, bacteria that cannot neutralize the toxicity of copper are more susceptible to copper-related toxicity of macrophages.[53, 60]

Antimicrobial and Host-Defense Peptides Utilizing Metal Ions

One way that nutritional immunity is mediated in the host-pathogen interface is through expression of high-affinity metal chelators by the immune system. Indeed, several HDPs are known to sequester transition metals, the largest and most characterized of which are proteins belonging to the S100 family.[75] Members of the S100 protein family (~20 identified and characterized to date) are EF-hand containing, Ca^{2+}-binding

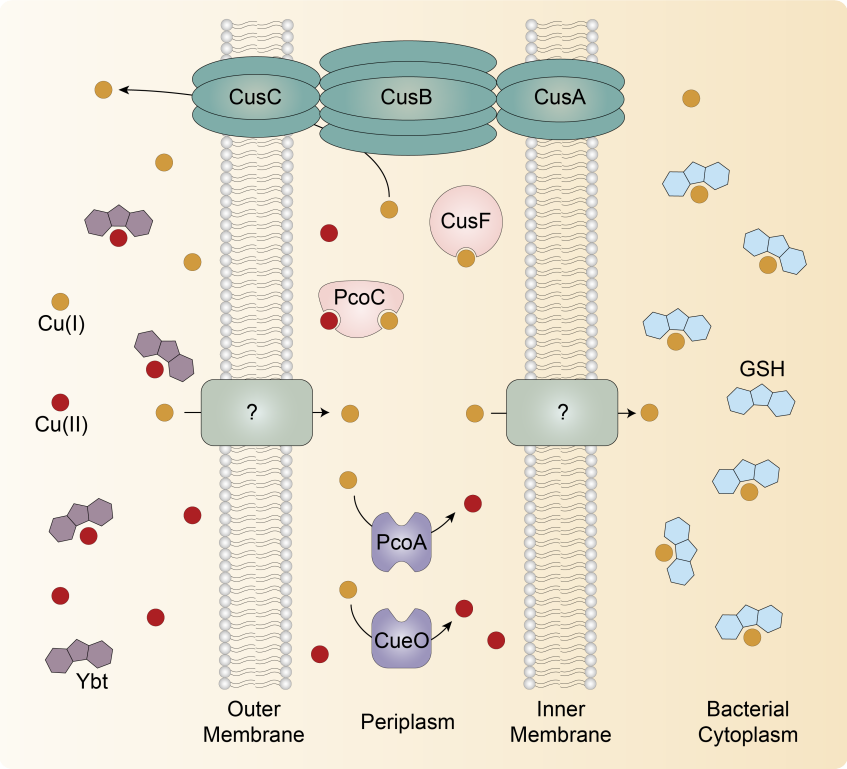

Figure 1.8. Copper chaperones in bacteria. Copper is transported into the bacterial cytosol by uncharacterized importers and are exported by the Cus system. Labile copper ions exits in the periplasmic space bound to small organic ligands and are converted to the +2 state by periplasmic oxidases.

polypeptides expressed by higher vertebrates that perform several functions in innate immunity. Psoriasin (S100A7), expressed by keratinocytes, binds to Zn(II) and is the main *E. coli*-killing protein in the skin.[76] Calprotectin (S100A8/A9) and Calgranulin (S100A12) are expressed by neutrophils, monocytes and macrophages; and are secreted in response to inflammation. Calprotectin binds Zn(II), Mn(II), and Fe(II) while Calgranulin binds Zn(II) and Cu(II).[77-79] In some cases, HDPs bind metal complexes, such is the case for Lipocalin-2 (Siderocalin). Expressed in neutrophils and macrophages, Lipocalin-2 binds the iron-siderophore complex and interferes with intracellular bacterial iron

acquisition.[80] Apart from metal withholding, HDPs also utilize transition metals for structural purposes. Dermcidin, an AMP from human sweat uses Zn^{2+} to form a trimer of antiparallel dimers, its active conformation. This hexameric bundle inserts into the bacterial bilayer and acts as a transmembrane channel dissipating the membrane potential.[81] Furthermore, Zn^{2+} in the catalytic domain of matrix metalloproteinase 12 (MMP12, macrophage elastase) serves to stabilize the protein tertiary structure. MMP12 binds to bacterial bilayers and causes membrane disruption through its antimicrobial C-terminal domain.[82]

While largely studied in the context of human infections, transition metal utilization of HDPs is certainly not unique to vertebrates. For instance, Microplusin from the hard tick *R. microplus* was found to sequester Cu^{2+} likely from terminal oxidases resulting in inhibition of aerobic respiration.[83] Furthermore, Clavanin A from the tunicate *Styela clava* was recently shown to use Zn^{2+} for its antibacterial action, however, the exact mechanism remains a question.[84]

Finally, the metal binding sites in the aforementioned HDPs come from residues belonging to different domains of the polypeptide. There are however, short sequences that bind to metals directly, and therefore require a shorter primary structure. The Zn^{2+} binding sequence, His-Glu-X-X-His (HEXXH) is present in histatins – a group of salivary AMPs known to have fungicidal activities.[16, 85] While the exact target and mechanism of histatins are still subject to debate, its ability to promote mitochondrial dysfunction and oxidative stress is widely accepted.[86]

The Amino Terminal Copper and Nickel (ATCUN) Binding Motif in Peptide and Proteins

Analogous to the HEXXH sequence in histatins, another short metal binding sequence is the Amino Terminal Copper and Nickel (ATCUN) binding motif. It consists of any two amino acids in the first two positions and histidine in the third (i.e. XXH). It binds to Cu^{2+} and Ni^{2+} ions with high affinity through a free amino terminal $–NH_2$ group, two intervening backbone amide nitrogens (from residue 2 and His3) and the imidazole δ-N from His3 (Figure 1.9).[87] The ATCUN motif is found in many copper-binding proteins, most notable of which are the serum albumins where they are believed to function as systemic copper shuttles.[88] Bound to copper or nickel, the resulting metallopeptide adopts a distorted square planar geometry optimally poised to bind to the minor groove of DNA.[89]

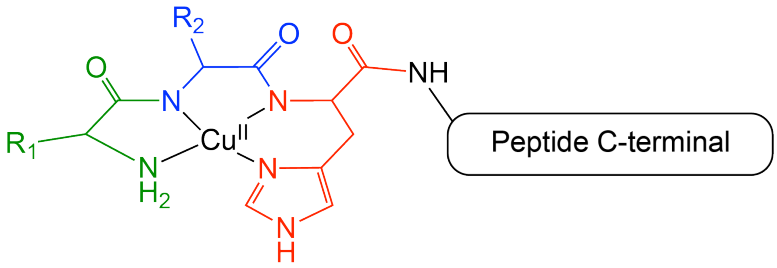

Figure 1.9. Schematic Representation of ATCUN-containing AMP. R1, and R2 represent the first and second amino acid residue. Each amino acid is color coded in this scheme. Cu(II) binds to the N-terminal of ATCUN-containing peptides leaving the C-terminal fragment free.

From a chemical and antimicrobial standpoint, the ATCUN motif is interesting because it has the ability to form ROS under physiological conditions.[90, 91] While most ligands prevent the redox cycling of metals, the peptidic backbone actually promotes it. The redox activity involves Cu(II) and Cu(III) species where the trivalent state is stabilized

by the strong Lewis basicity of the peptide amide nitrogens.[91] The reduction potential of the Cu(III)-ATCUN/Cu(II)-ATCUN couple is >900 mV (vs NHE) making the redox cycling accessible to biological reductants.[91] Indeed, redox cycling of the ATCUN complexes have been demonstrated using ascorbic acid and NADH.[90] While electrochemical methods have established the oxidation states pertinent to the redox cycling, the nature and identity of the ROS formed however, is still a topic of debate. The most accepted form of the ROS is a metal-bound hydroxo group,[90] which is chemically distinct from the canonical hydroxyl radical, •OH. Because this hydroxo species is bound to a heavy element, it is far less diffusible than •OH; but because it is bound to a more electropositive atom, it is far more oxidizing. Indeed Cu-ATCUN and Ni-ATCUN complexes have been demonstrated to effectively oxidize small organic fluorophores, phospholipids and oxidatively cleave DNA.[66, 91, 92]

Of direct relevance to this dissertation is the fact that a number of naturally-occurring AMPs and HDPs contain an ATCUN motif. Notable examples of which are members of the histatin family. In addition to containing a Zn^{2+}-binding sequence, histatins 3 and 5 also contain an ATCUN motif.[16] Taking into consideration the relative abundance of copper in the saliva and the ability of the Cu-ATCUN complex to form ROS, it's easy to assume that histatins can cause oxidative stress in the oral fungal flora. However, contrasting reports have shown that this is not the case. While some believe that histatins' ROS formation is the major fungicidal mechanism, recent reports have shown that histatins can also inhibit enzymatic activity, act as ionophores to disrupt ionic balance, and activate signaling cascades that lead to apoptosis.[85] While multiple modes of inhibition are expected from AMPs, its tempting to hypothesize a single major driving

force for fungal death following exposure to histatins. Clearly, more elaborative work is needed to build a complete picture of cell death, and find harmony in a sea of contrasting mechanisms.

Apart from their role in histatins, the ATCUN motif have been implicated in the activity of other naturally occurring AMPs as well. For instance, the activity of myxinidin (GIHDILKYGKPS) – an AMP from the epidermal mucous of hagfish – against *E. coli*, *K. pneumoniae*, and *S. aureus* is attenuated when the histidine residue is replaced by alanine.[93, 94] In the clavanin AMP family, peptides isolated from the hemocytes of the tunicate *Styela clava*, the ATCUN-containing clavanin C is three times more active than clavanins A and B.[95] Peptides that do not have antimicrobial properties but nevertheless have biological activity also seem to utilize the ATCUN motif. For instance, human protamine 2 (HP2), a protein that perform key functions in spermatogenesis and which contains the sequence Arg-Thr-His (RTH) in its N-terminal, was shown to generate ROS after binding to copper. Studies in model peptides show that the DNA damaging properties of HP2 is due in part to the presence of the ATCUN motif.[96] Finally, Cu^{2+} binding in the neuropeptide neuromedin C, containing the ATCUN motif Gly-Asn-His, is believed to inhibit neurotransmission or the growth factor effects of the peptide.[97]

Overview of the Dissertation – What we did, why we did it, and what we learned

As previously mentioned, a number of naturally occurring AMPs and HDPs contain an ATCUN motif (Figure 1.10). A simple AMP database search yields >50 ribosomally synthesized, mature peptides containing an XXH sequence in its N-terminal (hereon referred to as ATCUN-AMPs). These ATCUN-AMPs were isolated from all domains of life (including bacteria), and exhibit diversity in length, sequence, cellular and tissue distribution, and biological activity. Although currently unexplored, there is great potential for ATCUN-AMPs to utilize copper for their antimicrobial mechanism. This hypothesis is predicated on the fact that copper is upregulated in sites of infection and that the resulting Cu-ATCUN complex have redox cycling potential under physiological conditions. Furthermore, because these ATCUN-AMPs were isolated from various organisms, they may represent a generalized defensive strategy by unrelated groups of organisms.

While reallocating the inherently antimicrobial copper ion into sites of infection poses certain physiological advantages, a simplistic view of the bactericidal response by the immune system – one that is based on toxicity of a single element – is certainly unrealistic. Indeed, in the context of an infection, multiple antimicrobial effectors likely synergize with each other to eradicate the invading microbe. We therefore propose in this study that copper redistribution during infection serves two purposes; to generate a pool of inherently toxic copper (a function that is known and well appreciated) and to provide a metallic co-factor to other host-derived antimicrobial effectors such as AMPs.

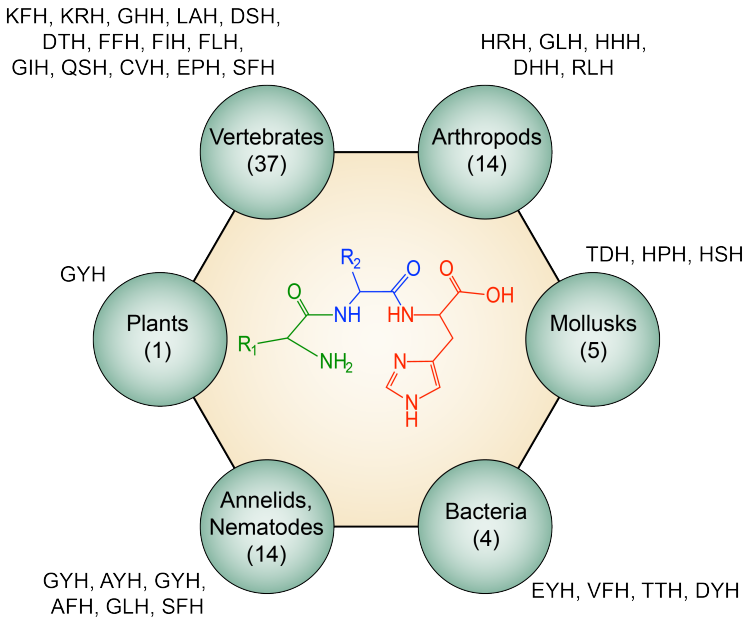

Figure 1.10. Diversity of ATCUN Motifs found in nature. This schematic shows the phylum of the organisms from which an ATCUN-AMP have been isolated and the sequences of the metal-binding motif. Numbers in the parenthesis represent the number of peptides characterized to date belonging to the family.

This dissertation showcases both fundamental and translational aspects of the ATCUN motif in the context of AMPs. First, the role that the ATCUN motif plays in the activity of naturally occurring ATCUN-AMPs is investigated. Chapter 2 describes copper-mediated membrane lipid oxidation by the ATCUN-AMP Ixosin as a requirement for synergy with another AMP, Ixosin B. Chapter 3 details the copper-mediated oxidative cleavage of DNA by two homologous ATCUN-AMPs, Piscidins 1 and 3. We uncover how copper-related bioactivities can vary significantly among bacteria in different lifestyles. Second, the ATCUN motif is used to modify other AMPs to develop more potent antimicrobials. Chapters 4 and 5 focus on our efforts to develop dual-acting peptides to target a wide-spectrum of bacteria, while chapter 6 shows the development of an ATCUN-based antimicrobial designed to target intracellular *M. tuberculosis*.

Throughout this dissertation, a central theme will become apparent, one that will expand the catalog of mechanisms by which AMPs and HDPs utilize metal ions for their activity. That is, in addition to metal sequestration and using transition metals for structural purposes, we propose that HDPs and AMPs use transition metals as direct chemical co-factors as well. Here, we put forth the idea that ATCUN-containing peptides leverages the chemical properties of the resulting copper complex to cause oxidative stress and elicit synergy with other antimicrobial effectors.

Chapter References:

[1] Zasloff, M. (2002) Antimicrobial peptides of multicellular organisms, *Nature 415*, 389-395.

[2] Brogden, K. A. (2005) Antimicrobial peptides: pore formers or metabolic inhibitors in bacteria?, *Nat Rev Microbiol 3*, 238-250.

[3] Nguyen, L. T., Haney, E. F., and Vogel, H. J. (2011) The expanding scope of antimicrobial peptide structures and their modes of action, *Trends Biotechnol 29*, 464-472.

[4] Hancock, R. E., Haney, E. F., and Gill, E. E. (2016) The immunology of host defence peptides: beyond antimicrobial activity, *Nat Rev Immunol 16*, 321-334.

[5] Hilchie, A. L., Wuerth, K., and Hancock, R. E. (2013) Immune modulation by multifaceted cationic host defense (antimicrobial) peptides, *Nat Chem Biol 9*, 761-768.

[6] Hancock, R. E., and Sahl, H. G. (2006) Antimicrobial and host-defense peptides as new anti-infective therapeutic strategies, *Nat Biotechnol 24*, 1551-1557.

[7] Fjell, C. D., Hiss, J. A., Hancock, R. E., and Schneider, G. (2011) Designing antimicrobial peptides: form follows function, *Nat Rev Drug Discov 11*, 37-51.

[8] Wimley, W. C. (2010) Describing the mechanism of antimicrobial peptide action with the interfacial activity model, *ACS Chem Biol 5*, 905-917.

[9] Le, C. F., Fang, C. M., and Sekaran, S. D. (2017) Intracellular Targeting Mechanisms by Antimicrobial Peptides, *Antimicrob Agents Chemother 61*.

[10] Nicolas, P. (2009) Multifunctional host defense peptides: intracellular-targeting antimicrobial peptides, *FEBS J 276*, 6483-6496.

[11] Park, C. B., Kim, H. S., and Kim, S. C. (1998) Mechanism of action of the antimicrobial peptide buforin II: buforin II kills microorganisms by penetrating the cell membrane and inhibiting cellular functions, *Biochem Biophys Res Commun 244*, 253-257.

[12] Yonezawa, A., Kuwahara, J., Fujii, N., and Sugiura, Y. (1992) Binding of tachyplesin I to DNA revealed by footprinting analysis: significant contribution of secondary structure to DNA binding and implication for biological action, *Biochemistry 31*, 2998-3004.

[13] Mardirossian, M., Grzela, R., Giglione, C., Meinnel, T., Gennaro, R., Mergaert, P., and Scocchi, M. (2014) The host antimicrobial peptide Bac71-35 binds to bacterial ribosomal proteins and inhibits protein synthesis, *Chem Biol 21*, 1639-1647.

[14] Patrzykat, A., Friedrich, C. L., Zhang, L., Mendoza, V., and Hancock, R. E. (2002) Sublethal concentrations of pleurocidin-derived antimicrobial peptides inhibit macromolecular synthesis in Escherichia coli, *Antimicrob Agents Chemother 46*, 605-614.

[15] Boman, H. G., Agerberth, B., and Boman, A. (1993) Mechanisms of action on Escherichia coli of cecropin P1 and PR-39, two antibacterial peptides from pig intestine, *Infect Immun 61*, 2978-2984.

[16] Kavanagh, K., and Dowd, S. (2004) Histatins: antimicrobial peptides with therapeutic potential, *J Pharm Pharmacol 56*, 285-289.

[17] Otvos, L., Jr., O, I., Rogers, M. E., Consolvo, P. J., Condie, B. A., Lovas, S., Bulet, P., and Blaszczyk-Thurin, M. (2000) Interaction between heat shock proteins and antimicrobial peptides, *Biochemistry 39*, 14150-14159.

[18] Subbalakshmi, C., and Sitaram, N. (1998) Mechanism of antimicrobial action of indolicidin, *FEMS Microbiol Lett 160*, 91-96.
[19] Peschel, A., and Sahl, H. G. (2006) The co-evolution of host cationic antimicrobial peptides and microbial resistance, *Nat Rev Microbiol 4*, 529-536.
[20] Anaya-Lopez, J. L., Lopez-Meza, J. E., and Ochoa-Zarzosa, A. (2013) Bacterial resistance to cationic antimicrobial peptides, *Crit Rev Microbiol 39*, 180-195.
[21] LaRock, C. N., and Nizet, V. (2015) Cationic antimicrobial peptide resistance mechanisms of streptococcal pathogens, *Biochim Biophys Acta 1848*, 3047-3054.
[22] Chaly, Y. V., Paleolog, E. M., Kolesnikova, T. S., Tikhonov, II, Petratchenko, E. V., and Voitenok, N. N. (2000) Neutrophil alpha-defensin human neutrophil peptide modulates cytokine production in human monocytes and adhesion molecule expression in endothelial cells, *Eur Cytokine Netw 11*, 257-266.
[23] Mookherjee, N., Brown, K. L., Bowdish, D. M., Doria, S., Falsafi, R., Hokamp, K., Roche, F. M., Mu, R., Doho, G. H., Pistolic, J., Powers, J. P., Bryan, J., Brinkman, F. S., and Hancock, R. E. (2006) Modulation of the TLR-mediated inflammatory response by the endogenous human host defense peptide LL-37, *J Immunol 176*, 2455-2464.
[24] Elssner, A., Duncan, M., Gavrilin, M., and Wewers, M. D. (2004) A novel P2X7 receptor activator, the human cathelicidin-derived peptide LL37, induces IL-1 beta processing and release, *J Immunol 172*, 4987-4994.
[25] Yu, J., Mookherjee, N., Wee, K., Bowdish, D. M., Pistolic, J., Li, Y., Rehaume, L., and Hancock, R. E. (2007) Host defense peptide LL-37, in synergy with inflammatory mediator IL-1beta, augments immune responses by multiple pathways, *J Immunol 179*, 7684-7691.
[26] Niyonsaba, F., Ushio, H., Nakano, N., Ng, W., Sayama, K., Hashimoto, K., Nagaoka, I., Okumura, K., and Ogawa, H. (2007) Antimicrobial peptides human beta-defensins stimulate epidermal keratinocyte migration, proliferation and production of proinflammatory cytokines and chemokines, *J Invest Dermatol 127*, 594-604.
[27] Davidson, D. J., Currie, A. J., Reid, G. S., Bowdish, D. M., MacDonald, K. L., Ma, R. C., Hancock, R. E., and Speert, D. P. (2004) The cationic antimicrobial peptide LL-37 modulates dendritic cell differentiation and dendritic cell-induced T cell polarization, *J Immunol 172*, 1146-1156.
[28] van der Does, A. M., Beekhuizen, H., Ravensbergen, B., Vos, T., Ottenhoff, T. H., van Dissel, J. T., Drijfhout, J. W., Hiemstra, P. S., and Nibbering, P. H. (2010) LL-37 directs macrophage differentiation toward macrophages with a proinflammatory signature, *J Immunol 185*, 1442-1449.
[29] Ong, P. Y., Ohtake, T., Brandt, C., Strickland, I., Boguniewicz, M., Ganz, T., Gallo, R. L., and Leung, D. Y. (2002) Endogenous antimicrobial peptides and skin infections in atopic dermatitis, *N Engl J Med 347*, 1151-1160.
[30] Gallo, R. L., and Hooper, L. V. (2012) Epithelial antimicrobial defence of the skin and intestine, *Nat Rev Immunol 12*, 503-516.
[31] Gaspar, D., Veiga, A. S., and Castanho, M. A. (2013) From antimicrobial to anticancer peptides. A review, *Front Microbiol 4*, 294.
[32] Buchau, A. S., Morizane, S., Trowbridge, J., Schauber, J., Kotol, P., Bui, J. D., and Gallo, R. L. (2010) The host defense peptide cathelicidin is required for NK cell-mediated suppression of tumor growth, *J Immunol 184*, 369-378.

[33] Mangoni, M. L., and Shai, Y. (2009) Temporins and their synergism against Gram-negative bacteria and in lipopolysaccharide detoxification, *Biochim Biophys Acta 1788*, 1610-1619.
[34] Rahnamaeian, M., Cytrynska, M., Zdybicka-Barabas, A., Dobslaff, K., Wiesner, J., Twyman, R. M., Zuchner, T., Sadd, B. M., Regoes, R. R., Schmid-Hempel, P., and Vilcinskas, A. (2015) Insect antimicrobial peptides show potentiating functional interactions against Gram-negative bacteria, *Proc Biol Sci 282*, 20150293.
[35] Agier, J., Efenberger, M., and Brzezinska-Blaszczyk, E. (2015) Cathelicidin impact on inflammatory cells, *Cent Eur J Immunol 40*, 225-235.
[36] Rahnamaeian, M., Cytrynska, M., Zdybicka-Barabas, A., and Vilcinskas, A. (2016) The functional interaction between abaecin and pore-forming peptides indicates a general mechanism of antibacterial potentiation, *Peptides 78*, 17-23.
[37] Westerhoff, H. V., Zasloff, M., Rosner, J. L., Hendler, R. W., De Waal, A., Vaz Gomes, A., Jongsma, P. M., Riethorst, A., and Juretic, D. (1995) Functional synergism of the magainins PGLa and magainin-2 in Escherichia coli, tumor cells and liposomes, *Eur J Biochem 228*, 257-264.
[38] Feng, Q., Huang, Y., Chen, M., Li, G., and Chen, Y. (2015) Functional synergy of alpha-helical antimicrobial peptides and traditional antibiotics against Gram-negative and Gram-positive bacteria in vitro and in vivo, *Eur J Clin Microbiol Infect Dis 34*, 197-204.
[39] Ejim, L., Farha, M. A., Falconer, S. B., Wildenhain, J., Coombes, B. K., Tyers, M., Brown, E. D., and Wright, G. D. (2011) Combinations of antibiotics and nonantibiotic drugs enhance antimicrobial efficacy, *Nat Chem Biol 7*, 348-350.
[40] Andreini, C., Bertini, I., Cavallaro, G., Holliday, G. L., and Thornton, J. M. (2008) Metal ions in biological catalysis: from enzyme databases to general principles, *J Biol Inorg Chem 13*, 1205-1218.
[41] Hood, M. I., and Skaar, E. P. (2012) Nutritional immunity: transition metals at the pathogen-host interface, *Nat Rev Microbiol 10*, 525-537.
[42] Chang, C. J. (2015) Searching for harmony in transition-metal signaling, *Nat Chem Biol 11*, 744-747.
[43] Skaar, E. P., and Raffatellu, M. (2015) Metals in infectious diseases and nutritional immunity, *Metallomics 7*, 926-928.
[44] Kehl-Fie, T. E., and Skaar, E. P. (2010) Nutritional immunity beyond iron: a role for manganese and zinc, *Curr Opin Chem Biol 14*, 218-224.
[45] Faraldo-Gomez, J. D., and Sansom, M. S. (2003) Acquisition of siderophores in gram-negative bacteria, *Nat Rev Mol Cell Biol 4*, 105-116.
[46] Johnstone, T. C., and Nolan, E. M. (2015) Beyond iron: non-classical biological functions of bacterial siderophores, *Dalton Trans 44*, 6320-6339.
[47] Djoko, K. Y., Ong, C. L., Walker, M. J., and McEwan, A. G. (2015) The Role of Copper and Zinc Toxicity in Innate Immune Defense against Bacterial Pathogens, *J Biol Chem 290*, 18954-18961.
[48] Lemire, J. A., Harrison, J. J., and Turner, R. J. (2013) Antimicrobial activity of metals: mechanisms, molecular targets and applications, *Nat Rev Microbiol 11*, 371-384.
[49] Besold, A. N., Culbertson, E. M., and Culotta, V. C. (2016) The Yin and Yang of copper during infection, *J Biol Inorg Chem 21*, 137-144.

[50] Samanovic, M. I., Ding, C., Thiele, D. J., and Darwin, K. H. (2012) Copper in microbial pathogenesis: meddling with the metal, *Cell Host Microbe 11*, 106-115.
[51] Fu, Y., Chang, F. M., and Giedroc, D. P. (2014) Copper transport and trafficking at the host-bacterial pathogen interface, *Acc Chem Res 47*, 3605-3613.
[52] Achard, M. E., Stafford, S. L., Bokil, N. J., Chartres, J., Bernhardt, P. V., Schembri, M. A., Sweet, M. J., and McEwan, A. G. (2012) Copper redistribution in murine macrophages in response to Salmonella infection, *Biochem J 444*, 51-57.
[53] White, C., Lee, J., Kambe, T., Fritsche, K., and Petris, M. J. (2009) A role for the ATP7A copper-transporting ATPase in macrophage bactericidal activity, *J Biol Chem 284*, 33949-33956.
[54] Solioz, M., Abicht, H. K., Mermod, M., and Mancini, S. (2010) Response of gram-positive bacteria to copper stress, *J Biol Inorg Chem 15*, 3-14.
[55] Ding, C., Festa, R. A., Chen, Y. L., Espart, A., Palacios, O., Espin, J., Capdevila, M., Atrian, S., Heitman, J., and Thiele, D. J. (2013) Cryptococcus neoformans copper detoxification machinery is critical for fungal virulence, *Cell Host Microbe 13*, 265-276.
[56] Frieden, E. (1968) The biochemistry of copper, *Sci Am 218*, 103-114.
[57] Wagner, D., Maser, J., Lai, B., Cai, Z., Barry, C. E., 3rd, Honer Zu Bentrup, K., Russell, D. G., and Bermudez, L. E. (2005) Elemental analysis of Mycobacterium avium-, Mycobacterium tuberculosis-, and Mycobacterium smegmatis-containing phagosomes indicates pathogen-induced microenvironments within the host cell's endosomal system, *J Immunol 174*, 1491-1500.
[58] Cernat, R. I., Mihaescu, T., Vornicu, M., Vione, D., Olariu, R. I., and Arsene, C. (2011) Serum trace metal and ceruloplasmin variability in individuals treated for pulmonary tuberculosis, *Int J Tuberc Lung Dis 15*, 1239-1245, i.
[59] Kocyigit, A., Erel, O., Gurel, M. S., Avci, S., and Aktepe, N. (1998) Alterations of serum selenium, zinc, copper, and iron concentrations and some related antioxidant enzyme activities in patients with cutaneous leishmaniasis, *Biol Trace Elem Res 65*, 271-281.
[60] Wolschendorf, F., Ackart, D., Shrestha, T. B., Hascall-Dove, L., Nolan, S., Lamichhane, G., Wang, Y., Bossmann, S. H., Basaraba, R. J., and Niederweis, M. (2011) Copper resistance is essential for virulence of Mycobacterium tuberculosis, *Proc Natl Acad Sci U S A 108*, 1621-1626.
[61] Subashchandrabose, S., Hazen, T. H., Brumbaugh, A. R., Himpsl, S. D., Smith, S. N., Ernst, R. D., Rasko, D. A., and Mobley, H. L. (2014) Host-specific induction of Escherichia coli fitness genes during human urinary tract infection, *Proc Natl Acad Sci U S A 111*, 18327-18332.
[62] Outten, F. W., and Munson, G. P. (2013) Lability and liability of endogenous copper pools, *J Bacteriol 195*, 4553-4555.
[63] Macomber, L., and Imlay, J. A. (2009) The iron-sulfur clusters of dehydratases are primary intracellular targets of copper toxicity, *Proc Natl Acad Sci U S A 106*, 8344-8349.
[64] Varadwaj, P. R., Varadwaj, A., and Jin, B. Y. (2015) Ligand(s)-to-metal charge transfer as a factor controlling the equilibrium constants of late first-row transition metal complexes: revealing the Irving-Williams thermodynamical series, *Phys Chem Chem Phys 17*, 805-811.

[65] Hong, R., Kang, T. Y., Michels, C. A., and Gadura, N. (2012) Membrane lipid peroxidation in copper alloy-mediated contact killing of Escherichia coli, *Appl Environ Microbiol 78*, 1776-1784.
[66] Wang, T. Y., Libardo, M. D., Angeles-Boza, A. M., and Pellois, J. P. (2017) Membrane oxidation in cell delivery and cell killing applications, *ACS Chem Biol*.
[67] Arguello, J. M., Raimunda, D., and Padilla-Benavides, T. (2013) Mechanisms of copper homeostasis in bacteria, *Front Cell Infect Microbiol 3*, 73.
[68] Gold, B., Deng, H., Bryk, R., Vargas, D., Eliezer, D., Roberts, J., Jiang, X., and Nathan, C. (2008) Identification of a copper-binding metallothionein in pathogenic mycobacteria, *Nat Chem Biol 4*, 609-616.
[69] Finney, L. A., and O'Halloran, T. V. (2003) Transition metal speciation in the cell: insights from the chemistry of metal ion receptors, *Science 300*, 931-936.
[70] Chaturvedi, K. S., Hung, C. S., Crowley, J. R., Stapleton, A. E., and Henderson, J. P. (2012) The siderophore yersiniabactin binds copper to protect pathogens during infection, *Nat Chem Biol 8*, 731-736.
[71] Chaturvedi, K. S., Hung, C. S., Giblin, D. E., Urushidani, S., Austin, A. M., Dinauer, M. C., and Henderson, J. P. (2014) Cupric yersiniabactin is a virulence-associated superoxide dismutase mimic, *ACS Chem Biol 9*, 551-561.
[72] Huffman, D. L., Huyett, J., Outten, F. W., Doan, P. E., Finney, L. A., Hoffman, B. M., and O'Halloran, T. V. (2002) Spectroscopy of Cu(II)-PcoC and the multicopper oxidase function of PcoA, two essential components of Escherichia coli pco copper resistance operon, *Biochemistry 41*, 10046-10055.
[73] Rowland, J. L., and Niederweis, M. (2013) A multicopper oxidase is required for copper resistance in Mycobacterium tuberculosis, *J Bacteriol 195*, 3724-3733.
[74] Rae, T. D., Schmidt, P. J., Pufahl, R. A., Culotta, V. C., and O'Halloran, T. V. (1999) Undetectable intracellular free copper: the requirement of a copper chaperone for superoxide dismutase, *Science 284*, 805-808.
[75] Zackular, J. P., Chazin, W. J., and Skaar, E. P. (2015) Nutritional Immunity: S100 Proteins at the Host-Pathogen Interface, *J Biol Chem 290*, 18991-18998.
[76] Glaser, R., Harder, J., Lange, H., Bartels, J., Christophers, E., and Schroder, J. M. (2005) Antimicrobial psoriasin (S100A7) protects human skin from Escherichia coli infection, *Nat Immunol 6*, 57-64.
[77] Corbin, B. D., Seeley, E. H., Raab, A., Feldmann, J., Miller, M. R., Torres, V. J., Anderson, K. L., Dattilo, B. M., Dunman, P. M., Gerads, R., Caprioli, R. M., Nacken, W., Chazin, W. J., and Skaar, E. P. (2008) Metal chelation and inhibition of bacterial growth in tissue abscesses, *Science 319*, 962-965.
[78] Nakashige, T. G., Zhang, B., Krebs, C., and Nolan, E. M. (2015) Human calprotectin is an iron-sequestering host-defense protein, *Nat Chem Biol 11*, 765-771.
[79] Cunden, L. S., Gaillard, A., and Nolan, E. M. (2016) Calcium Ions Tune the Zinc-Sequestering Properties and Antimicrobial Activity of Human S100A12, *Chem Sci 7*, 1338-1348.
[80] Flo, T. H., Smith, K. D., Sato, S., Rodriguez, D. J., Holmes, M. A., Strong, R. K., Akira, S., and Aderem, A. (2004) Lipocalin 2 mediates an innate immune response to bacterial infection by sequestrating iron, *Nature 432*, 917-921.
[81] Song, C., Weichbrodt, C., Salnikov, E. S., Dynowski, M., Forsberg, B. O., Bechinger, B., Steinem, C., de Groot, B. L., Zachariae, U., and Zeth, K. (2013) Crystal

structure and functional mechanism of a human antimicrobial membrane channel, *Proc Natl Acad Sci U S A 110*, 4586-4591.
[82] Houghton, A. M., Hartzell, W. O., Robbins, C. S., Gomis-Ruth, F. X., and Shapiro, S. D. (2009) Macrophage elastase kills bacteria within murine macrophages, *Nature 460*, 637-641.
[83] Silva, F. D., Rezende, C. A., Rossi, D. C., Esteves, E., Dyszy, F. H., Schreier, S., Gueiros-Filho, F., Campos, C. B., Pires, J. R., and Daffre, S. (2009) Structure and mode of action of microplusin, a copper II-chelating antimicrobial peptide from the cattle tick Rhipicephalus (Boophilus) microplus, *J Biol Chem 284*, 34735-34746.
[84] Juliano, S. A., Pierce, S., deMayo, J. A., Balunas, M. J., and Angeles-Boza, A. M. (2017) Exploration of the Innate Immune System of Styela clava: Zn2+ Binding Enhances the Antimicrobial Activity of the Tunicate Peptide Clavanin A, *Biochemistry 56*, 1403-1414.
[85] Puri, S., and Edgerton, M. (2014) How does it kill?: understanding the candidacidal mechanism of salivary histatin 5, *Eukaryot Cell 13*, 958-964.
[86] Koshlukova, S. E., Araujo, M. W., Baev, D., and Edgerton, M. (2000) Released ATP is an extracellular cytotoxic mediator in salivary histatin 5-induced killing of Candida albicans, *Infect Immun 68*, 6848-6856.
[87] Harford, C., and Sarkar, B. (1997) Amino Terminal Cu(II)- and Ni(II)-Binding (ATCUN) Motif of Proteins and Peptides: Metal Binding, DNA Cleavage, and Other Properties, *Acc Chem Res 30*, 123-130.
[88] Rozga, M., and Bal, W. (2010) The Cu(II)/Abeta/human serum albumin model of control mechanism for copper-related amyloid neurotoxicity, *Chem Res Toxicol 23*, 298-308.
[89] Long, E. C. (1999) Ni(II)-Xaa-Xaa-His Metallopeptide - DNA/RNA Interactions, *Acc Chem Res 32*, 827-836.
[90] Jin, Y., and Cowan, J. A. (2005) DNA cleavage by copper-ATCUN complexes. Factors influencing cleavage mechanism and linearization of dsDNA, *J Am Chem Soc 127*, 8408-8415.
[91] Jin, Y., Lewis, M. A., Gokhale, N. H., Long, E. C., and Cowan, J. A. (2007) Influence of stereochemistry and redox potentials on the single- and double-strand DNA cleavage efficiency of Cu(II) and Ni(II) Lys-Gly-His-derived ATCUN metallopeptides, *J Am Chem Soc 129*, 8353-8361.
[92] Neupane, K. P., Aldous, A. R., and Kritzer, J. A. (2013) Macrocyclization of the ATCUN motif controls metal binding and catalysis, *Inorg Chem 52*, 2729-2735.
[93] Cantisani, M., Finamore, E., Mignogna, E., Falanga, A., Nicoletti, G. F., Pedone, C., Morelli, G., Leone, M., Galdiero, M., and Galdiero, S. (2014) Structural insights into and activity analysis of the antimicrobial peptide myxinidin, *Antimicrob Agents Chemother 58*, 5280-5290.
[94] Cantisani, M., Leone, M., Mignogna, E., Kampanaraki, K., Falanga, A., Morelli, G., Galdiero, M., and Galdiero, S. (2013) Structure-activity relations of myxinidin, an antibacterial peptide derived from the epidermal mucus of hagfish, *Antimicrob Agents Chemother 57*, 5665-5673.
[95] Zhao, C., Liaw, L., Lee, I. H., and Lehrer, R. I. (1997) cDNA cloning of Clavanins: antimicrobial peptides of tunicate hemocytes, *FEBS Lett 410*, 490-492.

[96] Liang, R., Senturker, S., Shi, X., Bal, W., Dizdaroglu, M., and Kasprzak, K. S. (1999) Effects of Ni(II) and Cu(II) on DNA interaction with the N-terminal sequence of human protamine P2: enhancement of binding and mediation of oxidative DNA strand scission and base damage, *Carcinogenesis 20*, 893-898.

[97] Harford, C., and Sarkar, B. (1995) Neuromedin C binds Cu(II) and Ni(II) via the ATCUN motif: implications for the CNS and cancer growth, *Biochem Biophys Res Commun 209*, 877-882.

Chapter 2

The ATCUN Motif in Membrane Lipid Oxidation

Copper-mediated Fatty Acyl Chain Peroxidation by Ixosin Promotes Synergistic Interactions with Ixosin B

Adapted entirely from:

Libardo, M.D.J., Gorbatyuk, V.Y., Angeles-Boza, A.M. *ACS Infect Dis,* **2016**, 2, 71-81

and in part from:

Wang, T.Y., **Libardo, M.D.J.**, Angeles-Boza, A.M., Pellois, J.-P. *ACS Chem Biol*, **2017**, 12, 1170-1182

Libardo, M.D.J., Wang, T.Y., Pellois, J.-P., Angeles-Boza, A.M. *Trends in Biotech*, **2017**, *in press*

Introduction

Ticks are the most important arthropod vectors of human diseases, highlighting their ability to control infections when challenged with various pathogens.[98] Unlike vertebrates, ticks lack an adaptive immune system, which indicates that the mechanisms by which microbial loads are maintained at a tolerable level solely depend on phagocytic cells and their humoral response including AMPs.[98-100] Most of what is known about tick immune response comes from experiments oh phagocytes found in their hemocoel. Fortunately, tick AMPs gained attention and many peptides with novel functions have been isolated from various species. Microplusin, a 10 kDa polypeptide expressed in hemocytes of the cattle tick *Rhipicephalus (Boophilus) microplus* was found to sequester Cu(II) from terminal oxidases to short circuit aerobic respiration.[83] In addition, hemoglobin fragments produced by various proteases in the tick midgut have been implicated in ROS production, which may help control bacterial levels.[101, 102]

Although its importance is mostly overlooked, tick saliva contains multiple bioactive molecules that participate in immune modulation and inflammatory responses in the host-vector interface.[103] In fact, during tick feeding – opportunity when bacteria can be transferred between reservoirs – bacteria encounter the tick saliva first following collection and last prior to transmission. A survey of genetic data revealed that of the 14 AMPs expressed by various tick species belonging to the genus *Ixodes*, seven are found in the salivary glands.[100] This information seems to support the hypothesis that the tick saliva plays a major role in sterilizing materials ingested during feeding, preventing infections in the tick body. One can also theorize that ticks strategically express a variety of AMPs in the saliva that can act synergistically to mount an effective immune response.

Ixosin is a 23-amino acid AMP isolated from the salivary glands of the hard tick *Ixodes sinensis* with the following amino acid sequence: GLHKVMREVLGYERNSYKKFFLR.[104] Interestingly, unlike other AMPs isolated from ticks, ixosin does not have a cysteine residue in its primary structure. Moreover, ixosin contains basic and acidic residues in the *i-* and *i+1* positions analogous to α-defensins expressed by higher vertebrates.[105] Ixosin activity was proven against *E. coli*, *S. aureus*, and *C. albicans* with minimum inhibitory concentrations (MICs) in the low micromolar range.[104] We became interested in ixosin because of the presence of the ATCUN motif in its primary structure.

In this chapter, we probe several molecular determinants of ixosin bioactivity (including hydrophobicity and cationic character) with a strong emphasis on the role of the ATCUN motif. Systematic residue substitutions and deletions at the copper binding site and key positions throughout the peptide were done to piece out individual contributions of the aforementioned structural properties. Our results reveal that whereas the ATCUN motif is not essential in the potency of ixosin, it is found to be necessary for its oxidative mechanism of action. This oxidative damage was found to be exploited by another tick salivary gland AMP, Ixosin B,[106] resulting in a synergistic interaction between the two peptides.

Results

Sequence, antimicrobial activity and cytotoxicity of designed peptides

We sought to determine the contribution of the copper-binding sequence in ixosin to the peptide's bioactivity. We systematically varied the sequence by substitutions and

deletions of residues at and around the ATCUN motif and then measured their respective MICs against a panel of microbes. First, we synthesized the wild type (WT) ixosin and its H3A mutant (to abolish copper binding) and found that they had equal potencies (from the geometric mean of MICs, Table 1 and 2). When the ATCUN motif was completely deleted (ixosin$_{4-23}$), the potency decreased two-fold. The minimum (H3A substitution) versus maximum (ATCUN deletion leading to loss of both a positively charged and hydrophobic residue) perturbations in ixosin's primary sequence indicate that the ATCUN motif is not essential to the peptide's potency.

Our studies on truncated ixosin derivatives showed that the C-terminal region (KFFLR) is necessary for its activity (Appendices, Table S2.2) as its deletion (ixosin$_{1-18}$) completely abrogated activity. We then asked whether increasing the hydrophobicity and cationic character of ixosin$_{1-18}$ would restore its activity, therefore we introduced three point mutations (E8K, E13L, and S16V) to generate ixosin-*pch* (*pch* for plus cationic & hydrophobic, Table 1 and 2), a derivative that is an order of magnitude more potent than the WT. This result is consistent with known facts that positive charge and hydrophobicity are important factors in antimicrobial activity.[2, 107] To study the contribution of the ATCUN motif to this highly hydrophobic derivative, we synthesized ixosin-*pch* derivatives harboring ATCUN mutations. We found that ixosin-*pch*-H3A was two-fold less potent while deletion of the ATCUN motif (ixosin-*pch*$_{4-18}$) decreased the potency 5-fold. This suggests that the ATCUN motif is essential for the activity of a highly positively charged and hydrophobic ixosin derivative.

Table 2.1. Sequence and Calculated Helicity of the Designed Peptides.

Peptide name	Sequence	% conformation in TFE		% conformation in 3:1 POPE:DOPG LUVs	
		α-helix	β-sheet	α-helix	β-sheet
ixosin (Cu-Ixosin)	GLHKVMREVLGYERNSYKKFFLR	50 (50)	11 (10)	14 (13)	34 (33)
ixosin H3A	GLAKVMREVLGYERNSYKKFFLR	50	10	16	31
$ixosin_{4-23}$	KVMREVLGYERNSYKKFFLR	32	18	11	40
$Ixosin_{1-18}$ E8K, E13L, S16V / ixosin-*pch*	GLHKVMRKVLGYLRNVYK	62	8	9	44
$Ixosin_{1-18}$ H3A, E8K, E13L, S16V / ixosin-*pch*-H3A	GLAKVMRKVLGYLRNVYK	63	7	14	45
$Ixosin_{4-18}$ E8K, E13L, S16V / ixosin-pch_{4-18}	KVMRKVLGYLRNVYK	50	11	10	42

[a] CD spectra were deconvoluted and percent helix was calculated using the software CDNN. [b] Large unilamellar vesicles were composed of 3:1 mol ratio of POPE:DOPG suspended in 20 mM MOPS buffer, pH 7.4. [c] Percent helix in TFE was obtaines at 50% (v/v) 50 mM sodium phosphate buffer, pH 7.4, and 50% trifluoroethanol.

Table 2.2. Antimicrobial and Cytotoxic Activity of the Peptides under Study.

Peptide name	Minimum Inhibitory Concentration, μM					% cell viability (@ MIC vs *E. coli*)	
	S. aureus	***E. coli* (MG1655)**	***P. aeruginosa***	***C. albicans***	**Geometric Mean[a]**	**HeLa**	**HEK293**
Ixosin WT	64	16 – 32	128	16 – 32	53.8	91 ± 14	107 ± 6
ixosin H3A	64	16	128	64 *	53.8	92 ± 13	101 ± 8
$ixosin_{4-23}$	>128 *	128 *	>128	128 *	128	81 ± 2	100 ± 14
ixosin-*pch*	8 *	1 *	8 *	8 *	4.7	76 ± 8	86 ± 17
ixosin-*pch*-H3A	4 – 8	2 – 4 #	8	16 – 32 #	9.5	72 ± 27	77 ± 15
ixosin-pch_{4-18}	128 #	2	32	32	22.6	81 ± 8	85 ± 3

*, $P < 0.05$ when compared to ixosin; #, $P < 0.05$ when compared to ixosin-*pch*. MICs presented here are the range of MICs obtained from three independent trials. [a] When MIC > 128 μM, the value 128 was used to calculate the geometric mean.

Spectroscopic characterization of conformation and Cu^{2+}-binding site in ixosin

The activity of AMPs is not only dependent on its primary structure but is also tightly linked to its three-dimensional shape.[107] To eliminate the possible conformational effects in the activity of ixosin and its derivatives, we determined their respective secondary structure using Circular Dichroism (CD) Spectroscopy in two different media. First, in the presence of Large Unilamellar Vesicles (LUVs) composed of a 3:1 mole ratio of 1-Palmitoyl-2-oleoyl-phosphatidylethanolamine (POPE) to dioleoylphosphatidylglycerol (DOPG), we observed CD traces resembling a hybrid between helical and β-sheet structures (Figure 2.1A). We used a neural network artificial intelligence program called CDNN[108] to deconvolute and calculate the contributions between different conformations and found that in the presence of a membrane environment, ixosin and its derivatives predominantly adopt either a β-sheet structure or is in an unordered state. On the other hand, in the presence of the membrane mimicking solvent, trifluoroethanol (TFE), all peptides adopt a predominant α-helical structure (Appendices, Figure S2.2). This flexibility in conformations demonstrates the ability of ixosin to respond to changes in its environment possibly encouraging different interactions. Regardless of the environment, we observed minute differences in conformations between the GLH- and GLA-containing peptides (Table 1, 1-3% for ixosin WT vs ixosin H3A and 1-5% for ixosin-*pch* vs ixosin-*pch*-H3A). This suggests that the differences in their potency are likely not a result of the extent to which they adopt their secondary structures. In the contrary, ixosin-*pch* was found to have more ordered structures compared to ixosin WT (Table 1, 5-9%), which could have contributed to their large difference in potencies. Finally, we note that metalation of ixosin WT showed a

negligible change in % conformation relative to free ixosin, suggesting that copper-binding neither promotes nor inhibits secondary structure formation.

When a Cu^{2+} (or Ni^{2+}) ion binds to the ixosin ATCUN motif, the backbone amide nitrogens of Leu-2 and His-3 get deprotonated to accommodate the metal in a distorted square planar geometry,[109] generating a Cu-ixosin complex having a molecular mass of 2931.96 Da. We mixed 1 eq of ixosin WT with 0.8 eq of Cu^{2+} and injected the mixture to an ESI-MS. We observed multiply charged species bearing *m/z* values consistent with a 1:1 Cu:ixosin stoichiometry (Figure 2.1B). The peaks attributed to $[Cu\text{-}Ix+3H]^{3+}$ and $[Cu\text{-}Ix+4H]^{4+}$ showed large similarities to the simulated isotopic distribution pattern (Appendices, Figure S2.3), suggesting that these peaks are not an artifact from the analysis. Furthermore, ixosin H3A did not seem to bind Cu^{2+} based on our MS analysis (Appendices, Figure S2.4), indicating that His-3 is required for metal binding.

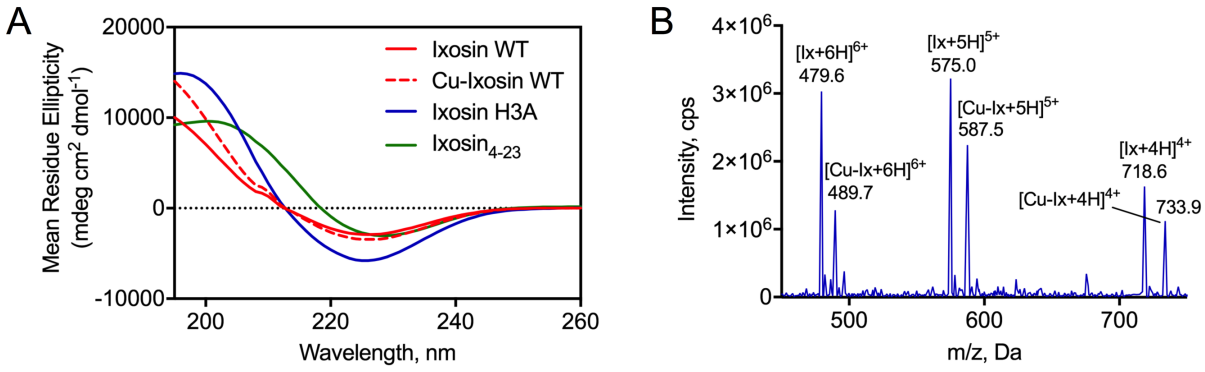

Figure 2.1. Spectroscopic Characterization of Conformation and Copper-binding. (A) Circular dichroism (CD) spectra obtained in the presence of 3:1 POPE:DOPG LUVs at a peptide:lipid ratio of 1:30. (B) ESI-MS spectra of Cu-ixosin WT complex showing 1:1 stoichiometry of binding.

We then mapped the actual copper-binding site via Heteronuclear Single Quantum Correlation (HSQC) approach. Upon gradual addition of Cu^{2+}, we observed signal intensity degradation for a set of protons, while the rest of the HSQC spectra remained unperturbed. This indicates that, except for the metal coordination site, there are no conformational changes in the peptide backbone upon Cu^{2+} complexation. We observed the loss of ^{1}H-^{15}N correlation starting at ratio Cu:ixosin WT of 1:5 for Leu-2 and at 1:2 for His-3 amide protons (Figure 2.2A). This is consistent with the deprotonation of these backbone amides upon copper binding. In addition, we monitored the ^{1}H-^{13}C correlations and found that at the lowest studied metal concentration (1:5 Cu:ixosin), the HSQC signals of the imidazole protons ε1-H (~8.55 ppm) and δ2-H (~7.25 ppm) of His-3 become undetectable while signals from other aromatic residues are unchanged (Figure 2.2B). Furthermore, the ^{1}H-^{13}C correlations of the α-H of Gly-1 also disappear starting at a 1:2 ratio (inset in Figure 2.2B). Due to the paramagnetic nature of Cu^{2+}, any proton in its vicinity will experience a shortened transverse relaxation time leading to a significant broadening of its NMR signal.[110] While deprotonation of imidazole residue of His-3 and α-CH2 of Gly-1 is not expected upon copper complexation, we believe that the bound Cu^{2+} broadened the HSQC resonances of these protons beyond recognition. At higher metal concentrations (up to 1:1 ratio), the α-H of Gly-1 and amide proton of Lys-4 broadens beyond detection as well. Taken together with our MS data, we definitively show that ixosin WT indeed binds to Cu^{2+} through its ATCUN motif, and that any other potential ligands within the peptide chain do not have a high-enough affinity to compete with the N-terminal sequence. Since the motif is conserved between ixosin WT and ixosin-*pch*, we expect the two peptides to have similar Cu^{2+}-binding behavior.

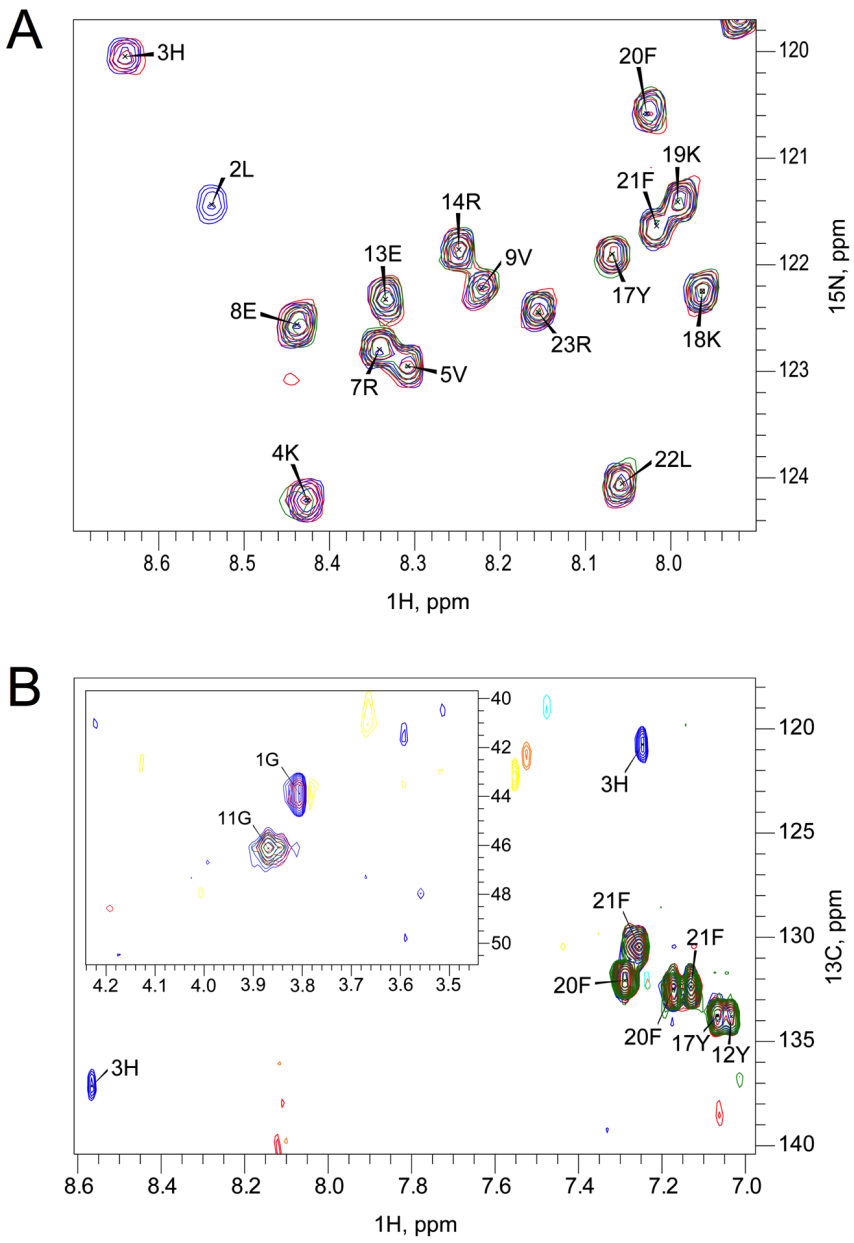

Figure 2.2. Mapping the Cu^{2+}-binding site in Ixosin. (A) ^{1}H-^{15}N HSQC and (B) ^{1}H-^{13}C HSQC spectra of free ixosin WT (blue), 1:5 ratio of Cu^{2+}:ixosin WT (red), and 1:2 Cu^{2+}:ixosin WT ratio (green) recorded in 93% 20 mM acetate buffer pH 4.4, and 7% D_2O. NMR spectra indicate that ixosin WT binds to Cu^{2+} via its ATCUN motif.

Ixosin is a bactericidal peptide localizing in the membrane

The initial interaction between AMPs and bacteria occur in the membrane.[111] While some AMPs have been found to cross the membrane and perturb various intracellular processes,[3, 112] most AMPs are membrane active.[6] To determine the bacterial localization of ixosin and its derivatives, we employed laser confocal microscopy. The 5(6)-carboxyfluorescein-labeled peptides were synthesized on-resin by coupling the dye to the ε-amino group of Lys-18, this was done to preserve copper binding (whenever possible) in the N-terminal as a free –NH2 group is required.[109] Thirty minutes post-exposure to the peptides at their MIC, we observed fluorescent hollow ellipsoids indicative of membrane localization for ixosin WT, ixosin-*pch* and their respective H3A derivatives (Figure 2.3). Furthermore, green fluorescence was not found to co-localize with blue fluorescence from Hoescht 33342, a DNA tracer (Appendices, Figure S2.5). A closer examination of the ixosin H3A panel shows some cells stained homogenously while others appear as hollow ellipsoids (indicated by the white arrow). This observation is consistent with the model of self-induced peptide uptake where AMPs (and other cell-penetrating peptides) generate transient pores which they use to cross the membrane and equilibrate its concentration.[111, 113] We also observed this for ixosin WT when incubated for 1 hr as a more intracellular staining was observed (inset in Figure 2.3). Our microscopy studies revealed that the structural changes we applied to ixosin did not significantly alter its localization during the time scale of our experiments.

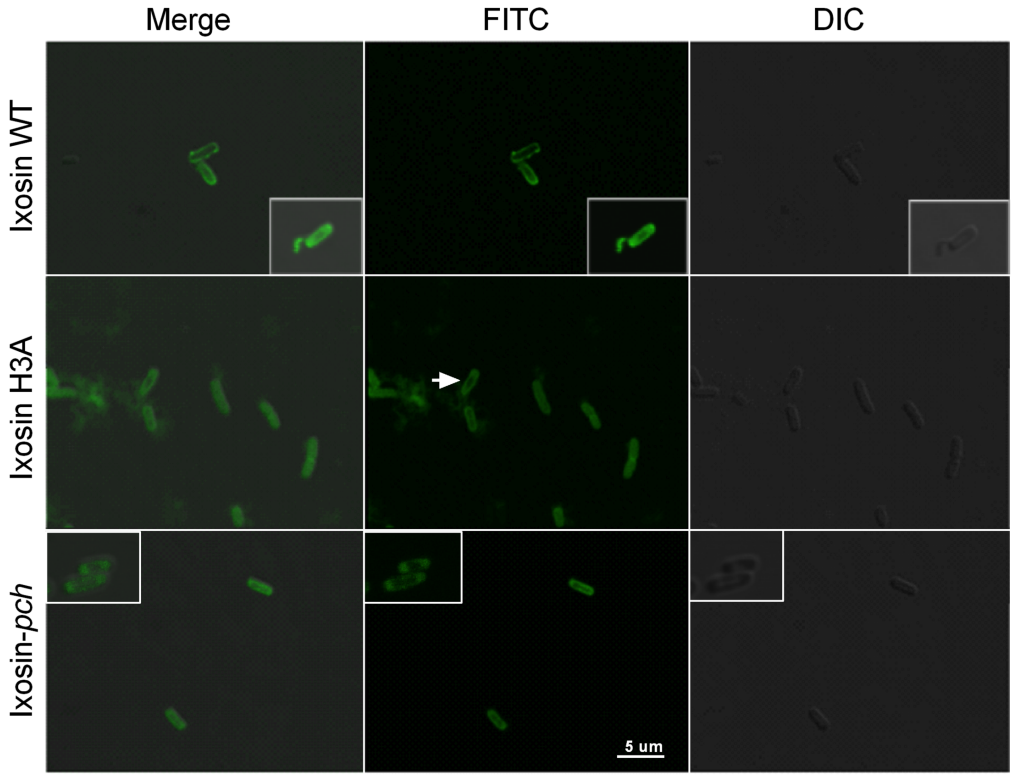

Figure 2.3. Cellular Localization of Ixosin. Bacterial localization of ixosin WT (inset: ixosin WT for 1 h), ixosin H3A, and ixosin-*pch* (inset: ixosin-*pch*-H3A) revealed via laser confocal microscopy. Fluorescence micrographs show extensive membrane staining by all ixosin derivatives during a 30 min incbubation period.

An increasing number of evidence suggests that initial membrane binding and destabilization of AMPs at their MICs is not the determining factor for cell death.[114-116] To investigate this, we looked at the killing kinetics of ixosin and its derivatives (Figure 2.4). We found that at the MIC, ixosin WT is bactericidal (decreasing bacterial content by two orders of magnitude at the first 4 hrs) with cell death commencing 1 hr post-exposure. On the other hand, ixosin H3A exhibited a weak bacteriostatic effect at its MIC. Taken together with our microscopy results, we believe that initial membrane localization (observed at 30 mins) contributes negligibly to cell death as bacterial population was

relatively constant for the first hour of incubation. In the case of ixosin-*pch*, we observed a decrease in viable bacteria followed by a steady growth beginning at 2 hrs. This trend was a lot less pronounced for ixosin-*pch*-H3A where there were little fluctuations in viability over 8 hrs. Derivatives of ixosin WT and ixosin-*pch* containing D-amino acids were also found to be bactericidal (Appendices, Figure S2.6). Our time-kill kinetics results suggest that the ATCUN-containing peptides are bactericidal at their MIC while their corresponding H3A mutants are bacteriostatic. This dramatic change in mechanism arising from a single amino acid substitution suggests the possibility that ATCUN-containing ixosin derivatives, apart from membrane binding and destabilization, may utilize an independent pathway which may be more destructive to the cell.

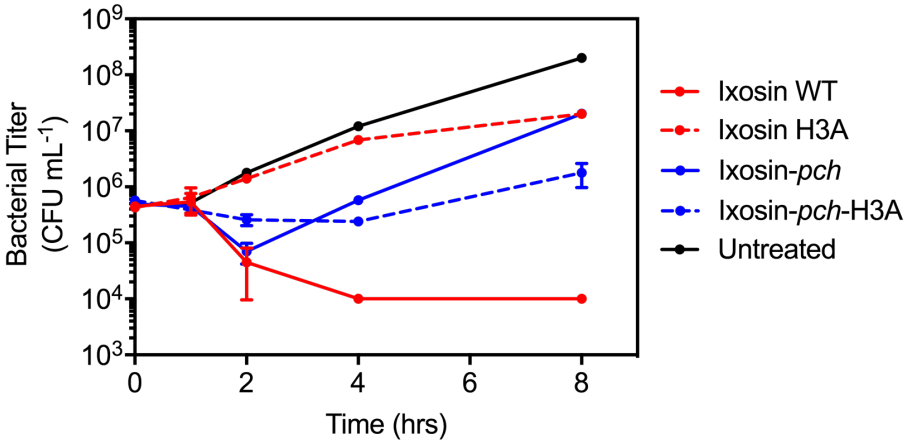

Figure 2.4. Time-Kill Curves of Ixosin-treated *E. coli*. Killing kinetics of ixosin and its derivatives showing that ATCUN-containing peptides are bactericidal, whereas the corresponding H3A mutants are bacteriostatic.

Activity of ATCUN-containing derivatives are dependent on Cu^{2+} and O_2 levels

Our time-kill kinetics studies suggested the involvement of the ATCUN motif in the bactericidal action of ixosin. The Cu-ATCUN complex has repeatedly been shown to form

reactive oxygen species in combination with biologically relevant reducing agents.[90, 91, 117] Given that the ROS production by the ATCUN motif requires the presence of both Cu^{2+} and O_2 (Equations 1-3, L = ATCUN),[90] we next asked whether their concentration affects the activity of ixosin and its derivatives.

$$2L\text{-}Cu^{II} + O_2 + 2e^- \rightarrow L\text{-}Cu^{II}\text{-}O\text{-}O\text{-}Cu^{II}\text{-}L \quad (1)$$

$$L\text{-}Cu^{II}\text{-}O\text{-}O\text{-}Cu^{II}\text{-}L \rightarrow 2L\text{-}Cu^{II} + HO2^- \quad (2)$$

$$2L\text{-}Cu^{II} + HO2^- + H^+ + e^- \rightarrow 2L\text{-}Cu^{II}\text{-}OH + OH^- \quad (3)$$

We studied the activity of ixosin and its derivatives with and without copper chelators (Figure 2.5A), and under normal- and low-oxygen levels (Figure 2.5B). We resuspended *E. coli* in a medium that maintains the viability of cells while inhibiting their growth (HEPES minimal medium),[118] this allowed us to have a baseline bacterial count per trial. After which, we exposed the cells to peptides at their MIC, incubated for two hours and then plated in LB agar for colony enumeration. We reasoned that a decrease in copper or oxygen levels will lead to fewer ROS formed and hence will result in lower potency. We observed a marked increase in the number of colonies when the copper chelators triethylenetetramine (TETA) or penicillamine ($PenNH_2$) was added and when oxygen was depleted (Appendices, Figure S2.7). This indicates that individual depletion of copper or oxygen rescued the growth of bacteria when exposed to ATCUN-containing peptides, that is, the ATCUN-containing peptides were more active in the presence of copper and oxygen (Figure 2.5). This however was not the case for the H3A mutants and the derivatives lacking the ATCUN motif completely. For those peptides, no statistically significant difference was observed upon Cu^{2+} or O_2 depletion. This data showed that

there is indeed an involvement of ROS in the activity of the ATCUN-containing ixosin derivatives, and that ROS formation may even be critical to its bactericidal property.

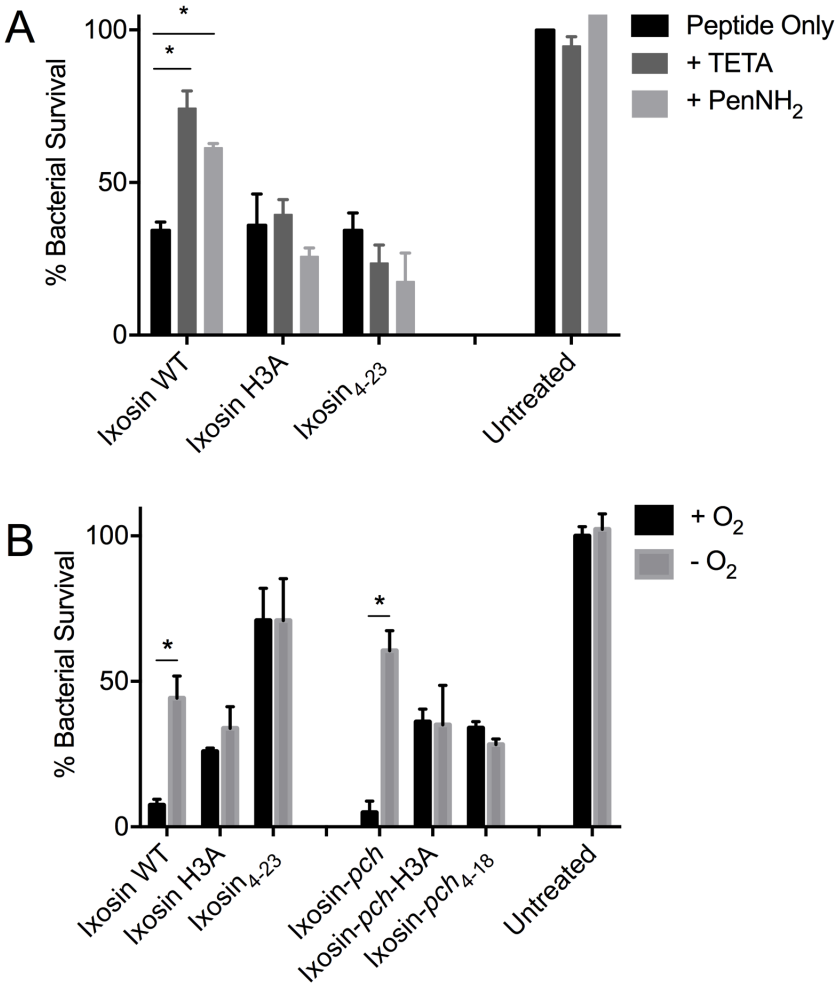

Figure 2.5. Oxidative Activity of Ixosin is due to the Presence of the ATCUN Motif. (A) Bacterial survival was determined in the presence of copper chelators, triethylenetetramine (TETA) and penicillamine ($PenNH_2$). Data highlight the importance of Cu^{2+} to the activity of ixosin WT. *, $P<0.05$. (B) Activity of ixosin and derivatives under normoxic ($+O_2$) and hypoxic ($-O_2$) conditions shows that O_2 plays a role in the activity of ATCUN-containing peptides suggesting a possible involvement of ROS. *, $P<0.01$.

A closer examination of Figure 2.5A shows that copper chelation with 200 μM TETA did not restore ~100% bacterial survival. While this may be a function of competition for copper between ixosin and the copper chelator, the added TETA was in a large excess relative to the copper content of the medium (previously measured as 5 ppm, ~78 μM)[119] and to the concentration of ixosin WT (32 μM). It can therefore be assumed that, at these conditions, most (if not all) Ixosin exists in the non-metallated form. The fact that free ixosin WT was still able to kill ~25% of the cells (Figure 2.5A) suggests a pathway leading to cell death that does not involve Cu^{2+} binding. Our MIC results coupled with our mutational analysis showed relevance of hydrophobicity and cationic charge to the activity of ixosin (Table 2). Incidentally, these physico-chemical properties also dictate the extent of membrane activity. Hence, as one would expect from any prototypical AMP, ixosin may also possess membrane disruption capability – a copper-independent mechanism – which may lead to cell death.

ATCUN-containing ixosin derivatives peroxidize lipids in E. coli

Since ixosin is found to localize at the membrane and that ROS is implicated in its activity, we investigated whether ixosin can oxidize the lipids in the membrane of *E. coli*. We hypothesized that the ROS formed is localized in the membrane environment and hence will target unsaturations found in the bilayer. We employed a standard assay to measure the extent of lipid peroxidation brought about by our peptides at three different time points. The peroxidation products (thiobarbituric acid reactive substances, TBARS) were then quantified using analytical HPLC (Appendices, Figure S2.8). Our data show that there is an immediate increase in peroxidized lipid following exposure to ixosin WT. This peroxidation increased sharply through the first hour of incubation. On the other

hand, a lag phase was observed for ixosin H3A and ixosin$_{4-23}$ which then modestly increased after 30 mins. After 60 mins, lipid peroxidation by ixosin WT was three-fold greater (P<0.001) than its ATCUN-free derivatives. This coincides with the onset of bacterial killing we observed from our time-kill kinetics studies (Figure 2.6). Taken together, our results suggest that oxidatively damaging the membrane may be a significant step in the bactericidal activity of ixosin. Moreover, addition of the copper chelator, TETA, lead to ~35% reduction in lipid peroxidation (at 60 mins post-exposure), suggesting that peroxidation is indeed Cu^{2+}-dependent.

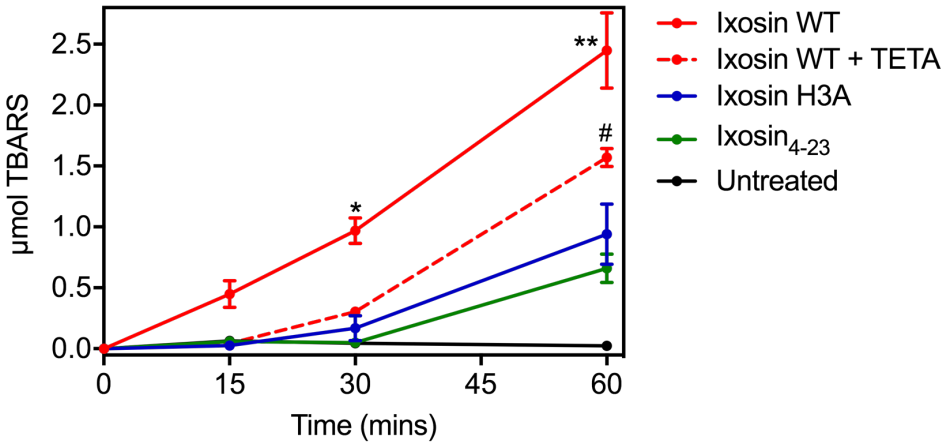

Figure 2.6. Lipid Peroxidation Activity of Ixosin. The extent of lipid peroxidation promoted by ixosin measured over the first hour of incubation and calculated as micromoles of thiobarbituric acid reactive substances (TBARS). A significant increase in peroxidized lipids by ixosin WT was observed, indicating a major role in its activity. * and #, P<0.005; **, P<0.001.

The MIC of the ATCUN-containing peptides were measured after pre-incubation with Cu^{2+} and found to be similar to those of the naïve peptide. Furthermore, an attempt to boost bacterial copper content was made by growing *E. coli* in media containing 50 µM

Cu^{2+} (a concentration far below its MIC which was determined to be 1 mM). The MIC against the "copper-loaded" bacteria was also unchanged. In contrast, the tick AMP, microplusin, was rendered inactive by exogenous Cu^{2+} in the media.[83] Silva, et. al. hypothesized based on their O_2 consumption experiments in the presence of cyanide and the energy uncoupler carbonyl cyanide m-chlorophenylhydrazone (CCCP), that microplusin might be sequestering Cu^{2+} from one or more of the heme-copper terminal oxidases (member of the electron transport chain which act to reduce O_2 to H_2O).[83] We hypothesize a distinct mechanism of action for ixosin – one that does not involve sequestration of essential copper for the following reasons: (1) there exists a pool of labile copper ions in *E. coli* (and other bacteria), most of which are found in the periplasm bound to methionine, cysteine, or glutathione.[62, 120, 121] This labile pool of copper ions is most likely in the +2 state (preferentially bound by the ATCUN motif) due to the presence of multicopper copper oxidases which act to detoxify Cu(I) by oxidizing it to Cu(II).[51] Therefore, pre-loading ixosin with Cu^{2+} contributes negligibly since there is plenty of labile copper that ixosin can theoretically scavenge. (2) Our normoxic and hypoxic experiment (Figure 2.5B) showed increased survival of ixosin-treated cells when O_2 was depleted. If ixosin bound copper belonging to a respiratory metalloprotein (or any copper-binding protein), a decrease in oxygen is expected to force the ixosin-treated cells into a metabolically impaired state (untreated cells would be in a metabolically dormant state), perhaps even pushing the cells to extreme starvation which should lead to cell death. Hence, it is clear that even though microplusin and ixosin both seem to utilize Cu^{2+} in their activity, the manner at which they do so is very different. Finally, we found that ixosin generated high levels of peroxidized lipids (Figure 2.6), a phenotype expected only if the

peptide is metallated. In theory, if ixosin WT did not bind copper, the amount of TBARS between ixosin WT and ixosin H3A would have been comparable. Overall, our results thus far indicate the likely possibility that ixosin is metallated *in cella* and that this metalation is causing peroxidation of lipids in the membrane.

The ATCUN motif in ixosin promotes synergy with ixosin B

Multiple secreted salivary gland peptide orthologs have been identified in hard ticks.[100] Because of the crucial role played by tick saliva in modulating the immune response at the host-tick interface, expression of an arsenal of salivary gland AMPs suggests possible synergistic interactions between these molecules.[5, 122] Like ixosin, ixosin B (QLKVDLWGTRSGIQPEQHSSGKSDVRRWRSRY) is an AMP isolated from the salivary glands of *Ixodes sinensis*.[106] We examined possible synergy between ixosin and ixosin B through the context of lipid oxidation. Using a 1:1 mixture of ixosin and ixosin B, we measured the fractional inhibitory concentration (FIC) index, which is assessed as: FIC = [AMP1]/MIC_{AMP1} + [AMP2]/MIC_{AMP2}, where MIC_{AMP1} and MIC_{AMP2} are the MICs of AMPs 1 and 2 alone and [AMP1] and [AMP2] are the MICs of the AMPs in combination. An FIC index < 0.5 indicates good synergy (representing a ≥ 4-fold increase in activity), whereas an FIC index of 0.5 to 1.0 represents additive activity. When tested against *E. coli* PDJ1, a parental strain, we found that all 1:1 peptide mixtures used exhibited additive activity (Table 3). To confirm importance of lipid oxidation in the synergistic effect, we measured FIC indices in *E. coli* MWF1 (an isogenic mutant derived from PDJ1), a strain containing elevated levels of unsaturated fatty acids in its membrane.[65] Not surprisingly, we observed a synergistic interaction between ixosin and ixosin B while the additive activity of ixosin H3A and ixosin B was preserved. Furthermore, when ixosin and ixosin

H3A was mixed, a synergistic interaction was also observed albeit to a lesser extent. These results indicate that the ATCUN motif is imperative in eliciting a synergistic interaction between ixosin and ixosin B. Moreover, the differences observed from the two *E. coli* strains indicate that membrane lipid unsaturations – a substrate for peroxidation – is a requirement for synergy.

Table 2.3. Interactions between Ixosin Derivatives and Ixosin B Expressed as the FIC[a].

Peptide Combination	FIC Index (effect)	
	***E. coli* PDJ1**	***E. coli* MWF1**
ixosin WT + ixosin B	0.562 (Additive)	0.281 (Synergistic)
ixosin H3A + ixosin B	0.625 (Additive)	0.625 (Additive)
$ixosin_{4-23}$ + ixosin B	1.000 (Additive)	1.000 (Additive)
ixosin WT + ixosin H3A	0.750 (Additive)	0.375 (Synergistic)

[a] Fractional Inhibitory Concentration (FIC). Because regulation and relative expression of ixosin and ixosin B are currently unknown, we measured FIC indices using a 1:1 mixture of both peptides.

Ixosin B interacts differently with membranes containing oxidized phospholipids

It has been previously suggested that oxidized phospholipids in the lipid bilayer can be a potential target of AMPs.[123, 124] The amine groups from the AMP may act as nucleophiles toward the electrophilic carbonyl groups in oxidized lipids to generate Schiff bases.[125] To test whether this is a potential avenue of synergy between ixosin and ixosin B, we studied the interaction of ixosin B with model membranes by following quenching

of tryptophan fluorescence as a consequence of acrylamide titration. We used 3:1 POPE:DOPG LUVs and pre-oxidized them using the copper complex of ixosin for 36 hrs. Since we were working with a purified system, we added ascorbic acid to promote ROS formation.[91] We confirmed that our oxidation did not alter the diameter and size distribution of the LUVs by dynamic light scattering (Appendices, Figure S2.9). To determine the membrane interaction of ixosin B, we generated a Stern-Volmer plot from which we calculated K_{SV} (Stern-Volmer quenching constant), a direct measure of Trp accessibility from the aqueous environment.[123] Compared to free ixosin B, our data showed a decrease in quenching constant when native LUVs are added, furthermore, a statistically significant decrease was observed when oxidized LUVs are used. There is therefore a greater membrane interaction by ixosin B when the lipids in the membrane are oxidized. These results are consistent with the results obtained by Matilla et. al. utilizing oxidized phospholipids to generate LUVs instead of oxidizing the LUVs. We note, however, that while Matilla et. al. observed ~90% decrease in KSV, we only saw a ~30% difference in our experiments.[123] This can be attributed to several factors, including LUV composition, amount of oxidized lipids in LUVs, and more likely, the fact that ixosin B has two Trp residues close to both the N- (W7) and C-terminal (W28). While the relative orientation and affinity of ixosin B within the membrane is unknown, there is a slim probability that both tryptophans are projected away from the aqueous phase. This leads us to speculate on a conformation where only one is protected from acrylamide while the other is kept accessible. However, we can say with certainty that ixosin B has a stronger membrane interaction in the presence of oxidized phospholipids.

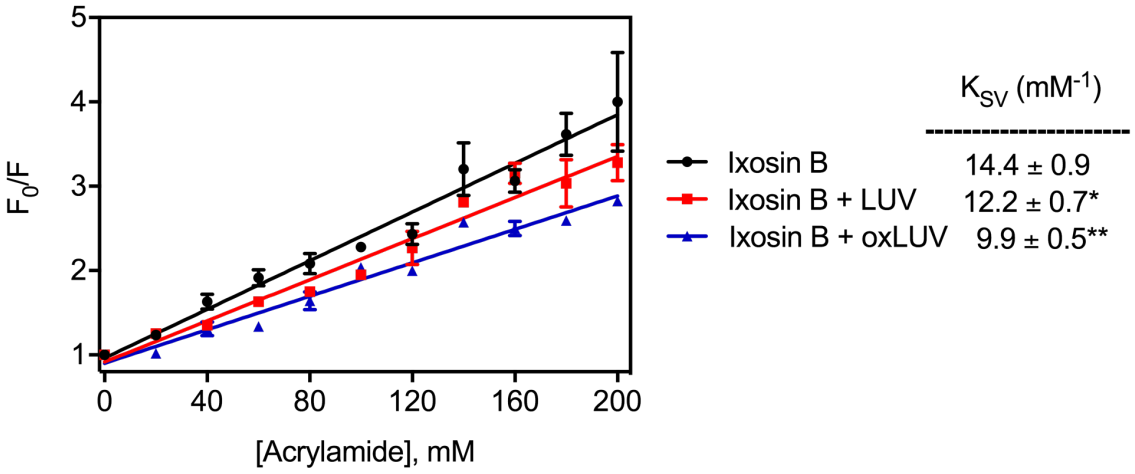

Figure 2.7. Measurement of Ixosin B Affinity Toward Oxidized Membranes. The decrease in tryptophan fluorescence resulting from titration of the water-soluble collisional quencher, acrylamide is a direct readout of the degree of accessibility of Trp residues in the peptide. F and F_0 are fluorescence intensity with and without quencher. K_{SV} is a direct measure of solvent accessibility of Trp residue and a reporter of membrane interaction. *, *P*<0.01 compared to free ixosin B; **, *P*<0.01 compared to ixosin B + LUV.

The ATCUN motif in ixosin causes ixosin B to delocalize into the bacterial membrane

To identify a cellular basis of the synergy between ixosin and ixosin B, we looked at their interaction in live *E. coli*. We labeled ixosin B with 5(6)-carboxytetramethylrhodamine at its N-terminal and observed its co-localization with ixosin WT and ixosin H3A. We found that ixosin B alone stains the cells homogenously indicative of diffusion throughout the entire cell (Figure 2.8A). From the plot of fluorescence intensities (Figure 2.8B), one can see a clear co-localization of ixosin B with DNA stained by Hoescht 33342. When E. coli was co-treated with ixosin and ixosin B (at their FIC for 30 mins), a strong co-localization between the green and red fluorescence is observed which manifested as yellow hollow ellipsoids (Figure 2.8C). Furthermore, intracellular

staining by ixosin B seems to have decreased, as did its co-localization with DNA. This shows that in the presence of ixosin, the affinity of ixosin B to the bacterial membrane is increased. On the other hand, the intracellular localization of ixosin B was not affected by co-treatment with ixosin H3A because ixosin B again co-localized with DNA (Figure 2.8E). Taken together, our results demonstrate that the presence of the ATCUN motif in ixosin causes ixosin B to delocalize to the bacterial membrane, a phenomenon that (to the best of our knowledge) has not been reported to date.

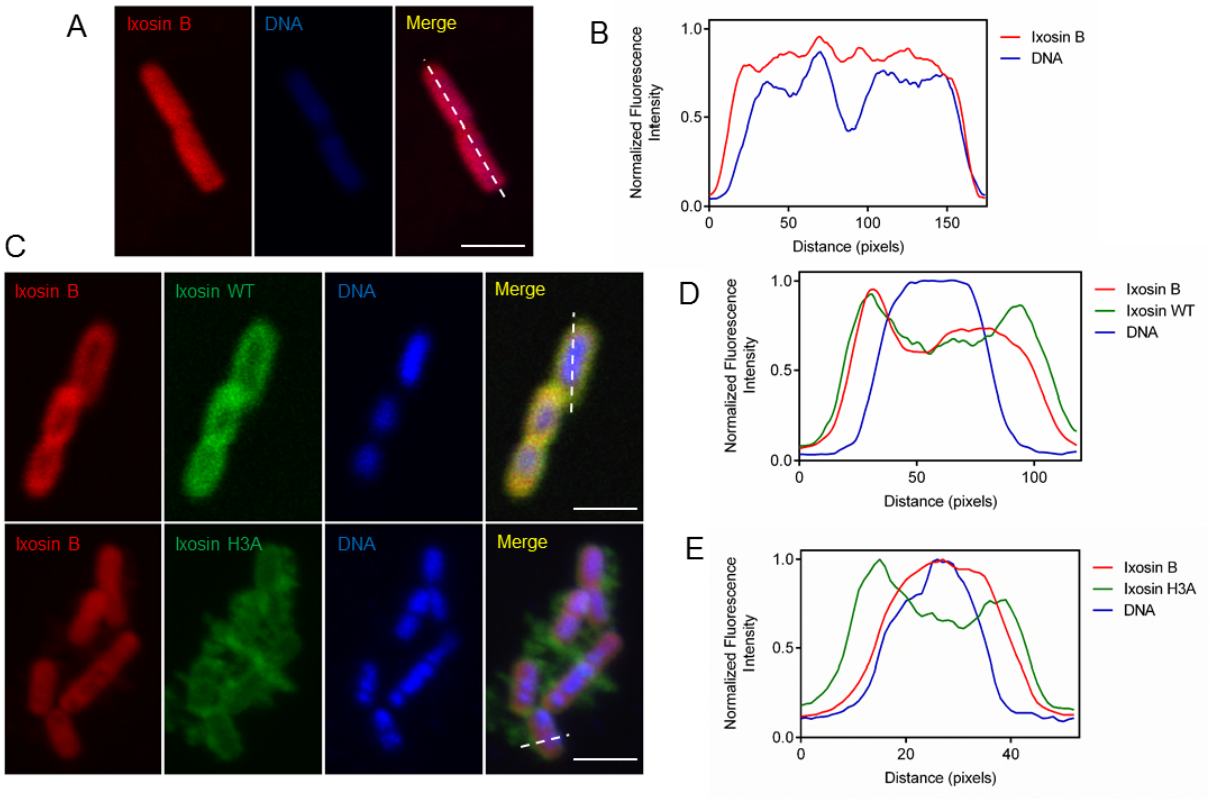

Figure 2.8. Cellular evidence for Ixosin and Ixosin B Synergy. (A) Localization of TAMRA-ixosin B and (B) fluorescence intensity curves showing ixosin B co-localizing with bacterial nucleoid. (C) Co-localization studies of *E. coli* MWF1 cotreated with ixosin (WT and H3A) and ixosin B; (D) Increased localization of ixosin B to the bacterial periphery as a result of co-treatment with ixosin WT. (E) Restoration of native ixosin B localization via co-treatment with ixosin H3A.

The proposed mechanism of action of ixosin highlights the central role of the ATCUN motif

Pooling our data together, we propose a plausible mechanism of action of ixosin, the details of which are illustrated in Figure 2.9. Ixosin expression is induced when the tick is challenged with bacteria. Ixosin then binds copper either endogenously located in the target bacteria or from the host. Human serum albumin (also containing an ATCUN motif, Asp-Ala-His) has been proposed to function as a copper transporter with a picomolar affinity.[126] Since isolated ATCUN motifs and shorter peptides containing this sequence have been reported to bind copper with affinities in the same range (or even higher), ixosin can also compete and sequester Cu^{2+} from albumins. Once bound to copper, the complex resides in the bacterial membrane. Non-metalated ixosin residing in the membrane can sequester labile copper from the bacteria itself. Once bound to the membrane, ixosin may induce local perturbations leading to membrane disruption. With the aid of dioxygen, Cu-ixosin forms ROS, which then diffuse to and react with nearby unsaturations in the bilayer causing lipid (per)oxidation. The (per)oxidized lipids then become a target to other AMPs (including ixosin B) leading to a synergistic effect. Work is currently being done to elucidate the exact molecular details of the oxidized lipid targeting by ixosin B. We hypothesize however that if Schiff bases are indeed formed,[123] this leads to ixosin B being covalently anchored to the membrane as opposed to binding via dispersion and ionic forces. What this implies is that ixosin B (and other AMPs) has the potential to generate “non-transient” pores due to their increased residence time in the membrane. While this may not lead to cell death directly, it gives other antimicrobial effectors a continued access to the bacteria, a scenario where bacterial recovery is virtually impossible. It should also be noted that the ROS formation by Cu-ATCUN

complexes are highly catalytic.[117] This means that even a small amount of copper-bound ixosin has the potential to elicit the same biological effect.

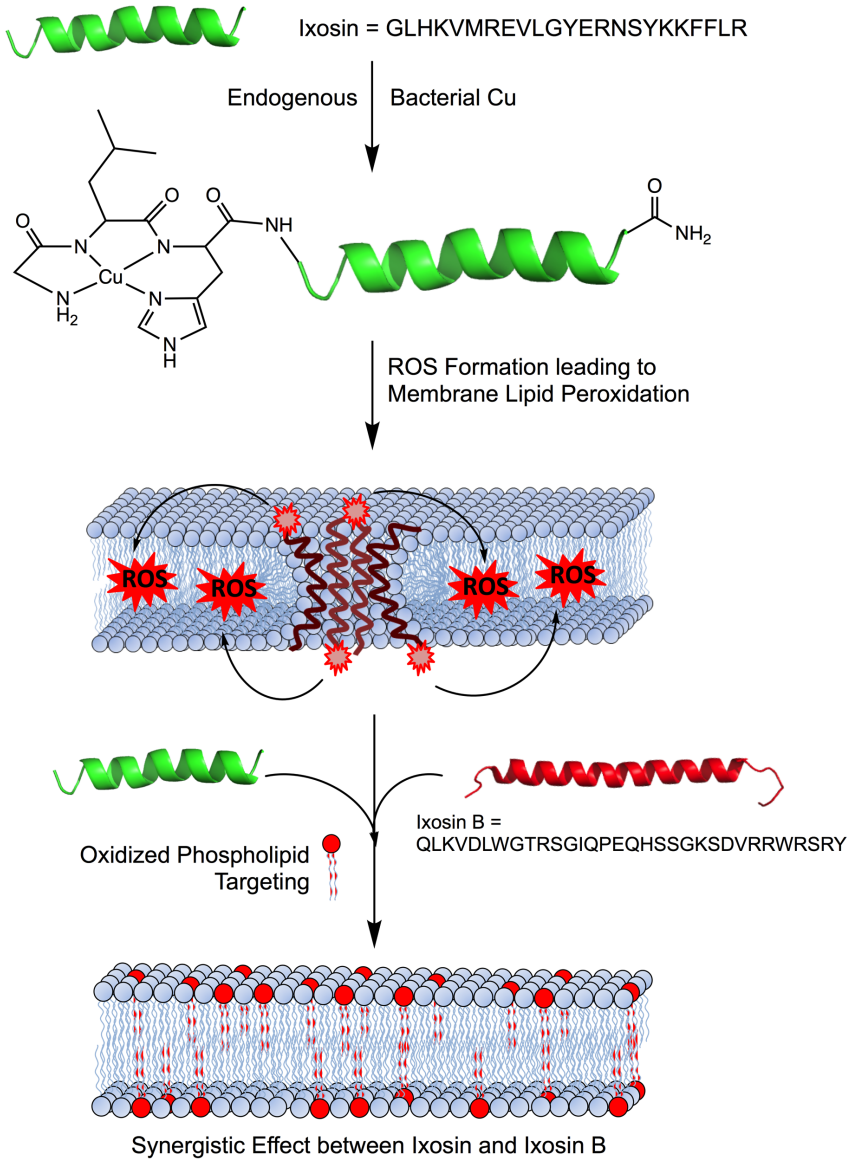

Figure 2.9. Proposed Mechanism of Action of Ixosin and its Synergy with Ixosin B. Both peptides are depicted as helical, and ixosin is shown to form toroidal pores in the membrane are for illustration purposes only. Oxidized phospholipid targeting would not be possible without copper-mediated lipid oxidation.

Discussion

AMPs represent a large class of molecules that multicellular organisms use for defense against pathogens. Considered as one of nature's oldest antibiotics, AMPs rely on their overall positive charge, and conformational plasticity to recognize multiple targets and have broad-spectrum activities. Many modes of action have been proposed and proven for a lot of AMPs, most of which converge on the idea that AMPs bind electrostatically to the anionic bacterial membrane, induce local perturbations and generate pores. In addition, AMPs have been found to translocate across the membrane and inhibit intracellular processes including protein, and DNA synthesis. This seemingly diverse mechanism of action can be intuitively attributed to the AMP's inherent flexibility allowing it to recognize a wide variety of targets. Regardless of the mechanism, three distinct physical properties seem to dictate a peptide's biological activity; amphipathicity, hydrophobicity, and cationic charge. Herein, we study the molecular determinants to ixosin's bioactivity and find that it is indeed, in part dictated by its hydrophobicity and positive charge. Although largely unexplored in this study, ixosin, much like any canonical AMP (due to its membrane affinity) may also generate membrane pores. We focused on the contribution of the copper-binding motif (Gly1-Leu2-His3) to the biological activity of ixosin. Our findings reveal that the ATCUN motif GLH, confers bactericidal properties to ixosin at its MIC. The affinity of ixosin for the bacterial membrane allows the ATCUN motif in ixosin to produce oxidative damage to the membrane lipid unsaturation in a copper- and oxygen-dependent manner. Once the lipids are peroxidized, it paves the way for other AMPs to act synergistically via an unknown mechanism. Taken altogether, our results indicate that there are at least two modes of action by ixosin – membrane

binding/disruption (from the hydrophobic and positively charged portion) and membrane oxidation (from the ATCUN domain). We believe the two domains likely act in a cooperative fashion (as highlighted by the synergy between ixosin WT and ixosin H3A) and that the ATCUN motif requires the rest of the peptide to generate its full oxidative effect. From a molecular standpoint, this may represent economic efficiency and an evolutionary advantage because the tick expressing ixosin gets multiple modes of action from one single molecule allowing it to combat a deluge of microorganisms. We present an undocumented case of an AMP acting in concert with Cu2+ to generate oxidative effects as part of its mechanism of action and as a key element for its synergy with ixosin B – another AMP expressed in the same tick gland. Surely AMPs and other antimicrobial effectors – no matter how seemingly unrelated they are – exhibit a dynamic interplay to generate a quick, amplified, and effective immune response. This paradigm is becoming more apparent in recent literature.

The fact that ATCUN-containing AMPs have been isolated from very diverse forms of life, may represent a generalized defense mechanism from unrelated organisms. Of special relevance to this is that metchnikowin, an ATCUN-containing AMP from Drosophila has been shown to be induced constitutively in response to any microbial challenge (Gram +/- and Fungi), while other AMPs (e.g. Diptericin, Cecropin A, and Drosocin) have been induced only selectively.[127] It is tantalizing to assume that the ATCUN-containing AMPs may be a point of convergence for most AMPs since their capability to form ROS may sensitize microbes to attack by other AMPs. In particular, *Borrelia burgdorferi*, the causative agent of Lyme disease transmitted by ticks, possess membranes enriched with polyunsaturated fatty acids that are particularly sensitive to

attack by ROS.[128] Our study also reveals another avenue to which tick AMPs utilize copper in their activity (much like microplusin) at the same time, unifying it with ROS production (like hemoglobin fragments).

While we are unsure of the molecular details of their synergy, our results may have important ramifications in the understanding of the tick innate immune response, more specifically a possible reason for its vector competence. Indeed, a comparison of three tick species based on their expression of ixosin and their relative ability to transmit *B. burgdorferi*, an inverse relationship seems to arise. That is, ticks that express ixosin do not act as vectors for the spirochete but species that lack ixosin in their saliva are able to transmit the bacteria. Furthermore, evidence for a borreliacidal activity of *A. americanum* and non-borreliacidal activity of *I. ricinus* have been reported.[129] We therefore posit that expression of ixosin in the tick salivary glands causes membrane lipid peroxidation in *B. burgdorferi*, attenuating the spirochete prior to assimilation or transmission – perhaps to levels that would cause bacterial death. Work is underway to test this hypothesis.

Methodology

Peptide Synthesis, Purification, and Quantification. Peptides in their C-terminal amidated forms were synthesized manually on a Rink Amide resin (ChemPep Inc, Wellington, FL) using standard Fmoc-protected L-amino acids (Matrix Innovation, Quebec, Canada). Coupling reactions were done with 4 eq of amino acids and 4 eq of HBTU, deprotection using 20% piperidine in DMF and cleavage using 95:2.5:2.5 TFA/H_2O/TIS. Free peptides were purified via RP-HPLC (Schimadzu LC-20AD) on a C18 semi-prep 250x10mm column (Grace Davison, Deerfield, IL) using 0.1% TFA in H2O

(Buffer A) and 0.1% TFA in ACN (Buffer B). Peptides were purified (up to >95% purity as confirmed by analytical RP-HPLC) using a linear gradient of 30-60% Buffer B over 30 mins. 5(6)-Carboxyfluorescein (Sigma Aldrich) labeled peptides were synthesized on-resin by attaching the fluorophore to the peptide N-terminal. Pure fractions were collected and the identities confirmed by ESI-MS ran on a positive ionization mode. All peptides were quantified using a method suggested by Gruppen. Briefly, lyophilized pure peptides were dissolved in nanopure water and a small aliquot was diluted in 80:20:0.1 H_2O/ACN/Formic Acid and absorbance of this solution was read using a Varian Cary 50Scan UV-Vis Spectrometer at 214 nm. Molar extinction coefficient of each peptide was calculated on a sequence-specific manner based on the reported values for each amino acid and the peptide bond.

Antimicrobial Assay. Antimicrobial susceptibility testing were done using the broth microdilution method as suggested by Hancock.[130] Gram positive *Staphylococcus aureus* (ATCC 25923); Gram negatives *Escherichia coli* (DL7), and *Pseudomonas aeruginosa* (PAO1) were grown in Mueller-Hinton Broth (MHB, Difco) until mid-log phase for 3-5 hrs. The fungus *Candida albicans* were grown in Yeast Mold Broth. Peptide stock solutions were diluted in PBS (Gibco) pH 7.40, 50 µL two-fold serial dilutions (starting from 32 µM) were placed on a sterile 96-well poplypropylene plate (Greiner). To each well, 50 µL of a bacterial suspension was added resulting to a final inoculum of $5x10^5$ CFU/mL per well. Ampicillin (Sigma Aldrich) was used as positive control and PBS as negative control. Plates were incubated at 37°C for 18-20 hrs. Minimum Inhibitory Concentration (MIC) was defined as the concentration that prevented visual growth of bacteria. MICs reported here are the mode of three independent trials. To test synergy between ixosin and ixosin B, a

1:1 molar ratio of peptides were mixed and added to a culture of *E. coli* PDJ1 and *E. coli* MWF1. FIC Index was calculated using the formula: FIC Index = ([A]mix / MIC A) + ([B]mix / MIC B). A FIC Index of <0.5 indicated good synergy (a four-fold increase in MIC in combination) and a FIC Index = 1.0 indicates additive effects.

Cytotoxicity Studies. The cytotoxicity of ixosin and its derivatives were assessed using a standard MTT (3-(4,5-dimethylthizol-2-yl)-2,5-diphenyltetrazolium bromide) Assay on the Cervical Carcinoma (HeLa) cell line, and the Human Embryonic Kidney (HEK293) cell line. HeLa and HEK293 cells were grown in Dubelco's Modified Eagle Medium (DMEM, Gibco) supplemented with 10% Fetal Bovine Serum and incubated at 37°C in a 5% CO_2 incubator. 5000 cells were seeded per well and incubated overnight prior to exposure to a two-fold serial dilution of the peptides for 24 hours. After which, the media was aspirated out and replaced with complete growth medium containing 5 mg/mL of MTT and the cells were returned to the incubator for another 4 hours. Then, the media was removed and 200 µL of DMSO was used to extract insoluble formazan product. The absorbance at 570 nm was read and used against a negative control (treatment with buffer) to estimate % viability. The values reported here are the Mean ± SD obtained from three independent experiments performed in duplicates.

Circular Dichroism Spectroscopy. Spectra were recorded on a Jasco J-710 Spectropolarimeter. 50 µM of peptide solutions in 50% (v/v) TFE in 50 mM sodium phosphate buffer, pH 7.40 in a 1 mM cuvette. For spectra recorded with LUVs, 30 µM of peptide was added to 900 µM of LUV (P:L ratio of 1:30) both in 20 mM MOPS buffer at pH 7.4. Spectra were collected as the average of 15 scans and the two trials were found to be <2% different from each other.

Time-Kill Kinetics. The number of viable cells was determined after 1, 2, 4, and 8 hours of exposure to the peptide. A 350 µL aliquot of peptide at concentration 2X the MIC was mixed with 350 µL of 10^6 CFU/mL of (*E. coli* MG1655) bacterial suspension in MHB, to yield a final inoculum containing $5x10^5$ CFU/mL and peptide at MIC. At each specified time-point, 10 µL of the mixture was withdrawn and was diluted 1000-fold and spread on LB agar plates and allowed to grow for an additional 16 hrs. The number of single colonies were counted and plotted against time to generate curves representative of three independent trials.

Nuclear Magnetic Resonance Studies. NMR data were collected at 25°C on an Agilent (Varian) INOVA 600 MHz NMR spectrometer equipped with a cold probe. The standard BioPack pulse sequences were used. The NMR sample of 2.3 mM of unlabeled ixosin in 20mM acetate buffer at pH 4.4, 7% D_2O was used to obtain the sequence specific chemical shift assignment of the NMR resonances. For this, a set of spectra was collected and analyzed: 2D ^1H-^{15}N HSQC, ^1H-^{13}C HSQC, ^1H-^1H TOCSY (mixing time 0.07 s) and NOESY (mixing time 0.15 s), and 3D ^{15}N-edited TOCSY (mixing time 0.07 s) and NOESY (mixing time 0.3 s). The spectra were processed with NMRPipe[131] and analyzed with CCPNMR[132] Analysis. The binding of Cu^{2+} to Ixosin was studied by HSQC titration approach. The NMR signals from nuclei participating in coordination with a metal will disappear from the HSQC spectrum due to deprotonation. In addition, since Cu^{2+} exhibits paramagnetic properties, the NMR signals of peptide nuclei adjacent to the metal coordination site will experience broadening and decrease of their intensities compared to the free peptide spectra. Thus, to identify the metal binding site, the NMR sample of

unlabeled Ixosin was titrated with $CuCl_2$ and ^{1}H-^{15}N and ^{1}H-^{13}C HSQC spectra were collected at stoichiometric ratios 5:1, 2:1, 1:1, 1:2 and 1:5.

Confocal Fluorescence Microscopy Imaging. Images were acquired on a Nikon A1R spectral confocal microscope using a 100X oil immersion objective at a pixel resolution of 1024 × 1024. *E. coli* MG1655 were labeled by incubating them with 5(6)-carboxyfluorescein labeled peptides at their MIC for 30 mins. The cells were then pelleted and resuspended in PBS prior to imaging. For co-localization studies, the same treatment was done except that E. coli MWF1 strain was used. Fluorescence intensity was obtained from micrograph analysis using ImageJ.

Activity of Ixosin in O_2- and Cu^{2+}- starved Conditions. 50 µL of 10^6 CFU/mL bacterial (*E. coli* MG1655) suspension (in 5 mM HEPES, 100 mM KCl, 5 mM glucose, pH 7.30) was mixed with 50 µL of peptide at 2X its MIC. The resulting mixture was split into two 50 µL aliquots, one of which was incubated in a 37°C incubator, while the other is placed in a gas tight anaerobic chamber at the same temperature. After two hours, 10-fold dilutions were plated onto LB agar plates and allowed to grow overnight. For the copper-chelation experiments, the same manipulations were done except that the cells were co-treated with 200 µM triethylenetetramine or 50 µM penicillamine. Colonies were counted manually and the bars represent the Mean ± SEM from three independent trials.

Lipid Peroxidation Assay.[133] *E. coli* strain MWF1, *fabR*::*kan recD*::*Tn*10 (containing a higher level of unsaturated fatty acid in its membrane) were grown, washed and resuspended in 20 mM HEPES, 100 mM NaCl pH 7.40 and was incubated with peptides at their MIC without addition of exogenous Cu^{2+} for 2 hours. After which the suspension was subjected to a standard thiobarbituric acid (TBA) assay to determine amount of

peroxidation product. Briefly, 50 µL of treated bacteria was added to 150 µL of $HClO_4$ and 150 µL of 40 mM TBA. The mixture was heated in a dry block for 60 mins at 97ºC followed by a 20 min cool-down at -20ºC. Then 300 µL of methanol and 100 µL of 20% trichloroacetic acid was added. A 100 µL aliquot was injected in a C18 analytical column and eluted at 1 mL/min (for 15 mins) using 72:17:11 50 mM KH_2PO_4 pH 7:MeOH:ACN. A 97% tetramethoxypropane (Sigma) at different concentrations were used as external standard to quantify µmoles of TBARS. Bars represent Mean ± SEM obtained from three independent trials.

Tryptophan Fluorescence Quenching. LUVs composed of 3:1 POPE:DOPG was prepared and a sample was pre-oxidized with 100 µM Cu-ixosin WT and 1 mM ascorbate for 36 hrs. Ixosin B was added to native or oxidized LUVs to a final concentration of 20 µM (with LUV at 200 µM). Initial fluorescence was recorded using a Varian Cary50 Spectrofluorometer with excitation set at 295 nm, emission at 310-390 nm and PMT voltage at 650. Then a small aliquot of acrylamide was titrated into the mixture with subsequent recording of fluorescence quenching. Points represent Mean ± SEM from three independent experiments obtained from different LUV preps.

Statistical Analysis. Data were analyzed for statistical differences using Graph-Pad Prism® v6.0 software. One-Way or Two-Way ANOVA was used to determine statistical significance and was set at $P < 0.05$.

Chapter References:

[1] Hajdusek, O., Sima, R., Ayllon, N., Jalovecka, M., Perner, J., de la Fuente, J., and Kopacek, P. (2013) Interaction of the tick immune system with transmitted pathogens, *Front Cell Infect Microbiol 3*, 26.

[2] Tonk, M., Cabezas-Cruz, A., Valdes, J. J., Rego, R. O., Grubhoffer, L., Estrada-Pena, A., Vilcinskas, A., Kotsyfakis, M., and Rahnamaeian, M. (2015) Ixodes ricinus defensins attack distantly-related pathogens, *Dev Comp Immunol 53*, 358-365.

[3] Smith, A. A., and Pal, U. (2014) Immunity-related genes in Ixodes scapularis--perspectives from genome information, *Front Cell Infect Microbiol 4*, 116.

[4] Silva, F. D., Rezende, C. A., Rossi, D. C., Esteves, E., Dyszy, F. H., Schreier, S., Gueiros-Filho, F., Campos, C. B., Pires, J. R., and Daffre, S. (2009) Structure and mode of action of microplusin, a copper II-chelating antimicrobial peptide from the cattle tick Rhipicephalus (Boophilus) microplus, *J Biol Chem 284*, 34735-34746.

[5] Horn, M., Nussbaumerova, M., Sanda, M., Kovarova, Z., Srba, J., Franta, Z., Sojka, D., Bogyo, M., Caffrey, C. R., Kopacek, P., and Mares, M. (2009) Hemoglobin digestion in blood-feeding ticks: mapping a multipeptidase pathway by functional proteomics, *Chem Biol 16*, 1053-1063.

[6] Cruz, C. E., Fogaca, A. C., Nakayasu, E. S., Angeli, C. B., Belmonte, R., Almeida, I. C., Miranda, A., Miranda, M. T., Tanaka, A. S., Braz, G. R., Craik, C. S., Schneider, E., Caffrey, C. R., and Daffre, S. (2010) Characterization of proteinases from the midgut of Rhipicephalus (Boophilus) microplus involved in the generation of antimicrobial peptides, *Parasit Vectors 3*, 63.

[7] Francischetti, I. M., Sa-Nunes, A., Mans, B. J., Santos, I. M., and Ribeiro, J. M. (2009) The role of saliva in tick feeding, *Front Biosci (Landmark Ed) 14*, 2051-2088.

[8] Yu, D., Sheng, Z., Xu, X., Li, J., Yang, H., Liu, Z., Rees, H. H., and Lai, R. (2006) A novel antimicrobial peptide from salivary glands of the hard tick, Ixodes sinensis, *Peptides 27*, 31-35.

[9] Lehrer, R. I., and Lu, W. (2012) alpha-Defensins in human innate immunity, *Immunol Rev 245*, 84-112.

[10] Liu, Z., Liu, H., Liu, X., and Wu, X. (2008) Purification and cloning of a novel antimicrobial peptide from salivary glands of the hard tick, Ixodes sinensis, *Comp Biochem Physiol B Biochem Mol Biol 149*, 557-561.

[11] Fjell, C. D., Hiss, J. A., Hancock, R. E., and Schneider, G. (2012) Designing antimicrobial peptides: form follows function, *Nat Rev Drug Discov 11*, 37-51.

[12] Brogden, K. A. (2005) Antimicrobial peptides: pore formers or metabolic inhibitors in bacteria?, *Nat Rev Microbiol 3*, 238-250.

[13] Bohm, G., Muhr, R., and Jaenicke, R. (1992) Quantitative analysis of protein far UV circular dichroism spectra by neural networks, *Protein Eng 5*, 191-195.

[14] Harford, C., and Sarkar, B. (1997) Amino Terminal Cu(II)- and Ni(II)-Binding (ATCUN) Motif of Proteins and Peptides: Metal Binding, DNA Cleavage, and Other Properties, *Acc Chem Res*, 123-130.

[15] Koval, I. A., van der Schilden, K., Schuitema, A. M., Gamez, P., Belle, C., Pierre, J. L., Luken, M., Krebs, B., Roubeau, O., and Reedijk, J. (2005) Proton NMR spectroscopy and magnetic properties of a solution-stable dicopper(II) complex bearing a single mu-hydroxo bridge, *Inorg Chem 44*, 4372-4382.

[16] Last, N. B., Schlamadinger, D. E., and Miranker, A. D. (2013) A common landscape for membrane-active peptides, *Protein Sci 22*, 870-882.
[17] Nguyen, L. T., Haney, E. F., and Vogel, H. J. (2011) The expanding scope of antimicrobial peptide structures and their modes of action, *Trends Biotechnol 29*, 464-472.
[18] Cudic, M., and Otvos, L., Jr. (2002) Intracellular targets of antibacterial peptides, *Curr Drug Targets 3*, 101-106.
[19] Hancock, R. E., and Sahl, H. G. (2006) Antimicrobial and host-defense peptides as new anti-infective therapeutic strategies, *Nat Biotechnol 24*, 1551-1557.
[20] Bechara, C., and Sagan, S. (2013) Cell-penetrating peptides: 20 years later, where do we stand?, *FEBS Lett 587*, 1693-1702.
[21] Park, C. B., Yi, K. S., Matsuzaki, K., Kim, M. S., and Kim, S. C. (2000) Structure-activity analysis of buforin II, a histone H2A-derived antimicrobial peptide: the proline hinge is responsible for the cell-penetrating ability of buforin II, *Proc Natl Acad Sci U S A 97*, 8245-8250.
[22] Falla, T. J., Karunaratne, D. N., and Hancock, R. E. (1996) Mode of action of the antimicrobial peptide indolicidin, *J Biol Chem 271*, 19298-19303.
[23] Hsu, C. H., Chen, C., Jou, M. L., Lee, A. Y., Lin, Y. C., Yu, Y. P., Huang, W. T., and Wu, S. H. (2005) Structural and DNA-binding studies on the bovine antimicrobial peptide, indolicidin: evidence for multiple conformations involved in binding to membranes and DNA, *Nucleic Acids Res 33*, 4053-4064.
[24] Jin, Y., and Cowan, J. A. (2005) DNA cleavage by copper-ATCUN complexes. Factors influencing cleavage mechanism and linearization of dsDNA, *J Am Chem Soc 127*, 8408-8415.
[25] Jin, Y., Lewis, M. A., Gokhale, N. H., Long, E. C., and Cowan, J. A. (2007) Influence of stereochemistry and redox potentials on the single- and double-strand DNA cleavage efficiency of Cu(II) and Ni(II) Lys-Gly-His-derived ATCUN metallopeptides, *J Am Chem Soc 129*, 8353-8361.
[26] Joyner, J. C., Reichfield, J., and Cowan, J. A. (2011) Factors influencing the DNA nuclease activity of iron, cobalt, nickel, and copper chelates, *J Am Chem Soc 133*, 15613-15626.
[27] Roversi, D., Luca, V., Aureli, S., Park, Y., Mangoni, M. L., and Stella, L. (2014) How many antimicrobial peptide molecules kill a bacterium? The case of PMAP-23, *ACS Chem Biol 9*, 2003-2007.
[28] Fernandez-Mazarrasa, C., Mazarrasa, O., Calvo, J., del Arco, A., and Martinez-Martinez, L. (2009) High concentrations of manganese in Mueller-Hinton agar increase MICs of tigecycline determined by Etest, *J Clin Microbiol 47*, 827-829.
[29] Helbig, K., Bleuel, C., Krauss, G. J., and Nies, D. H. (2008) Glutathione and transition-metal homeostasis in Escherichia coli, *J Bacteriol 190*, 5431-5438.
[30] Outten, F. W., and Munson, G. P. (2013) Lability and liability of endogenous copper pools, *J Bacteriol 195*, 4553-4555.
[31] Fung, D. K., Lau, W. Y., Chan, W. T., and Yan, A. (2013) Copper efflux is induced during anaerobic amino acid limitation in Escherichia coli to protect iron-sulfur cluster enzymes and biogenesis, *J Bacteriol 195*, 4556-4568.
[32] Fu, Y., Chang, F. M., and Giedroc, D. P. (2014) Copper transport and trafficking at the host-bacterial pathogen interface, *Acc Chem Res 47*, 3605-3613.

[33] Choi, K. Y., Chow, L. N., and Mookherjee, N. (2012) Cationic host defence peptides: multifaceted role in immune modulation and inflammation, *J Innate Immun 4*, 361-370.
[34] Hilchie, A. L., Wuerth, K., and Hancock, R. E. (2013) Immune modulation by multifaceted cationic host defense (antimicrobial) peptides, *Nat Chem Biol 9*, 761-768.
[35] Hong, R., Kang, T. Y., Michels, C. A., and Gadura, N. (2012) Membrane lipid peroxidation in copper alloy-mediated contact killing of Escherichia coli, *Appl Environ Microbiol 78*, 1776-1784.
[36] Mattila, J. P., Sabatini, K., and Kinnunen, P. K. (2008) Oxidized phospholipids as potential molecular targets for antimicrobial peptides, *Biochim Biophys Acta 1778*, 2041-2050.
[37] Steinbrecher, U. P. (1987) Oxidation of human low density lipoprotein results in derivatization of lysine residues of apolipoprotein B by lipid peroxide decomposition products, *J Biol Chem 262*, 3603-3608.
[38] Kurvinen, J. P., Kuksis, A., Ravandi, A., Sjovall, O., and Kallio, H. (1999) Rapid complexing of oxoacylglycerols with amino acids, peptides and aminophospholipids, *Lipids 34*, 299-305.
[39] Rozga, M., Sokolowska, M., Protas, A. M., and Bal, W. (2007) Human serum albumin coordinates Cu(II) at its N-terminal binding site with 1 pM affinity, *J Biol Inorg Chem 12*, 913-918.
[40] Lemaitre, B., Reichhart, J. M., and Hoffmann, J. A. (1997) Drosophila host defense: differential induction of antimicrobial peptide genes after infection by various classes of microorganisms, *Proc Natl Acad Sci U S A 94*, 14614-14619.
[41] Boylan, J. A., Lawrence, K. A., Downey, J. S., and Gherardini, F. C. (2008) Borrelia burgdorferi membranes are the primary targets of reactive oxygen species, *Mol Microbiol 68*, 786-799.
[42] Ledin, K. E., Zeidner, N. S., Ribeiro, J. M., Biggerstaff, B. J., Dolan, M. C., Dietrich, G., Vredevoe, L., and Piesman, J. (2005) Borreliacidal activity of saliva of the tick Amblyomma americanum, *Med Vet Entomol 19*, 90-95.
[43] Wiegand, I., Hilpert, K., and Hancock, R. E. (2008) Agar and broth dilution methods to determine the minimal inhibitory concentration (MIC) of antimicrobial substances, *Nat Protoc 3*, 163-175.
[44] Delaglio, F., Grzesiek, S., Vuister, G. W., Zhu, G., Pfeifer, J., and Bax, A. (1995) NMRPipe: a multidimensional spectral processing system based on UNIX pipes, *J Biomol NMR 6*, 277-293.
[45] Vranken, W. F., Boucher, W., Stevens, T. J., Fogh, R. H., Pajon, A., Llinas, M., Ulrich, E. L., Markley, J. L., Ionides, J., and Laue, E. D. (2005) The CCPN data model for NMR spectroscopy: development of a software pipeline, *Proteins 59*, 687-696.
[46] Boylan, J. A., and Gherardini, F. C. (2008) Determining the cellular targets of reactive oxygen species in Borrelia burgdorferi, *Methods Mol Biol 431*, 213-221.

Chapter 3

The ATCUN Motif in Microbial DNA Oxidation

Copper-mediated Nuclease Activity of Piscidin 1 and 3 Coupled with their Contrasting Expression Profiles Reveal Novel Insights into Vertebrate Immune Response

Adapted entirely from:

Hayden, R.M., Goldberg, G.K., Ferguson, B.M., Schoeneck, M.W., **Libardo, M.D.J.**, … Angeles-Boza, A.M., Fu, R., Cotten, M.L. *J. Phys Chem B*, **2015**, 119, 15235-46

Libardo, M.D.J., Bahar, A.A., Ma, B., Fu, R., Zhao, J., Nussinov, R., Ren, D., Angeles-Boza, A.M., Cotten, M.L. **2017**, *submitted*

Introduction

Two of the first Antimicrobial Peptides (AMPs) discovered in the mast cells of vertebrates were piscidin 1 (p1, FFHHIFRGIVHVGKTIHRLVTG-NH_2) and piscidin 3 (p3, FIHHIFRGIVHAGRSIGRFLTG-NH_2), members of the Class I piscidins that exhibit activities against a wide panel of bacteria.[134, 135] While piscidins were initially isolated from the hybrid striped seabass, there is now significant evidence of piscidins being expressed by several fish species belonging to a range of taxonomic families.[136-138] Moreover, piscidins were found to be omnipresent in several cell types including phagocytic immune cells, hematopoietic cells, epithelial cells, chondrocytes and cells of the mucosal tissues.[139, 140] The ubiquity of piscidins in both the organism and ecological levels, coupled with their potency against various pathogens, is reflective of their important role in the fish innate immune response.[139]

The piscidins p1 and p3, much like other AMPs, are multifunctional molecules. Aside from direct microbial killing, p1 and p3 exhibit immunomodulatory properties,[141] have wound-healing effects[142] and anesthetic[143] activities. The ability to bind to and act on different molecular targets highlight the conformational plasticity that p1 and p3 possess due to their inherently disordered nature. From the antimicrobial standpoint, p1 and p3 represent good archetypes of AMPs that have membrane disruptive abilities because they are cationic, amphipathic and α-helical when bound to model membranes.[144, 145] However, no studies thus far have definitively linked p1 and p3's membrane activity to their bactericidal action. Numerous evidence in literature have shown that some AMPs translocate across the bacterial membrane and bind to internal targets leading to perturbation of essential processes.[10] Indeed, p1 and p3 were shown

to localize intracellularly at sub-inhibitory concentrations and bind to DNA in vitro,[146] however, there exists no evidence of a direct association between DNA binding and cell death. Clearly, other factors are involved and need to be uncovered before a comprehensive narrative of piscidin-induced bacterial death can be made. At present, it is clear that p1 and p3 have complementary effects on phosphate-containing targets, that is, p1 seems to be more membrane disruptive while p3 is more DNA condensing.[146]

Initial examination of p1 and p3's primary structure reveals that both isoforms contain an Amino Terminal Copper and Nickel (ATCUN) binding motif, FFH- for p1 and FIH- for p3. Chapter 1 of this dissertation showed that the ATCUN motif in the tick AMP, Ixosin, was necessary for its lipid oxidation mechanism leading to synergistic interactions with another AMP (Ixosin B) via oxidized phospholipid targeting.[147] While it is very likely that the ATCUN motif in p1 and p3 can afford these peptides a similar oxidative mode of attack, the demonstration that both piscidins traverse the bacterial membrane at sub-inhibitory concentrations lead us to test the possibility that they could oxidatively damage not only phospholipids but also DNA. The ROS formed by the copper-ATCUN complex retains the oxidizing power of classical ROS, and have been shown to effectively damage DNA within minutes.[117] Taken together with the fact that both peptides bind to DNA in vitro, we speculated that copper-bound p1 and p3 have nuclease activity that might be involved in its bactericidal action.

In this chapter, we demonstrate that p1 and p3 have nuclease activity and show how it relates to the antimicrobial activity of the peptides against planktonic cells, persisters, and biofilms. We use structural, electrochemical, computational, and kinetic information obtained from in vitro studies to rationalize the observed trends in the

biological activity of the peptides. We found that whereas Cu-p1 is a stronger oxidizing agent, Cu-p3 has a faster rate of oxidative DNA cleavage likely due to its stronger DNA interaction. Treatment of log phase *E. coli* with both peptides resulted in a dose- and copper-dependent DNA damage, with p3 being more effective. *P. aeruginosa* biofilms and persister cells were found to be more susceptible to Cu-p3 than to Cu-p1. We found that this trend in susceptibility is correlated with the nuclease activity of the peptides as Cu-p3 was more efficient in degrading extracellular DNA in biofilms and elicited a stronger SOS response (DNA repair) in persister cells relative to Cu-p1. Finally, we couple our results to the genomic and localization studies performed by others to unveil a sophisticated defensive strategy employed by fish against invading microbes.

Results

Both p1 and p3 bind to Cu^{2+} in vitro

To confirm and determine stoichiometry of Cu^{2+} binding by p1 and p3, we incubated equimolar solutions of peptide and Cu^{2+}, and subjected it to ESI-MS analysis. We observed *m/z* values of 878.9, 659.3, and 527.8 for Cu-p1, and *m/z* 852.8, 639.7, and 512.2 for Cu-p3. These values are consistent with the $[M+3H]^{3+}$, $[M+4H]^{4+}$, and $[M+5H]^{5+}$ multiply charged species of a 1:1 complex of both isoforms (Figure 3.1A). We then employed two-dimensional solution NMR to confirm that Cu^{2+} binds to the ATCUN motif. Because Cu^{2+} is paramagnetic, any proton in its vicinity will exhibit a significant broadening of its NMR signal. To circumvent this problem, we used Ni^{2+} as a spectroscopic probe (both Cu^{2+} and Ni^{2+} bind to the ATCUN motif in a similar fashion and with comparable dissociation constants).[109] Upon titration of Ni^{2+} to either p1 or p3, we

observed an upfield shift of the aromatic proton signals in His-3 (Figure 3.1B), consistent with a previous report,[148] indicating metal binding to the ATCUN motif of the peptides. Our results suggest that p1 and p3 bind to Cu^{2+} in vitro in a 1:1 fashion via their ATCUN motif, and that no other potential ligands in the peptide backbone can compete for the Cu^{2+} ions.

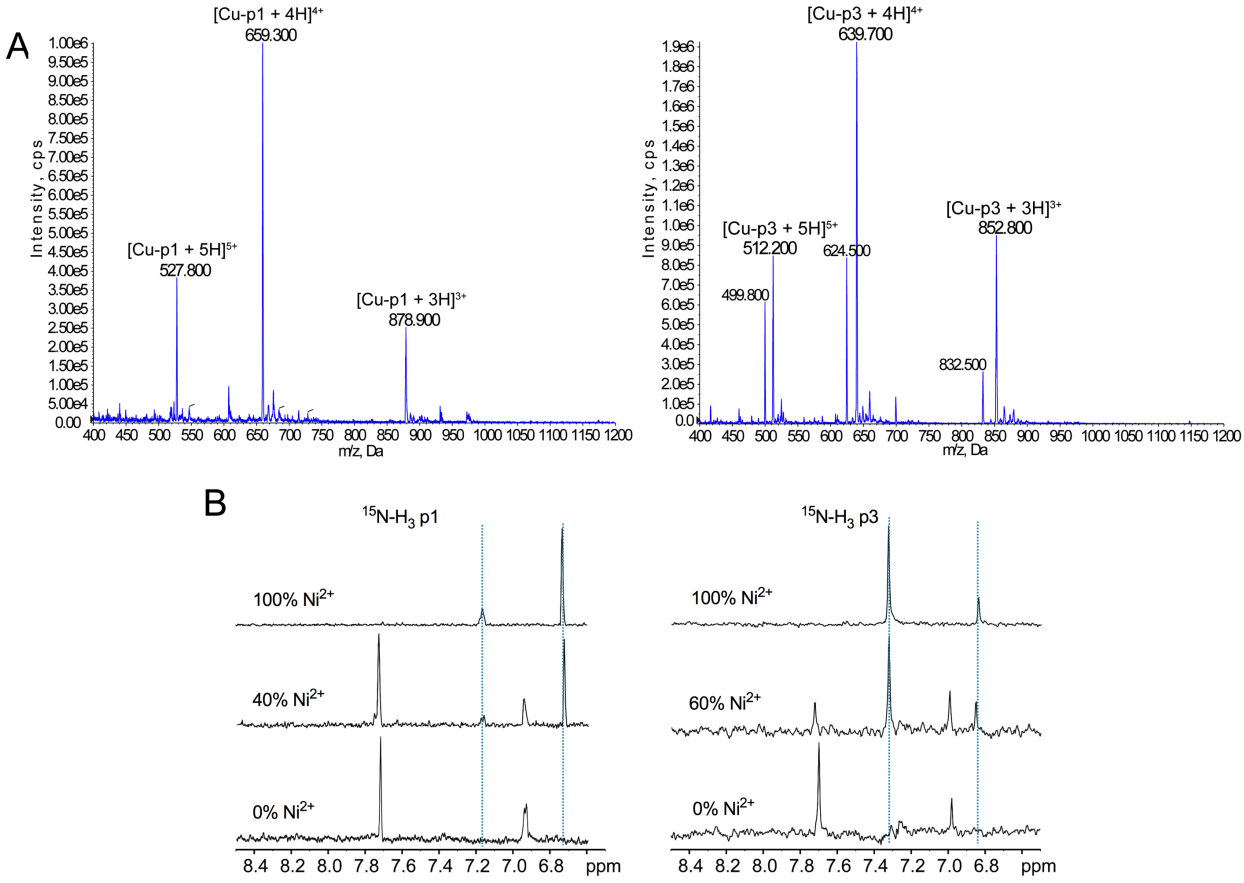

Figure 3.1. Spectroscopic Characterization of Piscidin Copper-binding. (A) ESI-MS spectra of a 1:1 mixture of piscidin and Cu^{2+}. m/z values show p1 and p3 bind to copper with a 1:1 stoichiometry. (B) One dimensional slices from solution NMR heteronuclear quantum correlation (HMQC) spectra of ^{15}N-H_3-labeled p1 and p3 titrated with Ni^{2+} indicating perturbation of chemical shifts of δ-proton (7.0 ppm) and ε-proton (7.7 ppm of His3. *Experiment in (B) was performed by Prof. Myriam L. Cotton (W&M) and Dr. Riquiang Fu (NHMFL)*.

p3 binds DNA more strongly than p1

Having proven copper binding, we set out to determine whether both peptides bind to DNA *in vitro*. To this end, we utilized the electrophoretic mobility shift assay (EMSA) to determine relative strengths of DNA binding between p1 and p3 (Figure 3.2). Using a constant amount of linearized pNEB206A plasmid and increasing amounts of each peptide, we observed a progressive decrease in the fraction of migrating DNA. This suggests that *in vitro*, both p1 and p3 are able to bind DNA, perhaps causing charge neutralization and/or aggregation resulting in a markedly lower electrophoretic mobility. When the data were fitted to a simple one-site binding model, the peptide weight that caused 90% inhibition of migration was found to be 730 ng and 650 ng for p1 and p3, respectively. These IC_{90} values suggests that p3 has a stronger interaction with DNA.

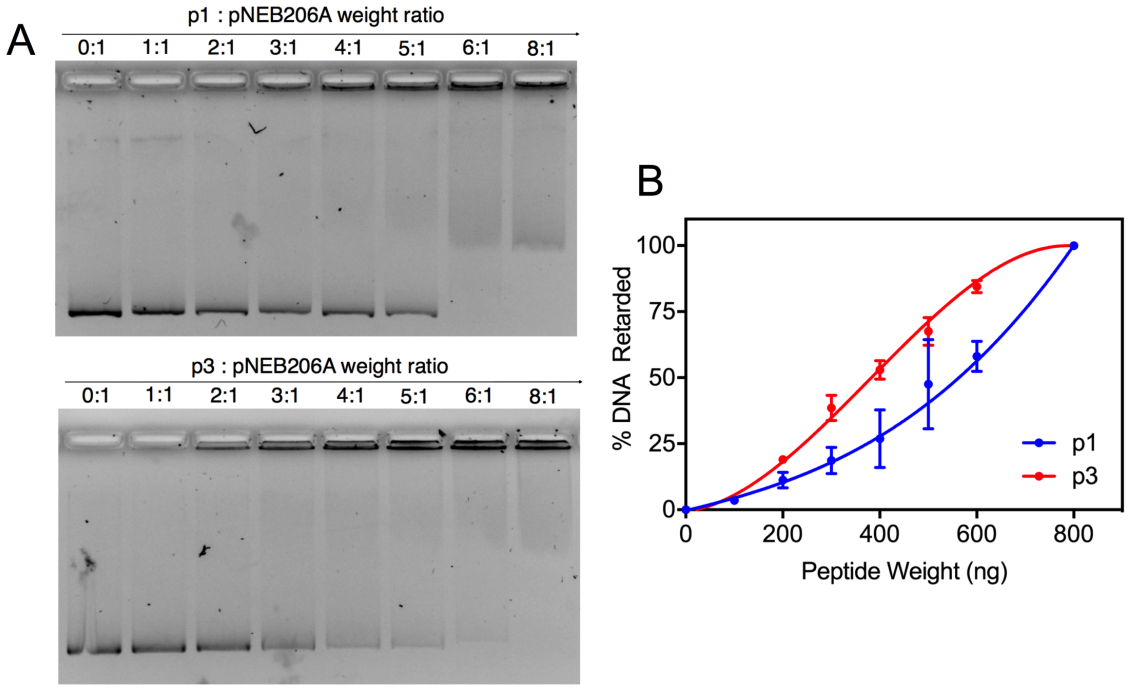

Figure 3.2. *in vitro* DNA binding of Piscidins 1 and 3. (A) Electrophoretic mobility shift assay was used to assess the degree of DNA binding by p1 and p3. (B). Curve fits for the gel images shown in (A). Curves show that p3 bind to DNA cooperatively.

We set out to provide molecular-level insight of the DNA-p1/3 interactions using MD simulations. The DNA duplex structure formed by the sequence AAATACACTTTTGGT and its complement was used for molecular simulations focusing on the binding of monomeric (non-aggregated) piscidin to DNA, that is, without considering the subsequent aggregation step. Under these conditions, the most stable conformation of DNA-p3 was found to have a binding energy to DNA that was favorable (-1.4 ± 10.1 kcal/mol) while its p1 equivalent was unfavorable (81.4 ± 14.1 kcal/mol). The Arg7 in p3 engages in five H-bonds with DNA while Arg7 in p1 only has two (Figure 3.3A and 3.3B). Moreover, the Arg14 residue in p3 is engaged in a stronger interaction with DNA than the Lys14 in p1 (Appendices, Figure S3.1). Neither p3 nor p1 formed stable soluble binary complexes with DNA (binding energies > 0 for both p1 and p3 ensembles), reflecting that DNA-peptide complexes form polymeric aggregated states in solution. Indeed, the most stable DNA-p3 complex shows exposure of p3's hydrophobic surface (black arrows in Figure 3.3C). We then calculated the binding energy when the monomeric complex was allowed to form dimers. We observed more favorable binding energies for both piscidin isoforms, -189.3 ± 18.7 kcal/mol for $(p3\text{-}DNA)_2$ and -69.6 ± 27.6 kcal/mol for $(p1\text{-}DNA)_2$, confirming that higher order oligomerization promote binding between peptide and DNA. Not surprisingly, the most stable conformation of the dimers (Figure 3.4) show the hydrophobic residues interacting in a manner analogous to leucine zippers. Overall, our simulations support our multiple observation of p3 binding to DNA more tightly.

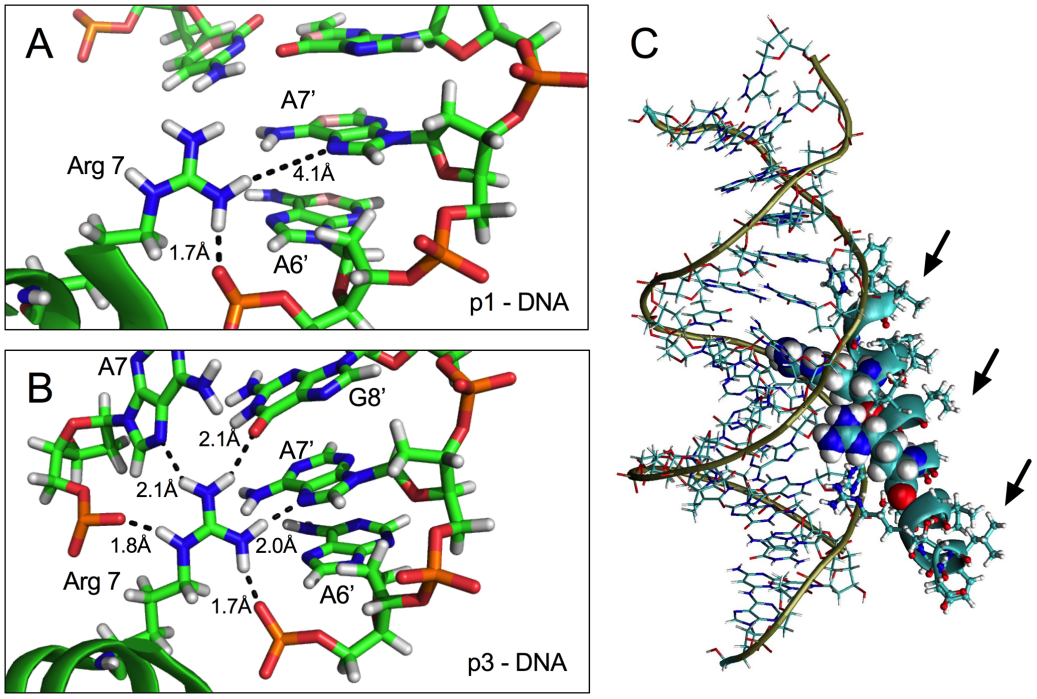

Figure 3.3. Molecular Dynamics Simulation of Monomeric Piscidin-DNA Complex. Hydrogen-bonding network between Arg7 of p1 (A) and p3 (B) shows more interactions in p3, confirming its tighter DNA binding. (C) When p1 or p3 form a binary complex with DNA, a surface of hydrophobic residues (indicated by black arrows) is exposed to the solvent. *Structures were calculated by Dr. Buyong Ma, Dr. Jun Zhao, and Dr. Ruth Nussinov (NCI, NIH)*.

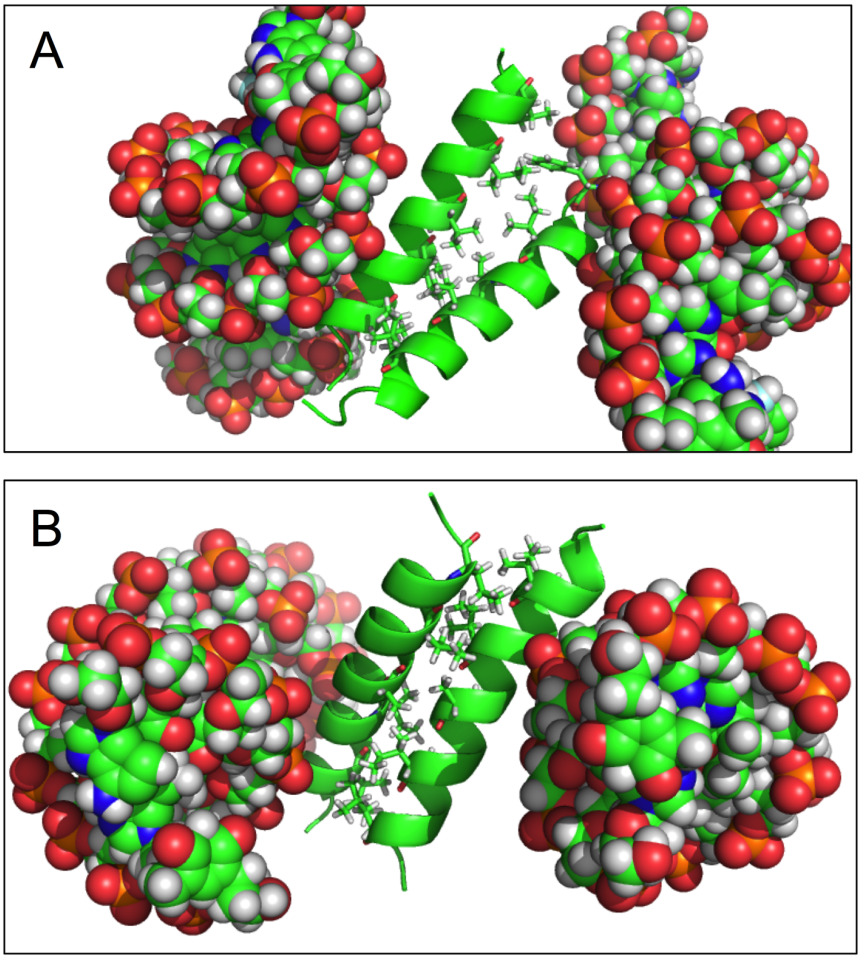

Figure 3.4. Molecular Dynamics Simulation of Aggregated Piscidin-DNA Complex.

The solvent-exposed hydrophobic residues in the monomeric complex promotes dimerization of piscidin-DNA complexes as shown here for p1 (A) and p3 (B). *Structures were calculated by Dr. Buyong Ma, Dr. Jun Zhao, and Dr. Ruth Nussinov (NCI, NIH)*.

The N-terminal of piscidins adopts a structure optimized for metal coordination when bound to DNA

We next wanted to determine whether metal binding leads to structural changes at the N-end of piscidin when bound to DNA. Because DNA is aggregated in the presence of piscidin, we also employed rotational-echo double-resonance (REDOR) solid state NMR on a ^{13}C-carbonyl and ^{15}N-amide labeled p1 and p3 for distance measurement at

the N-terminal. The isotopic labels were placed in *i* and *i* + *4* positions to span the length of hydrogen-bonding partners in a canonical α-helix (~4.2 Å). Notably, we found that Ni-p1 exhibited a $^{13}C\text{-}F_2$ – $^{15}N\text{-}F_6$ distance of 3.55 ± 0.29 Å (Figure 3.5), comparable to the distance (3.46 ± 0.51 Å) in the non-metallated p1. The same was true for p3, where metalation did not significantly change the $^{13}C\text{-}I_2$ – $^{15}N\text{-}F_6$ distance. These distances are shorter than the expected distance in an α-helical pitch indicating twisted configuration of the peptides when bound to DNA, in contrast to the fraying observed when bound to lipid bilayers.[144] These results also indicate that the ATCUN motif is poised for metal coordination when p1 or p3 is bound to DNA. When a similar technique was done to measure the distance between residue 8 and 12 of both p1 and p3 bound to DNA, we also observed distances within the α-helical range suggesting the possibility of a fully helical peptide fold when p1 and p3 are bound to DNA, experimentally validating the structures calculated in Figure 3.3.

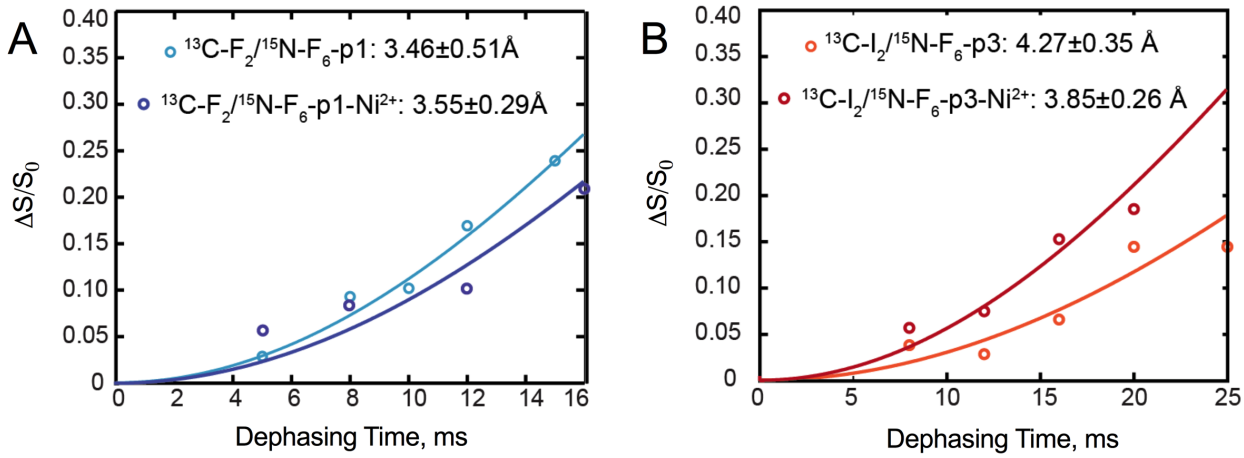

Figure 3.5. Distance Measurements in Piscidin N-terminal. Solid state NMR was used to measure distance between H-bonding pairs in p1 (A) and p3 (B) with and without Ni^{2+}. Curves suggest that structures at the ATCUN motif of p1 and p3 are unchanged upon metalation. *Experiments performed by Dr. Myriam Cotten and Dr. Riquiang Fu*.

Cu-p3 cleaves DNA more efficiently that Cu-p1 in vitro

The Cu-ATCUN complex has been shown to have DNA cleavage activity, effecting DNA damage within minutes in the presence of pro-oxidants.[117] To confirm a similar *in vitro* nuclease activity of the peptides, we monitored the time-dependent cleavage of the plasmid pUC19 when incubated with Cu-p1/p3 in the presence of H_2O_2 and ascorbic acid. We observed a progressive loss of the supercoiled (S) form with a concomitant increase in the nicked (N) and linearized (L) forms of the plasmid (Figure 3.6A and Appendices Figure S3.2). When the data was fitted into a pseudo-first order rate equation ($d[DNA]/dt = -k_{cleavage}t$, Figure 3.6B), Cu-p3 was found to have approximately three-fold greater DNA cleavage rate constant than Cu-p1 (Table 3.1). This is counterintuitive to what we observed from our voltammetric studies which indicates that Cu-p1 is a stronger oxidizing agent (E° in Table 3.1). To justify the observed trend in DNA cleavage, we applied the Freifelder-Trumbo (F-T) statistical analysis. F-T analysis suggests that when single strand breaks occur at sites that are close to each other (as a result of localized ROS formation), the forces that tend to stabilize the doible helix is overcome resulting in linearization of plasmid DNA. The F-T relationship suggests that if the cleavage occurs via random mechanisms, 100 single strand breaks (at interspersed regions of the DNA) is required for linearization,[149] that is $n_1/n_2 \geq 100$ (where n_1 = number of single strand breaks and n_2 = number of double strand breaks). We calculated n_1 and n_2 values from the fraction of supercoiled and linearized plasmids remaining after each time point and reasoned that since p3 has a stronger DNA binding ability, it should have a lower n_1/n_2 ratio. Indeed, we found a lower ratio for Cu-p3 relative to Cu-p1 (Table 3.1), suggesting a more concerted mechanism of DNA cleavage by Cu-p3 likely resulting from the longer lifetime of the Cu-

p3:DNA complex. Altogether, our data indicate that Cu-p3 has a better nuclease activity than Cu-p1, despite the latter being a stronger oxidant.

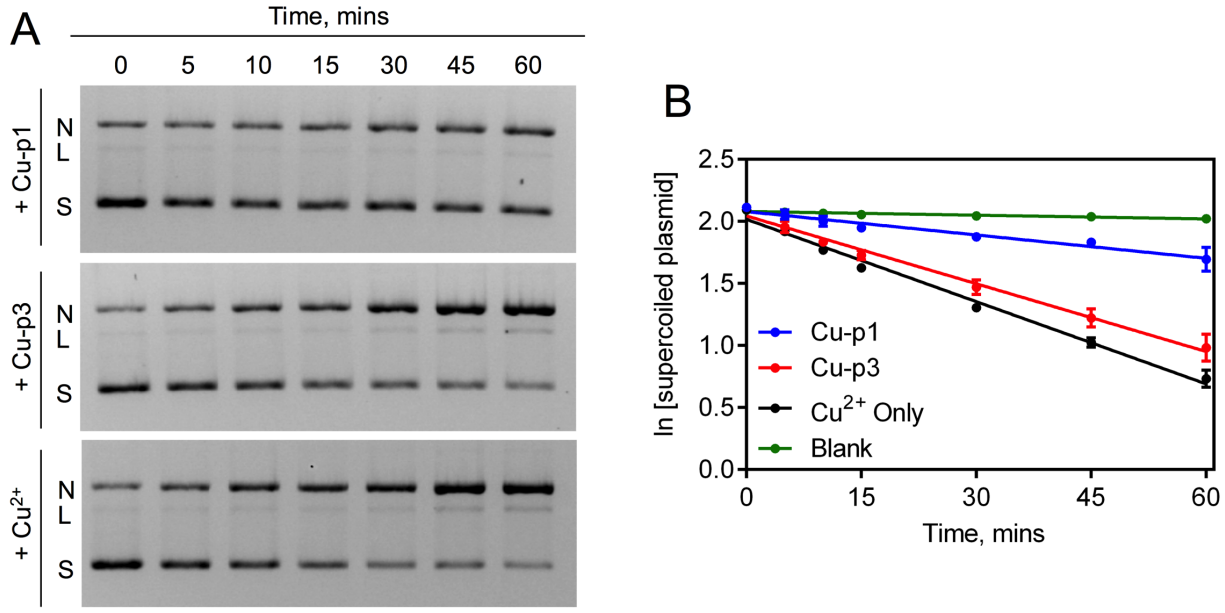

Figure 3.6. in vitro DNA Cleavage of Cu-piscidin Complexes. (A) Electrophoretic monitoring of piscidin-induced cleavage of pUC19 showing loss of supercoiled (S) plasmid with corresponding increase in the nicked (N) and linearized (L) form. (B) Pseudo-first order intergrated rate law plots of *in vitro* DNA cleavage promoted by piscidins. Blank runs represent experiments with H_2O_2 and ascorbic acid but without any metallopeptide.

Table 3.1. Summary of values obtained from electrochemical, kinetic and statistical analysis of metallopeptides.

Parameter	Cu-p1	Cu-p3	Cu^{2+}
E° vs NHE (V)	0.990	0.972	n.d.
$k_{clevagae}$ (min^{-1})	6.3 ± 0.5	18.2 ± 0.7	22.1 ± 0.6
n_1/n_2	34	27	27

n.d. = not determined

p1 and p3 both use copper in their bactericidal activity against planktonic bacteria

Having confirmed *in vitro* redox activity of the corresponding copper complexes, we set out to determine their respective antimicrobial activity against planktonic bacteria. We measured the Minimum Inhibitory Concentration (MIC) of p1 and p3 with or without pre-incubation with an equimolar amount of Cu^{2+}. Consistent with previous studies,[150] we found that for all Gram-negative bacteria tested, p1 was more active than p3, and that against the Gram-positive *S. aureus*, both peptides exhibited similar MICs (Table 3.2). Interestingly, no change in MIC was observed upon pre-incubation of the peptides with Cu^{2+}. Since the Mueller-Hinton Broth contains ~78 μM of copper,[119] a concentration in excess of the highest peptide concentration tested (16 μM), it is likely that both p1 and p3 are copper-saturated in the growth medium. Moreover, the pool of labile copper ions in bacteria (bound to methionine, cysteine or glutathione)[120, 121] may act as a copper source for p1 and p3, since the peptides have a considerably higher affinity towards the metal. These two possibilities reasonably explain the similar MICs obtained with and without pre-loading of copper. When tested against the isogenic mutant strain *E. coli* TD172 (a strain harboring a deletion in the *recA* gene, essential for DNA damage repair), a four-fold increase in p3 activity was observed (relative to WT *E. coli*) whereas p1 activity was unchanged. This result implicates DNA damage in the mechanism of action of p3, at par with the strong DNA binding and cleavage observed *in vitro*.

Table 3.2. Antimicrobial Activity of Piscidin Isoforms.

Bacteria	Minimum Inhibitory Concentration (MIC), μM			
	p1	Cu-p1	p3	Cu-p3
E. coli WT	4	4	8	8
E. coli (Δ*recA*)	4	4	2	2
S. aureus	2	2	2	2
P. aeruginosa	16	16	32	32

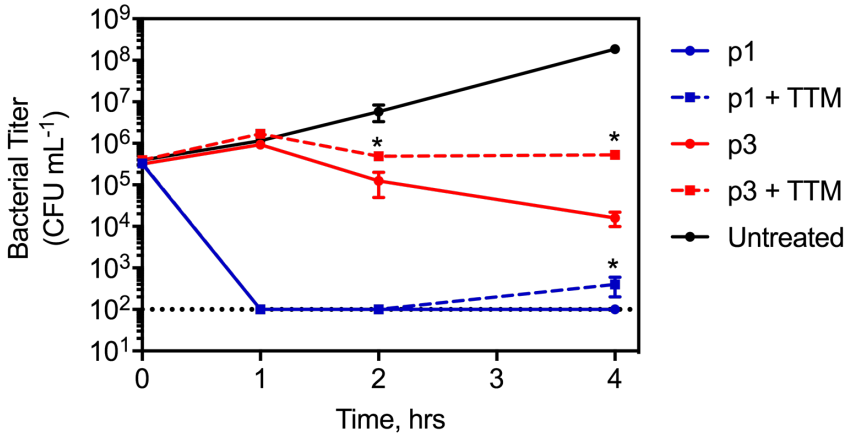

Figure 3.7. Bactericidal Property of Piscidins. Time-kill curves of piscidin-treated *E. coli* in the presence and absence of 100 μM of the copper-chelator, tetrathiomolybdate (TTM). *, *P*<0.01 compared to corresponding runs without TTM.

To test the copper-dependence of the activity of p1 and p3, we monitored the killing kinetics of the peptides at their MIC in the presence and absence of 100 μM tetrathiomolybdate (TTM), a copper-selective, cell-permeable chelator.[151] We reasoned that if p1 and p3 uses Cu^{2+} for its activity, copper depletion should result in a lower

bactericidal activity. We observed rapid sterilization of the culture – decreasing viable count by 4 orders of magnitude – by p1 with and without TTM within the first hour of exposure (Figure 3.7). However, p1 + TTM exhibited a resumption of growth two hours post-exposure, likely arising from a slower rate of inhibition relative to the rate of bacterial growth. On the other hand, p3 showed a slow and steady decline in bacterial viability (~1.5 log) which slowed down further when TTM was added. Our results indicate that copper depletion affects the activity of p1 and p3 negatively, and suggests that both isoforms use Cu^{2+} for their bactericidal action.

Piscidins, like most AMPs, have membrane binding and disruptive properties on model membranes and live cells;[146] furthermore, ATCUN-containing AMPs are known to oxidatively damage lipid bilayers (Chapter 2).[147] For this reason, we tested whether lipid peroxidation is an important step in the mechanism of p1 and p3. Using a standard thiobarbituric acid assay, we found a three-fold increase in peroxidized lipids in *E. coli* treated with p1 or p3 at their MIC (Figure 3.8A). However, no statistical difference between p1- and p3-treated cells were observed, indicating that the differences in MICs between the two isoforms is likely not a result of oxidative attack on the lipid bilayer. Piscidin 1 has been reported to be highly membranolytic, able to effect cell lysis in the span of minutes.[146, 150] Despite the lack of a significant difference between p1 and p3 in terms of lipid peroxidation, we proceeded to characterize the affinity of p1 to oxidized membranes. We performed titrations of lipid vesicles into a solution of p1 and monitored membrane partitioning of the peptide via CD spectroscopy. We utilized large unilamellar vesicles (LUVs) composed of either 70:30 POPE:POPG of 65:25:10 POPE:POPG:AldoPC (1-palmitoyl-2-(9'-oxo-nonanoyl)-sn-glycero-3-phosphocholine, a phospholipid containing

an aldehyde functionality). We find that p1 adopts significantly more pronounced helical conformations in the presence of vesicles containing oxidized phospholipids (Figure 3.8B). When partition coefficient and free energy of binding was calculated based on published procedures,[152, 153] we found that p1 has a significantly greater partition coefficient in oxidized LUVs ($6.1X10^3$) compared to normal LUVs ($1.8X10^3$). This result indicates that p1 indeed has a higher affinity toward oxidized membranes. Ixosin B exhibits a similar behavior, as shown in Chapter 2.

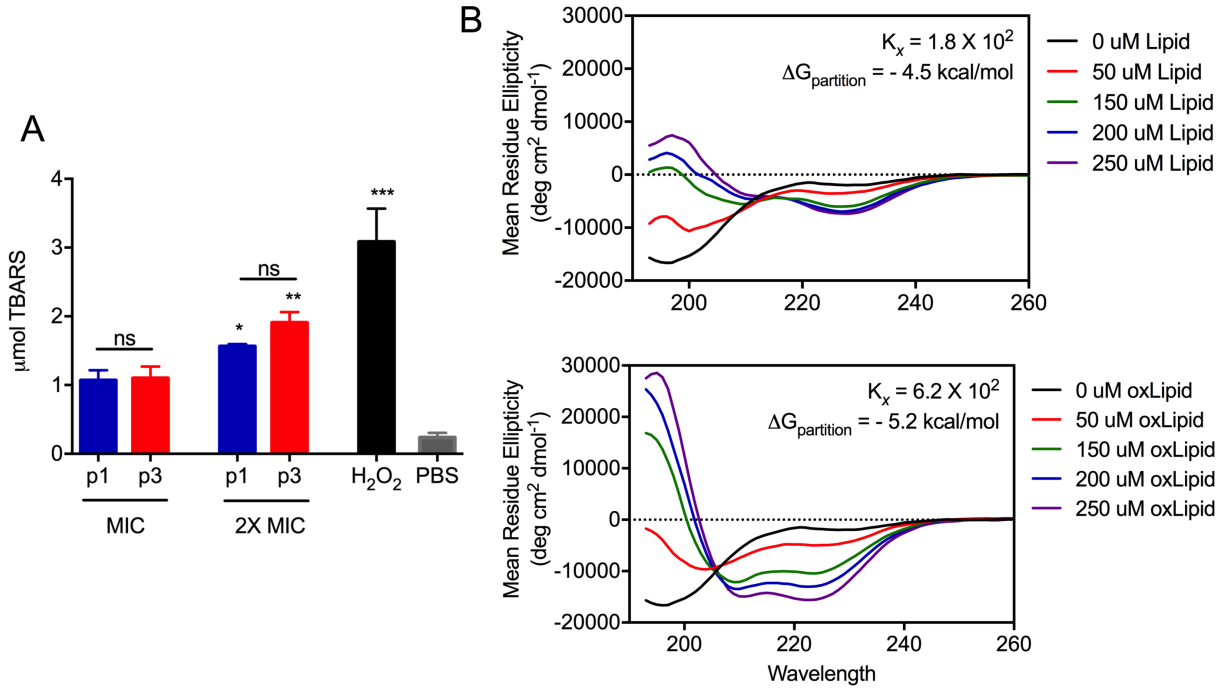

Figure 3.8. Membrane Oxidizing and Affinity of Piscidins. (A) *E. coli* cells were treated with p1 or p3 at the indicated concentrations and subsequently harvested for peroxidized lipid quantification using a standard thiobarbituric acid assay. TBARS = thiobarbituric reactive substances. *, $P<0.05$; **, $P<0.01$; ***, $P<0.005$ compared to the PBS control. ns = not significant. (B) Relative affinity of p1 toward bilayers containing normal phospholipids (top) and oxidized phospholipids (bottom) measured using CD spectroscopy. Wimley-white paramters are shown within the CD spectra and indicates that p1 has greater affinity towards oxidized membranes.

To definitively piece out whether p1 and p3 can competitively sequester copper and to determine whether the copper is coming from extracellular (in the media) or intracellular (inside the bacteria) sources, we tested their activities in different growth media. We first grew the bacteria in either copper-containing complex media (MHB) or in copper-deprived minimal media (M9 + glucose). Then we washed the bacteria and resuspended them in the either MHB or M9 prior to treatments. This set-up gave us three conditions: (*i*) A, bacteria both grown and tested in MHB will have both extracellular and intracellular copper, (*i*) B, bacteria grown in MHB but tested in M9 will only have intracellular copper, and (*iii*) C, bacteria both grown and tested in M9 will have neither extracellular nor intracellular copper. We determined relative activity by plating dilutions of cultures following exposure to apopeptides or their corresponding metallated forms. In agreement with our MIC data, we found that pre-loading the peptides with copper (Cu-p1 and Cu-p3) does not yield an increased potency only in MHB. However, conditions lacking extracellular copper exhibited a markedly higher potency upon pre-incubation with copper (Figure 3.9). This indicates the clear synergy between p1 or p3 with copper ions. Comparing bacterial survival in condition A with that in B shows that both p1 and p3 utilize extracellular copper. However, removal of intracellular copper only seemed to positively affect p1 (Figure 3.9). Taken together, these results suggest that p1 has the ability to (sequester and) utilize both extracellular and intracellular copper while p3 synergizes only with extracellular copper.

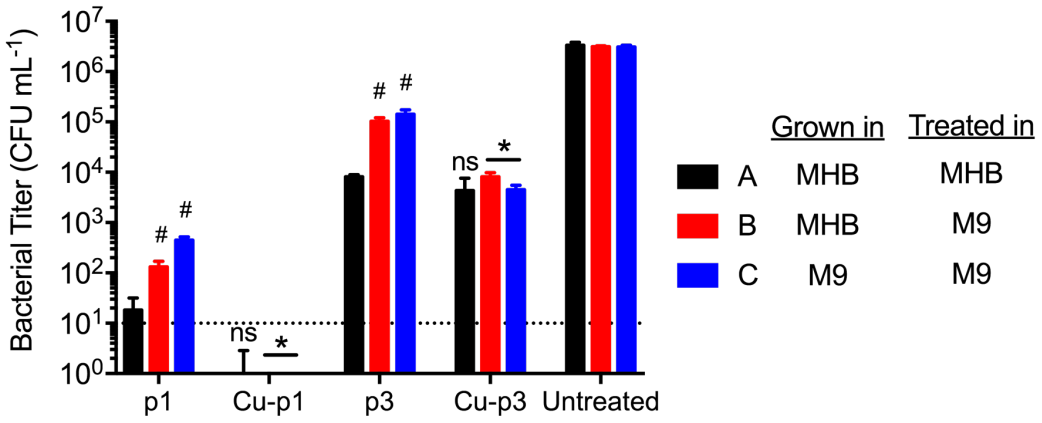

Figure 3.9. Synergy between Cu^{2+} and Piscidins Against Planktonic Bacteria. To determine piscidin's copper source and synergy with copper, bacteria were grown and tested at different conditions. MHB is a complex medium containing copper, able to suppy both extracellular and intracellular copper. M9 is a minimal medium that has trace amounts of copper and cannot supply copper. #, $P<0.05$ compared to condition A; *, $P<0.05$ compared to non-metallated piscidin, ns = not significant. Dotted line represents the limit of detection of the assay.

Only p3 has the ability to damage DNA in live E. coli in a Cu^{2+}-dependent manner

Since p1 and p3 have been shown to cross bacterial membranes even at sub-lethal concentration, and their corresponding complexes was found to cleave isolated DNA, we tested whether this nuclease activity is preserved *in cella*. We utilized the Terminal deoxynucleotidyl transferase dUTP Nick End Labeling (TUNEL) assay to assess intracellular DNA damage in wild type *E. coli*. Since pre-incubating the peptides did not alter the MICs, we mixed the naïve peptides with bacteria in the presence or absence of 100 μM TTM. Our results show that there is indeed DNA damage in piscidin-treated cells (Figure 3.10A). When p1 was used at 2X MIC, a two-fold increase in DNA nicked ends was observed which was unchanged upon co-treatment with TTM (Figure 3.10B). Meanwhile, p3 at its MIC afforded a statistically significant 1.5-fold increase in TUNEL

fluorescence which decreased slightly in the presence of TTM (P<0.05). Furthermore, when used at 2x MIC, p3 affords a four-fold greater DNA damage which decreased considerably upon addition of TTM. Our data demonstrates that only p3 has a significant copper-dependent nuclease activity in live bacteria. It should be noted that TTM treatment alone did not alter the TUNEL fluorescence of the control cells (Appendices, Figure S3.3), suggesting that the observed decrease in fluorescence is a consequence of decreased copper availability. While several reports have shown that treatment of bacteria with bactericidal antibiotics result in buildup of ROS (which could lead to DNA damage),[154, 155] the fact that we observed a copper-dependence in TUNEL response suggests that the DNA damage is likely a direct result of the oxidative capacity of p3. Furthermore, the p3-induced DNA damage was observed at 2 hours post-exposure, a time at which cell killing have already commenced (Figure 3.7), suggesting that oxidative DNA cleavage may be a major contributor to p3's bactericidal action.

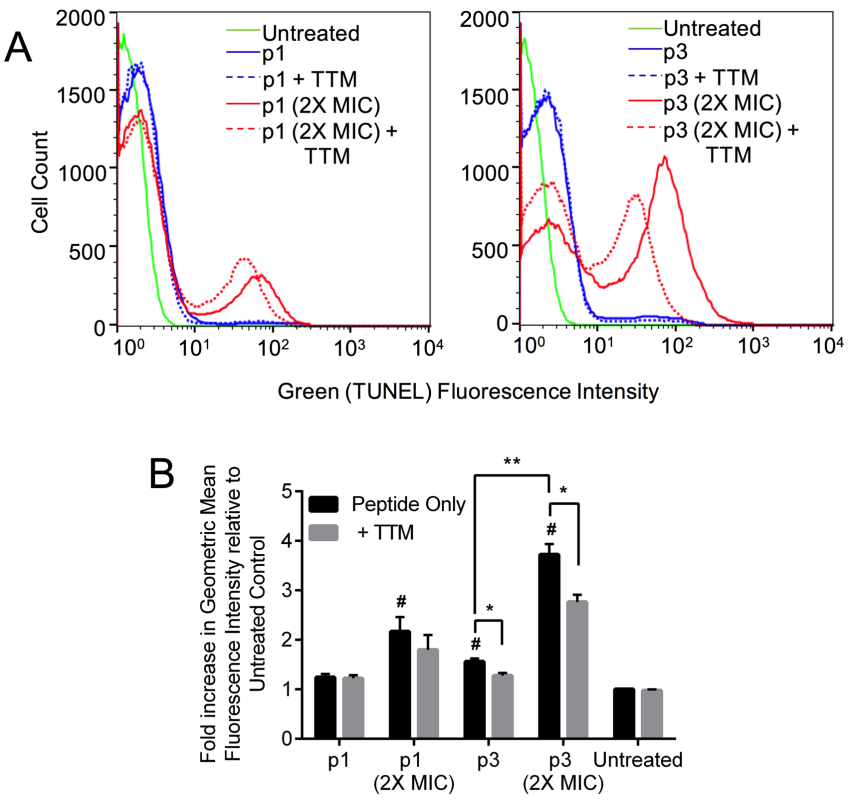

Figure 3.10. DNA Cleavage in Live Bacteria by Piscidins. (A) Representative histograms obtained from flow cytometric analysis of piscidin-treated *E. coli*. The fluorescence intensity is directly proportional to the amount of DNA strand breaks. (B) The geometric mean fluorescence intensity was normalized against that of the untreated cells (assigned a value of 1) to compare relative nuclease efficiency of p1 and p3 in live bacteria. *, $P<0.05$; **, $P<0.01$; and $^{\#}$, $P<0.05$ compared to untreated control.

Synergy between p1 and p3 is possible only in the absence of a robust DNA repair mechanisms

Having seen effective cidal activities of both p1 and p3 against planktonic cells, we next wanted to determine whether the two peptides interact synergistically and effect a stronger sterilizing effect in combination. In a physiological setting, both p1 and p3 are expressed simultaneously (albeit to varying levels), hence we postulated on a dynamic interplay between the two homologous peptides. We performed the checkerboard assay

to determine fractional inhibitory concentration (FIC) indices of p1 and p3 in combination. When tested against WT *E. coli*, we observed, at best additive interactions between the two peptides as evidence by FIC indices >0.50 (Figure 3.11A). Because we have been observing a strong implication of DNA damage to the activity of these peptides, we repeated the checkerboard assay using *E. coli* TD172 – a strain harboring a deletion in the DNA repair enzyme RecA. Not surprisingly, in the mutant strain we observed actual synergistic interactions between p1 and p3, with and FIC index of 0.38. Moreover, a combination of both peptides, clearly and visually prevent growth of the mutant *E. coli* in culture (Figure 3.11B).

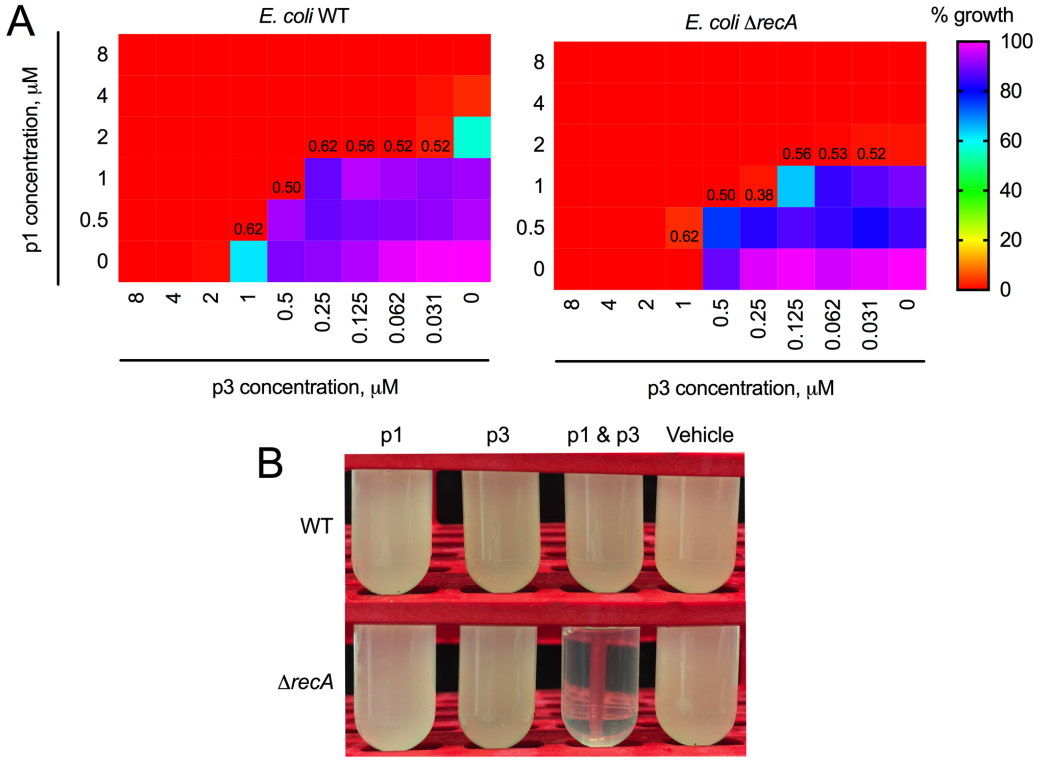

Figure 3.11. Synergy Between p1 and p3. (A) The checkerboard assay was used to assess synergy between p1 and p3 following overnight incubation with varying ratios of both peptides to either WT *E. coli* (left) or *recA* deletion mutant (right). Numbers at the boundary of the zone of inhibition and zone of growth represent FIC indices calculated

from the corresponding well at which they appear. (B) Sub-inhibitory concentrations of p1 and p3 either alone or in combination was used to treat *E. coli*. Growth was inhibited only when the *recA* mutant was treated with both peptides.

p1 and p3 act synergistically with Cu^{2+} to disperse preformed biofilms

Since p1 and p3 exhibit potency against planktonic cells, we sought to determine if they can inhibit *P. aeruginosa* PA01 growth in the context of biofilms. To determine the importance of copper-binding to this activity, we treated pre-formed biofilms (grown in rich medium) with peptides and their corresponding copper complexes in copper-free MOPS buffer (all subsequent assays hereon after were performed in MOPS buffer pH 7.40). We reasoned that by using a medium with defined components, the only source of copper for the peptides is the exogenously added Cu^{2+} or the bacterial bioavailable pool. We observed a modest inhibitory activity for both non-metallated pisicidin isoforms, effecting only an order of magnitude decrease in viable bacteria at 16 μM (Figure 3.12). When the peptides were pre-incubated with Cu^{2+}, a stronger biofilm clearance effect was observed which was more pronounced at higher concentrations. It is important to note that while *P. aeruginosa* biofilms are susceptible to the toxic effects of free Cu^{2+} (it was previously shown that PA01 biofilms are sensitive to 1 mM Cu^{2+}),[156] we observed a statistically significant (P<0.01) difference in the inhibitory activities of the metallated piscidins and Cu^{2+}. This indicates that piscidin and Cu^{2+} act synergistically and suggests that the toxicity of Cu-p1 and Cu-p3 is not a result of the biofilm's sensitivity to oxidative effects by Cu^{2+}. We further note that from 2 through 8 μM, Cu-p3 was more active than Cu-p1, mirroring the trends we observed in the *in vitro* (Figure 3.6) and *in cella* (Figure 3.10) DNA cleavage

experiments. This lead us to speculate an involvement of oxidative DNA damage to the anti-biofilm mechanism of copper-bound piscidins.

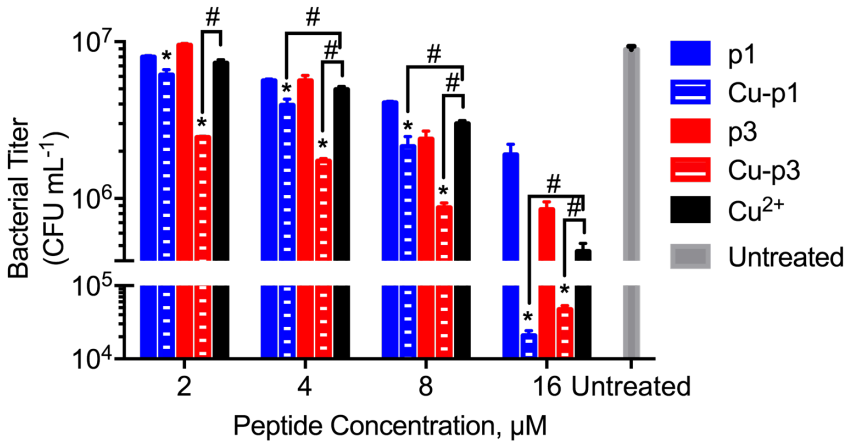

Figure 3.12. Synergy between Piscidin and Copper against Biofilms. 24-hour old *P. aeruginosa* PA01 biofilms were treated with piscidins at the indicated concentrations for 3 hours followed by CFU enumeration. *, $P<0.05$ compared to the corresponding non-metallated peptide; #, $P<0.01$. *Experiment performed by Dr. Ali Adem Bahar and Dr. Dacheng Ren (Syracuse).*

Cleavage of biofilm extracellular matrix occurs during piscidin treatment

The biofilm extracellular matrix is composed of a multitude of secreted biomolecules that mostly serve structural and signaling functions.[157] Studies show that extracellular DNA (eDNA) in biofilms function in strengthening the matrix and as such are necessary for biofilm formation.[158] Therefore, eDNA represents an important point of attack for anti-biofilm agents, especially the ones that have nuclease activity. We treated 24-hour old *P. aeruginosa* PA01 biofilms with p1 and p3 with and without pre-incubation with Cu^{2+}, extracted the biofilm eDNA, and characterized it using electrophoresis. Untreated biofilms contained eDNA of ~11 kbp in length (Figure 3.13), far from the size of the PA01 genomic DNA (6.3 Mbp)[159] confirming no intracellular DNA contamination in

the assay. Piscidin treatment of the biofilms resulted in eDNA cleavage as evidenced by the smearing pattern in the treated lanes. Our results show that naïve p1 and p3 cleave eDNA to similar extents in a dose-dependent manner. Because nuclease activity is a phenotype expected only if the peptides are metallated, our results also suggest that p1 and p3 were able to sequester copper from the biofilm's bioavailable pool. Indeed, the exopolysaccharide (EPS) matrix of *P. aeruginosa* biofilms was shown to retain Cu^{2+} and that a similar metal-sequestration phenotype protected *Erwinia amylovora* biofilms from copper stress.[160, 161] In this context, the EPS may very well be the copper source for p1 and p3. When Cu^{2+} is added, it is apparent that Cu-p3 cleaved eDNA more efficiently than Cu-p1. Because the trends we observed for the eDNA cleavage parallel the potency trends in our biofilm inhibition assay (Figure 3.12), we believe that eDNA cleavage plays a major role in the action of p1 and p3 against biofilms – a hypothesis supported by the demonstration that DNAse I effectively dispersed 60-hour old PA01 biofilms.[158] Since other biomolecules in the biofilm extracellular matrix are potentially susceptible to oxidative attack, we cannot discount other pathways leading to biofilm growth inhibition without exhaustive investigation.

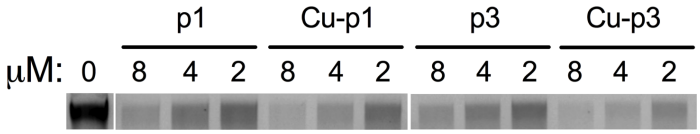

Figure 3.13. Biofilm eDNA Cleavage by Piscidins. Electrophoretic characterization of cleavage of biofilm extracellular DNA (eDNA) following exposure to peptides at the indicates concentrations. MW of eDNA isolated ~11 kDa.

Only the copper complex of p3 is bactericidal against P. aeruginosa persisters

Persisters are a subpopulation of transiently antibiotic-tolerant bacteria that are often the cause of recurring infections. Although target recognition is not abolished, a lack of downstream effects due to the metabolic idleness of persister cells renders current antibiotics less effective.[162] Recent studies showed efficient persister cell eradication via ROS production by conventional anti-TB drugs.[163] It has also been suggested that multi-hit agents that can damage DNA can be potentially cytotoxic to persisters.[162] For this reason, we tested the activity of p1, p3, and their corresponding copper complexes against *P. aeruginosa* PA01 persisters. We found that naïve p1 and p3 have moderate bactericidal activity against persisters, reaching a maximum of 1 log of reduction in viability at 16 μM (Figure 3.14). While several studies have reported different Cu^{2+} MIC values against *P. aeruginosa* persisters ranging from low micromolar[164] to millimolar[160] values, in our hands, they succumbed to ≥4 μM of the metal. Across all concentrations, we observed a similar activity between free Cu^{2+} and Cu-p1, suggesting that Cu-p1 toxicity has very likely, the same oxidative effect on PA01 as cupric ion. On the contrary, Cu-p3 exhibited a stronger bactericidal effect than Cu^{2+} alone, indicating that p3 is synergistic with the metal in eradicating persisters. Once again, it was evident that Cu-p3 was more active than Cu-p1 across all concentrations, echoing the trends we have been observing thus far, leading us to wonder whether DNA damage has a role in piscidin-induced persister cell death.

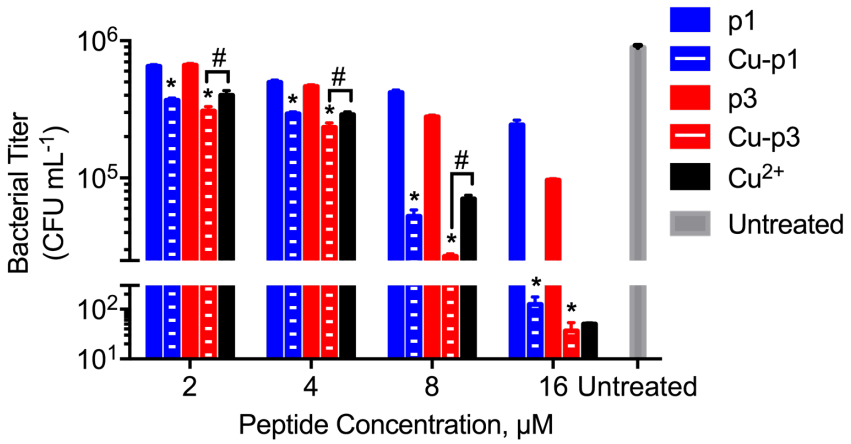

Figure 3.14. Synergy between Piscidin and Copper against Persister Cells. *P. aeruginosa* PA01 persisters were treated with the indicated concentrations of peptides for 3 hours prior to CFU enumeration. *, P<0.01 compared to corresponding non-metallated peptide; #, P<0.05. *Experiment performed by Dr. Ali Adem Bahar and Dr. Dacheng Ren (Syracuse).*

Cu-p1 and Cu-p3 trigger the SOS response in E. coli persisters

Exposure to DNA damaging agents lead to the induction of the SOS response. Having shown that Cu-p3 eradicates PA01 persisters, we set out to determine whether DNA damage is part of its bactericidal mechanism. For this purpose, we used the GFP fluorescence of the E. coli reporter strain AT15[165] (Δ*attλ*::*sulA*pΩ*gfp-mut2* Tet^R) as a direct readout of the SOS response. We exposed *E. coli* AT15 persisters to varying concentrations of p1, p3 and their corresponding Cu^{2+} complex for 2 hours and then counterstained the cells with propidium iodide (PI). This set-up allowed us to monitor the number of dead cells bearing a damaged DNA by comparing the levels of doubly fluorescent cells, that is, both GFP and PI positive cells. Our treatments resulted in a significant increase in GFP(+), PI(+) cells (Q2 in the scatter plots of Figure 3.15A). At concentrations greater than 1 μM, we observed an increase in GFP(+), PI(+) cells upon

metallation of both p1 and p3 (Figure 3.15B). While Cu-p1 and Cu^{2+} had similar potencies against PA01 persisters, induction of SOS response in *E. coli* persisters was significantly smaller during Cu^{2+} treatment compared to Cu-p1. This disparity likely arises from differences in copper-homeostasis pathways[67] and in the SOS response[166] between the different bacteria used. The strong SOS response following Cu-p1 and Cu-p3 treatment suggests that their oxidative DNA cleavage activity is playing a role in *E. coli* persister cell death. In addition, p3 also elicited a strong SOS response suggesting two possibilities; that p3 was able to scavenge Cu^{2+} and cause direct DNA cleavage; or, that p3 bound strongly to genomic DNA in the non-metallated form eliciting SOS response as observed for the non-DNA cleaving fluoroquinolones.[167] Indeed, our MD simulation suggests that the binary complex between piscidin and DNA is intermediary to the more stable aggregated form (Figure 3.4). It is therefore possible that p3 can non-covalently "crosslink" DNA strands when they condense to form aggregates which ultimately leads to induction of the SOS response. Finally, we note that there are no significant differences in terms of GFP(-), PI(+) cells (dead cells without DNA damage, Q1) between naïve and metallated piscidin (Figure 3.15B), suggesting that persister cell death pathways induced by p1 and p3 that are independent of oxidative DNA damage is not a function of copper binding.

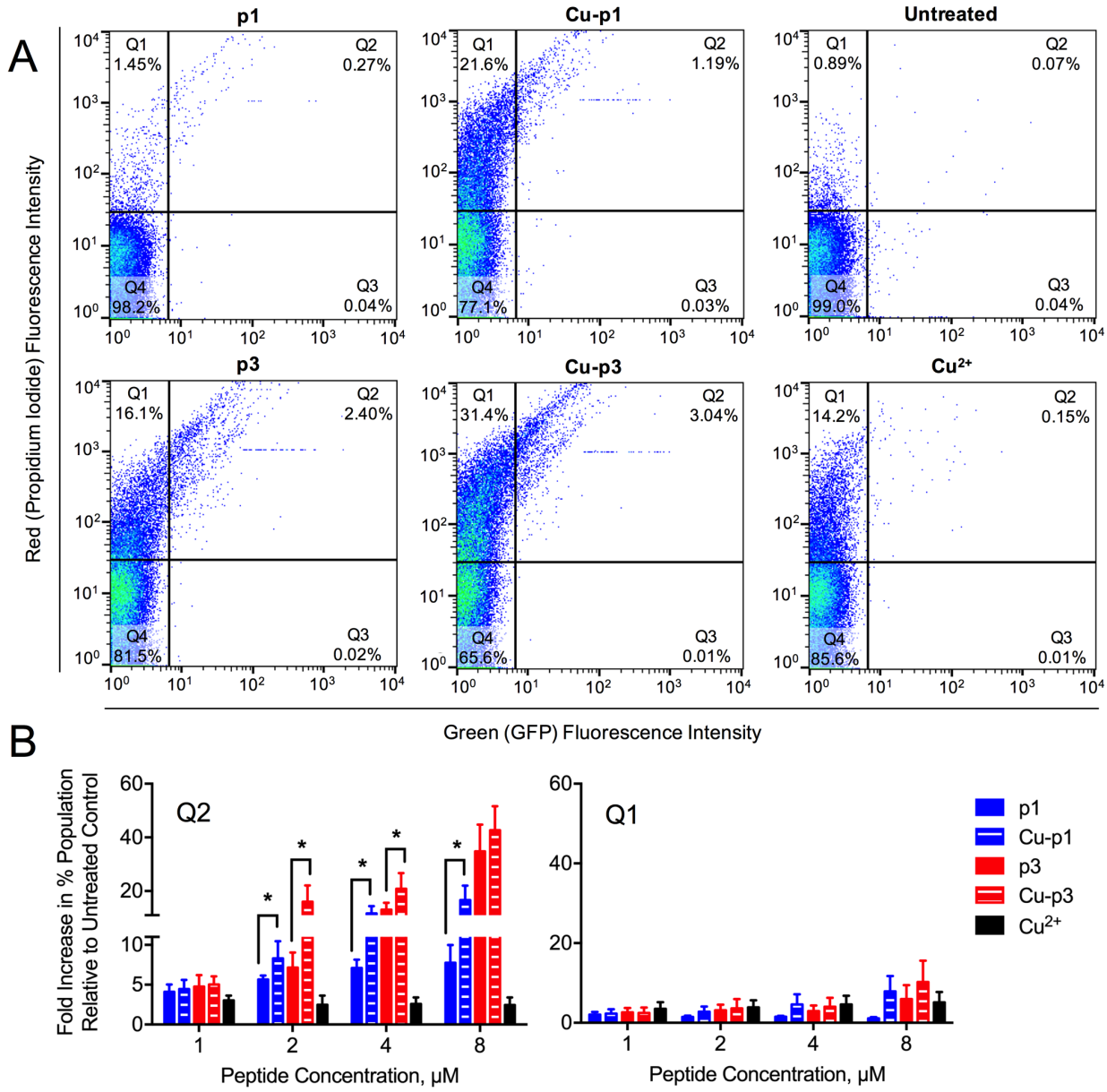

Figure 3.15. Induction of SOS Response in *E. coli* Persisters by Piscidins. (A) Representative scatter plots from flow cytometric analysis of *E. coli* AT15 persisters treated with piscidins and stained with propidium iodide. Expression of GFP is a readout for DNA damage, and influx of PI is a measure of cell death. (B) Quantitative analysis of the increase in doubly dead cells bearing damaged DNA (Q2, left) or dead cells without DNA damage (Q1, right) following *E. coli* AT15 persisters treatment with the indicated peptide. *, $P<0.05$.

Discussion

Thousands of AMPs have been isolated and their activity against bacteria has been described, but the majority of the literature focuses on their membranolytic activity. Even though several AMPs have been demonstrated to be non-membranolytic, a detailed description of AMP-induced cell death is usually lacking. Non-membrane active AMPs have been shown to bind to intracellular targets, but so far, none have been shown to covalently damage their binding partners. In this chapter, we illustrate the first demonstration of a nuclease activity for the natural AMPs, p1 and p3, as a function of copper binding, and how their relative activities translate to their bactericidal action against bacteria.

Here, we show that p1 and p3 form strong interactions with DNA *in vitro* and that this interaction is not disrupted upon metallation of the peptides as their N-terminal domain is ordered irrespective of the presence of copper. This is interesting from a biophysical standpoint because it shows that DNA allows piscidin to adopt a conformation that is poised to accommodate the metal and is conducive for the nuclease function it has to perform. Furthermore, we studied p1 and p3's DNA binding with atomic resolution and show that Arg7 and Arg14 in p3 engages in more hydrogen bonding interactions with DNA than Arg7 and Lys14 in p1, reasonably explaining the higher DNA affinity of p3.

Cu-p1 is a stronger oxidizing agent, however, our *in vitro* DNA cleavage results show that the reaction with Cu-p3 has a larger rate constant. We believe that the stronger DNA binding by p3, compensates for the small edge in free energy of oxidation that Cu-p1 affords from a slightly more positive E°, leading to a more effective nuclease activity for p3. Indeed, in all biological contexts tested in this study, p3 (or Cu-p3) was superior to

p1 (or Cu-p1) in cleaving DNA. The trend in nuclease activity mirrored the potency of p1 and p3 against bacteria and biofilms, suggesting that oxidative DNA cleavage plays a determining role in the bactericidal mechanism of p3. Since p1 and p3 have identical MICs against a large number of bacteria, a compensatory mechanism that p3 relies on to make up for its weaker membranolytic effect have been previously hypothesized.[146] The stronger nuclease activity by p3 may very well be the supplemental mode of attack that p3 uses to "level-off" its potency with p1.

Comparing p1 and p3 according to their relative ability to target the phosphate containing biomolecules, DNA and phospholipids, it becomes apparent that p1 is more membrane-active, whereas p3 is more DNA-active.[146] While at first glance, contrasting effects towards these potential targets maybe counterproductive in the context of homologous peptides, one has to wonder whether a functional complementarity explains the success of homologous AMP pairs against pathogens. Here, we strengthen this notion by showing that p1 and p3 have complementary growth inhibition rates. It is logical for a highly membrane active AMP, like p1, to be able to sterilize a culture rapidly because of the accessibility of the membrane as its main target. The resumption of growth after 2 hours in p1 + TTM, however, suggests that p1 finds copper in the cellular environment and utilizes a copper-dependent pathway, independent of membrane disruption, leading to sustained cell death, possibly because the more versatile mechanism of action of Cu-p1 relative to naïve p1 is more effective at sensitizing bacteria in the long term. On the other hand, acting on the DNA not only requires translocation across membranes, but also circumventing the redundant DNA damage repair pathways. It is therefore sensible that p3, which has stronger effects than p1 on DNA, exhibits a slower killing kinetics.

Removal of copper from p3 (and by extension, loss of its nuclease activity) resulted in attenuation of p3's bactericidal action, further solidifying the idea that oxidative DNA damage is central to p3's antimicrobial mechanism. Collectively, our results suggest that while Cu-p1 exhibits nuclease activity, it may not be its primary mode of attack simply because p1 is highly membranolytic, and that bacterial DNA is much less accessible than the membrane. The alternative mode of attack we propose here highlights the promiscuity of p1 and p3 (and of other α-helical AMPs) for various targets, and underpins the challenge of generating a detailed mechanistic account of AMP-induced bacterial death. We further note that this apparent synergy between copper and both piscidin isoforms have been previously observed in piscidin 2 (FFHHIFRGIVHVGKTIHKLVTG), which differs from p1 only through a conservative substitution at position 18, against the fish parasites *Saprolegnia* and *Tetrahymena*.[168] It was reasoned that since both agents are membrane active, their combination resulted in a synergistic effect. We believe that the copper-binding ability of p2, which affords the peptide oxidative capabilities on critical cellular components such as the membrane and DNA, logically explains the observed synergy.

Since the proposed nuclease activity by p1 and p3 is imparted by their metal co-factor, the copper sources of the peptides need to be addressed. We reasoned that the growth medium or the bacteria themselves contain enough bioavailable and exchangeable copper for p1 or p3 to sequester. In *E. coli*, there is an estimated 18 μM of cell-associated copper.[169] Although the reducing environment of the cytosol favors Cu(I), the presence of multicopper oxidases – that act to detoxify Cu(I) and convert it to Cu(II) – in several bacteria,[51, 69] likely generates a pool of exchangeable Cu(II), the preferred

oxidation state of the ATCUN motif. While relying solely on intrinsic copper reserves may not saturate the peptides with the metal, the fact that ROS formation by the Cu-ATCUN complexes is catalytic, suggests that a small amount of metallated piscidin may be sufficient to give rise to the observed nuclease activity. However, this still begs the question: Are p1 and p3 expressed in nature in their metallated form? First, genomic information indicates that piscidins are expressed as pre-propeptides that need to be proteolytically cleaved to liberate their active form.[135] Second, piscidins were originally isolated in mast cells[134] and were later found to be stored in granules.[170] It is known that both proteolysis and trafficking to cytoplasmic vesicles involve the trans-Golgi network, an organelle that houses the copper-transporters ATP7A and 7B which metallate newly synthesized cuproenzymes.[171] Therefore, the fundamental processes that act to ensure proper piscidin expression and localization place these peptides in copper-rich sites of the cell. For this reason, we propose that both p1 and p3 are likely expressed as metallopeptides postranscriptionally.

Finally, because of the ability of mast cells and acidophilic granulocytes to circulate systemically, piscidins were proposed to be involved in the non-specific killing of both extracellular (via mast cell degranulation) and intracellular (following phagocytosis) microbes.[170] Indeed, previous immunolocalization studies showed a high p1, p2, and p3 expression near the luminal surface of several species of teleost fish, and that p1 was highly expressed in epithelial cells of the Atlantic cod.[140] These surfaces are lined with a protective layer of mucous which can support bacterial growth.[172] It is therefore logical to express potent and broad-spectrum piscidins at regions that contact pathogens more often. While expression of all piscidin isoforms may be redundant, the inherent viscosity

of the mucous might prevent efficient dispersal of these peptides. Therefore, even though the pathogens encounter a lower effective piscidin concentration, their combinations might lead to synergistic effects – a phenotype promoted by a weak DNA repair system, which likely exists in some aquatic pathogens. We also show here that both Cu-p1 and Cu-p3 are active in eradicating biofilms, which are more relevant in the external surface of fish. Conversely, it was shown via qPCR that p3 RNA levels in the gills, intestines and spleen of hybrid striped bass is higher than those of p1,[135] and that an ortholog of p3 is highly expressed in the gills of the Nile tilapia.[138] These are highly vascularized organs in the fish and therefore, expression of the less hemolytic p3 would be advantageous. Moreover, in the context of an infection, bacteria that were able to infiltrate the connective tissue, evade the effects of immune cells and circulate through the bloodstream can cause recurring infections and persist within the fish. We find here that only Cu-p3 is active against bacterial persisters, making its expression in highly vascularized organs all the more profitable.

Methodology

Mass Spectrometry and Cyclic Voltammetry. To determine the stoichiometry of binding, mass spectrometry was employed. 100 μM of p1 or p3 was mixed with an equal volume of 100 μM Cu^{2+} and incubated at room temp for 30 mins. The mixture was diluted 1:500 with 1% formic acid in acetonitrile (ACN) and injected into an electrospray ionization-mass spectrometer. Resulting spectra was reported without further manipulation. To determine the standard reduction potential of the respective copper complexes, we used cyclic voltammetry. A 250 μM solution of p1 or p3 was prepared in 20 mM MOPS, 100 mM KCl pH 7.40, an equal volume of 225 μM Cu^{2+} was then added

(slight excess of peptide is present to ensure that no free Cu^{2+} exists) and incubated for 30 mins. The solution was transferred into a microcell for voltammetry using Ag/AgCl as reference electrode, glassy carbon as working electrode and a platinum mesh as counter electrode; a 100 mV/s scan rate over a 1.1 V range was used.

Molecular dynamics simulation of Piscidin and DNA conformations. (Experiment performed by Dr. Buyong Ma, Dr. Jun Zhao and Dr. Ruth Nussinov, NCI). The initial Piscidins 1 and 3 conformations were taken from NMR structures (PDB code 2ojm (piscidin 1) and 2mcx (piscidin 3)). The DNA structure were initially modeled using DNA response element E-box structure as template and mutating sequence to AAATACACTTTTGGT. With constraints of hydrogen bonds between base pairs, the DNA duplex structure was refined using MD simulations, as described below. The piscidin-DNA complex structures were searched using Haddock docking and additional manual adjustment to accommodate/optimize the charge interactions between piscidin and DNA. Six starting conformations with best initial energy were used to run MD simulations for p3-DNA complex, and three of them were replaced by p1 to compare their DNA interactions. The most stable conformation was selected from the MD simulations using protonated histidines based on free energies. Starting from this select conformation, a round of MD simulations was performed to test the structural stability of the peptide-DNA complex at 300 K. The simulations were stopped after confirming the convergence of the conformation in the MD simulations. For the unstable docking pose, the simulations were terminated when peptide moves out of docked binding pocket. Images were prepared in VMD and Pymol.

Molecular Dynamics Simulations. (Experiment performed by Dr. Buyong Ma, Dr. Jun Zhao and Dr. Ruth Nussinov, NCI). Two charged states for piscidins were simulated, with neutral and protonated histidine residues respectively. The simulation times for the isolated piscidins were 100 ns at 310 K. For the peptide-DNA complexes, the simulations were 100 ns for neutral histidine simulation and 30 ns for protonated histidines in the complexes. MD simulations of the solvated variant models were performed in NPT ensemble using the NAMD program[173] with the CHARMM36 force-field. The models were explicitly solvated with TIP3P water molecules,[174, 175] with a minimum distance of 10 Å from any edge of the box to any protein atom. Sodium Chloride ions were added at random locations to neutralize the peptide charge and to maintain the ionic strength at 150 mM salt concentrations. The Langevin piston method[173, 176, 177] with a decay period of 100 fs, and a damping time of 50 fs was used to maintain a constant pressure of 1 atm. The temperature (300 K) was controlled by Langevin thermostat with a damping coefficient of 10 ps^{-1}.[173] The short-range van der Waals (VDW) interactions were calculated using the switching function, with a twin range cutoff of 10.0 and 12.0 Å. Long-range electrostatic interactions were calculated using the particle mesh Ewald method with a cut-off of 12.0 Å for all simulations.[178, 179] The equations of motion were integrated using the leapfrog integrator with a step of 2 fs. The hydrogen atoms were constrained to the equilibrium bond using the SHAKE algorithm.[180] To obtain the relative structural stability of the variant models, the trajectories were first extracted from the explicit MD simulation excluding water molecules. The solvation energies of all systems were calculated using the Generalized Born Method with Molecular Volume (GBMV).[181, 182] In the GBMV calculations, the dielectric constant of water was set to 80.0. The hydrophobic

solvent-accessible surface area (SASA) term factor was set to 0.00592 kcal/mol·Å2. Each variant is minimized 500 cycles and the conformation energy was evaluated by grid-based GBMV.

Nuclear Magnetic Resonance. (Experiments performed by Prof. Myriam L. Cotten, College of William and Mary and Dr. Riquiang Fu, NHMFL). *Solution NMR:* Solution NMR titration of p3 with Ni^{2+} was achieved using a buffered solution of either $^{15}N_3$-His3 p1 or $^{15}N_3$-His3 p3 with a nickel chloride aqueous solution (Fluka). P3 was dissolved at 0.50 mM in Bis-Tris (10 mM, pH 6.8) and aliquots of nickel chloride were added to achieve specific peptide to nickel molar ratios. Progress of the titrations was monitored using Heteronuclear Multiple Quantum Coherence (HMQC) solution NMR experiments previously established.[183, 184] The experiments were peformed at the Rensselaer Polytechnic Institute (Troy, NY) on 800 and 600 MHz Bruker instruments fitted with cryoprobes. *Solid-state NMR*: Solid-state samples were made as previously described (14), with the exception that the peptide (about 2-3 mg) was titrated with an equimolar amount of Ni^{2+} prior to binding to DNA. The sequence of the duplex DNA was AAATACACTTTTGGT, as used in the molecular dynamics simulations. Upon addition of the peptide to the DNA, aggregation occurred, allowing us to collect hydrated peptide-DNA complex for solid-state NMR. The NMR experiments were performed on a midbore 800 MHz magnet equipped with a Bruker Avance III console and fitted with a 3.2 mm low-E triple-resonance biosolids MAS probe at the National High Magnetic Field Laboratory (NHMFL). Experimental conditions for the NMR experiments were as previously published.[146] Briefly, for each dephasing time (i.e., a multiple of rotor periods), two sets of data were recorded: one without the train of ^{15}N 180° pulses and one with the train of

pulses, corresponding to the ^{13}C signals without (S_0) and with (S) ^{15}N dephasing, respectively. We collected 10,240 to 30,720 transients depending on the dephasing time. Since the difference ΔS ($S-S_0$) over S_0 depends exclusively on the $^{13}C-^{15}N$ dipolar coupling, we used a MATLAB program to fit the $\Delta S/S_0$ ratio as a function of the dephasing time, and obtained the internuclear $^{13}C/^{15}N$ distance. Additional details about fitting the data and obtaining error bars were previously published.[146]

In vitro DNA cleavage Assay. The cleavage reactions consisted of 10 μM base pair pUC19, 100 nM Cu-peptide (or Cu^{2+}), 1 mM sodium ascorbate, and 1 mM H_2O_2 in 20 mM HEPES, 100 mM NaCl pH 7.40. Reactions were run at room temperature for the indicated time points where 10 μL was withdrawn. The reactions were stopped using 3X loading dye containing 1 mM EDTA. The samples were loaded onto a 1% agarose gel containing ethidium bromide and ran for 60 mins at 100 V. The gels were imaged using a Bio-Rad GelDoc XR+ imager and the bands were quantified using the accompanying Image Lab 5.0 software. Due to its diminished capacity to intercalator ethidium bromide, the intensity of the bands corresponding to the supercoiled form were multiplied by 1.47. Data shown represent Mean ± SEM obtained from three independent trials. The n_1/n_2 values were calculated using equations (1) and (2) from the Poisson distribution and Freifelder-Trumbo equation where f(I) and f(III) are the fraction of supercoiled and linearized plasmid remaining per time point.

$$f(III)= n_2\, e^{(-n_2)} \quad (1)$$

$$f(I)= e^{(-(n_1+n_2))} \quad (2)$$

Antimicrobial Assay and Time-Kill Kinetics. Antimicrobial susceptibility testing were done using the broth microdilution method as suggested by Hancock. Gram positive

Staphylococcus aureus (ATCC 25923); Gram negatives *Escherichia coli* (MG1655, TD172 – ΔrecA), and *Pseudomonas aeruginosa* (PAO1) were grown in Mueller-Hinton Broth (MHB, Difco) until mid-log phase for 3-5 hrs. Peptide stock solutions were diluted in PBS (Gibco) pH 7.40, 50 µL two-fold serial dilutions were placed on a sterile 96-well poplypropylene plate (Greiner). To each well, 50 µL of a bacterial suspension was added resulting to a final inoculum of $5x10^5$ CFU/mL per well. Plates were incubated at 37°C for 18-20 hrs. Minimum Inhibitory Concentration (MIC) was defined as the concentration that prevented visual growth of bacteria. MICs reported are the mode obtained from three independent trials. For time-kill experiments, 350 µL of peptide at 2X the MIC was mixed with bacteria to yield the same inoculum density as the antimicrobial assay. Every time point, 10 µL was withdrawn and diluted 1000-fold. Then 100 µL of either the 1:1000 or the 1:100 dilution was plated on LB agar plates. Colonies were counted manually after overnight incubation. Curves represent data obtained from two independent trials done in duplicates.

In cella DNA damage Assay. The Terminal deoxyribonucleotidyl transferase (TdT)-mediated dUTP Nick End Labeling (TUNEL) assay was used to assess extent of DNA damage in live *E. coli*. A 350 µL aliquot of a 10^8 CFU/mL E. coli culture was mixed with an equal volume of the peptides at 2X and 4X its MIC and incubated for 2 hrs. The cells were pelleted and washed twice with ice-cold PBS. The cells were then fixed with 4% paraformaldehyde for 30 mins, washed, and permeabilized with 0.1% triton X-100 in 0.1% sodium citrate for 2 mins. The cells were then pelleted and resuspended in 1X TUNEL reaction mixture (1 part TdT enzyme, 9 parts label solution; Roche Molecular Biochemicals, Indianapolis, IN) and were incubated in the dark for 1 hr at 37°C. The cells

were then pelleted, washed twice with ice cold PBS and resuspended in PBS containing Propidium iodide for DNA staining. The green and red fluorescence of 100,000 cells were obtained using a BD FACSCalibur flow cytometer and data were analyzed using FlowJo v 10 software. Histograms are representative of three independent trials, and bars represent Mean ± SEM.

Determination of the copper source of p1 and p3. Single colonies of *E. coli* MG1655 was taken from a LB agar plate and were inoculated into MHB or minimal media, M9 supplemented with glucose. To encourage growth of bacteria in M9, cells were passaged thrice prior to being used in the experiment. This also ensured infinite dilution of copper that may have originated from the LB agar plate. Cells were grown in liquid medium to mid-log phase after which cells were harvested and washed in the corresponding growth medium they were treated in. A 350 μL, $5x10^5$ CFU/mL suspension was mixed with an equal volume of peptides (non-metallated or pre-incubated with equimolar concentration of Cu^{2+}) for 30 mins (for p1 and Cu-p1), 4 hrs (for p3 and Cu-p3) and 2 hrs (for the untreated controls). The incubation times were selected using the Time-Kill assay as a guideline and to make sure maximum phenotypic resolution. The cells were incubated at 37°C and diluted up to 1:1000. Then, 100 μL of each dilution were plated into LB agar plates and incubated overnight for colony enumeration. Bars represent data obtained from three trials done in duplicates.

Biofilm Inhibition and Biofilm eDNA Cleavage Assay. (Biofilm inhibition experiment performed by Dr. Ali Alem Bahar and Dr. Dacheng Ren, Syracuse University). An exponentially growing *P. aeruginosa* PAO1 culture was used to inoculate 25 mL of fresh LB broth to an OD_{600} of 0.05. Biofilms were grown in glass cover slips for 24 hrs at 37°C.

The cover slips were rinsed by dipping carefully in 20 mM MOPS buffer, pH 7.40, before transferring to a 10 mm sterile petri plate containing piscidin at varying concentrations. Following 3 hrs of incubation at 37°C, the coverslips were transferred into conical tubes containing 10 mL of MOPS buffer, sonicated for 4 mins (at 15 sec intervals), and vortexed. The cells were concentrated by centrifugation and resuspension in 100 µL of MOPS buffer. Four 10 µL portions (of each treatment) were then plated into separated LB agar plates, incubated overnight after which the colonies were counted manually. Bars represent data obtained from three independent trials. For the eDNA cleavage experiments, the same treatments were done, following an overnight incubation with the peptides, coverslips were transferred to conical tubes containing 20 mM Tris-HCl, 5 mM $CaCl_2$ buffer, pH 8.0 and vortexed for 1 min. the coverslips were removed and 5 µg/mL Proteinase K was added and incubated at 37°C for 1 hr. After which, the suspension was centrifuged at maximum speed for 10 mins (to remove planktonic cells and other debris) and the supernatant was collected. Qiagen spin columns were used to purify extracellular DNA, using the Qiagen wash buffer provided. The eDNA was eluted using 50 µL of sterile nanopure water. The DNA was quantified by nanodrop spectroscopy (A_{260}/A_{280} were all > 1.80) and a total of 150 µg of DNA was loaded into a 1% agarose gel containing 1X Sybr Green, ran at 150 V for 2 hrs. Data is representative of three trials done independently of each other.

Persister Cell Inhibition Assay. (Experiment performed by Dr. Ali Alem Bahar and Dr. Dacheng Ren, Syracuse University). An overnight *P. aeruginosa* PAO1 culture was treated with 200 µg/mL Ciprofloxacin for 3.5 hrs with shaking at 37°C to kill off non-persister cells. The culture was spun down and washed with MOPS buffer three times

before resuspending in MOPS buffer at 4°C. A total of 500 µL total volume containing the indicated peptide concentrations was used, and treatment was done for 3 hrs at 37°C with shaking. Aliquots were diluted in room temperature MOPS buffer and dilutions were plated in LB agar plates. After overnight incubation, colonies were counted manually. Bars represent data from three independent experiments done in triplicates.

Measurement of SOS response via Flow Cytometry. An exponentially growing culture of E. coli AT15 (a kind gift from Prof Kim Lewis, Northeastern University) was treated with 50 µg/mL of Ampicillin for 4 hrs at 37°C to kill non-persister cells. The culture was spun down and cells were washed three times with MOPS buffer before resuspending to an OD_{600} of 0.1. A total of 700 µL total volume was used for piscidin treatment at the indicated concentration. After 2 hrs of exposure to the peptides, the cells were spun down, washed twice, and resuspended in 15 µL of MOPS buffer containing 0.5 mg/mL of Propidium Iodide (PI). A 10 µL aliquot was used for flow cytometry analysis in a BD FACSCalibur cytometer, and fluorescence of 100,000 cells were measured. The gates were established using the Untreated control, and % populations were calculated (by FlowJo v 10) after applying the same gating parameters through all treatments. Bars represent data from three independent experiments.

Checkerboard Assay and Synergy Testing. A method analogous to MIC determinations was used to measure FIC indices. Two-fold serial dilutions of p3 (in MHB broth) was added to the columns of a sterile 96-well polypropylene plate (except the last column). Then 50 µL of two-fold serial dilutions of p1 (in MHB) was added to the rows of the plate (except the last row). The plate was then inoculated with a suspension of 10^6 CFU/mL of either *E. coli* MG1655 (WT) or *E. coli* TD172 (ΔrecA) and incubated overnight

at 37°C. The growth was determined by OD_{600} measurements using a plate reader and absorbance values were converted to % growth values by dividing it with the untreated well. The heat map represents Mean ± SEM obtained from three trials done in duplicates. For visual assessment of synergy, a 3mL culture of $5x10^5$ CFU/mL of bacteria was treated with ½ MIC of p1 or p3 either alone or in combination. The culture tubes were incubated in a shaker at 37°C overnight and photographed.

Statistical Analysis. Data were analyzed for statistical differences using Graph-Pad Prism® v6.0 software. One-Way or Two-Way ANOVA was used to determine statistical significance and was set at $P < 0.05$.

Chapter References:

[1] Silphaduang, U., and Noga, E. J. (2001) Peptide antibiotics in mast cells of fish, *Nature 414*, 268-269.

[2] Salger, S. A., Cassady, K. R., Reading, B. J., and Noga, E. J. (2016) A Diverse Family of Host-Defense Peptides (Piscidins) Exhibit Specialized Anti-Bacterial and Anti-Protozoal Activities in Fishes, *PLoS One 11*, e0159423.

[3] Andrews, M., Battaglene, S., Cobcroft, J., Adams, M., Noga, E., and Nowak, B. (2010) Host response to the chondracanthid copepod Chondracanthus goldsmidi, a gill parasite of the striped trumpeter, Latris lineata (Forster), in Tasmania, *J Fish Dis 33*, 211-220.

[4] Dezfuli, B. S., Pironi, F., Giari, L., and Noga, E. J. (2010) Immunocytochemical localization of piscidin in mast cells of infected seabass gill, *Fish Shellfish Immunol 28*, 476-482.

[5] Peng, K. C., Lee, S. H., Hour, A. L., Pan, C. Y., Lee, L. H., and Chen, J. Y. (2012) Five different piscidins from Nile tilapia, Oreochromis niloticus: analysis of their expressions and biological functions, *PLoS One 7*, e50263.

[6] Silphaduang, U., Colorni, A., and Noga, E. J. (2006) Evidence for widespread distribution of piscidin antimicrobial peptides in teleost fish, *Dis Aquat Organ 72*, 241-252.

[7] Ruangsri, J., Fernandes, J. M., Rombout, J. H., Brinchmann, M. F., and Kiron, V. (2012) Ubiquitous presence of piscidin-1 in Atlantic cod as evidenced by immunolocalisation, *BMC Vet Res 8*, 46.

[8] Lee, E., Shin, A., Jeong, K. W., Jin, B., Jnawali, H. N., Shin, S., Shin, S. Y., and Kim, Y. (2014) Role of phenylalanine and valine10 residues in the antimicrobial activity and cytotoxicity of piscidin-1, *PLoS One 9*, e114453.

[9] Huang, H. N., Chan, Y. L., Hui, C. F., Wu, J. L., Wu, C. J., and Chen, J. Y. (2015) Use of tilapia piscidin 3 (TP3) to protect against MRSA infection in mice with skin injuries, *Oncotarget 6*, 12955-12969.

[10] Chen, W. F., Huang, S. Y., Liao, C. Y., Sung, C. S., Chen, J. Y., and Wen, Z. H. (2015) The use of the antimicrobial peptide piscidin (PCD)-1 as a novel anti-nociceptive agent, *Biomaterials 53*, 1-11.

[11] Perrin, B. S., Jr., Tian, Y., Fu, R., Grant, C. V., Chekmenev, E. Y., Wieczorek, W. E., Dao, A. E., Hayden, R. M., Burzynski, C. M., Venable, R. M., Sharma, M., Opella, S. J., Pastor, R. W., and Cotten, M. L. (2014) High-resolution structures and orientations of antimicrobial peptides piscidin 1 and piscidin 3 in fluid bilayers reveal tilting, kinking, and bilayer immersion, *J Am Chem Soc 136*, 3491-3504.

[12] Chekmenev, E. Y., Jones, S. M., Nikolayeva, Y. N., Vollmar, B. S., Wagner, T. J., Gor'kov, P. L., Brey, W. W., Manion, M. N., Daugherty, K. C., and Cotten, M. (2006) High-field NMR studies of molecular recognition and structure-function relationships in antimicrobial piscidins at the water-lipid bilayer interface, *J Am Chem Soc 128*, 5308-5309.

[13] Nicolas, P. (2009) Multifunctional host defense peptides: intracellular-targeting antimicrobial peptides, *FEBS J 276*, 6483-6496.

[14] Hayden, R. M., Goldberg, G. K., Ferguson, B. M., Schoeneck, M. W., Libardo, M. D., Mayeux, S. E., Shrestha, A., Bogardus, K. A., Hammer, J., Pryshchep, S., Lehman,

H. K., McCormick, M. L., Blazyk, J., Angeles-Boza, A. M., Fu, R., and Cotten, M. L. (2015) Complementary Effects of Host Defense Peptides Piscidin 1 and Piscidin 3 on DNA and Lipid Membranes: Biophysical Insights into Contrasting Biological Activities, *J Phys Chem B 119*, 15235-15246.

[15] Libardo, M. D. J., Gorbatyuk, V. Y., and Angeles-Boza, A. M. (2016) Central Role of the Copper-Binding Motif in the Complex Mechanism of Action of Ixosin: Enhancing Oxidative Damage and Promoting Synergy with Ixosin B, *ACS Infectious Diseases 2*, 71-81.

[16] Joyner, J. C., Reichfield, J., and Cowan, J. A. (2011) Factors influencing the DNA nuclease activity of iron, cobalt, nickel, and copper chelates, *J Am Chem Soc 133*, 15613-15626.

[17] Harford, C., and Sarkar, B. (1997) Amino Terminal Cu(II)- and Ni(II)-Binding (ATCUN) Motif of Proteins and Peptides: Metal Binding, DNA Cleavage, and Other Properties, *Acc Chem Res*, 123-130.

[18] Eshelman, M. R., Aldous, A. R., Neupane, K. P., and Kritzer, J. A. (2014) Solution structure of a designed cyclic peptide ligand for nickel and copper ions, *Tetrahedron 70*, 7651-7654.

[19] D. Freifelder, B. T. (1969) Matching of single-strand breaks to form double-strand breaks in DNA, *Biopolymers 7*, 681-693.

[20] Chekmenev, E. Y., Vollmar, B. S., Forseth, K. T., Manion, M. N., Jones, S. M., Wagner, T. J., Endicott, R. M., Kyriss, B. P., Homem, L. M., Pate, M., He, J., Raines, J., Gor'kov, P. L., Brey, W. W., Mitchell, D. J., Auman, A. J., Ellard-Ivey, M. J., Blazyk, J., and Cotten, M. (2006) Investigating molecular recognition and biological function at interfaces using piscidins, antimicrobial peptides from fish, *Biochim Biophys Acta 1758*, 1359-1372.

[21] Fernandez-Mazarrasa, C., Mazarrasa, O., Calvo, J., del Arco, A., and Martinez-Martinez, L. (2009) High concentrations of manganese in Mueller-Hinton agar increase MICs of tigecycline determined by Etest, *J Clin Microbiol 47*, 827-829.

[22] Helbig, K., Bleuel, C., Krauss, G. J., and Nies, D. H. (2008) Glutathione and transition-metal homeostasis in Escherichia coli, *J Bacteriol 190*, 5431-5438.

[23] Fung, D. K., Lau, W. Y., Chan, W. T., and Yan, A. (2013) Copper efflux is induced during anaerobic amino acid limitation in Escherichia coli to protect iron-sulfur cluster enzymes and biogenesis, *J Bacteriol 195*, 4556-4568.

[24] Brewer, G. J. (2009) Zinc and tetrathiomolybdate for the treatment of Wilson's disease and the potential efficacy of anticopper therapy in a wide variety of diseases, *Metallomics 1*, 199-206.

[25] White, S. H., Wimley, W. C., Ladokhin, A. S., and Hristova, K. (1998) Protein folding in membranes: determining energetics of peptide-bilayer interactions, *Methods Enzymol 295*, 62-87.

[26] Wimley, W. C., and White, S. H. (1996) Experimentally determined hydrophobicity scale for proteins at membrane interfaces, *Nat Struct Biol 3*, 842-848.

[27] Dwyer, D. J., Belenky, P. A., Yang, J. H., MacDonald, I. C., Martell, J. D., Takahashi, N., Chan, C. T., Lobritz, M. A., Braff, D., Schwarz, E. G., Ye, J. D., Pati, M., Vercruysse, M., Ralifo, P. S., Allison, K. R., Khalil, A. S., Ting, A. Y., Walker, G. C., and Collins, J. J. (2014) Antibiotics induce redox-related physiological alterations as part of their lethality, *Proc Natl Acad Sci U S A 111*, E2100-2109.

[28] Kohanski, M. A., Dwyer, D. J., Hayete, B., Lawrence, C. A., and Collins, J. J. (2007) A common mechanism of cellular death induced by bactericidal antibiotics, *Cell 130*, 797-810.
[29] Teitzel, G. M., and Parsek, M. R. (2003) Heavy metal resistance of biofilm and planktonic Pseudomonas aeruginosa, *Appl Environ Microbiol 69*, 2313-2320.
[30] Flemming, H. C., Wingender, J., Szewzyk, U., Steinberg, P., Rice, S. A., and Kjelleberg, S. (2016) Biofilms: an emergent form of bacterial life, *Nat Rev Microbiol 14*, 563-575.
[31] Whitchurch, C. B., Tolker-Nielsen, T., Ragas, P. C., and Mattick, J. S. (2002) Extracellular DNA required for bacterial biofilm formation, *Science 295*, 1487.
[32] Stover, C. K., Pham, X. Q., Erwin, A. L., Mizoguchi, S. D., Warrener, P., Hickey, M. J., Brinkman, F. S., Hufnagle, W. O., Kowalik, D. J., Lagrou, M., Garber, R. L., Goltry, L., Tolentino, E., Westbrock-Wadman, S., Yuan, Y., Brody, L. L., Coulter, S. N., Folger, K. R., Kas, A., Larbig, K., Lim, R., Smith, K., Spencer, D., Wong, G. K., Wu, Z., Paulsen, I. T., Reizer, J., Saier, M. H., Hancock, R. E., Lory, S., and Olson, M. V. (2000) Complete genome sequence of Pseudomonas aeruginosa PAO1, an opportunistic pathogen, *Nature 406*, 959-964.
[33] Harrison, J. J., Turner, R. J., and Ceri, H. (2005) Persister cells, the biofilm matrix and tolerance to metal cations in biofilm and planktonic Pseudomonas aeruginosa, *Environ Microbiol 7*, 981-994.
[34] Ordax, M., Marco-Noales, E., Lopez, M. M., and Biosca, E. G. (2010) Exopolysaccharides favor the survival of Erwinia amylovora under copper stress through different strategies, *Res Microbiol 161*, 549-555.
[35] Lewis, K. (2010) Persister cells, *Annu Rev Microbiol 64*, 357-372.
[36] Grant, S. S., Kaufmann, B. B., Chand, N. S., Haseley, N., and Hung, D. T. (2012) Eradication of bacterial persisters with antibiotic-generated hydroxyl radicals, *Proc Natl Acad Sci U S A 109*, 12147-12152.
[37] Huang, H. I., Shih, H. Y., Lee, C. M., Yang, T. C., Lay, J. J., and Lin, Y. E. (2008) In vitro efficacy of copper and silver ions in eradicating Pseudomonas aeruginosa, Stenotrophomonas maltophilia and Acinetobacter baumannii: implications for on-site disinfection for hospital infection control, *Water Res 42*, 73-80.
[38] Theodore, A., Lewis, K., and Vulic, M. (2013) Tolerance of Escherichia coli to fluoroquinolone antibiotics depends on specific components of the SOS response pathway, *Genetics 195*, 1265-1276.
[39] Arguello, J. M., Raimunda, D., and Padilla-Benavides, T. (2013) Mechanisms of copper homeostasis in bacteria, *Front Cell Infect Microbiol 3*, 73.
[40] Cirz, R. T., O'Neill, B. M., Hammond, J. A., Head, S. R., and Romesberg, F. E. (2006) Defining the Pseudomonas aeruginosa SOS response and its role in the global response to the antibiotic ciprofloxacin, *J Bacteriol 188*, 7101-7110.
[41] Qin, T. T., Kang, H. Q., Ma, P., Li, P. P., Huang, L. Y., and Gu, B. (2015) SOS response and its regulation on the fluoroquinolone resistance, *Ann Transl Med 3*, 358.
[42] Zahran, E., and Noga, E. J. (2010) Evidence for synergism of the antimicrobial peptide piscidin 2 with antiparasitic and antioomycete drugs, *J Fish Dis 33*, 995-1003.

[43] Nies, D. H. (2007) Bacterial Transition metal Homeostasis, In *Molecular Biology of Heavy Metals* (Nies, D. H., and Silver, S., Eds.), pp 117-142, Springer-Verlag, Heidelberg, Germany.
[44] Fu, Y., Chang, F. M., and Giedroc, D. P. (2014) Copper transport and trafficking at the host-bacterial pathogen interface, *Acc Chem Res 47*, 3605-3613.
[45] Finney, L. A., and O'Halloran, T. V. (2003) Transition metal speciation in the cell: insights from the chemistry of metal ion receptors, *Science 300*, 931-936.
[46] Mulero, I., Noga, E. J., Meseguer, J., Garcia-Ayala, A., and Mulero, V. (2008) The antimicrobial peptides piscidins are stored in the granules of professional phagocytic granulocytes of fish and are delivered to the bacteria-containing phagosome upon phagocytosis, *Dev Comp Immunol 32*, 1531-1538.
[47] Polishchuk, R., and Lutsenko, S. (2013) Golgi in copper homeostasis: a view from the membrane trafficking field, *Histochem Cell Biol 140*, 285-295.
[48] Rakers, S., Niklasson, L., Steinhagen, D., Kruse, C., Schauber, J., Sundell, K., and Paus, R. (2013) Antimicrobial peptides (AMPs) from fish epidermis: perspectives for investigative dermatology, *J Invest Dermatol 133*, 1140-1149.
[49] Kale, L., Skeel, R., Bhandarkar, M., Brunner, R., Gursoy, A., Krawetz, N., Phillips, J., Shinozaki, A., Varadarajan, K., and Schulten, K. (1999) NAMD2: Greater scalability for parallel molecular dynamics, *J Comput Phys 151*, 283-312.
[50] Mahoney, M. W., and Jorgensen, W. L. (2000) A five-site model for liquid water and the reproduction of the density anomaly by rigid, nonpolarizable potential functions, *Journal of Chemical Physics 112*, 8910-8922.
[51] Jorgensen, W. L., Chandrasekhar, J., Madura, J. D., Impey, R. W., and Klein, M. L. (1983) Comparison of Simple Potential Functions for Simulating Liquid Water, *Journal of Chemical Physics 79*, 926-935.
[52] Martyna, G. J., Tobias, D. J., and Klein, M. L. (1994) Constant-Pressure Molecular-Dynamics Algorithms, *J Chem Phys 101*, 4177-4189.
[53] Feller, S. E., Zhang, Y. H., Pastor, R. W., and Brooks, B. R. (1995) Constant-Pressure Molecular-Dynamics Simulation - the Langevin Piston Method, *J Chem Phys 103*, 4613-4621.
[54] Darden, T., York, D., and Pedersen, L. (1993) Particle Mesh Ewald - an N.Log(N) Method for Ewald Sums in Large Systems, *Journal of Chemical Physics 98*, 10089-10092.
[55] Essmann, U., Perera, L., Berkowitz, M. L., Darden, T., Lee, H., and Pedersen, L. G. (1995) A Smooth Particle Mesh Ewald Method, *Journal of Chemical Physics 103*, 8577-8593.
[56] Ryckaert, J. P., Ciccotti, G., and Berendsen, H. J. C. (1977) Numerical-Integration of Cartesian Equations of Motion of a System with Constraints - Molecular-Dynamics of N-Alkanes, *J Comput Phys 23*, 327-341.
[57] Lee, M. S., Feig, M., Salsbury, F. R., and Brooks, C. L. (2003) New analytic approximation to the standard molecular volume definition and its application to generalized born calculations, *J Comput Chem 24*, 1348-1356.
[58] Lee, M. S., Salsbury, F. R., and Brooks, C. L. (2002) Novel generalized Born methods, *J Chem Phys 116*, 10606-10614.

[59] Dawson, J. E., Seckute, J., De, S., Schueler, S. A., Oswald, A. B., and Nicholson, L. K. (2009) Elucidation of a pH-folding switch in the Pseudomonas syringae effector protein AvrPto, *Proc Natl Acad Sci U S A 106*, 8543-8548.
[60] Pelton, J. G., Torchia, D. A., Meadow, N. D., and Roseman, S. (1993) Tautomeric states of the active-site histidines of phosphorylated and unphosphorylated IIIGlc, a signal-transducing protein from Escherichia coli, using two-dimensional heteronuclear NMR techniques, *Protein Sci 2*, 543-558.

Chapter 4

The ATCUN Motif in General Antimicrobial Drug Development – Part I

ATCUN motif Conjugation to AMPs Results in a Gain-of-Function Phenotype Affording Membrane Lipid Peroxidation

Adapted entirely from:

Libardo, M.D.J., Cervantes, J.L., Salazar, J.C., Angeles-Boza, A.M.
ChemMedChem, **2014**, 9, 1892-1901

Libardo, M.D.J., Nagella, S., Lugo, A., Pierce, S., Angeles-Boza, A.M.
Biochem Biophys Res Comms, **2015**, 456, 446-451

Introduction

The rise of bacterial resistance against small-molecule antibiotics is a growing global health problem that has led to increased interest in the discovery of agents with a unique mode of action. Due to their broad-spectrum activity, antimicrobial peptides (AMPs) have arisen as a paradigm for the design of novel antibiotics. AMPs are a component of the innate immune system of many organisms, from bacteria and fungi to vertebrates, invertebrates and plants.[1, 6, 185] AMPs have membrane solubilizing, cell penetrating and DNA/RNA binding abilities.[7, 8] Because of their diverse mode of action, a large effort has been made to develop new classes of anti-infective agents based on AMPs.[6, 7] While some peptides have entered clinical trials, so far, no AMP-based antibiotics are available in the market right now. Work on the field continues to improve both efficacy and selectivity against microbes, and prolonging serum stability of peptides.[186, 187]

Recent evidence has shown that small molecule bactericidal antibiotics, apart from their canonical microbial targets, also stimulate the formation of deleterious hydroxyl radicals. The ROS induction occurs following collapse of the tricarboxylic acid cycle and subsequent destabilization of iron-sulfur clusters. This liberates free ferrous ions which catalyze the Fenton reaction, contributing to cell death. [154, 155, 188] While strong arguments exist against this observation,[189, 190] there is generally a consensus in the field that ROS do play a role in bacterial death by classical antibiotics due to confirmatory work by several research groups.[191, 192] A similar induction of ROS was observed for the AMP indolicidin, although it was postulated that the •OH radical source was distinct from that of bactericidal antibiotics.[193] In a related note, increasing ROS levels in bacteria either by

targeting the endogenous ROS-producing mechanism[194] or by using silver ions to directly form ROS,[195] have been shown to enhance the bactericidal action of antibiotics *in vitro* and *in vivo*. These studies suggest that synthesis of bactericidal agents with dual actions – microbial targeting and ROS formation – could lead to the development of clinically useful molecules.

Numerous peptide-small molecule conjugates have been synthesized to improve the efficacy of AMPs. Conjugates relevant to this work include amine-based metal binding groups,[196, 197] porphyrins,[198-200] and chromophores.[200-202] The latter two conjugates are dual acting in that they directly generate ROS in addition to their classical antibiotic action. The resulting ROS renders the bacteria more susceptible to the conjugates. Because of the ability of the ATCUN motif to directly produce ROS, it has also been used to develop dual-acting antimicrobials. Reports that came out at the same time as the work in this chapter was being reported have shown that addition of the ATCUN motif to AMPs do in fact result in higher potencies.[203-205] In this chapter, several ATCUN sequences were assayed for their ability to form ROS when bound to Cu^{2+} ions. The most active sequences were added at the amino-terminus of two AMPs with membrane permeabilizing ability – Anoplin (GLLKRIKTLL-NH_2) and the pro-apoptotic peptide (PAP, KLAKLAKKLAKLAK-NH_2).[206, 207] We found that addition of the metal-binding motif leads to a gain-of-function phenotype that affords the resulting conjugate a secondary oxidative mode of attack.

Results

Screening for a favorable rate of ROS formation in a small library of tripeptides

A 13-member ATCUN library was prepared by established methods using solid-phase peptide synthesis (SPPS) using standard Fmoc protocols. Most of these ATCUN sequences occur naturally in a variety of proteins (Table 4.1). We first assessed the ability of these ATCUN sequences to produce ROS after binding copper ions with an assay that measures the rate at which the Cu-ATCUN complexes undergo multiple turnover redox process (Table 4.1).[91] The rate at which reduced ascorbic acid is consumed was monitored to measure the turnover rate of the Cu-ATCUN complexes using either O_2 or H_2O_2 as co-reactant. Initial rates in the presence of H_2O_2 are higher than in its absence, a behavior that has been observed in other copper peptide complexes.[91] Cu-GGH and Cu-VIH gave the highest rates for ascorbic acid consumption under both conditions indicating rapid electrochemical turnover by these complexes. We next examined the rate at which hydroxyl radicals are formed via reaction with Rhodamine B.[117] In agreement with our ascorbic acid consumption assays, Cu-GGH and Cu-VIH were the most active complexes (Table 4.1). Taken together, our results indicate that GGH and VIH form ROS with the fastest kinetics.

Since the four most efficient catalysts for ROS formation were GGH > VIH > RTH > LKH, these sequences were selected for addition to the AMP sequences. Asp-Ala-His (DAH) showed slower rates of ROS formation in comparison to the four previously mentioned, thus, it was selected to serve as a low ROS-producing control sequence. These tripeptides were appended directly to the N-terminal of Anoplin and PAP without any amino acid linker. That is, GGH-Anoplin corresponds to GGHGLLKRIKTLL-NH_2.

Table 4.1. Summary of calculated rates for ROS formation by Cu-ATCUN complexes.

Complex	Source Protein	Initial Rate of Ascorbic Acid Consumption (μM/min)		Initial Rate of Hydroxyl Radical Formation (μM/min)	
		with H_2O_2	no H_2O_2	with H_2O_2	no H_2O_2
Cu-DAH	Human serum albumin	1.45 ± 0.07	0.20 ± 0.02	2.44 ± 0.12	0.13 ± 0.03
Cu-DMH	Neuromedin K	1.36 ± 0.02	0.16 ± 0.01	2.57 ± 0.29	0.22 ± 0.02
Cu-DSH	Histatin 5	1.31 ± 0.03	0.13 ± 0.01	2.02 ± 0.06	0.04 ± 0.005
Cu-DTH	Bovine serum albumin	2.89 ± 0.07	1.28 ± 0.06	2.39 ± 0.23	0.56 ± 0.04
Cu-EAH	Rat serum albumin	1.14 ± 0.04	0.12 ± 0.02	2.65 ± 0.06	0.47 ± 0.04
Cu-GGH	Simplest ATCUN	52.54 ± 0.76	19.35 ± 0.43	4.31 ± 0.27	0.92 ± 0.09
Cu-GKH	-	1.21 ± 0.09	0.13 ± 0.01	2.42 ± 0.12	0.19 ± 0.02
Cu-GNH	Neuromedin C	1.15 ± 0.04	0.10 ± 0.002	2.44 ± 0.04	0.07 ± 0.03
Cu-LKH	Xnf7	10.8 ± 0.27	4.52 ± 0.17	3.14 ± 0.14	0.69 ± 0.04
Cu-NGH	Met Lyase	1.29 ± 0.09	0.18 ± 0.01	1.81 ± 0.04	0.14 ± 0.01
Cu-RTH	Human protamine 2	13.12 ± 0.27	5.67 ± 0.20	2.72 ± 0.08	0.72 ± 0.06
Cu-SMH	Human TBX3	1.39 ± 0.04	0.11 ± 0.01	1.79 ± 0.04	0.07 ± 0.04
Cu-VIH	Designed	39.21 ± 1.08	15.5 ± 0.07	4.08 ± 0.10	0.90 ± 0.09
Cu^{2+} only	-	57.21 ± 0.81	20.03 ± 0.37	5.03 ± 0.43	0.98 ± 0.09
No Cu-XXH	-	1.13 ± 0.03	0.19 ± 0.02	0.10 ± 0.02	0.05 ± 0.003

Antimicrobial activity of the ATCUN-AMP conjugates

The efficacy of the ATCUN-AMPs was assessed by determining their Minimum Inhibitory Concentration (MIC) against four different bacterial strains: Gram-positive *Bacillus subtilis* and *Staphylococcus epidermidis* and Gram-negative *Escherichia coli* and *Enterobacter aerogenes*. Data obtained using standard antimicrobial susceptibility testing are shown in Table 4.2. The microbiological characterization showed that the ATCUN-AMPs were generally more effective against the Gram-positive bacteria used in this study. Incorporation of the ATCUN motif to Anoplin and PAP largely resulted in an increase of their activity, particularly when the ATCUN sequence was VIH. For instance, against *E. coli*, VIH-Anoplin was 8-times more active than the parent peptide. GGH was the second most active ATCUN sequence when bound to the membrane-active peptides Anoplin and PAP. Since the ATCUN-AMPs bind metal ions, we tested whether the addition of copper ions could affect its antimicrobial activity. When medium was supplemented with 32 μM Cu^{2+}, we did not observe a decrease in the activity of the peptides against *B. subtilis* and *E. coli* (Table X). These results suggest that this family of peptides do not induce starvation for copper ions.

Table 4.2. Antimicrobial Activity of ATCUN-conjugated AMPs.

Peptide	Minimum Inhibitory Concentration[a] (MIC), μM			
	B. subtilis	***S. epidermidis***	***E. coli***	***E. aerogenes***
Anoplin	4 (4)	8	16 (16)	>32
DAH-Anoplin	2 (2)	16	8 (8)	>32
GGH-Anoplin	2 (2)	8	4 (4)	>32
LKH-Anoplin	2	n.d.	4	n.d.
RTH-Anoplin	1	n.d.	4	n.d.
VIH-Anoplin	0.5 (0.5)	2	2 (2)	32
PAP	0.5 (0.25)	4	1 (1)	>32
DAH-PAP	0.25 (0.5)	4	0.25 (0.25)	>32
GGH-PAP	0.125 (0.06)	1	0.125 (0.06)	>32
VIH-PAP	0.125 (0.03)	0.25	0.25 (0.125)	32

[a] Numbers in parenthesis are MICs upon addition of 32 μM to the growth medium.

ATCUN motif conjugation changes the conformation and amphipathicity but not the cellular localization of Anoplin

We examined the secondary structure adopted by Anoplin and ATCUN-Anoplin using CD spectroscopy with and without the addition of the membrane mimicking agent, 2,2,2-trifluoroethanol. Figure 4.1 shows that Anoplin and ATCUN-Anoplin adopts a random coil conformation in buffer. However, when TFE is added to a final concentration

of 50% (v/v), characteristic curves indicative of an α-helix is observed. This suggests that Anoplin and ATCUN-Anoplin adopt a helical conformation when interacting with the bacterial membrane. The resulting curves were used to calculate the percent α-helical content of each peptide from the observed ellipticity at 222 nm. We found a minor decrease in the helical content when the ATCUN motif was added to the N-terminal of Anoplin (Table 4.3). Since protein and peptide function is highly tied to its propensity to adopt a functional secondary structure, we believe that the activity of ATCUN-Anoplin is not due to its formation of structured conformations. Since Anoplin has been shown to adopt an α-helical conformation, its amphipathicity can be analyzed using a helical wheel diagram (Figure 4.2). An increase in amphipathicity is not expected for the RTH and LKH derivatives, due to the presence of the helix breakers, Lys 2 and Thr 2 in the hydrophobic phase of the helix. This explains why the addition of the ATCUN motifs LKH and RTH resulted in lower percent α helical content for the ATCUN-Anoplin conjugates.

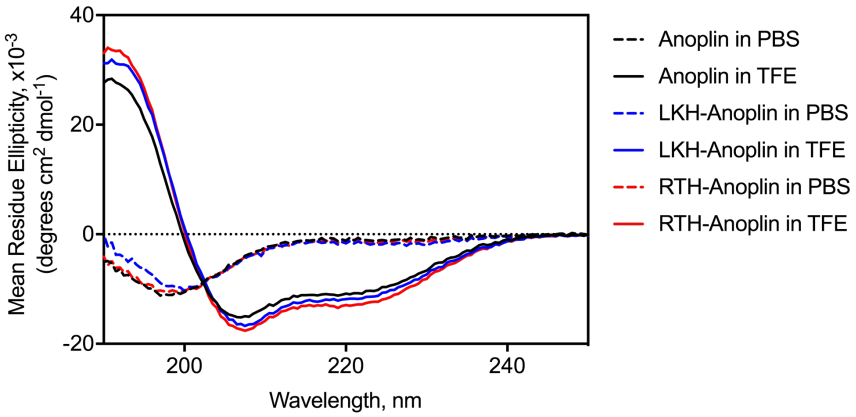

Figure 4.1. Secondary Structure of ATCUN-conjugated Peptides. Circular dichroism spectra of Anoplin and ATCUN-Anoplin in 25 mM phosphate buffer pH 7.40 (dashed lines) and in 50% trifluoroethanol in phosphate buffer (solid lines). Spectra show that all peptides adopt a helical conformation in membrane mimicking solvents.

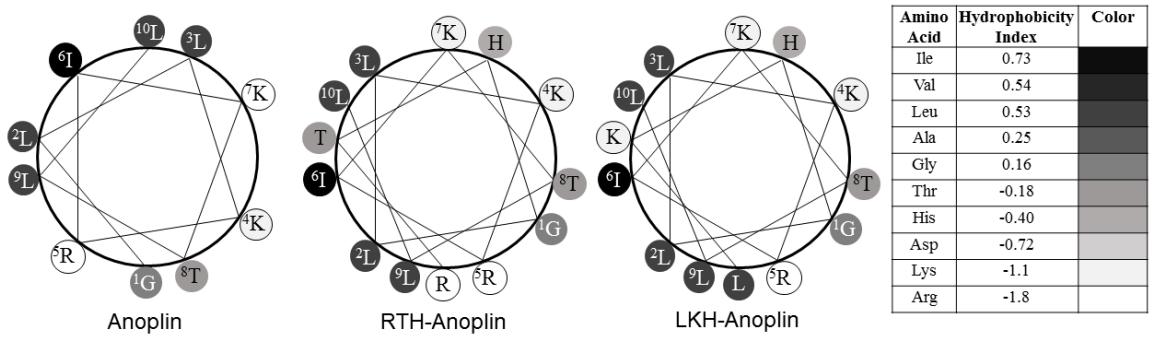

Amino Acid	Hydrophobicity Index	Color
Ile	0.73	
Val	0.54	
Leu	0.53	
Ala	0.25	
Gly	0.16	
Thr	-0.18	
His	-0.40	
Asp	-0.72	
Lys	-1.1	
Arg	-1.8	

Figure 4.2. Helical Wheel Diagram of ATCUN-conjugated Anoplin. Amphipathicity is shown here as clusters of amino acids having similar hydrophobicities when viewed along the helical axis. Thr 2 and Lys 2 in ATCUN-Anoplin break the continuum of hydrophobic residues in each helix. The Eisenberg concensus hydrophobicity scale was used.

Table 4.3. Calculated Percent α-Helix for ATCUN-containing Peptides.

Peptide	% α-helix	
	PBS	50% TFE
Anoplin	0	56
LKH-Anoplin	0	45
RTH-Anoplin	0	51

To evaluate whether the addition of the ATCUN motif changes the localization of Anoplin, we used laser confocal microscopy to visualize the fluorescently-labeled peptides upon incubation with *E. coli*. The 5(6)-carboxyfluorescein-labeled peptides were synthesized by coupling the fluorescent probe to the ε-amino group of an extra Lys residue placed between the ATCUN motif and Anoplin domains. Laser confocal microscopy showed that fluorescent peptides localized in the bacterial membrane and

that addition of LKH and RTH to the sequence of Anoplin does not change its localization (Figure 4.3). This result also suggests that the major target of Anoplin is retained. A similar localization was observed for PAP (Appendices, Figure S4.1).

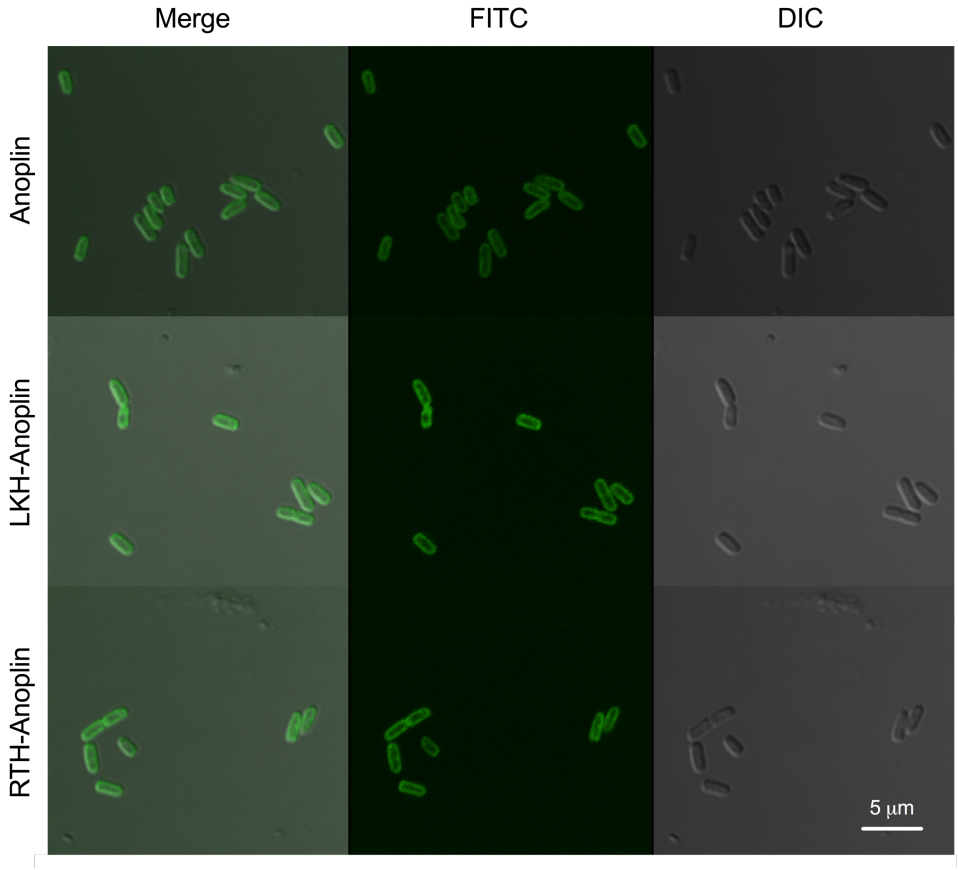

Figure 4.3. Cellular Localization of ATCUN-conjugated Peptides. Laser confocal microscopy (middle) and differential interface contrast (DIC, right) images of live *E. coli* cells exposed to fluorescein-conjugated peptides for 30 mins. Micrographs show that peptides localize in the bacterial membrane.

The ATCUN motif increases the membrane-permeabilizing activity of Anoplin and PAP

Since the addition of the ATCUN motif could affect the ability of the AMPs to turn the bacterial membranes permeable and allow the cellular contents to leak out, we assayed membrane permeabilization in *E. coli* by measuring the amount of β-

galactosidase leakage from the bacterial cytoplasm after exposure to the ATCUN-AMPs. After isolating the leaked β-galactosidase, its activity was monitored by adding 2-nitrophenyl-β-D-galactopyranoside and measuring the increase in absorbance at 405 nm. Upon addition of the DAH motif to Anoplin, we found that the membrane lytic activity of the AMP was improved (Figure 4.4). The addition of GGH and VIH to Anoplin did not result in an enhancement of the membrane-permeabilizing property of the peptide. In contrast to the ATCUN-Anoplin peptides, the addition of the GGH and VIH motifs to PAP increased its membrane-permeabilizing activity, while DAH conjugation to PAP did not result in increased lytic activity. These results are to be expected as ATCUN motif conjugation adds three extra residues, one of which contributes to the overall cationic charge of the peptide, which potentially increases membrane binding affinity.

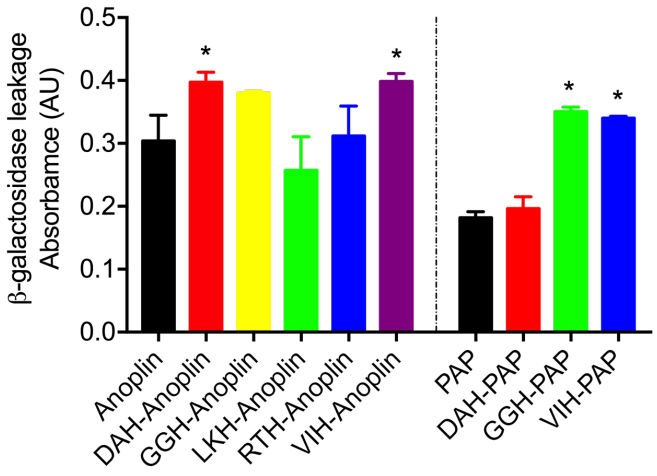

Figure 4.4. Membrane Permeabilizing Activity of ATCUN-AMPs. *E. coli* cells were treated with peptides at their MIC and levels of β-galactosidase that leaked out as a result of peptide treatment was quantified using a colorimetric assay at 405 nm. *, $P<0.05$.

ATCUN-AMPs bound to copper ions can peroxidize phospholipids

Since ROS formation can induce damage to bacterial membranes (Chapter 2), we next evaluated whether the diffusible and short-lived ROS generated by the ATCUN-AMPs bound to copper ions (Cu-ATCUN-AMP) could potentially destabilize the bacterial membrane through oxidative stress. The oxidative damage brought about by ROS production was assessed by measuring lipid peroxidation in either small unilamellar vesicles (SUVs) that mimic the *E. coli* outer membrane or live *E. coli* MWF1 (a strain that contains elevated levels of unsaturated fatty acids in its membrane). The Cu-ATCUN-AMP complexes were prepared by mixing 1.5 equivalents of peptide with 1 equivalent of Cu^{2+} and pre-incubating at room temperature for 30-45 minutes. The slight excess of ATCUN-AMP is used to ensure no free copper ions are present. Cu-ATCUN-AMPs were incubated with 80:20 DOPE:DOPG SUVs in the presence of H_2O_2 and sodium ascorbate or with live *E. coli* in complex media. The malonyldialdehyde formed was then tested via a standard thiobarbituric acid test.

As can be seen in Figure 4.5, the Cu-ATCUN-PAP complexes showed no differences among themselves in the amount of peroxidized lipid formed. Interestingly, the Cu-ATCUN-Anoplin peptides show a trend that trails the observed MICs of the ATCUN-AMPs, i.e. Cu-VIH-Anoplin and Cu-GGH-Anoplin being more active than Cu-DAH-Anoplin. Moreover, lipid peroxidation was observed in live bacteria, suggesting relevance of this mechanism in the activity of this family of ATCUN-AMPs. These results taken together suggest that the increased antimicrobial action of the ATCUN derivatives of the membrane-disrupting peptide Anoplin is largely influenced by the oxidative stress caused by the peptides on the microbial membrane.

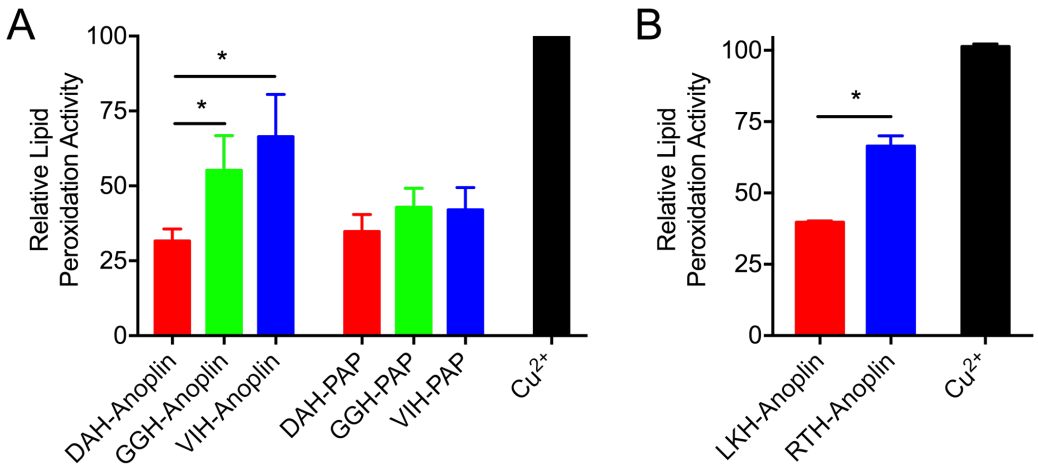

Figure 4.5. Lipid Peroxidation Activity of ATCUN-AMPs. Oxidation of fatty acyl lipid chains in the bacterial membrane as a result of peptide treatment was assessed by measuring levels of malonyldialdehyde (MDA) – a product of lipid peroxidation. Percent lipid peroxidized was normalized against activity of free Cu^{2+}, whose activity was assigned the value of 100%. Data show that ATCUN-AMPs peroxidize phospholipids both in (A) purified vesicles and (B) live bacteria. *, $P<0.05$.

ATCUN-AMPs exhibit low hemolytic activity against human erythrocytes

To assess the selectivity of the tested compounds towards bacteria over mammalian cells, their hemolytic activity was investigated. Release of hemoglobin from packed human red blood cells (RBCs) was measured spectrophotometrically and hemolysis of the peptides was normalized against the hemolytic activity of Triton X-100. As observed in Table 4.4, all the synthesized peptides had low hemolytic activity at the observed MIC for *E. coli* as all of the peptides had less than 10% hemolysis (with the exception of VIH-PAP with 13%), suggesting a selectivity of these peptides to lyse bacterial cells instead of RBCs. The data also showed that upon addition of the ATCUN motif to Anoplin and PAP, general membrane lytic activity increased.

Table 4.4. Hemolytic Activity and Selectivity Parameters of ATCUN-AMPs.

Peptide	% Hemolysis (@ MIC vs *E. coli*)	HD_{10} (μM)[a]	Therapeutic Index[b]
Anoplin	6 ± 1	> 64	> 4
DAH-Anoplin	7 ± 3	64	8
GGH-Anoplin	6 ± 2	16	4
LKH-Anoplin	6 ± 1	64	4
RTH-Anoplin	6 ± 2	16	4
VIH-Anoplin	7 ± 1	4	2
PAP	3 ± 1	64	64
DAH-PAP	4 ± 1	8	32
GGH-PAP	4 ± 1	4	32
VIH-PAP	13 ± 5	< 1	< 1

[a] Peptide concentration that results in lysis of 10% of red blood cells. [b] The therapeutic index was calculated by dividing the MIC (vs *E. coli*) by the HD_{10} values.

Discussion

This study presents the development of bifunctional antimicrobial agents that combine the bactericidal/bacteriostatic action of AMPs with the ROS-forming ability of a Cu^{II}-ATCUN complex. We hypothesize that the new ATCUN-AMPs will take advantage of the presence of the existing pool of labile copper ions in bacteria that flux in response to environmental stimuli. The large affinity of the ATCUN motif for copper ions (log K ~

14-15) would allow successful competition for this endogenous pool of copper.[91] For this purpose, the ability of certain ATCUN sequences to form ROS was initially assessed by monitoring consumption of reduced ascorbic acid. In the presence of the oxidant H2O2 and reductant ascorbic acid, hydroxyl radicals (•OH) and other ROS are produced via the Fenton reaction, as the bound copper cycles back and forth between its +2 and +3 oxidation states.[91, 92] Our experiments showed that both Cu-GGH and Cu-VIH produced ROS at the highest rates, and as such were chosen to be added at the N-terminus of Anoplin, and PAP. The DAH derivatives were used as a control for sequences that weakly form ROS.

When the ATCUN-AMPs were tested for their potency against a panel of four different bacteria the ATCUN motif was found to increase the activity of Anoplin and PAP up to a maximum of 16-fold (in the case of VIH-PAP against S. Epidermis). Some AMPs use metal-chelation as their mechanism of action and do not involve the production of ROS.[83] In those cases, the addition of metal ions such as Cu2+ to the medium affects negatively their antimicrobial activity. This is not the case for the ATCUN-AMPs presented in this study, since when 32 μM of Cu^{2+} ions were deliberately added to the peptide before incubation with the bacteria, the antibacterial activity of the ATCUN derivatives of all peptides were retained. This clearly indicates, that metal depletion due to the chelating ability of the ATCUN-AMPs synthesized in this work is not the mechanism of action used by these peptides. The ATCUN-AMPs have a low toxicity towards mammalian cells, as tested by an assay that measures their hemolytic activity. Although the ATCUN derivatives are slightly more hemolytic than their parent peptides, none of them cause more than 33% hemolysis at a concentration as high as 32 μM.

Anoplin is a membrane-acting AMP isolated from the venom of the wasp *Anoplius samariensis* with a broad-spectrum antimicrobial activity.[206] The fluorescently labeled Anoplin and ATCUN-Anoplin localize on the bacterial membrane, indicating that the addition of the ATCUN motif does not change to a major extent the affinity of the Anoplin sequence for its target. The highest antibacterial activity in the four bacterial strains tested was observed for VIH-Anoplin. The pore-forming ability of the ATCUN derivatives seems to be larger than that of Anoplin; however, no correlation between the membrane-permeabilizing activity and the MIC values is found. Importantly, ROS-mediated damage of lipids by the ATCUN-Anoplin peptides in combination with copper ions correlates with the antimicrobial activity. Thus, it is reasonable to suggest that the increased antimicrobial activity of the Anoplin derivatives has as origin the nonenzymatic oxidative damage of membrane phospholipids.[208] The process is likely initiated by hydroxyl radicals since peroxyl radicals are unable to react with fatty acids with rates that are biochemically important.[209] The •OH produced via the ATCUN-Cu^{III}/ ATCUN-Cu^{II} cycling can initiate membrane peroxidation through a hydrogen atom abstraction from a –CH2 group alpha to a carbon-carbon double bond of an unsaturated fatty acid (Equation (1)). Next, a lipid peroxyl radical can be formed from the reaction of dioxygen with the lipid radical (Equation (2)). The radical can then be propagated via reaction 3.

$$RH + HO\bullet \rightarrow R\bullet + HOH \quad (1)$$

$$R\bullet + O2 \rightarrow ROO\bullet \quad (2)$$

$$RH + ROO\bullet \rightarrow R\bullet + ROOH \quad (3)$$

The de novo peptide PAP was designed to be amphipathic in its helical conformation and strongly interact with bacterial membranes.[207] Initial studies have

established that PAP is a highly active AMP with low toxicity towards mammalian cells.[207, 210] Overall, the addition of the ATCUN motif increased the antimicrobial activity of PAP. The addition of both GGH and VIH doubled the membrane-permeabilizing activity of PAP, whereas no significant difference was observed with the DAH derivative. The larger ability to disrupt the membrane structure by the VIH and GGH derivatives can be explained by analyzing the helical wheel diagram of the three peptides (Figure 4.6). If a peptide adopts an α-helical conformation, as expected for PAP, the helical wheel diagram provides a simple tool for the analysis of amphipathicity.[211] As observed in Figure 4.6, VIH-PAP can potentially have the highest amphipathicity, followed by GGH-PAP. The Asp residue in DAH-PAP is detrimental to the amphipaticity of the peptide, since it would appear surrounded by hydrophobic residues. The close correlation between the membrane-permeabilizing activity and antimicrobial activity is an indication that the main mechanism of action of the ATCUN-PAP peptides is the disruption of the prokaryotic cell membrane.

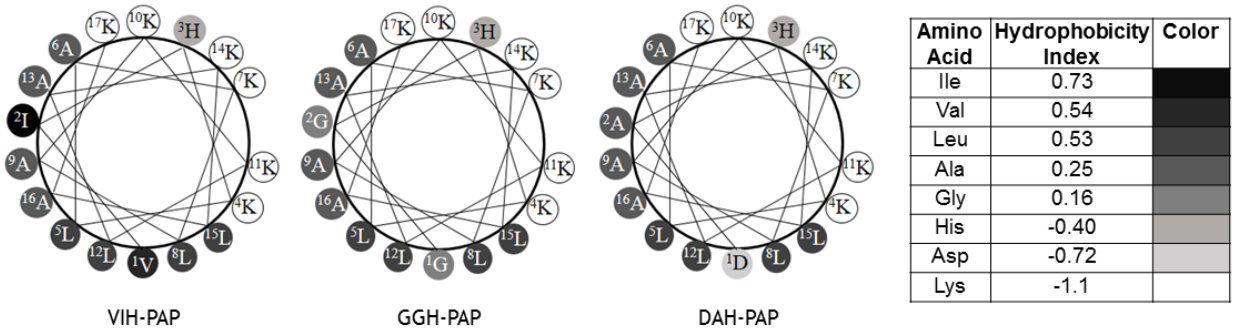

Amino Acid	Hydrophobicity Index	Color
Ile	0.73	
Val	0.54	
Leu	0.53	
Ala	0.25	
Gly	0.16	
His	-0.40	
Asp	-0.72	
Lys	-1.1	

Figure 4.6. Helical Wheel Diagram of ATCUN-conjugated PAP. The better membranolytic activity of ATCUN-PAP may be related to an increased amphipathic character. Shown here are the clusters of hydrophobic residues in ATCUN-PAP making a significant hydrophobic phase of the helix. Eisenberg hydrophobicity values are used.

The present study reveals that the addition of the ATCUN motifs leads to an increase in antimicrobial activity of the parental AMPs Anoplin, and PAP. Although the ATCUN-AMPs can induce the formation of ROS, the mechanistic mode of action differs among peptides and depends largely on the parental peptide. The addition of the ATCUN motif to Anoplin and PAP results in an increase of their membrane-permeabilizing activity. In the case of Anoplin, the membrane-permeabilization is caused by ROS-mediated damage to the lipids; whereas the activity of the PAP derivatives is related to the increase in amphipathicity. In the field of drug design, it is well accepted that the ability to attack microbes with multiple mechanisms of activity may have better chances of generating new antibiotics with broader-spectrum and enhanced antimicrobial activity. Therefore, agents such as the ATCUN-AMPs synthesized in this work are promising lead compounds that deserve further studies to fully describe their mechanism of action and their potential therapeutic applications.

Methodology

Peptide Synthesis, Purification, and Quantification. Peptides in their C-terminal amidated forms were synthesized manually on a Rink Amide resin (ChemPep Inc, Wellington, FL) using standard Fmoc-protected L-amino acids (Matrix Innovation, Quebec, Canada). Coupling reactions were done with 4 eq of amino acids and 4 eq of HBTU, deprotection using 20% piperidine in DMF and cleavage using 95:2.5:2.5 TFA/H_2O/TIS. Free peptides were purified via RP-HPLC (Schimadzu LC-20AD) on a C18 semi-prep 250x10mm column (Grace Davison, Deerfield, IL) using 0.1% TFA in H_2O (Buffer A) and 0.1% TFA in ACN (Buffer B). Tripeptides were subjected to a linear gradient of 5-95% Buffer B over 20 mins and ATCUN-AMPs were purified using a linear gradient

of 30-60% Buffer B over 30 mins. 5(6)-Carboxyfluorescein (Sigma Aldrich) labeled peptides were synthesized by attaching the fluorophore to the ε-amino group of an additional Lysine residue and were purified in the same way as the ATCUN-AMPs. Pure fractions were collected and the identities confirmed by ESI-MS ran on a positive ionization mode. All purified Peptides were subsequently reinjected on a C18 analytical 250x4.6 mm column (Grace Davison, Deerfield, IL) and were found to be ≥ 95% pure. All peptides were quantified using a method suggested by Gruppen. Briefly, lyophilized pure peptides were dissolved in nanopure water and a small aliquot was diluted in 80:20:0.1 H2O/ACN/Formic Acid and absorbance of this solution was read using a Varian Cary 50Scan UV-Vis Spectrometer at 214 nm. Molar extinction coefficient of each peptide was calculated on a sequence-specific manner based on the reported values for each amino acid and the peptide bond.

Peptide Handling and Preparation. All water used in this study was obtained from a Barnstead NANOpure Diamond filtration system with a 0.2 μm pore size filter. Purified peptides dissolved in nanopure water were stored at 4°C, and were diluted to the required concentration on the day of use. Concentrations were regularly checked via UV-Vis spectrophotometry. To form CuII-peptide complexes, 1.5 eq of peptide was mixed with 1 eq of Cu^{2+} (to ensure no free metal ion is present) and were pre-incubated at room temperature for 30-45 mins.

Determination of Ascorbic Acid Consumption. The rate at which ascorbic acid was consumed by the Cu^{II}-ATCUN complex was measured by the decrease in absorbance of reduced ascorbic acid. Reaction mixture contained 10 μM Cu^{II}-XXH complex with 1 mM Ascorbic acid with and without 1 mM H_2O_2 in 20 mM HEPES, 100 mM NaCl at pH 7.40.

Absorbance at 300 nm was measured on a clear 96-well plate using a Molecular Devices FlexStation 3 Plate Reader. Absorbance was plotted versus time and the slope of the linear portion of the curve was used to determine the rate constant of reaction. Ascorbic acid molar absorptivity was used to convert units of rate to μM ascorbic acid/min. Average values were taken from three trials and presented as Mean ± SD.

Antimicrobial Assay. Antimicrobial susceptibility testing was done using the broth microdilution method as suggested by Hancock. Gram-positives *Bacillus subtilis* (PS832), *Staphylococcus epidermidis* (ATCC 12228) and Gram-negatives *Escherichia coli* (DL7), and *Enterobacter aerogenes* (ATCC 13048) were grown in Mueller-Hinton Broth (MHB, Difco) until mid-log phase for 3-5 hrs. Peptide stock solutions were diluted in PBS (Gibco) pH 7.40, 50 μL two-fold serial dilutions (starting from 32 μM) were placed on a sterile 96-well poplypropylene plate (Greiner). To each well, 50 μL of a bacterial suspension was added resulting to a final inoculum of $5x10^5$ CFU/mL per well. Ampicillin (Sigma Aldrich) was used as positive control and PBS as negative control. Plates were incubated at 37°C (30°C for *E. aerogenes*) for 18-20 hrs. For experiments with the Cu-ATCUN-AMP complexes, the same dilutions and bacterial manipulations were done using MHB containing Cu^{2+}. A small aliquot of a concentrated Cu^{2+} solution was added to the MHB to bring the final Cu^{2+} concentration to 32 μM (well below the toxic level of Cu^{2+} in E. coli which is 3.5 mM). Minimum Inhibitory Concentration (MIC) was defined as the concentration that prevented visual growth of bacteria, and results were confirmed by matching to a plate reader $OD_{600\ nm}$ measurement. MICs reported here is the average of three independent trials.

β-Galactosidase Leakage Assay. The membrane disruption caused by the peptides was assessed by measuring the amount of leaked β-galactosidase. Overnight cultures of *E. coli* were inoculated in fresh LB broth and were grown to $OD_{600\ nm} \approx 0.6$. Overexpression of β-galactosidase was induced for 1 hr by addition of isopropyl-β-D-thiogalactopyranoside (IPTG, Fisher) at 1 mM final concentration. The cells were washed three times with PBS and resuspended in fresh LB broth. 75 µL of the bacterial suspension was mixed with 75 µL of two-fold serial dilutions of the peptides (starting from 32 µM) in sterile microcentrifuge tubes. The mixture was incubated at 37°C for 1 hr. After incubation, tubes were spun down at 4400 rpm at 4°C for 10 mins, then 100 µL of the supernatant was transferred to a clear 96-well plate. 50 µL of 2-nitrophenyl-β-D-galactopyranoside (ONPG, Thermo Scientific) in PBS was added at 0.8 mg/mL final concentration. The β-galactosidase activity was monitored by measuring the increase in absorbance at 405 nm every 5 mins for a period of 1 hr. Data shown are the final absorbance readings for three independent trials and presented as Mean ± SD.

Lipid Peroxidation Assay. The extent of Oxidative damage in the surface of the cell was measured by quantifying the peroxidation products of unsaturated phospholipids. A model E. coli membrane was made from an 80:20 mole percent mixture of 1,2-dioleoyl-sn-glycero-3-phosphoethanolamine (DOPE, Avanti Polar Lipids, Alabaster, AL) and 1,2-dioleoyl-sn-glycero-3-phospho-1'-rac-glycerol sodium salt (DOPG, Avanti Polar Lipids, Alabaster, AL). The chloroform was evaporated by a steady stream of N_2 and was dried further overnight in a high vacuum line. The lipid cake was rehydrated with 20 mM HEPES, 100 mM NaCl at pH 7.40 for 1 hour, vortexed 5 times and was sonicated for 20 mins to generate Small Unilamellar Vesicles (SUV). A 100 µM total lipid solution of SUV

was incubated with 10 μM of Cu^{II}-ATCUN-AMP complexes with 1 mM H_2O_2 and 1 mM sodium ascorbate in rehydration buffer for 1 hour. Then 50 μL of Butylated Hydroxytoluene was added followed by 1.5 mL of 0.44 M H_3PO_4. The mildly acidic mixture was incubated for 10 mins prior to addition of 500 μL of 2-thiobarbituric acid (TBA). The mixture was then heated on a dry block heater set at 90°C for 30 mins. After cooling down to room temperature, the amount of malonyldialdehyde-TBA adduct was quantified by injecting 50 μL of the final reaction mixture in a C18 analytical column. Elution was done at 35% methanol and 65% 50 mM KH_2PO_4/KOH buffer at pH 7.00 and monitored at 532 nm. The peak at ~4.6 mins represents the amount of the pink MDA-TBA adduct. The average of the peak area obtained from three independent trials are reported and presented as Mean ± SD.

Confocal Fluorescence Microscopy Imaging. Images were acquired on Zeiss LSM-510 confocal microscope using a 63X (1.4 N.A.) oil immersion objective at a pixel resolution of 512 × 512, and then processed utilizing ImageJ (National Institutes of Health).

Hemolytic Assay. To assess selectivity of the peptides towards bacterial membrane disruption, extent of hemolysis was measured. Packed Human Erythrocytes (ZenBio Inc, Research Triangle, NC) with anticoagulant Citrate Dextrose were washed three times with sterile PBS. A small aliquot of washed cells were resuspended in fresh PBS to make a 0.8 % (v/v) solution of RBC. Then 75 μL of RBC was mixed with 75 μL of a two-fold serial dilution series of the peptides and incubated at 37°C for 1 hr. Triton X-100 and PBS were used as positive and negative controls, respectively. The tubes were then spun down at 4400 rpm at 4°C for 10 mins and 100 μL of the supernatant was

transferred to a clear 96-well plate. The absorbance at 414 nm was measured and was normalized against the absorbance of the positive and negative controls. Data are obtained from four independent trials presented as Mean ± SD.

Statistical Analysis. Data were analyzed for statistical differences using Graph-Pad Prism® software. The Mann–Whitney asymptotic U-test was used for comparison because a Gaussian distribution could not be assumed. Whenever ties were present, comparison was done using Chi-square test. Statistical significance for all tests was set at $P < 0.05$.

Chapter References:

[1] Hancock, R. E., and Sahl, H. G. (2006) Antimicrobial and host-defense peptides as new anti-infective therapeutic strategies, *Nat Biotechnol 24*, 1551-1557.

[2] Lai, Y., and Gallo, R. L. (2009) AMPed up immunity: how antimicrobial peptides have multiple roles in immune defense, *Trends Immunol 30*, 131-141.

[3] Zasloff, M. (2002) Antimicrobial peptides of multicellular organisms, *Nature 415*, 389-395.

[4] Fjell, C. D., Hiss, J. A., Hancock, R. E., and Schneider, G. (2011) Designing antimicrobial peptides: form follows function, *Nat Rev Drug Discov 11*, 37-51.

[5] Wimley, W. C. (2010) Describing the mechanism of antimicrobial peptide action with the interfacial activity model, *ACS Chem Biol 5*, 905-917.

[6] Greber, K. E., and Dawgul, M. (2017) Antimicrobial Peptides Under Clinical Trials, *Curr Top Med Chem 17*, 620-628.

[7] Libardo, M. D. J., and Angeles-Boza, A. M. (2014) Bioinorganic chemistry of antimicrobial and host-defense peptides, *Comments Inorg Chem 34*, 42-58.

[8] Dwyer, D. J., Belenky, P. A., Yang, J. H., MacDonald, I. C., Martell, J. D., Takahashi, N., Chan, C. T., Lobritz, M. A., Braff, D., Schwarz, E. G., Ye, J. D., Pati, M., Vercruysse, M., Ralifo, P. S., Allison, K. R., Khalil, A. S., Ting, A. Y., Walker, G. C., and Collins, J. J. (2014) Antibiotics induce redox-related physiological alterations as part of their lethality, *Proc Natl Acad Sci U S A 111*, E2100-2109.

[9] Dwyer, D. J., Camacho, D. M., Kohanski, M. A., Callura, J. M., and Collins, J. J. (2012) Antibiotic-induced bacterial cell death exhibits physiological and biochemical hallmarks of apoptosis, *Mol Cell 46*, 561-572.

[10] Kohanski, M. A., Dwyer, D. J., Hayete, B., Lawrence, C. A., and Collins, J. J. (2007) A common mechanism of cellular death induced by bactericidal antibiotics, *Cell 130*, 797-810.

[11] Liu, Y., and Imlay, J. A. (2013) Cell death from antibiotics without the involvement of reactive oxygen species, *Science 339*, 1210-1213.

[12] Keren, I., Wu, Y., Inocencio, J., Mulcahy, L. R., and Lewis, K. (2013) Killing by bactericidal antibiotics does not depend on reactive oxygen species, *Science 339*, 1213-1216.

[13] Albesa, I., Becerra, M. C., Battan, P. C., and Paez, P. L. (2004) Oxidative stress involved in the antibacterial action of different antibiotics, *Biochem Biophys Res Commun 317*, 605-609.

[14] Becerra, M. C., and Albesa, I. (2002) Oxidative stress induced by ciprofloxacin in Staphylococcus aureus, *Biochem Biophys Res Commun 297*, 1003-1007.

[15] Liu, Z., Cai, Y., Young, A. W., Totsingan, F., Jiwrajka, N., Shi, Z., and Kallenbach, N. (2012) OH radical production stimulated by (RW)4D, a synthetic antimicrobial agent and indolicidin, *MedChemComm*, 1548-1554.

[16] Brynildsen, M. P., Winkler, J. A., Spina, C. S., MacDonald, I. C., and Collins, J. J. (2013) Potentiating antibacterial activity by predictably enhancing endogenous microbial ROS production, *Nat Biotechnol 31*, 160-165.

[17] Morones-Ramirez, J. R., Winkler, J. A., Spina, C. S., and Collins, J. J. (2013) Silver enhances antibiotic activity against gram-negative bacteria, *Sci Transl Med 5*, 190ra181.

[18] Pages, J. M., Kascakova, S., Maigre, L., Allam, A., Alimi, M., Chevalier, J., Galardon, E., Refregiers, M., and Artaud, I. (2013) New Peptide-based antimicrobials for tackling drug resistance in bacteria: single-cell fluorescence imaging, *ACS Med Chem Lett 4*, 556-559.

[19] Zheng, T., Bullock, J. L., and Nolan, E. M. (2012) Siderophore-mediated cargo delivery to the cytoplasm of Escherichia coli and Pseudomonas aeruginosa: syntheses of monofunctionalized enterobactin scaffolds and evaluation of enterobactin-cargo conjugate uptake, *J Am Chem Soc 134*, 18388-18400.

[20] Dosselli, R., Ruiz-Gonzalez, R., Moret, F., Agnolon, V., Compagnin, C., Mognato, M., Sella, V., Agut, M., Nonell, S., Gobbo, M., and Reddi, E. (2014) Synthesis, spectroscopic, and photophysical characterization and photosensitizing activity toward prokaryotic and eukaryotic cells of porphyrin-magainin and -buforin conjugates, *J Med Chem 57*, 1403-1415.

[21] Dosselli, R., Tampieri, C., Ruiz-Gonzalez, R., De Munari, S., Ragas, X., Sanchez-Garcia, D., Agut, M., Nonell, S., Reddi, E., and Gobbo, M. (2013) Synthesis, characterization, and photoinduced antibacterial activity of porphyrin-type photosensitizers conjugated to the antimicrobial peptide apidaecin 1b, *J Med Chem 56*, 1052-1063.

[22] Liu, F., Soh Yan Ni, A., Lim, Y., Mohanram, H., Bhattacharjya, S., and Xing, B. (2012) Lipopolysaccharide neutralizing peptide-porphyrin conjugates for effective photoinactivation and intracellular imaging of gram-negative bacteria strains, *Bioconjug Chem 23*, 1639-1647.

[23] Johnson, G. A., Ellis, E. A., Kim, H., Muthukrishnan, N., Snavely, T., and Pellois, J. P. (2014) Photoinduced membrane damage of E. coli and S. aureus by the photosensitizer-antimicrobial peptide conjugate eosin-(KLAKLAK)2, *PLoS One 9*, e91220.

[24] Johnson, G. A., Muthukrishnan, N., and Pellois, J. P. (2013) Photoinactivation of Gram positive and Gram negative bacteria with the antimicrobial peptide (KLAKLAK)(2) conjugated to the hydrophilic photosensitizer eosin Y, *Bioconjug Chem 24*, 114-123.

[25] Joyner, J. C., and Cowan, J. A. (2013) Target-directed catalytic metallodrugs, *Braz J Med Biol Res 46*, 465-485.

[26] Joyner, J. C., Hodnick, W. F., Cowan, A. S., Tamuly, D., Boyd, R., and Cowan, J. A. (2013) Antimicrobial metallopeptides with broad nuclease and ribonuclease activity, *Chem Commun (Camb) 49*, 2118-2120.

[27] Ross, M. J., Bradford, S. S., and Cowan, J. A. (2015) Catalytic metallodrugs based on the LaR2C peptide target HCV SLIV IRES RNA, *Dalton Trans 44*, 20972-20982.

[28] Konno, K., Hisada, M., Fontana, R., Lorenzi, C. C., Naoki, H., Itagaki, Y., Miwa, A., Kawai, N., Nakata, Y., Yasuhara, T., Ruggiero Neto, J., de Azevedo, W. F., Jr., Palma, M. S., and Nakajima, T. (2001) Anoplin, a novel antimicrobial peptide from the venom of the solitary wasp Anoplius samariensis, *Biochim Biophys Acta 1550*, 70-80.

[29] Foillard, S., Jin, Z. H., Garanger, E., Boturyn, D., Favrot, M. C., Coll, J. L., and Dumy, P. (2008) Synthesis and biological characterisation of targeted pro-apoptotic peptide, *Chembiochem 9*, 2326-2332.

[30] Jin, Y., Lewis, M. A., Gokhale, N. H., Long, E. C., and Cowan, J. A. (2007) Influence of stereochemistry and redox potentials on the single- and double-strand DNA cleavage efficiency of Cu(II) and Ni(II) Lys-Gly-His-derived ATCUN metallopeptides, *J Am Chem Soc 129*, 8353-8361.
[31] Joyner, J. C., Reichfield, J., and Cowan, J. A. (2011) Factors influencing the DNA nuclease activity of iron, cobalt, nickel, and copper chelates, *J Am Chem Soc 133*, 15613-15626.
[32] Neupane, K. P., Aldous, A. R., and Kritzer, J. A. (2013) Macrocyclization of the ATCUN motif controls metal binding and catalysis, *Inorg Chem 52*, 2729-2735.
[33] Silva, F. D., Rezende, C. A., Rossi, D. C., Esteves, E., Dyszy, F. H., Schreier, S., Gueiros-Filho, F., Campos, C. B., Pires, J. R., and Daffre, S. (2009) Structure and mode of action of microplusin, a copper II-chelating antimicrobial peptide from the cattle tick Rhipicephalus (Boophilus) microplus, *J Biol Chem 284*, 34735-34746.
[34] Girotti, A. W. (1998) Lipid hydroperoxide generation, turnover, and effector action in biological systems, *J Lipid Res 39*, 1529-1542.
[35] Bielski, B. H., Arudi, R. L., and Sutherland, M. W. (1983) A study of the reactivity of HO2/O2- with unsaturated fatty acids, *J Biol Chem 258*, 4759-4761.
[36] Kim, H. Y., Kim, S., Youn, H., Chung, J. K., Shin, D. H., and Lee, K. (2011) The cell penetrating ability of the proapoptotic peptide, KLAKLAKKLAKLAK fused to the N-terminal protein transduction domain of translationally controlled tumor protein, MIIYRDLISH, *Biomaterials 32*, 5262-5268.
[37] Kim, Y. S., and Cha, H. J. (2010) Disperse distribution of cationic amino acids on hydrophilic surface of helical wheel enhances antimicrobial peptide activity, *Biotechnol Bioeng 107*, 216-223.

Chapter 5

The ATCUN Motif in General Antimicrobial Drug Development – Part II

ATCUN motif Conjugation to AMPs Results in a Gain-of-Function Phenotype Imparting the Ability to Oxidatively Cleave Microbial DNA

Adapted entirely from:

Libardo, M.D.J., Cervantes, J.L., Salazar, J.C., Angeles-Boza, A.M.
ChemMedChem **2014**, 9, 1892-1901

Libardo, M.D.J., Paul, T.J., Prabhakar, R., Angeles-Boza, A.M.
Biochimie, **2015**, 113, 143-155

Introduction

In chapter 4, we appended the ATCUN motif to the membrane active AMPs Anoplin and PAP to address the influence of an exogenously added ATCUN motif to the activity of AMPs. The resulting ATCUN-AMP conjugates were found to be more active compared to the parental AMPs. We proposed that this increase in activity arises from the endogenous capability of the ATCUN-AMPs to inflict oxidative stress (when they bind to labile copper ions) on top of the classical antimicrobial action of the parent peptide. Our initial mechanistic evaluations lead us to believe that the ATCUN-AMPs ultimately cause membrane damage by lipid peroxidation on the natural target of the parent AMP.

The success of the ATCUN motif conjugation to Anoplin made us wonder whether the same phenotype can be observed on an AMP that naturally targeted the bacterial DNA. Cowan and Long have shown that Cu-ATCUN complexes possess nuclease activity via formation of ROS when the metal cycles back and forth its +2 and +3 oxidation states under physiologically relevant conditions.[90, 91, 212-215] In this regard, we conjugated ATCUN motifs to the DNA-binding AMP, Buforin II. We aimed at developing a conjugate that could bring the ATCUN motif in close proximity to bacterial DNA and generate ROS in the vicinity to effect DNA cleavage.

The rational design of AMPs largely depends on the understanding of the molecular characteristics responsible for the antimicrobial action. Here, to address the influence of a basic residue in the ATCUN motif in AMPs that target DNA, we have appended the RTH motif to sh-Buforin and compared it to a derivative containing a VIH motif. We hypothesize that the addition of a positively-charged ATCUN motif will allow a stronger interaction with DNA resulting in an AMP with increased antimicrobial activity.

We have also investigated the effects of a change in stereochemistry to the bioactivity of ATCUN-sh-Buforin conjugates. We hypothesize that increased antimicrobial activity of ATCUN-sh-Buforin is expected since L-to-D amino acid substitution have been shown to increase the ROS-generating activity of the ATCUN motif.[91] The results provided in this chapter are important information for the further optimization of ATCUN-based antimicrobial agents.

Results

Initial ATCUN motif conjugation to sh-Buforin generates a peptide-based nuclease

sh-Buforin is a truncated analogue of buforin II (TRSSRAGLQFPVGRVHRLLRK-NH_2), a potent AMP that kills bacteria without cell lysis and has a strong affinity for oligonucleotides.[11, 114, 216, 217] The N-terminal random structure (residues 1-4) does not appear to be important to the antibacterial activity of buforin II,[114] thus the addition of the ATCUN motif was not expected to perturb its mode of action. Driven by the calculated rates of ROS formation from Chapter 4, we proceeded to append the ATCUN motifs DAH, GGH and VIH to *sh*-Buforin (RAGLQFPVGRVHRLLRK-NH_2). A structure-activity relationship study showed that *sh*-Buforin had increased translocation activity across bacterial membranes relative to the full peptide.[114] ATCUN motif conjugation resulted in a two- to four-fold decrease in MIC against *E. coli* and *B. subtilis*. We postulated that this increase was likely a result of oxidative DNA cleavage being afforded by the exogenous ATCUN motif and we tested this hypothesis using an *in vitro* model of DNA cleavage. Damage to the DNA plasmid pUC19 by ROS was monitored after 30 mins and 2 hours of incubation with the Cu-ATCUN-*sh*-buforin complexes. Figure 5.1A shows a time-

dependent cleavage of plasmid DNA with the supercoiled form decreasing overtime and the linearized form simultaneously building up. We then measured the degree to which the peptides can affect general oxidative stress in live bacteria by monitoring the increase in fluorescence of an ROS-responsive fluorophore – 2',7'-dichlorofluoresceindiacetete. Figure 5.1B shows that ATCUN-*sh*-buforin can generate >3-fold amount of ROS within cells and this activity mirrored the rates of ROS formation by the isolated tripeptides. These evidences point to a capability of Cu-ATCUN-*sh*-buforin to induce generalized oxidative stress within bacteria, generating DNA nicks that could be responsible for the antibacterial action.

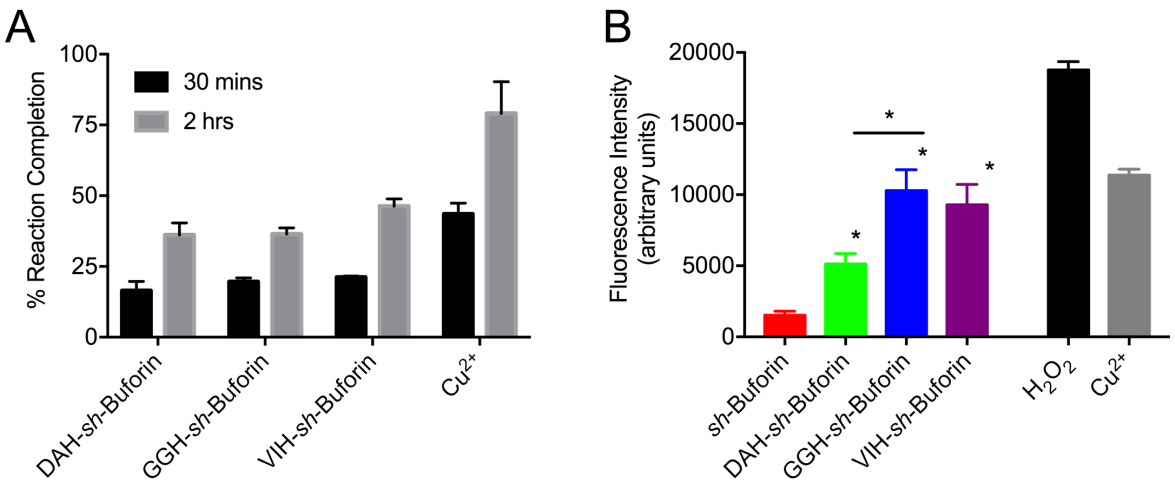

Figure 5.1. Initial Assessment of ATCUN-*sh*-Buforin Activity. (A) pUC19 plasmid DNA was used to monitor in vitro nuclease activity of ATCUN-*sh*-Buforin derivatives. Reactions were quenched at two time points showing a time-dependent cleavage of DNA promoted by the peptides. (B) General oxidative stress in *E. coli* was measured using the fluorescent reporter dichlorofluorescein. Cells pre-loaded with the dye were treated with the peptides and the indicated controls for 2 hrs. *, $P<0.05$.

Design principles to optimize nuclease activity of ATCUN-sh-buforin

We selected the ATCUN motif RTH not only because it has moderately high initial rates of ROS production, but also due to the structural similarities of the metal-bound ATCUN motif to DNA binding agents such as Netropsin and Hoescht 33258 as illustrated by Long.[218] We reasoned that these two factors could lead to an added interaction with DNA, generating a more potent antimicrobial. In addition, we synthesized ATCUN-*sh*-buforin peptides containing D-enantiomers since we wanted to explore the influence of amino acid stereochemistry in the activities of the peptides as it has been previously reported that changes in the stereochemistry can tune the reactivity of the copper-bound ATCUN motif.[91]

L-to-D amino acid substitution positively affects the potency of ATCUN-sh-buforin

To assess the relative efficacy of the synthesized peptides, the minimum inhibitory concentration (MIC) was determined against *E. coli*, and *E. aerogenes*. Our data shows that addition of the ATCUN motif generally leads to an increase in antimicrobial activity against all strains used. For the case of *E. coli* MG1655 (a wild type K-12 strain), a two-fold increase was observed when RTH was added to L-*sh*-buforin and a four-fold increase when RTH and VIH were added to D-*sh*-buforin. Table 1 also shows that the D-peptides are more active compared to the L-peptides. An 8-fold increase in activity was seen when the stereochemistry of L-*sh*-buforin was changed and up to a 32-fold increase was seen for the case of L-VIH-L-*sh*-buforin. Interestingly, the data also shows that changing the stereochemistry of the ATCUN motif does not affect the antimicrobial activity (L-ATCUN-L-*sh*-buforin vs D-ATCUN-L-*sh*-buforin) and that MIC seem to be largely dictated by the

stereochemistry of the parental peptide, *sh*-buforin. It is also worth noting that while all the other peptides exhibited MIC values in the high micromolar range, D-VIH-D-*sh*-buforin had an MIC of 16 μM against the problem pathogen *E. aerogenes*, the causative agent of many nosocomial infections. Buforin II and *sh*-buforin has been shown to exert its action by penetrating the bacterial membrane and interacting with both DNA and RNA. We hypothesize that ATCUN-*sh*-buforin can interact and directly damage the DNA via ROS formation. Because of this, a bacterial strain incapable of repairing DNA damage is expected to be more susceptible to ROS relative to the wild type strain. This phenomenon has been observed on several occasions. In this regard, we determined the MIC of our peptides against *E. coli* TD172, a strain wherein the DNA repair protein RecA has been deleted. Most of our peptides exhibited a two-fold increase in activity (Table 5.1) when tested against the *recA* deletion mutant compared to the wild type; this hints at the possibility that ATCUN-*sh*-buforin acts by damaging the DNA. We used as a control, the membrane active peptide, magainin 2, which generates tension-induced pores on the surface of bacterial membranes. We found that activity of magainin 2 was the same in both *E. coli* strains, further implicating DNA as the major target for *sh*-buforin and ATCUN-*sh*-buforin.

Chelating agents like the ATCUN motif can devoid cells of essential copper ions, perturbing metabolic functions, which can cause cell death. Notably, the Cu(II)-chelating antimicrobial peptide microplusin exerts its action by copper starvation. Excess Cu^{2+} in the medium was found to rescue the growth of bacteria exposed to microplusin. We determined the MIC of our peptides when the growth medium was supplemented with 32 μM (Table 5.1, +Cu^{2+}) and found that the additional Cu^{2+} does not reduce the activity of

our peptides. Interestingly, we observed a two-fold increase in activity for L-RTH-D-*sh*-buforin and D-VIH-D-*sh*-buforin when Cu^{2+} was supplemented, which might indicate full activity during a copper-saturated state for these peptides.

Table 5.1. Antimicrobial Activity of *sh*-Buforin and ATCUN-*sh*-Buforin Analogs.

Peptide	Minimum Inhibitory Concentration (MIC)[a], μM				
	***E. coli* MG1655 (WT)**		***E. coli* TD172 (Δ*recA*)**		***E. aerogenes***
	no Cu^{2+}	+ Cu^{2+}	no Cu^{2+}	+ Cu^{2+}	
L-*sh*-Buforin	64	64	32	32	>64
L-RTH-L-*sh*-Buforin	32 *	32 *	16 *	16 *	64
L-VIH-L-*sh*-Buforin	64	64	32	32	64
D-RTH-L-*sh*-Buforin	32 *	32 *	16 *	16 *	64 [b]
D-VIH-L-*sh*-Buforin	64	64	32	32	64 [b]
D-*sh*-Buforin	8 #	8 #	4 #	4 #	64
L-RTH-D-*sh*-Buforin	2 *	2 *	2 *	1 *,**	32
L-VIH-D-*sh*-Buforin	2 *	2 *	1 *	1 *	32
D-RTH-D-*sh*-Buforin	4 *,#	4 *,#	2 *,#	2 *,#	32 [b]
D-VIH-D-*sh*-Buforin	2 *,#	4 *,#	2 *,#	1 *,#,**	16
Magainin 2	8	8	8	8	N.D.
Ampicillin	2	N.D.	2	N.D.	16
Kanamycin	0.125	N.D.	0.125	N.D.	1

[a] + Cu^{2+} runs represent supplementation of growth medium with 32 μM of Cu^{2+}. [b] Significant reduction in growth was observed until 16 μM. *, *P*<0.001 compared to *sh*-Buforin; [#], *P*<0.001 compared to their enantiomer (pure L vs pure D); **, *P*<0.001 when compared to trials without Cu^{2+}.

D-sh-buforin have bactericidal activity against E. coli

To study the dynamics of bacterial killing, we quantified the number of viable cells for a specified period of time following exposure to the peptides. Since a change in stereochemistry of the ATCUN motif did not show a difference in MIC, we decided to study only the pure L- and pure D-enantiomers. Our data shows that the D-peptides are bactericidal at their MIC (exhibiting about four orders of magnitude decrease in population), in contrast to the bacteriostatic effects of the L-peptides. For the wild type (Figure 5.2), killing starts 2 hours after exposure to the peptide, whereas it only takes 1 hour to start killing off the *recA* mutant (Figure 5.2). This corroborates our MIC values, indicating that the peptides are more effective against the *recA* mutant. For both L-RTH-L-*sh*-buforin and L-VIH-L-*sh*-buforin, the rate of growth of bacteria seemed to exceed the rate of growth of inhibition by the peptides 4 hours post-exposure. This phenomenon has been observed for the all-D-enantiomer of the antimicrobial peptide KLAKLAKKLAKLAK at its MIC against *P. aeruginosa*,[219] and recently for a Vancomycin analog at its MIC against MRSA.[220] This suggests that bacterial clearance is incomplete at the MIC for L-ATCUN-L-*sh*-buforin.

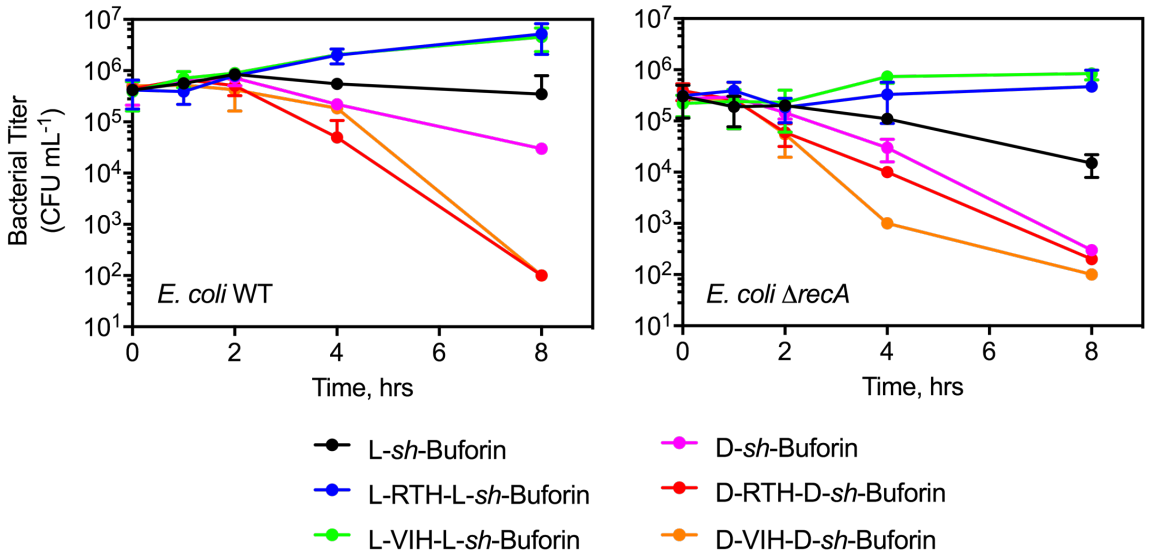

Figure 5.2. Bactericidal Activity of ATCUN-*sh*-Buforin. Time-kill kinetics curves following exposure to peptides at their MIC against *E. coli* WT (left) and *recA* mutant (right). Viable cells were enumerated at the indicated time points via spreading dilutions in LB agar plates.

Spectroscopic studies reveal that metalation of ATCUN-sh-buforin does not change its secondary structure

To determine the secondary structure adopted by the peptides we obtained the circular dichroism spectra of each peptide from 190 to 250 nm in a 50% (v/v) 2,2,2-trifluoroethanol (TFE) in 100 mM phosphate buffer pH 7.40. TFE mimics the bacterial membrane, hence, under these conditions; the functionally relevant conformations of the peptides can be determined. Figure 5.3 (and Appendices, Figure S5.1), shows that L-*sh*-buforin and L-ATCUN-L-*sh*-buforin adopts an alpha-helical conformation as evidence by the minimum negative peak at around 208 and 222 nm, and the maximum positive peak at 190 nm. The spectra of D-*sh*-buforin and D-ATCUN-D-*sh*-buforin were observed to be the exact mirror images of their respective enantiomers. We also determined the effect of

Cu^{2+} binding to the conformation of peptide and we found that complex formation does not affect the overall helicity (blue and green curves in Figure 5.3).

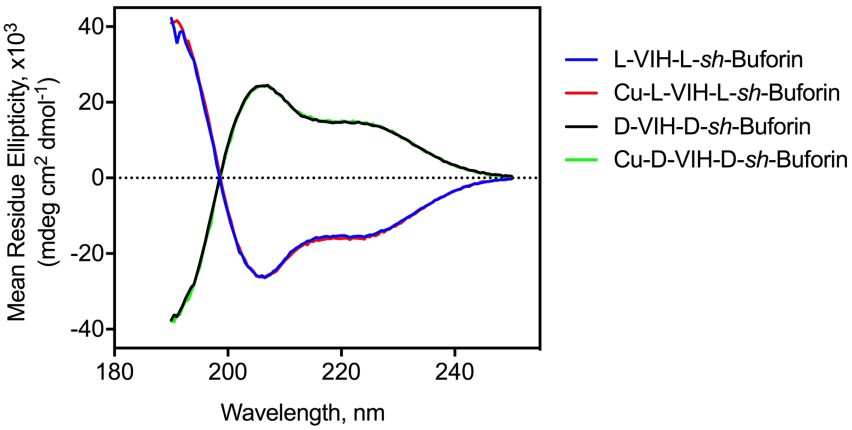

Figure 5.3. Spectroscopic Characterization of ATCUN-*sh*-Buforin Secondary Structure. CD Spectra of VIH-*sh*-Buforin with and without Cu^{2+} in 50% (v/v) trifluoroethanol and phosphate buffer. Spectra show characteristic curve for an α-helical peptide.

The amount of α-helix present was calculated based on the mean residue ellipticity at 222 nm using eqn 2 (Methodology). Our results show that all our peptides contain 35-43% α-helix, and counter intuitively, the addition of an ATCUN motif (of any stereochemistry) leads to a slight decrease in α-helical content. Buforin II contains three structured domains separated by a proline hinge at position 11 – the N-terminal random coil, an extended helical domain from the 5th to 10th amino acid, and a C-terminal regular helix.[114] In a structure-activity relationship study of buforin II, it was found that *sh*-buforin contained about 9% more helical content compared to the complete peptide.[114] The observed increase in helicity is probably due to the loss of the random coil domain of buforin II when the first four amino acids are truncated. When the ATCUN motif is added,

it occupies the region where a random coil is expected, which explains the decrease in helicity. No significant difference in values was observed when the stereochemistry of the peptides was changed, nor did it change upon addition of copper (Table 5.2).

Table 5.2. Calculated percent helicity for the synthesized peptides.

Peptide	% α helix	
	- Cu^{2+}	+ Cu^{2+}
L-*sh*-Buforin	42	-
L-RTH-L-*sh*-Buforin	36	38
L-VIH-L-*sh*-Buforin	40	41
D-RTH-L-*sh*-Buforin	39	39
D-VIH-L-*sh*-Buforin	40	39
D-*sh*-Buforin	43	-
L-RTH-D-*sh*-Buforin	40	40
L-VIH-D-*sh*-Buforin	36	36
D-RTH-D-*sh*-Buforin	35	37
D-VIH-D-*sh*-Buforin	37	39

ATCUN-sh-buforin does not exhibit a membranolytic activity

The extent to which *sh*-buforin and its analogs disrupt bacterial membranes was measured by quantifying the amount of leaked enzyme after exposure to the peptides. The β-galactosidase content of the supernatant was determined by a colorimetric reaction

monitored at 405 nm. When *E. coli* cells are exposed to *sh*-buforin and ATCUN-*sh*-buforin at their MIC, we observed very minimal membrane damage (four to five fold less) relative to the membrane active peptide, magainin 2 (Figure 5.4). No significant difference was found with either a change in stereochemistry or a change in the ATCUN motif. This suggests that both *sh*-buforin and ATCUN-*sh*-buforin (of either stereochemistry) exert very little perturbations in the integrity of bacterial membranes, in conjunction with the fact that buforin II is a cell-penetrating peptide able to kill bacteria without cell lysis.

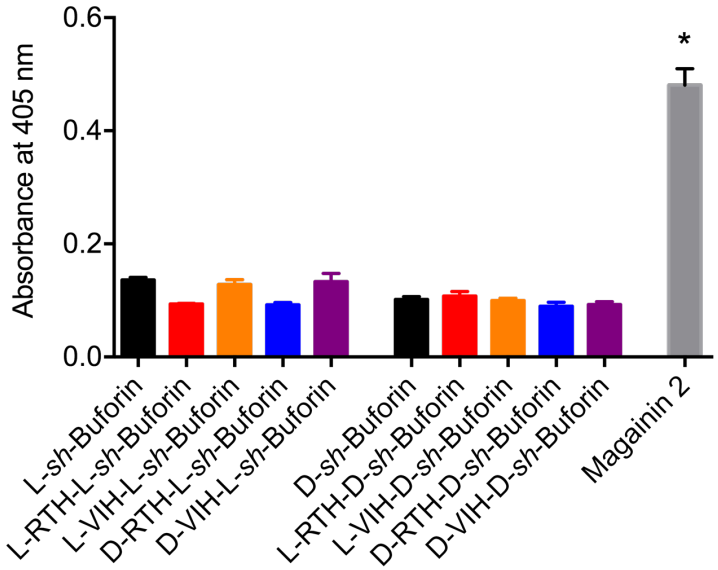

Figure 5.4. Membranolytic Activity of ATCUN-*sh*-Buforin. Hydrolysis of O-nitrophenyl-β-D-galactopyranoside (ONPG) to o-nitrophenol was used to quantify amount of leaked enzyme from *E. coli* exposed to peptides at their MIC. *, $P<0.001$ compared to L- and D-*sh*-Buforin.

ATCUN-sh-buforin induces oxidative stress in bacteria

Since the ATCUN-*sh*-buforin can form ROS when bound to Cu^{2+} ion, and because sh-buforin has been shown to traverse the membrane and localize in the cytoplasm, we studied the amount of ROS formed inside bacterial cells. We used the pro-fluoresent

probe 2',7'-dichlorofluorescein diacetate (dCFdA) to study generalized oxidative stress inflicted by our peptides. dCFdA can cross membranes, once inside, it gets deacetylated by cellular esterases. This non-fluorescent derivative is polar enough that it is essentially trapped inside the cell. When it gets oxidized by ROS, it generates the highly fluorescent 2',7'-dichlorofluorescein. We incubated *E. coli* MG1655 cells with the peptides at MIC (no Cu^{2+} added) for two hours – at which point killing has not started yet (as evidenced by the time-kill kinetics experiment) – and then we measured the fluorescence of 100,000 cells using a flow cytometer. Our treatments did not lead to a significant change in the cellular morphology as shown by the scatter plots (Appendices, Figure S5.2). Our results (Figure 5.5) indicate that there is a buildup of ROS inside the cell preceding cell death. A three- to seven-fold increase in intracellular ROS was observed when the bacteria were treated with our peptides. This may be related to the fact that antibiotics can induce formation of hydroxyl radicals via a pathway involving the tricarboxylic acid cycle and a transient destabilization of iron-sulfur clusters, a phenomenon that has been repeatedly reported by Collins.[155, 221, 222] This has also been observed for antimicrobial peptides, and respiratory proteins.[223, 224] Figure 5.5 shows that there is a greater amount of ROS induced by D-*sh*-buforin compared to L-*sh*-buforin. Curiously, The ATCUN-*sh*-buforin-treated cells formed the same amount of ROS as the *sh*-buforin-treated cells. A logical explanation for this observation is the model proposed by Cowan and Dervan where the ROS is intimately bound to the copper center and is not released to the surroundings. Thus, we believe that the ROS detected in this assay arises solely from the classical pathway as proposed by Collins and not from direct formation via the Cu-ATCUN complex.

The most accessible ROS, the superoxide anion ($O2^{-\bullet}$) – arising from a single electron reduction of molecular oxygen – can release iron from iron-sulfur clusters from metalloenzymes. The Fe^{2+} released can then undergo Fenton reaction to produce hydroxyl radicals, essentially amplifying the amount of ROS. To eliminate this effect, we repeated the ROS experiment with pre-incubation of the bacteria with the iron chelator, 2,2'-bipyridine (bpy). Our results show no significant difference when bpy is added indicating that the measured ROS is not due to endogenous ferrous ions.

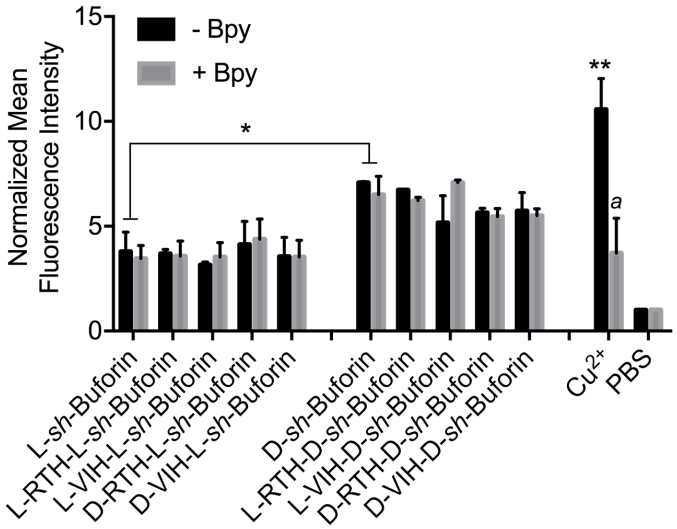

Figure 5.5. Intracellular ROS production of ATCUN-*sh*-Buforin. General oxidative stress was monitored using the ROS-responsive probe dichlorofluorescein. To study the effect of iron released from {4Fe-4S] clusters by ROS, the iron chelator 2,2'-bipyridine was added. a formation of $Cu(bpy)_3$ leads to less availability of copper to undergo redox cycling. *, $P<0.05$ and **, $P<0.01$ when compared to L- or D-*sh*-Buforin.

Next, we wanted to determine the extent to which ROS production is involved in the death of cells exposed to our peptides. We incubated *E. coli* MG1655 with the peptides at their MIC with and without the radical scavenger, thiourea for three hours and compared the survival rate. Thiourea has been shown to rescue the growth of bacteria

exposed to ROS-generating agents.[155, 225] Our results indicate that ROS is indeed contributing to the antibacterial action of the peptides and that quenching the ROS formed inside the cell diminishes their efficacy to varying degrees. Figure 5.6A shows a visible reduction in the number of colonies when thiourea (TU) is present. We also observed a greater difference in survival with thiourea when cells were incubated with ATCUN-*sh*-buforin (Figure 5.6B), which suggests that ROS production plays an important role in the mechanism of the conjugates.

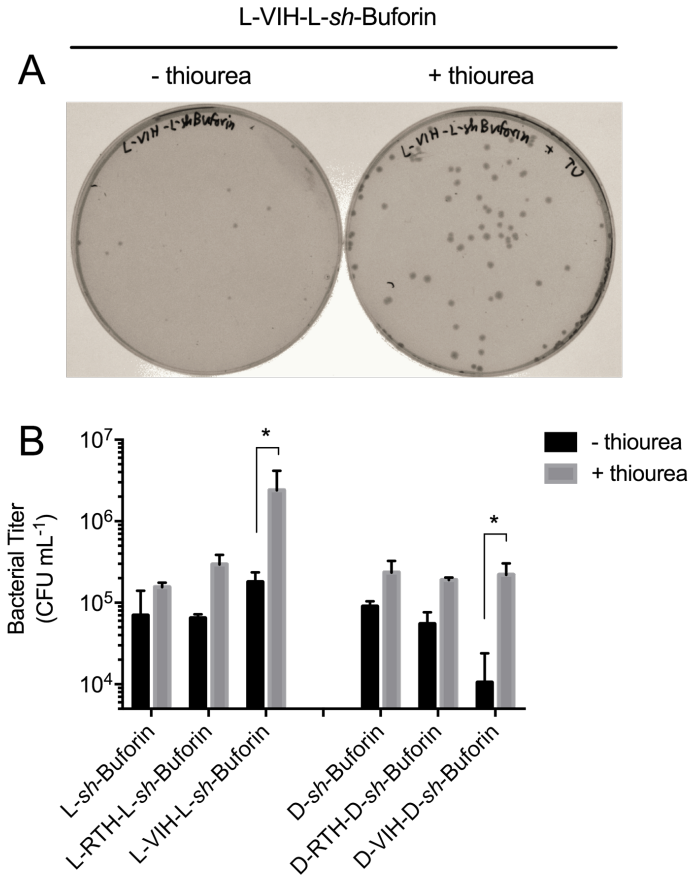

Figure 5.6. Involvement of ROS in ATCUN-*sh*-Buforin Activity. (A) Representative agar plates showing different bacterial susceptibility towards L-VIH-L-*sh*-Buforin in the presence of the radical scavenger, thiourea. (B) Presence of thiourea rescues survival of peptide-exposed *E. coli*. A greater degree of protection was observed during ATCUN-*sh*-Buforin treatments. *, $P<0.01$.

Positively charged ATCUN motifs promote DNA binding in vitro

Buforin II is found in the N-terminal region of Histone H2A of Xenopus,[226] and hence has DNA-binding capability as shown by previous *in vitro* experiments.[11, 227] We determined how the addition of the ATCUN motif changes the affinity of *sh*-buforin to DNA by employing a competition assay between Ethidium bromide (EtBr) and our peptides. We titrated a mixture of pUC19 plasmid and EtBr with the peptides (or pre-formed Cu-ATCUN-*sh*-buforin) and then measured the decrease in fluorescence after every addition. We observed no statistically significant difference in binding when the ATCUN motif is added (Figure 5.7A). This result was counterintuitive as addition of the tripeptide sequence increases the net charge, Z by 0.1 (for VIH) and by 1.1 (for RTH). On the other hand, when we utilized a 15-mer dsDNA oligonucleotide whose sequence was extracted from the portion of the DNA directly bound to the buforin II segment of Histone H2A (5'-AAATACACTTTTGGT-3'),[217] we observed an increase in binding when RTH is added to *sh*-Buforin (Figure 5.7B). Changing the stereochemistry of the peptides also did not give rise to a change in DNA binding. This suggests that the interaction between DNA and *sh*-buforin is largely ionic in nature. When pUC19 was titrated to pre-formed Cu^{II}-ATCUN-*sh*-buforin, a dramatic increase (up to four-fold) in binding affinity was observed. Cu^{II}-RTH-*sh*-buforin showed higher binding compared to Cu^{II}-VIH-*sh*-buforin (for both stereochemistries); this is likely a result of the key interactions between the guanidinium group of Arg and the nitrogenous bases in the DNA as mapped out by Long and co-workers for the Cu^{II}-Arg-Gly-His complex.[218] The Cu^{II}-ATCUN complex has high affinity towards A/T-rich regions of the DNA minor groove.[228, 229] We hypothesize that the large difference in binding affinity is caused by a change in binding mode – without Cu^{2+},

ATCUN-*sh*-buforin binds through the buforin portion, but with Cu^{2+}, it binds through both the buforin domain and the metal complex greatly increasing the formation constant of the peptide-DNA complex.

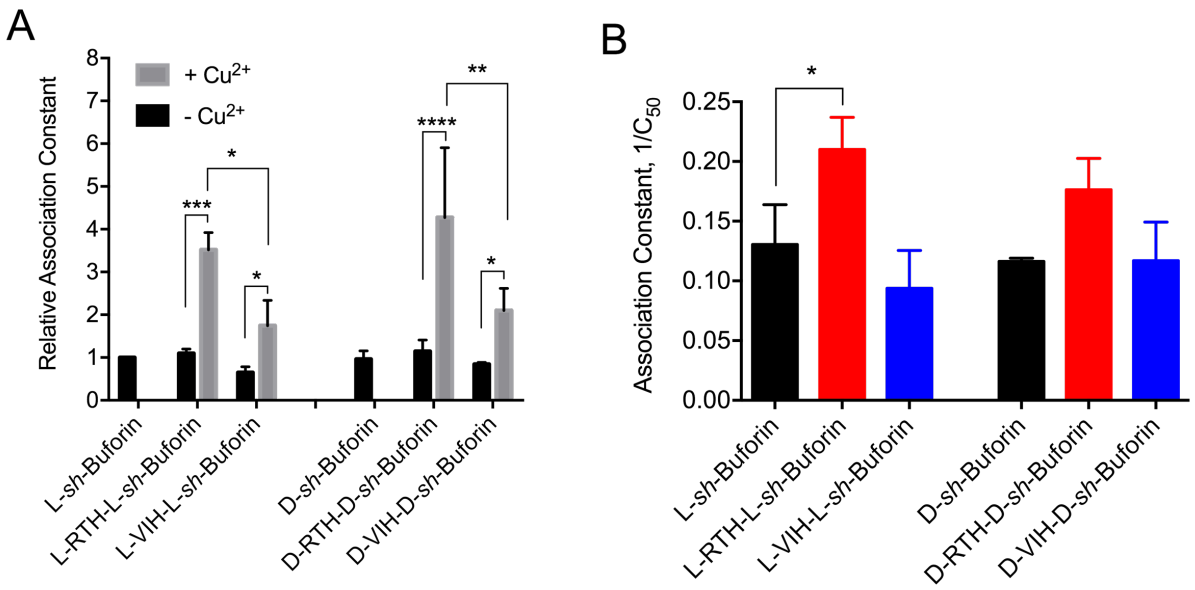

Figure 5.7. *In vitro* DNA binding of ATCUN-*sh*-Buforin. (A) Peptide-plasmid pUC19 association constant was calculated by measuring the decrease in ethidium bromide as a function of added peptide. Calculated values were normalized against L-*sh*-Buforin whose K_a = 1.00. A dramatic increase in binding was observed when Cu^{2+} is added. (B) Association constant defined as the concentration of peptide required to reduce initial fluorescence of ethidium bromide by half. RTH-*sh*-Buforin were found to bind tighter to a 15-mer oligonucleotide whose sequence was extracted from the portion of DNA directly bound to the Buforin II portion of Histone H2A. *, P<0.05; **, P<0.01; ***, P<0.005; and ****, P<0.001.

ATCUN-sh-buforin have catalytic nuclease activity in vitro

Since the ATCUN motif can form ROS and subsequently cleave DNA when bound to Cu^{2+}, we studied the extent of DNA linearization promoted by the Cu-ATCUN-*sh*-buforin complexes. We used as a model DNA target, a solution of the plasmid pUC19.

Our results showed a time-dependent decrease in the supercoiled form with a concomitant increase of the linearized form (Figure 5.8A, and Appendices Figure S5.3). We quantified the amount of supercoiled and linearized pUC19 at each time point and plotted it against time (Appendices Figure S5.3). The resulting curves show that rate of DNA cleavage is faster for ATCUN-D-*sh*-buforin compared to ATCUN-L-*sh*-buforin as evidenced by their slope. Our data show that the VIH-*sh*-buforin peptides cleave DNA faster compared to RTH-*sh*-buforin. This is not surprising because the oxidative nuclease activity is largely influenced by the sequence and stereochemistry of the ATCUN motif alone.[90, 91] Results also show that there is generally a smaller amount of supercoiled form that remains when it is incubated with ATCUN-D-*sh*-buforin, and that an L-to-D amino acid substitution in the ATCUN motif alone leads to a smaller (however statistically insignificant) amount of supercoiled DNA (Figure 5.8B). Taken together our results indicate that DNA cleavage is controlled largely by the stereochemistry of the parent peptide and to a smaller extent the stereochemistry of the ATCUN motif. Even though we did not study the rate of ROS formation of the D-ATCUN motifs alone, our DNA cleavage results agree with what Cowan and his co-workers pointed out that an L-to-D amino acid substitution leads to a greater rate of ROS-promoted DNA cleavage.[91]

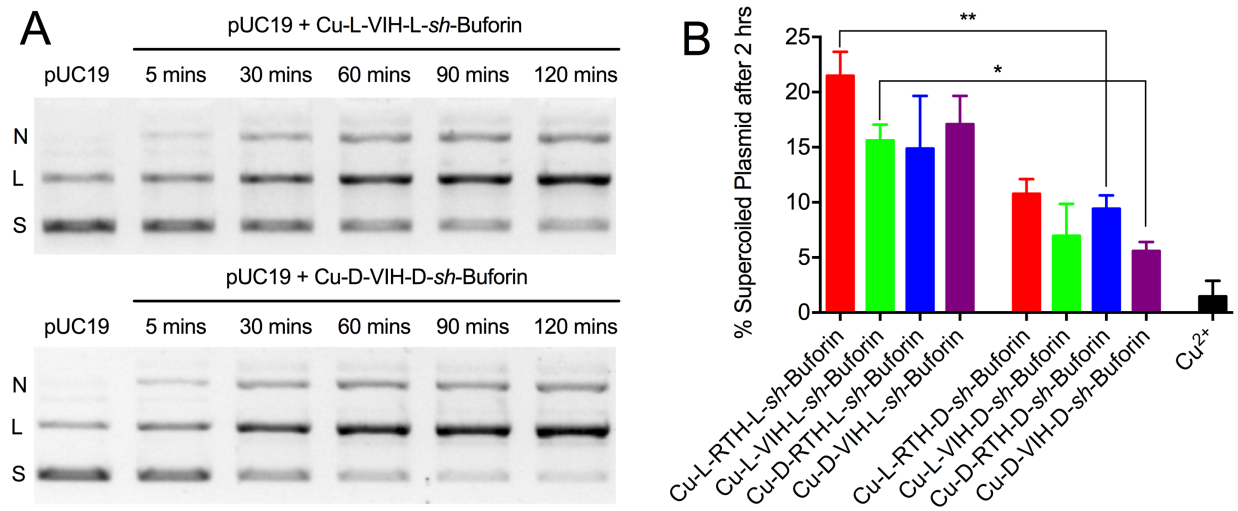

Figure 5.8. *In vitro* Nuclease Activity of ATCUN-*sh*-Buforin. (A) DNA cleavage was monitored using agarose gel electrophoresis at the indicated time points following incubation with the copper complexes of the peptides. N = nicked, L = linearized, and S = supercoiled form of the plasmid pUC19. (B) Amount of supercoiled plasmid remaining at the end of the experiment (a reporter of degree of reaction completion) shows that ATCUN-D-*sh*-Buforin cleaves DNA more efficiently compared to their enantiomer. *, $P<0.05$; **, $P<0.01$.

A closer examination of the cleavage patterns show a propensity for linearization, that is, the intensity of the bands corresponding to the nicked form seem to plateau out (around 60 mins) while that of the linearized form seem to continue increasing (Figure 5.8A). This suggests that double strand breaks are preferred over single strand breaks. Single-strand (ss) nicks in opposite strands of DNA can occur sufficiently close such that the forces stabilizing the double helix is weakened resulting to a double-strand (ds) break. Rationally, when the metallopeptide binds to a specific region on the DNA, the ROS produced diffuses to nearby regions resulting in a greater degree of dsDNA breaks. In light of this, we wanted to determine whether DNA cleavage occurs via a random process

or a concerted one using a standard statistical test.[230] The average number of ssDNA (n_1) and dsDNA (n_2) breaks per molecule was calculated from the fraction of linearized and supercoiled plasmid remaining after each time point. We then calculated the ratio n_1/n_2. The Freifelder-Trumbo relationship indicates that under completely random conditions, 100 ssDNA breaks occurs for every one dsDNA break, that is $n_1/n_2 \geq 100$ for a random cleavage event. Our calculations revealed n_1/n_2 values that were much less than 100 (Table 5.3) indicating that the ROS responsible for cleavage attack the DNA locally. The n_1/n_2 values were generally smaller for RTH-*sh*-buforin and for the L-peptides.

Table 5.3. Freifelder-Trumbo Analysis of *in vitro* DNA Cleavage by ATCUN-*sh*-Buforin.

Peptide Complex	n_1 / n_2	Peptide Complex	n_1 / n_2
L-RTH-L-*sh*-Buforin	2.1	L-RTH-D-*sh*-Buforin	2.7
L-VIH-L-*sh*-Buforin	2.1	L-VIH-D-*sh*-Buforin	4.2
D-RTH-L-*sh*-Buforin	1.8	D-RTH-D-*sh*-Buforin	3.7
D-VIH-L-*sh*-Buforin	2.6	D-VIH-D-*sh*-Buforin	4.9

ATCUN-sh-buforin cleave DNA in live E. coli

To determine whether the observed in vitro nuclease activity occurs in bacterial cells, we employed the Terminal deoxyribonucleotide transferase (TdT)-mediated dUTP Nicked End Labelling (TUNEL) Assay. The assay involves cell fixation and permeabilization with subsequent labeling of DNA strand breaks using an enzymatic, template-independent reaction. The TdT transfers a fluorescein-conjugated nucleotide to

free 3'-OH groups present in DNA strand breaks, hence, greater cell fluorescence means a greater amount of DNA damage. This assay has been used to assess DNA damage in *E. coli* and *H. volcanii* brought about by H_2O_2.[231] The data we obtained from measuring the TUNEL fluorescence of 100,000 cells proves the existence of DNA strand breaks in *E. coli* brought about by the peptides at their MIC (Figure 5.9). Moreover, the ATCUN-*sh*-buforin conjugates exhibited greater TUNEL fluorescence compared to *sh*-buforin alone, trailing the observed trend in MIC. It is worth noting that MIC of the D-peptides were about one-eighth those of the L-peptides, indicating that it requires a smaller amount of D-peptides to generate the same amount of DNA strand breaks. The D-ATCUN-D-*sh*-buforin analogs seem to have a higher nuclease activity *in cella*, consistent with our *in vitro* assay.

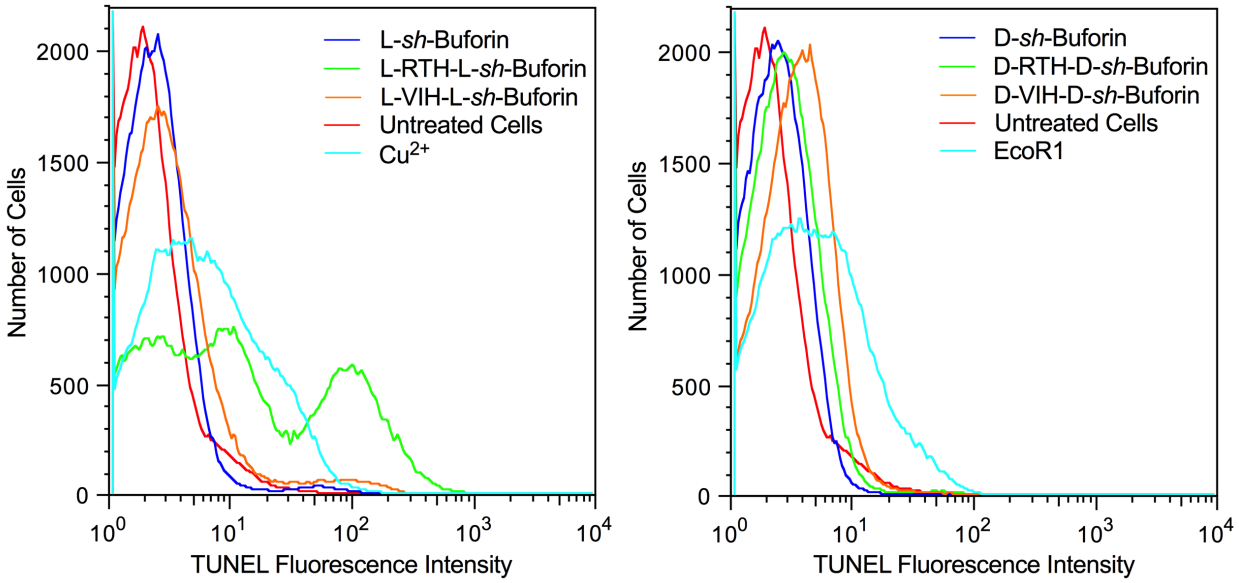

Figure 5.9. *In cella* DNA Cleavage by ATCUN-*sh*-Buforin. Representative histograms for detection of DNA damage in *E. coli* via the TUNEL assay. *E. coli* cells were treated with peptides at their MIC for 2 hrs. ATCUN-*sh*-Buforin showed higher nuclease activity relative to *sh*-Buforin alone.

ATCUN-sh-buforin are minimally cytotoxic to mammalian cells

Hemolysis assays were performed in PBS. Our data (Table 5.4) suggests that the synthesized peptides exhibit very low hemolytic activity at their MIC against *E. coli*. Addition of the ATCUN motif to *sh*-buforin does not seem to increase the peptide's hemolytic activity. All of the tested peptides were found to have less than 8% hemolysis at MIC, suggesting high selectivity towards bacterial cells. We calculated the concentration required to lyse 5% of the cells (Table 5.4) and used it to determine therapeutic indices, which were in the range of 0.14 through 13 suggesting good therapeutic potential. HeLa and HEK293 cells were used for the cytotoxicity studies of the peptides. The results depicted in Figure 5.10 indicate that all ATCUN-*sh*-buforin peptides showed very low toxicity or no toxicity to these cell lines up to 128 μM, a concentration well above their MIC values.

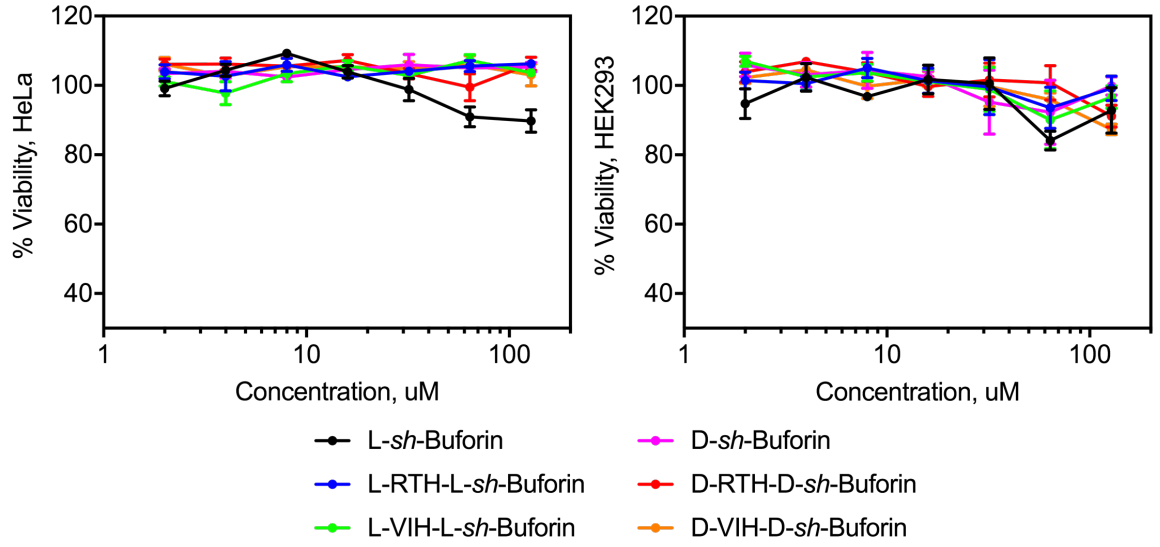

Figure 5.10. *In vitro* Cytotoxicity of ATCUN-*sh*-Buforin Against Mammalian Cells. HeLa and HEK293 cells were treated with peptides at varying concentrations for 24 hrs and viability was assessed by quantification of the insoluble formazan product from MTT oxidation. All tested peptides exhibit minimal toxicity.

Table 5.4. Hemolytic Activity and Calculated Therapeutic Indices of the Peptides.

Peptide	% Hemolysis	HD_5, μM	Therapeutic Index
L-*sh*-Buforin	5.5 ± 0.9	44	7
L-RTH-L-*sh*-Buforin	5.8 ± 0.6	26	4
L-VIH-L-*sh*-Buforin	5.9 ± 0.8	10	2
D-RTH-L-*sh*-Buforin	4.9 ± 0.5	54	11
D-VIH-L-*sh*-Buforin	7.4 ± 0.7	1	0.14
D-*sh*-Buforin	3.7 ± 0.1	45	11
L-RTH-D-*sh*-Buforin	4.2 ± 0.3	51	13
L-VIH-D-*sh*-Buforin	6.6 ± 0.9	1	0.14
D-RTH-D-*sh*-Buforin	5.4 ± 0.9	11	2
D-VIH-D-*sh*-Buforin	5.3 ± 1.0	3	0.60
Magainin 2	7.5 ± 2.4	2	0.25

Discussion

Buforin II and *sh*-buforin have been shown to exert their antimicrobial activity by traversing the bacterial membrane and binding to nucleic acids.[216, 217, 226] DNA is also the main target of the ATCUN-*sh*-buforin derivatives. The *ΔrecA* mutant *E. coli* TD172 was more susceptible to the ATCUN-*sh*-buforin peptides than wild-type *E. coli* MG1655. In this chapter, we studied the effect to the bioactivity of ATCUN-*sh*-buforin conjugates ($X_{aa}X_{aa}$HRAGLQFPVGRVHRLLRK-NH_2) upon: (1) inclusion of a basic amino acid in the ATCUN motif and (2) L-to-D amino acid substitution. The Arg-Thr-His (RTH) motif is expected to increase the affinity of the copper-bound ATCUN motif for the bacterial DNA; whereas the change in ATCUN stereochemistry is anticipated to result in an increased nuclease activity by metal complexes of this motif.[91]

sh-buforin has high affinity towards bacterial DNA. The addition of a positively charged ATCUN motif is expected to increase the binding affinity of the peptide for the negatively charged DNA. When we used a 15-mer sequence from a DNA sequence known to interact strongly with buforin II and its derivatives, our fluorescent intercalator displacement assay revealed that the RTH derivatives have larger affinities than the VIH peptides. The larger affinity displayed by the RTH peptides disappeared when pUC19 was used indicating that the peptide-nucleic acids interaction depends on the DNA sequence. Interestingly, the affinity towards pUC19 by the copper-bound peptides (Cu^{II}-ATCUN-*sh*-buforin) was three- to four-times larger than that of the apopeptide and a larger affinity was observed for the Cu^{II}-RTH-*sh*-buforin derivatives. The antimicrobial assays, however, showed that L-*sh*-buforin derivatives benefit from the positive charge, whereas the D-*sh*-buforin peptides had the same or lower activity when the RTH motif is

used. Thus, the charge of the ATCUN motif alone does not determine the overall activity of the peptide.

Results from our antimicrobial susceptibility testing revealed that the D-peptides are more active compared to the L-peptides. Within the same family, a change in stereochemistry of the ATCUN motif did not affect the antimicrobial activity (L-ATCUN-L-*sh*-buforin vs D-ATCUN-L-*sh*-buforin). Interestingly, the stereochemistry of the *sh*-buforin moiety dictates the potency (MIC of ATCUN-L-*sh*-buforin > MIC of ATCUN-D-*sh*-buforin, and DNA cleavage by ATCUN-D-*sh*-buforin > DNA cleavage by ATCUN-L-*sh*-buforin). Previous reports of L-to-D amino acid substitutions on membrane active peptides, wherein the key interactions are not chiral in nature, resulted in little to no increase in activity.[219, 232-235] However, in apidaecin and drosocin – AMPs thought of having intracellular targets – the antimicrobial activities of the all-L peptides differ from the all-D enantiomer.[236, 237] In both cases, the all-D peptides are less active than the all-L AMPs. It is interesting to note that the all-L and all-D enantiomers of the peptide WRWYCR, an AMP that induces DNA damage through Holliday junction-trapping, showed the same MIC values against a panel of bacteria.[238] Therefore, the observed eight-fold to 32-fold increase in activity for the all-D-ATCUN-*sh*-buforin peptides is to our knowledge unprecedented. This increase in activity is the result of the combined increased stability and higher DNA cleavage activity by the all-D peptides.

ROS formation plays a major role in the bacterial killing by ATCUN-*sh*-buforin. This was established by rescuing the bacterial population through the addition of the radical scavenger thiourea. When intracellular Cu^{2+} binds to ATCUN-*sh*-buforin, the resulting complex forms ROS, which then targets the major biomolecules in the cell causing the

bacteria to die of excessive oxidative stress. No significant difference in ROS production is observed when the ATCUN motif is added. This is likely due to the fact that the intermediate ROS formed by Cu-ATCUN complexes are non-diffusible; that is they are bound to the copper center.[90, 239] A scheme proposed by Cowan involves molecular oxygen undergoing a two-electron reduction, wherein two Cu-ATCUN complexes dimerizes via a peroxo bridge, and subsequently forms a hydroperoxyl anion. The resulting hydroperoxyl is reduced to form hydroxide ion and a copper-bound hydroxyl radical (Equations 1-3 in Chapter 1).[90]

In summary, the experiments described in this study allow us to better understand the role of the ATCUN motif in ATCUN-*sh*-buforin peptides. Comprehending the key factors that play a fundamental role in ATCUN-containing peptides is not only important to develop more potent AMPs but it will also allow us to understand the role of ATCUN motifs in AMPs found in nature. We found a strong correlation between the *in vitro* DNA cleavage results and the MICs (Figure 5.11A). For the group of D-peptides, we observed a strong correlation between the median TUNEL fluorescence and the MIC (Figure 5.11B), that is, a greater TUNEL fluorescence corresponds to a lower MIC. The same correlation was also observed for the L-peptides. Therefore, direct DNA damage plays a large and central role in the antimicrobial activity of ATCUN-*sh*-buforin peptides. A positively charged ATCUN motif contributes towards the DNA binding affinity but does not always result in an increased antimicrobial activity. We also found that changing the stereochemistry of the ATCUN-*sh*-buforin peptide leads to an increase in antimicrobial activity, as a result of the larger stability and enhanced nuclease activity of the peptides.

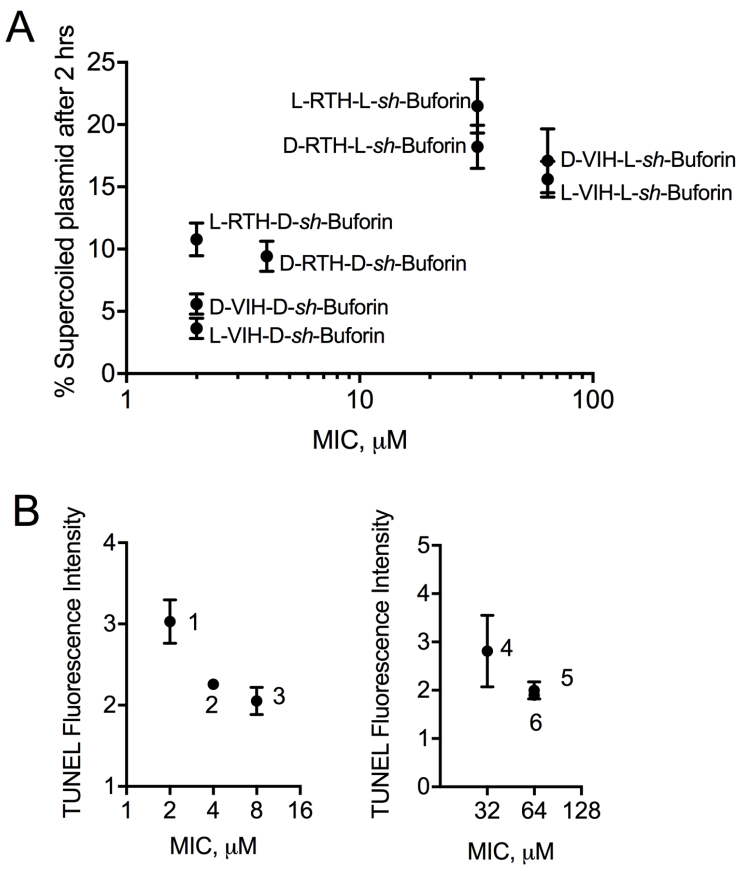

Figure 5.11. Nuclease and Antibacterial Activity Correlations of ATCUN-*sh*-Buforin. (A) Correlation between *in vitro* DNA cleavage and MIC of peptides. (B) Correlation between *in cella* DNA damage and observed MICs. Both panels show strong correlation between nuclease and antimicrobial activity of peptides, suggesting a strong involvement of DNA damage by ATCUN-*sh*-Buforin peptides.

Methodology

Peptide Synthesis, Purification, Quantification and Handling. Peptides were manually synthesized using standard Fmoc protocols and purified (≥95%) via reversed phase-HPLC on a C18 column. The purified fractions were characterized by ESI-MS ran in positive ion mode. The peptides were quantified using sequence-specific molar

extinction coefficients using reported values for each amino acid and the peptide bond as reported by Gruppen.[240] All purified peptides were dissolved in nanopure water and were stored at 4°C and were diluted to the required concentration on the day of the experiment. Finally, to form the Cu^{2+}-peptide complexes, 1.5 eq of peptide was mixed with 1 eq of Cu^{2+} (to ensure no free copper remains) and incubated at room temperature for 30-45 mins.

Antimicrobial Assay. Single colonies of *E. coli* (MG1655, WT), *E. coli* (TD172, *recA*)[241] and *E. aerogenes* (ATCC 13048) were grown in Mueller-Hinton Broth (MHB; Difco) for 3-5 hrs until mid-logarithmic phase. The peptide stock solutions were diluted in 1X sterile phosphate buffered saline (PBS; Gibco), pH 7.40 starting at 128 μM. Then 50 μL aliquots of a two-fold serial dilution series were placed on a sterile 96-well polypropylene plate (Greiner). To each well, 50 μL of a bacterial suspension was added to yield a final inoculum of $5x10^5$ CFU/mL per well. Ampicillin and Kanamycin (mixed isomers) were used as positive control. The plates were incubated at 37°C (30°C for *E. aerogenes*) for 18-20 hrs. For the experiments involving addition of Cu^{2+}, the same dilutions and manipulations were done using MHB containing 32 μM Cu^{2+}, but allowing for a 30 min incubation time prior to addition of bacteria. This concentration is well below the toxic level of Cu2+ for E. coli, which is 3.5 mM).[242] For both cases, the Minimum Inhibitory Concentration (MIC) was defined as the lowest concentration that prevent visual growth of bacteria. MIC values reported here is the mode of three independent trials.

Time-Kill Kinetics Experiment. The number of viable cells was determined 1, 2, 4, and 8 hrs after exposure. A 350 μL aliquot of peptide at concentration 2X the MIC was mixed with 350 μL of 10^6 CFU/mL bacterial suspension (*E. coli* MG1655 or *E. coli* TD172)

in MHB, to yield a final inoculum containing $5x10^5$ CFU/mL and peptide at the MIC. At each specified time point, 10 µL of the mixture was withdrawn and was serially diluted up to 1:1000. Then, 100 µL of the 10^{-3} dilution was spread on LB agar plates (the 10^{-2} dilutions were used when no colonies were detected from the 10^{-3}) and allowed to grow for an additional 16 hrs. The number of single colonies was counted and was plotted against time. The curves represent the average obtained from three independent trials.

Circular Dichroism Spectra. CD spectra were recorded on a Jasco J-710 Spectropolarimeter. Samples used were 100 µM of peptide in 50% (v/v) TFE in 50 mM sodium phosphate (NaPB), pH 7.40 in a 1 mm cuvette. Each spectrum was the average of 5 accumulations, and the spectra were recorded twice using peptides prepared at different time points to ensure reproducibility. The two average spectra showed <5% deviation from each other. For spectra of Cu-ATCUN-AMP, a 2 µL aliquot of a concentrated Cu^{2+} stock was added to the peptide sample to yield $[\text{Cu-ATCUN-AMP}]_{final}$ = 90 µM. Solution was allowed to equilibrate for 5 mins before obtaining CD spectra. The mean residue ellipticity, [θ] was calculated using eqn 1, where θ is the measured ellipticity, l is pathlength in cm, c is concentration in millimolars, and n is the number of residues in the peptide.[232]

$$[\theta] = (100 \cdot \theta) / (l \cdot c \cdot n) \qquad (1)$$

The percent alpha helical content was calculated using eqn 2, where $[\theta]_{222}$ is the mean residue ellipticity calculated at 222 nm.

$$\% \ \alpha \text{ helix} = ([\theta]_{222} - 3000) / 33000 \qquad (2)$$

β-galactosidase Leakage Assay. Overnight cultures of *E. coli* transformed with pUC19 were subcultured in fresh Luria-Bertani (LB) broth and were allowed to grow to

$OD_{600\ nm}$ ~ 0.6. Overexpression of β-galactosidase was induced for 1 hr by addition of isopropyl-β-D-thiogalactopyranoside (IPTG; Fisher) at 1 mM final concentration. The cells were washed three times with PBS and resuspended in fresh LB. Then, a 75 µL aliquot of the bacterial suspension was mixed with 75 µL aliquot of a two-fold serial dilutions of the peptides (starting from 64 µM) in sterile microcentrifuge tubes. The mixture was incubated for 1 hr at 37°C. The tubes were then spun down at 4400 rpm at 4°C for 10 min, then 100 µL of the supernatant was transferred to a clear 96-well plate. A 50 µL aliquot of 2-nitrophenyl-β-D-galactopyranoside (ONPG; Thermo Scientific) in PBS was added at 0.8 mg/mL final concentration. Color was allowed to develop for 1 hr in the dark, and then absorbance of each well was measured at 405 nm. Data shown are the average of three independent trials presented as Mean ± SD.

Measurement of Intracellular ROS Formation.[243] *E. coli* MG1655 cells in mid-logarithmic phase were washed twice with M9+glucose minimal media and resuspended in fresh M9+glucose containing 10 µM of the profluorescent probe 2',7'-dichlorofluorescein diacetate. The dye was loaded for 1 hr before washing the cells twice to remove unloaded dye. The cells were then suspended in fresh M9+glucose and were allowed to grow for an additional 30 mins, after which the cells were incubated with the peptides at MIC for 2 hrs. For experiments with the iron chelator, 2,2′-bipyridine, a small aliquot was added to the loaded cells to yield a 500 µM final concentration of bipyridine prior to incubation with the peptides. The fluorescence of 100,000 cells was read using a BD FACSCalibur flow cytometer with the following PMT voltage settings: E00 (FSC, primary collection parameter), 350 (SSC), and 600 (FL1). Data were analyzed using FlowJo 10.0 and the mean fluorescence intensity (MFI) of each experimental run was

normalized against the MFI of the negative control (PBS), which was set to 1.0. Results shown are obtained from three independent trials and presented as Mean ± SD.

Viable Colony Counting with Thiourea. Equal volumes of bacterial suspension containing 10^6 CFU/mL were mixed with peptide solution at 2X its MIC. This mixture was split into two portions, and to one of which were added thiourea to a final concentration of 100 μM. The cells were incubated at 37°C for 1 hr, after which a 10-μL aliquot was diluted 1:1000 using fresh MHB. Then 100 μL of the 10^{-3} dilution were spread onto fresh LB Agar plates and incubated overnight. The number of colonies was counted the next day. Results shown are obtained from two independent trials presented as Mean ± SD.

Fluorescent Intercalator Displacement Assay. *sh*-buforin, ATCUN-*sh*-buforin and preformed Cu^{II}-ATCUN-*sh*-buforin (1.2 eq of peptide with 0.9 eq of Cu^{2+}) were titrated into a 200 μL mixture containing 15 μM bp pUC19 and 7.5 μM Ethidium bromide in 10 mM NaCl and 10 mM sodium cacodylate buffer, pH 7.50. All measurements were done in a Molecular Devices FlexStation 3 with λex = 545 nm and λem = 595 nm. All fluorescence readings were corrected for dilution, and then fluorescence was plotted with concentration. The curves were fitted to a linear equation (all $R^2 > 0.91$) and C50 was calculated and defined as concentration of peptide required to decrease the fluorescence to half its original value. The Association constant K_a was the inverse of C50. Calculated values were normalized relative to L-*sh*-buforin which was assigned a value of 1.00. Data shown here are obtained from three independent experiments and presented as Mean ± SD.

In vitro DNA Cleavage Assay. The reaction mixtures contained 10 μM base pair pUC19, 100 nm Cu^{II}-ATCUN-AMP, 1 mM sodium ascorbate, and 1 mM H_2O_2 in 20 mM

HEPES, 100 mM NaCl pH 7.40. Reactions were run at room temperature for the indicated times and were stopped using 3X loading dye containing 1 mM EDTA. Then a 15 µL aliquot was loaded on a 1% agarose gel containing Ethidium bromide (EtBr) and ran at 100 V for 40 mins. The gels were imaged using a Bio-Rad GelDoc XR+ Imager, and bands were quantified using the accompanying Image Lab 5.0 software. A correction factor of 1.47 was applied to the intensity of supercoiled DNA due to its diminished ability to intercalate EtBr. Data shown here is the average of four trials reported as Mean ± SD.

Freifelder-Trumbo Analysis. The fraction of linearized DNA, f(III), is related to the number of double strand breaks, n_2, per molecule and can be calculated from the first term of the Poisson distribution (eq 3).

$$f(III)= n_2\, e^{(-n_2)} \qquad (3)$$

The number of single strand breaks, n_1, was then calculated from the fraction of supercoiled DNA, f(I), remaining after treatment with the Cu^{II}-ATCUN-AMP complexes using the Friefelder-Trumbo equation (eq 4).

$$f(I)= e^{(-(n_1+n_2))} \qquad (4)$$

This statistical test shows that the number of double-strand breaks arising from random single-strand nicks is less than 0.01, that is $(n_1/n_2) > 100$. Hence, by calculating the ratio of n_1 and n_2, one can determine whether linearization resulted from a random or concerted cleavage event.

TUNEL Assay. To assess the extent of *in cella* DNA damage brought about by the peptides, the Terminal deoxyribonucleotide transferase (TdT)-mediated dUTP Nick End Labelling (TUNEL) Assay was employed. An overnight culture of *E. coli* TD172 was subcultured 1:20 in fresh MHB and was allowed to grow for an additional 90 mins (~10^7

CFU/mL). A 350 µL aliquot of peptide at 2X the MIC was mixed with 350 µL of the bacterial suspension. The mixture was incubated at 37°C for 2 hrs, after which, the cells were pelletized and washed twice with ice-cold PBS. The cells were then fixed using 100 µL of 4% paraformaldehyde in 1X PBS for 30 mins. The cells were pelleted and resuspended in 100 µL of permeabilization solution (0.1% Triton X-100 in 0.1% sodium citrate) then incubated on ice for 2 minutes. The pellets were kept on ice. The positive control was resuspended in 50 µL of digestion buffer (CutSmart; New England Biolabs) containing 20 U of EcoR1 to generate single strand breaks. The digestion was allowed to proceed for 1 hr at 37°C, after which, the cells were pelleted. All tubes were resuspended in 50µL of 1X TUNEL reaction mixture (9 parts label solution, 1 part TdT enzyme; Roche Molecular Biochemicals, Indianapolis, IN) and were incubated in the dark at 37°C for 1 hr. The cells were then pelleted and washed once with ice-cold PBS. Cells were counterstained using the nuclear dye Propidium Iodide (PI). The PI staining was allowed to proceed for 10 mins, then 5 µL of the mixtures were diluted with 1 mL of PBS and the green and red fluorescence of 100,000 cells were analyzed using a BD FACSCalibur flow cytometer. Results shown are representative of three trials performed independently.

Hemolytic Assay. To assess the selectivity of the peptides against bacterial membranes, extent of hemolysis was measured in human red blood cells (RBCs). Packed human erythrocytes (ZenBio, Inc, Research Triangle, NC, USA) with anticoagulant citrate dextrose were washed three times with sterile PBS. A small aliquot of washed cells was resuspended in fresh PBS to yield a 0.8% (v/v) suspension of RBCs. Then 75 µL of RBCs were mixed with 75 uL aliquots of a two-fold serial dilution series of the peptides (starting from 64 µM). The mixture was incubated at 37°C for 1 hr. Triton X-100 and PBS were

used as positive and negative controls, respectively. The cells were then pelleted and 100 µL of the supernatant were carefully removed and transferred to a clear 96-well plate. The absorbance of each well at 414 nm was measured and was normalized against the positive and negative controls. Results shown are the average from three independent trials shown as Mean ± SD.

MTT Cell Viability Assay. HeLa and HEK293 cells were grown in DMEM supplemented with 10% Fetal Bovine Serum and incubated in a humidified atmosphere at 37°C and 5% CO2. Cytotoxicity studies were done using the MTT Assay (3-(4,5-dimethylthiazol-2-yl)-2,5-diphenyltetrazolium bromide, Invitrogen). Breifly, 5000 cells were seeded in each well of a sterile 96-well plate and incubated for 20 hours to allow cells to adhere. The media were aspirated and replaced with 200 uL of media containing serial dilutions of the peptide (starting from 128 uM). The cells were incubated for 24 hours after which 10 uL of 5 mg/mL solution of MTT was added to each well. The color development was allowed to proceed for 4 hours. The media was then removed and the purple formazan product was solubilized using pure DMSO. The absorbance of each well at 595 nm was recorded and used to calculate % viability.

Statistical Analysis. Data were analyzed for statistical differences using GraphPad Prism 6.0. One-Way or Two-Way ANOVA was used to determine statistical significane. The Sidak's or Turkey's multiple comparisons test was used as post-test. Statistical significance for all tests was set at $P < 0.05$.

Chapter References:

[1] Joyner, J. C., and Cowan, J. A. (2011) Targeted cleavage of HIV RRE RNA by Rev-coupled transition metal chelates, *Journal of the American Chemical Society 133*, 9912-9922.

[2] Jin, Y., and Cowan, J. A. (2005) DNA cleavage by copper-ATCUN complexes. Factors influencing cleavage mechanism and linearization of dsDNA, *Journal of the American Chemical Society 127*, 8408-8415.

[3] Jin, Y., Lewis, M. A., Gokhale, N. H., Long, E. C., and Cowan, J. A. (2007) Influence of stereochemistry and redox potentials on the single- and double-strand DNA cleavage efficiency of Cu(II) and Ni(II) Lys-Gly-His-derived ATCUN metallopeptides, *Journal of the American Chemical Society 129*, 8353-8361.

[4] Burke, S. K., Xu, Y., and Margerum, D. W. (2003) Cu(II)Gly2HisGly Oxidation by H2O2/Ascorbic Acid to the Cu(III) Complex and Its Subsequent Decay to Alkene Peptides, *Inorg. Chem. 42*, 5807-5817.

[5] Bossu, F. P., Chellappa, K. L., and Margerum, D. W. (1977) Ligand effects on the thermodynamic stabilization of copper(III)-peptide complexes, *J. Am. Chem. Soc. 99*, 2195-2203.

[6] Joyner, J. C., Hodnick, W. F., Cowan, A. S., Tamuly, D., Boyd, R., and Cowan, J. A. (2013) Antimicrobial metallopeptides with broad nuclease and ribonuclease activity, *Chem. Commun. (Cambridge, U. K.) 49*, 2118-2120.

[7] Elmore, D. E. (2012) Insights into buforin II membrane translocation from molecular dynamics simulations, *Peptides 38*, 357-362.

[8] Park, C. B., Kim, H. S., and Kim, S. C. (1998) Mechanism of action of the antimicrobial peptide buforin II: buforin II kills microorganisms by penetrating the cell membrane and inhibiting cellular functions, *Biochem Biophys Res Commun 244*, 253-257.

[9] Park, C. B., Yi, K. S., Matsuzaki, K., Kim, M. S., and Kim, S. C. (2000) Structure-activity analysis of buforin II, a histone H2A-derived antimicrobial peptide: the proline hinge is responsible for the cell-penetrating ability of buforin II, *Proceedings of the National Academy of Sciences of the United States of America 97*, 8245-8250.

[10] Uyterhoeven, E. T., Butler, C. H., Ko, D., and Elmore, D. E. (2008) Investigating the nucleic acid interactions and antimicrobial mechanism of buforin II, *FEBS letters 582*, 1715-1718.

[11] Fang, Y. Y., Ray, B. D., Claussen, C. A., Lipkowitz, K. B., and Long, E. C. (2004) Ni(II).Arg-Gly-His-DNA interactions: investigation into the basis for minor-groove binding and recognition, *Journal of the American Chemical Society 126*, 5403-5412.

[12] McGrath, D. M., Barbu, E. M., Driessen, W. H., Lasco, T. M., Tarrand, J. J., Okhuysen, P. C., Kontoyiannis, D. P., Sidman, R. L., Pasqualini, R., and Arap, W. (2013) Mechanism of action and initial evaluation of a membrane active all-D-enantiomer antimicrobial peptidomimetic, *Proceedings of the National Academy of Sciences of the United States of America 110*, 3477-3482.

[13] Yarlagadda, V., Akkapeddi, P., Manjunath, G. B., and Haldar, J. (2014) Membrane active vancomycin analogues: a strategy to combat bacterial resistance, *Journal of medicinal chemistry 57*, 4558-4568.

[14] Dwyer, D. J., Belenky, P. A., Yang, J. H., MacDonald, I. C., Chan, C. T. Y., Braff, D., Schwarz, E. G., Ye, J. D., Martell, J. D., Ting, A. Y., Takahashi, N., Vercruysse, M., Walker, G. C., Lobritz, M. A., Pati, M., Ralifo, P. S., Allison, K. R., Khalil, A. S., and Collins, J. J. (2014) Antibiotics induce redox-related physiological alterations as part of their lethality, *Proceedings of the National Academy of Sciences of the United States of America 111*, E2100-2109.

[15] Foti, J. J., Devadoss, B., Winkler, J. A., Collins, J. J., and Walker, G. C. (2012) Oxidation of the guanine nucleotide pool underlies cell death by bactericidal antibiotics, *Science (New York, N.Y.) 336*, 315-319.

[16] Kohanski, M. A., Dwyer, D. J., Hayete, B., Lawrence, C. A., and Collins, J. J. (2007) A common mechanism of cellular death induced by bactericidal antibiotics, *Cell 130*, 797-810.

[17] Liu, Z., Cai, Y., Young, A. W., Totsingan, F., Jiwrajka, N., Shi, Z., and Kallenbach, N. R. (2012) OH radical production stimulated by (RW)4D, a synthetic antimicrobial agent and indolicidin, *MedChemComm 3*, 1548-1554.

[18] Jiang, N., Tan, N. S., Ho, B., and Ding, J. L. (2007) Respiratory protein-generated reactive oxygen species as an antimicrobial strategy, *Nature immunology 8*, 1114-1122.

[19] Khodade, V. S., Sharath Chandra, M., Banerjee, A., Lahiri, S., Pulipeta, M., Rangarajan, R., and Chakrapani, H. (2014) Bioreductively Activated Reactive Oxygen Species (ROS) Generators as MRSA Inhibitors, *ACS medicinal chemistry letters 5*, 777-781.

[20] Park, C. B., Kim, M. S., and Kim, S. C. (1996) A novel antimicrobial peptide from Bufo bufo gargarizans, *Biochem Biophys Res Commun 218*, 408-413.

[21] Pavia, K. E., Spinella, S. A., and Elmore, D. E. (2012) Novel histone-derived antimicrobial peptides use different antimicrobial mechanisms, *Biochimica et biophysica acta 1818*, 869-876.

[22] Liang, Q., Ananias, D. C., and Long, E. C. (1998) Ni(II)-Xaa-Xaa-His Induced DNA Cleavage: Deoxyribose Modification by a Common "Activated" Intermediate Derived from KHSO5, MMPP, or H2O2, *J. Am. Chem. Soc. 120*, 248-257.

[23] Liang, Q., Eason, P. D., and Long, E. C. (1995) Metallopeptide-DNA Interactions: Site-Selectivity Based on Amino Acid Composition and Chirality, *J. Am. Chem. Soc. 117*, 9625-9631.

[24] Freifelder, D., and Trumbo, B. (1969) Matching of single-strand breaks to form double-strand breaks in DNA, *Biopolymers 7*, 681-693.

[25] Rohwer, F., and Azam, F. (2000) Detection of DNA damage in prokaryotes by terminal deoxyribonucleotide transferase-mediated dUTP nick end labeling, *Applied and environmental microbiology 66*, 1001-1006.

[26] Huang, J., Hao, D., Chen, Y., Xu, Y., Tan, J., Huang, Y., Li, F., and Chen, Y. (2011) Inhibitory effects and mechanisms of physiological conditions on the activity of enantiomeric forms of an alpha-helical antibacterial peptide against bacteria, *Peptides 32*, 1488-1495.

[27] Won, A., Khan, M., Gustin, S., Akpawu, A., Seebun, D., Avis, T. J., Leung, B. O., Hitchcock, A. P., and Ianoul, A. (2011) Investigating the effects of L- to D-amino acid substitution and deamidation on the activity and membrane interactions of antimicrobial peptide anoplin, *Biochimica et biophysica acta 1808*, 1592-1600.

[28] Wade, D., Boman, A., Wahlin, B., Drain, C. M., Andreu, D., Boman, H. G., and Merrifield, R. B. (1990) All-D amino acid-containing channel-forming antibiotic peptides, *Proceedings of the National Academy of Sciences of the United States of America 87*, 4761-4765.
[29] Wei, G. X., and Bobek, L. A. (2005) Human salivary mucin MUC7 12-mer-L and 12-mer-D peptides: antifungal activity in saliva, enhancement of activity with protease inhibitor cocktail or EDTA, and cytotoxicity to human cells, *Antimicrobial agents and chemotherapy 49*, 2336-2342.
[30] Casteels, P., and Tempst, P. (1994) Apidaecin-type peptide antibiotics function through a non-poreforming mechanism involving stereospecificity, *Biochem Biophys Res Commun 199*, 339-345.
[31] Bulet, P., Urge, L., Ohresser, S., Hetru, C., and Otvos, L., Jr. (1996) Enlarged scale chemical synthesis and range of activity of drosocin, an O-glycosylated antibacterial peptide of Drosophila, *European journal of biochemistry / FEBS 238*, 64-69.
[32] Gunderson, C. W., and Segall, A. M. (2006) DNA repair, a novel antibacterial target: Holliday junction-trapping peptides induce DNA damage and chromosome segregation defects, *Mol. Microbiol. 59*, 1129-1148.
[33] Mack, D. P., Iverson, B. L., and Dervan, P. B. (1988) Design and chemical synthesis of a sequence-specific DNA-cleaving protein, *J. Am. Chem. Soc. 110*, 7572-7574.
[34] Kuipers, B. J., and Gruppen, H. (2007) Prediction of molar extinction coefficients of proteins and peptides using UV absorption of the constituent amino acids at 214 nm to enable quantitative reverse phase high-performance liquid chromatography-mass spectrometry analysis, *Journal of agricultural and food chemistry 55*, 5445-5451.
[35] Dorr, T., Lewis, K., and Vulic, M. (2009) SOS response induces persistence to fluoroquinolones in Escherichia coli, *PLoS genetics 5*, e1000760.
[36] Grass, G., and Rensing, C. (2001) Genes involved in copper homeostasis in Escherichia coli, *Journal of bacteriology 183*, 2145-2147.
[37] Tavares, A. F., Teixeira, M., Romao, C. C., Seixas, J. D., Nobre, L. S., and Saraiva, L. M. (2011) Reactive oxygen species mediate bactericidal killing elicited by carbon monoxide-releasing molecules, *The Journal of biological chemistry 286*, 26708-26717.

Chapter 6

The ATCUN Motif in Targeted Antimicrobial Drug Development

Copper-binding and Cell-penetrating Antimicrobial Peptidomimetic Utilizes Phagosomal Copper to Target Intracellular *M. tuberculosis*

Adapted entirely from:

Libardo, M.D.J., Anand, K., Krishnamoorthy, G., Kaiser, P., Dietz, C., Smith, M.B., Kaufmann, S.H.E., Singh, A.S., Angeles-Boza, A.M., **2017**, *submitted*

Introduction

Resulting in close to two million deaths and more than 10 million new cases annually and with about two billion latent infections worldwide, tuberculosis (TB) remains the deadliest infectious disease known to humankind.[244] This problem is exacerbated by the alarming rate at which multidrug-resistant (MDR) and extensively drug-resistant (XDR) *M. tuberculosis* (Mtb) strains are emerging, extinguishing the efficacy of current anti-TB drugs. There is therefore an urgent need to develop medicines that target this pathogen in novel ways and a pressing demand to understand their mechanism of action.

It is widely known that transition metal trafficking within primary macrophages is altered in response to infection. In keeping with the concept of nutritional immunity, iron and manganese are limited within the phagosomes to deprive pathogens of these essential micronutrients.[41, 245] On the other hand, as substrate to the transporter ATP7A, copper is deliberately enriched in phagosomes and contributes to the macrophage microbicidal effect.[53] Considering its redox cycling, ability to displace metal cofactors of enzymes, iron-sulfur cluster targeting, and its thiophilic nature,[50, 246] it becomes apparent why reallocating this toxic metal to sites containing bacteria is advantageous. Indeed, Mtb-infected macrophages contain 25 – 400 μM of copper in the phagosome.[57] However, there exist redundant defense mechanisms which protect Mtb from copper-related toxicity. The bacilli express CtpV and MctB, membrane-bound copper efflux pumps that transport copper back to the phagosomal lumen.[60, 247] In addition, it expresses cytosolic metallothionein (MymT) which sequesters up to six Cu(I) ions,[68] and a periplasmic oxidase (MmcO) that converts Cu(I) to the less toxic Cu(II).[73] Together, these proteins whose expression is controlled by transcriptional repressors (CsoR and RicR) that bind

to Cu(I) in sub-attomolar ($<10^{-18}$) levels,[248-250] form an arsenal of defenses that confer Mtb resistance towards phagosomal copper stress.

The profusion of copper ions in the host-Mtb interface therefore represents an axis that can be exploited for therapeutic purposes. Indeed, several reports have shown that Mtb can be resensitized to copper by using small molecules that act as shuttles to boost the intracellular concentration of the metal. Compounds like thiolated semicarbazones,[251] disulfiram,[252] 8-hydroxyquinoline,[253] and cyclams[254] rely on a Trojan Horse strategy to inundate Mtb with copper and restore the metal's toxicity.

Whereas Mtb can withstand high copper concentrations, it is susceptible to reactive oxygen species (ROS). The pro-oxidant activity of ascorbic acid is responsible for the rapid and complete sterilization of an Mtb culture via perturbations in the NADPH/NADP+ ratio resulting in accumulation of hydroxylated fatty acids in the membrane.[255] Moreover, ROS induced by bactericidal antibiotics and inhibitors of sulfur metabolism were demonstrated to be effective in eradicating mycobacterial persisters.[163, 256] Reactive nitrogen species (RNS) liberated from intrabacterial reduction of PA-824 (a bicyclic nitroimidazole) and hydroquinone-based small molecules that generate superoxide radicals were shown to efficiently kill nonreplicating and drug-resistant Mtb.[257, 258] These studies suggest that ROS-forming compounds are potent alternatives to sterilize an Mtb infection, and perhaps shorten the treatment regimen in patients.

In this chapter, we utilized the peptidomimetic DAB-10 (D-VIH-D-*sh*-buforin from Chapter 5), composed of an Amino Terminal Copper and Nickel (ATCUN) binding motif, and a C-terminal domain from a cell-penetrating antimicrobial peptide (AMP) as an anti-mycobacterial agent. The Cu-ATCUN complex is known to produce ROS under

physiologically relevant conditions.[91, 204] By coupling it to a cell-permeable peptide, we aimed at developing a conjugate that could potentially bind intracellular copper (which Mtb is resistant to) and harness the chemical reactivity of the resulting metallopeptide to generate ROS (which Mtb is susceptible to). We demonstrate here that DAB-10 requires copper ions to kill mycobacteria via an oxidative stress mechanism and present the first unambiguous evidence that phagosomal copper plays a critical role in eliminating intracellular Mtb.

Results

Design principles and antimycobacterial activity of DAB-10

Our work on the ATCUN motif lead to the generation of D-ATCUN-D-*sh*-buforin-10 (DAB-10, Chapter 5), an all-D amino acid peptide with the sequence $_{D}$VIHRAGLQFPVGRVHRLLRK-NH_2. The ATCUN binding motif, Val-Ile-His (selected due to its high ROS forming activity, Chapter 4) was coupled to residues 5 through 21 of the AMP buforin II. Derived from Histone H2A, buforin II binds isolated DNA and is hypothesized to inhibit bacterial growth through the same manner.[114] Conversion from L- to D-amino acids served to increase oxidative turnover of the ATCUN motif[91] and to confer protease resistance to DAB-10. Previous chapters have shown that DAB-10 can oxidatively cleave DNA *in vitro* and in live *E. coli* (Chapter 5). Here we focus on its anti-mycobacterial activity and assess its potential to be activated by host-derived copper ions. As an internal control, we utilized DAB-6 ($_{D}$RAGLQFPVGRVHRLLRK-NH_2), a peptide identical to DAB-10 which lacks the ATCUN motif (and by extension, lacks direct oxidative capabilities), to determine the relevance of copper-binding to the mechanism of DAB-10.

We started by measuring the minimum inhibitory concentration (MIC) of both peptides against several *Mycobacterium* species in a standard broth microdilution assay. Across all species tested, we found that DAB-10 was more active than DAB-6 (Table 6.1). Pre-incubating DAB-10 with copper did not alter its MIC (Appendices, Table S6.1), hence, to examine the role of copper, we utilized the selective, cell-permeable copper chelator, tetrathiomolybdate (TTM).[151] In the presence of 100 μM TTM, DAB-10 activity against *M. smegmatis* was significantly attenuated as its MIC increased 16-fold while that of DAB-6 remained unchanged (Table 6.1). Supportive of this phenotype is our observation that the bactericidal activity of DAB-10 at its MIC is diminished in the presence of TTM (Figure 6.1). Taken together, our results show that DAB-10 indeed uses copper for its anti-mycobacterial activity.

Table 6.1. Antimycobacterial Activity of Peptidomimetics.

Mycobacterial Species	Minimum Inhibitory Concentration (MIC), μM	
	DAB-6 (+TTM)	DAB-10 (+TTM)
M. smegmatis mc^{2}155	0.5 (0.5 – 1)	0.125 (1 – 2)
M. bovis BCG (SSI 1331)	4 – 8	0.5 – 1
M. tuberculosis H37Rv	8	2
M. tuberculosis BND320[a]	8	4
M. tuberculosis Jal2287[a,b,c]	16	4
M. tuberculosis MYC431[a,b,c,d]	8	4

Resistance: [a] Isoniazid, [b] Streptomycin, [c] Rifampicin, [d] Ethionamide. TTM = Tetrathiomolybdate. *Experiments with M. tuberculosis were performed by Dr. Kushi Anand and Dr. Amit Singh (Indian Institute of Science)*.

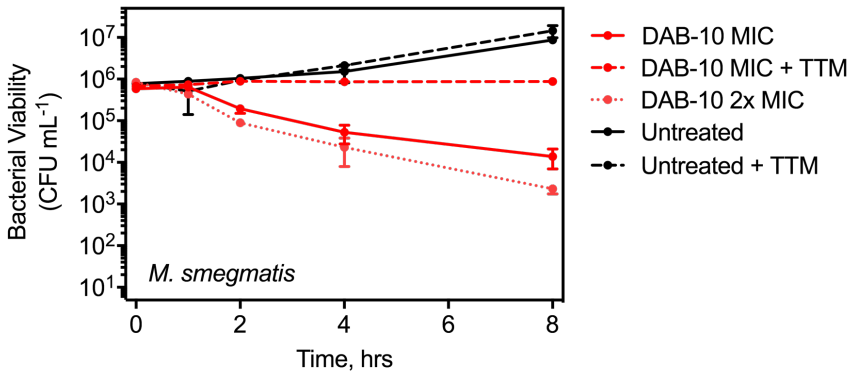

Figure 6.1. Copper-dependent Bactericidal Activity of DAB-10. Time-kill curves of *M. smegmatis* cells treated with DAB-10 in the presence or absence of 100 μM copper chelator, tetrathiomolybdate (TTM). Results show a strong copper-dependence of DAB-10 activity as bactericidal action is significantly attenuated upon co-treatment with TTM.

DAB-10 promotes copper-dependent oxidative stress, contributing to its potency

Following confirmation of the copper-dependence in the activity of DAB-10, we set out to determine whether it induces oxidative stress. For this purpose, we employed the genetically encoded, ratiometric, fluorescent probe Mrx1-roGFP2[259] – a fusion of mycoredoxin-1 and redox-sensitive GFP – to report on the redox state of DAB-10-treated mycobacteria. Oxidation of Mrx1-roGFP2 results in a decrease in the 488 nm excitation with a concomitant increase in the 405 nm excitation. The 405/488 ratio is therefore a direct readout of the relative amounts of oxidized and reduced mycothiol (MSH) which can then be converted to potential values (E_{MSH}) using the Nernst Equation (Appendices, Figure S6.1). We first generated a calibration curve using Mrx1-roGFP2-expressing *M. smegmatis* (Msm) treated with varying ratios of the oxidized and reduced form of dithiothreitol (DTT, 10 mM total) corresponding to known E_{MSH} values (Figure 6.2B). Treatment of Msm with DAB-10 at its MIC resulted in a population-wide shift in

fluorescence consistent with probe oxidation, while the fluorescence of DAB-6-treated cells virtually resembled the untreated ones (Figure 6.2A). Using DTT as reductant and cumene hydroperoxide (CHP) as oxidant controls, we confirmed that a shift towards more positive E_{MSH} values suggests that cells experience oxidative stress upon exposure to DAB-10, but not during DAB-6 treatment (Figure 6.2C). To confirm the copper dependence of DAB-10-induced oxidative stress, we utilized the TUNEL Assay as supplementary measure of oxidative DNA damage. We observed a two- to three-fold increase in TUNEL-positive cells upon DAB-10 treatment (Figure 6.2D). More importantly, we observed a statistically significant decrease upon addition of TTM, implying that intracellular oxidation by DAB-10 resulted from copper binding.

To determine whether oxidative activity of DAB-10 is a determining factor for its anti-mycobacterial activity, we tested the survival of Msm in Middlebrook 7H9 with or without catalase. Removal of catalase did not affect the potency of DAB-6 across all *Mycobacterium* species tested. On the other hand, DAB-10 activity increased six- to eight-fold upon removal of the enzyme, indicating that in the absence of an ROS scavenging system, DAB-10 activity was potentiated (Figure 6.3). Because catalase affects the potency of DAB-10 without gaining access to the mycobacterial cytosol, our results also suggest that extracellularly generated ROS by DAB-10 also plays a role in mycobacterial killing. Altogether, these results from three independent procedures demonstrate that DAB-10 induces copper-dependent oxidative stress in vitro which likely plays a major role in its bactericidal mechanism.

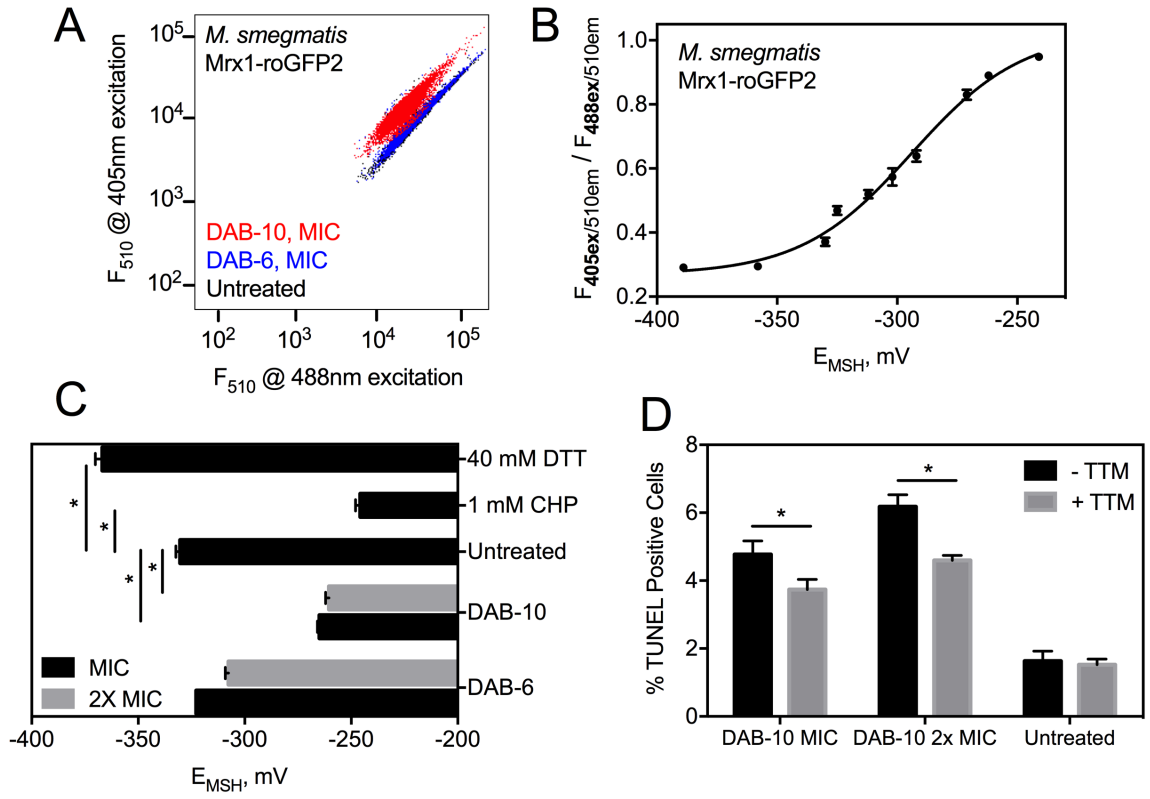

Figure 6.2. Oxidative Stress in *Mycobacteria* Induced by DAB-10. (A) Representative scatter plots obtained from flow cytometric determination of DAB-10-treated Msm, demonstrating oxidation of the probe Mrx1-roGFP2 indicating that only DAB-10 has oxidative activity. (B) Calibration curve relating 405/488 ratio to corresponding E_{MSH} value. Curve was obtained by titrating varying ratios of DTT_{ox} and DTT_{red} to Msm corresponding to known E_{MSH} values from the Nernst equation. (C) The 405/488 ratio of Mrx1-roGFP2 resulting from DAB-10 treatment were converted to E_{MSH} values using the calibration curve in (B). Results show that DAB-10 shifts E_{MSH} to more positive values, similarly to the oxidant control, cumene hydroperoxide, CHP. *, $P<0.05$. (D) TUNEL assay was used to quantify extent of genomic DNA damage arising from oxidative activity of DAB-10. Results show that oxidative stress is a function of copper binding because levels of TUNEL positive cells decreased upon addition of TTM. *, $P<0.05$.

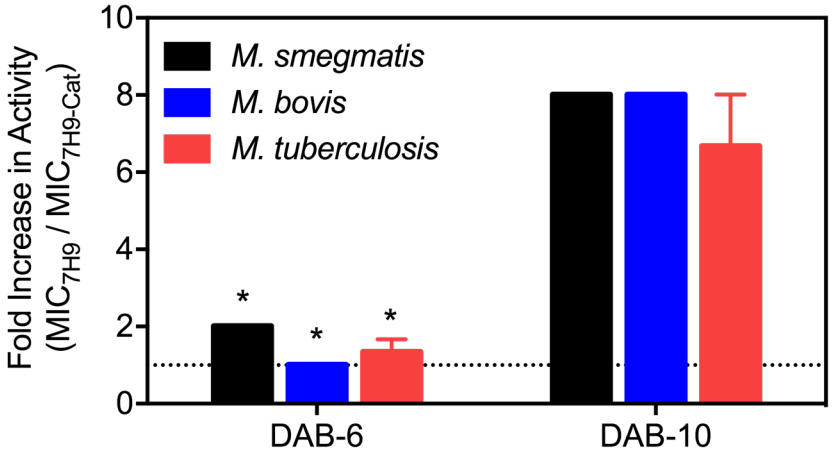

Figure 6.3. Effect of Catalase in the Oxidative Activity of DAB-10. Change in activity of the peptidomimetics as a result of removal of catalase from Middlebrook 7H9 was obtained from a ratio of MIC values with and without the enzyme. Results show that DAB-10 activity is positively affected by removal of catalase.

It was recently reported that silver ions potentiate the activity of bactericidal antibiotics through disruption of iron homeostasis eventually leading to production of ROS.[195] We therefore hypothesized that the ROS formed by copper-bound DAB-10 can enhance the activity of other antibiotics. To this end, we tested whether DAB-10 exhibits synergistic interactions with known anti-TB drugs. Of the four first-line drugs we tested, we observed synergistic interactions between DAB-10 and Rifampicin against both *M. tuberculosis* and *M. bovis* (Figure 6.4), suggesting the potential use of DAB-10 in combination chemotherapy.

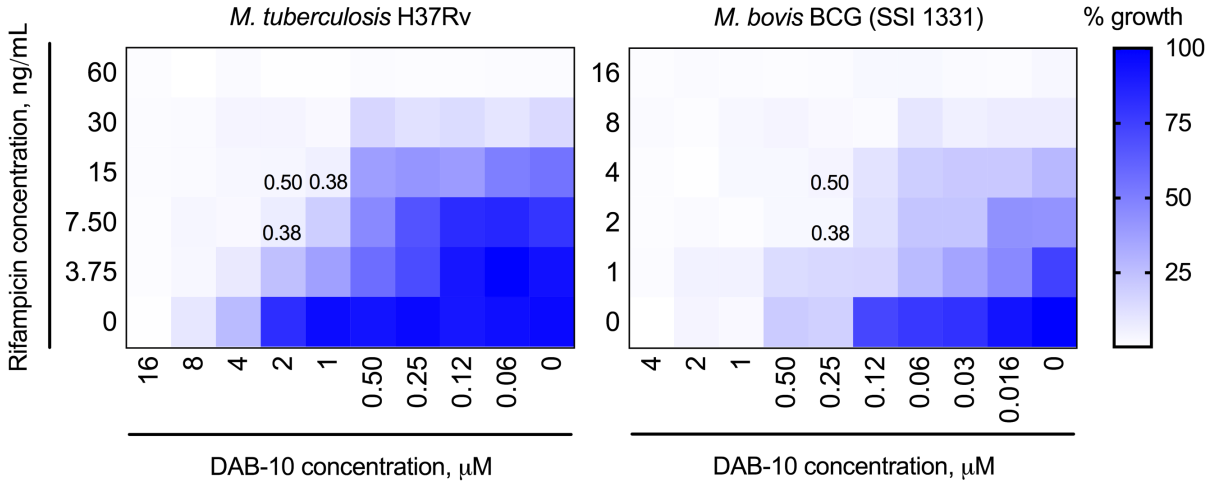

Figure 6.4. DAB-10 Synergy with Rifampicin. The checkerboard assay was used to assess interactions between DAB-10 and rifampicin. Heat maps show % survival determined via measurement of alamar blue fluorescence following overnight incubation. Values inside the heat maps are the fractional inhibitory concentration (FIC) indices for the corresponding well at which they appear in. FIC index < 0.50 indicates synergy.

Partial random transposon mutagenesis of Msm unravels networks necessary for DAB-10 resistance and provides hints to the nature of the ROS

To determine direct or indirect targets of DAB-10, we performed partial random transposon mutagenesis screen of Msm isolate DAB-10-resistant mutants (Figure 6.5). We failed to isolate truly resistant mutants from 7H11 plates containing DAB-6 or DAB-10 at 10X their MIC. Because AMPs are known to interfere with a wide range of biological functions (multi-hit mechanisms of action), we believe that pleiotropic effects dominate at this concentration making isolation of resistant clones challenging. However, we were able to isolate three mutants in 7H11 plates containing DAB-10 at 5X MIC. These mutants exhibited a markedly higher MIC relative to the wild type (WT) (Figure 6.6A). To determine the transposon insertion sites, we performed rescue cloning followed by DNA sequencing.

Briefly, genomic DNA of the resistant mutants were isolated, digested, religated, and reintroduced into *E. coli*. The rescued plasmids, containing the transposon (*Tn*::Kan^R) were sequenced using primers that annealed to the transposon termini. A BLAST search of the sequencing data identified transposon insertions in *MSMEG_6617*, *MSMEG_4041*, and *MSMEG_6091*; all comprise uncharacterized products but nevertheless express putative functions. Genetic complementation of these genes restored susceptibility of these mutants to DAB-10 similar to WT levels, confirming interactions of DAB-10 with the gene products. Surprisingly, when we tested the ROS resistance of the transposon mutants, all of them were equally susceptible as the WT strain to either 5 mM Menadione, 1 mM CHP, or 1 mM tert-butylhydroperoxide (tBHP) (Figure 6.6B). Despite its counterintuitive nature, our results are supported by the fact that the oxidative DNA cleavage of the ATCUN motif is not inhibited by DMSO, NaN3, or superoxide dismutase (SOD) which scavenges hydroxyl radicals, singlet oxygen, and superoxide, respectively.[90] Our results therefore suggest that none of the three aforementioned ROS is implicated in DAB-10 activity, and that the peptide likely generates an ROS of unknown nature. Indeed, a non-diffusible, copper-bound hydroxo species has been proposed as the formal ROS in this context.[90]

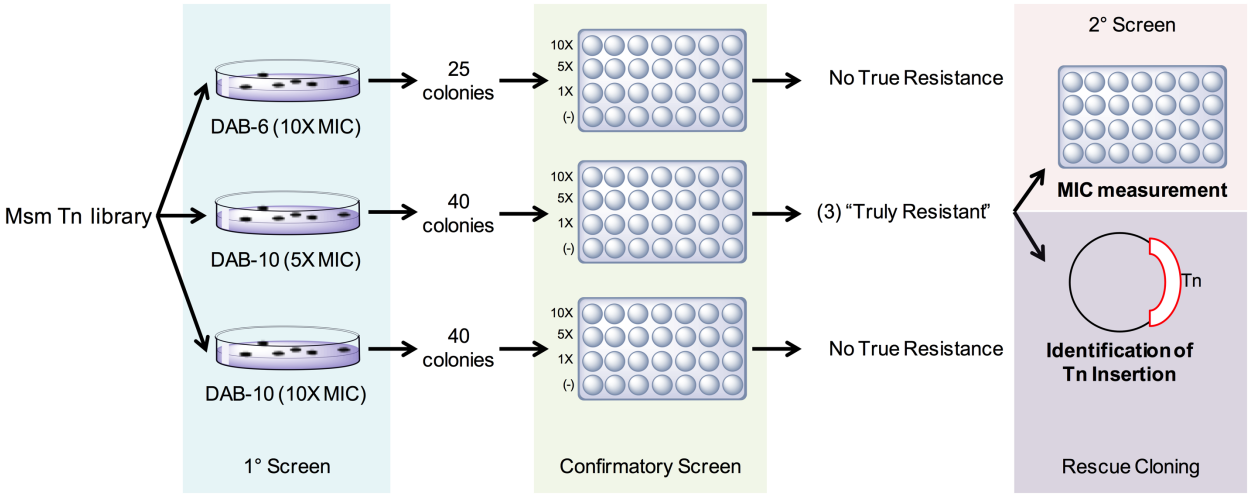

Figure 6.5. Schematic Representation of Msm Transposon Mutagenesis Screening. The library of Msm transposon mutants were plated in 7H11 plates containing indicated concentrations of peptidomimetics. The corresponding number of mutants were isolated and tested on liquid culture for determination of truly resistant mutants. Truly resistant mutants were used for MIC determination and rescue cloning.

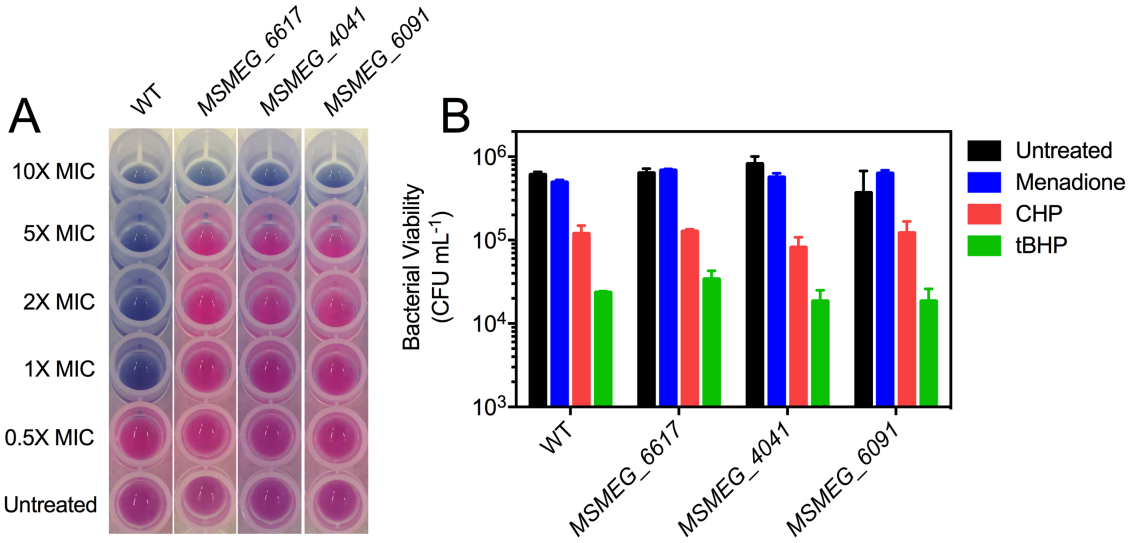

Figure 6.6. Genetic Screening for DAB-10 Target Identification. (A) Alamar blue viability assay of Msm Tn mutants truly resistant to DAB-10. Red wells indicate bacterial growth. (B) ROS susceptibility of the isolated Msm transposon mutants were tested by treatment with 5 mM Menadione, 1 mM CHP, or 1 mM tBHP. Results show that mutants were equally susceptible to superoxide and hydroxyl radicals as the WT.

We hypothesized that genetic interruptions that ultimately lead to hyperactive ROS scavenging systems (that detoxify the ROS formed by DAB-10) or proteases (that degrade oxidized proteins which become toxic in abundance) could reconcile the observed DAB-10 resistance in spite of the mutants' ROS susceptibility. Using the online database SmegmaList,[260] we found that none of the interrupted genes encoded for putative reductases or proteases (Table 6.2). However, a STRING analysis[261] of *MSMEG_4041* shows phylogenetic co-occurrence and genetic fusion with a putative reductase and that of *MSMEG_6091* showed functional associations with the chaperone DnaK and three Clp protease subunits (Appendices, Figure S6.2). Therefore, our analysis suggests that while a direct interaction of DAB-10 to the products of the interrupted genes are unlikely, the resulting mutant proteins interact with downstream effectors that can neutralize the toxicity of DAB-10.

Table 6.2. Msm Transposon Mutants Resistant to 5X MIC of DAB-10 vs WT.

Tn insertion site	Gene Product	Mtb ortholog	DAB-10 MIC, μM
WT	-	-	0.25 – 1
MSMEG_6617	NUDIX hydrolase	None	8
MSMEG_4041	Hydroxyquinol dioxygenase	None	8
MSMEG_6091	Negative regulator of Genetic Competence	*clpC1*	8

DAB-10 co-localizes with intracellular Mycobacteria

Since access to the mycobacteria-containing phagosome is imperative for efficient Mtb eradication, we next tested whether DAB-10 co-localizes with intracellular

Mycobacteria. We first incubated RAW264.7 macrophages with 4 μM of a tetramethylrhodamine (TMR)-labeled version of DAB-10. We observed distinct punctate localization reminiscent of cytosolic vesicles (Figure 6.7), indicating a possible mode of internalization involving endocytosis. When we co-treated macrophages with 50 μM Amiloride, a macropinocytosis inhibitor, we observed a DAB-10 localization similar to that of the untreated one. However, in the presence of 80 μM Dynasore which inhibits COP1-mediated endocytosis, DAB-10 was found to localize in the mitochondria. This observation suggests that while DAB-10 can translocate across biological membranes, it is preferably internalized by macrophages via COP1-mediated endocytosis.

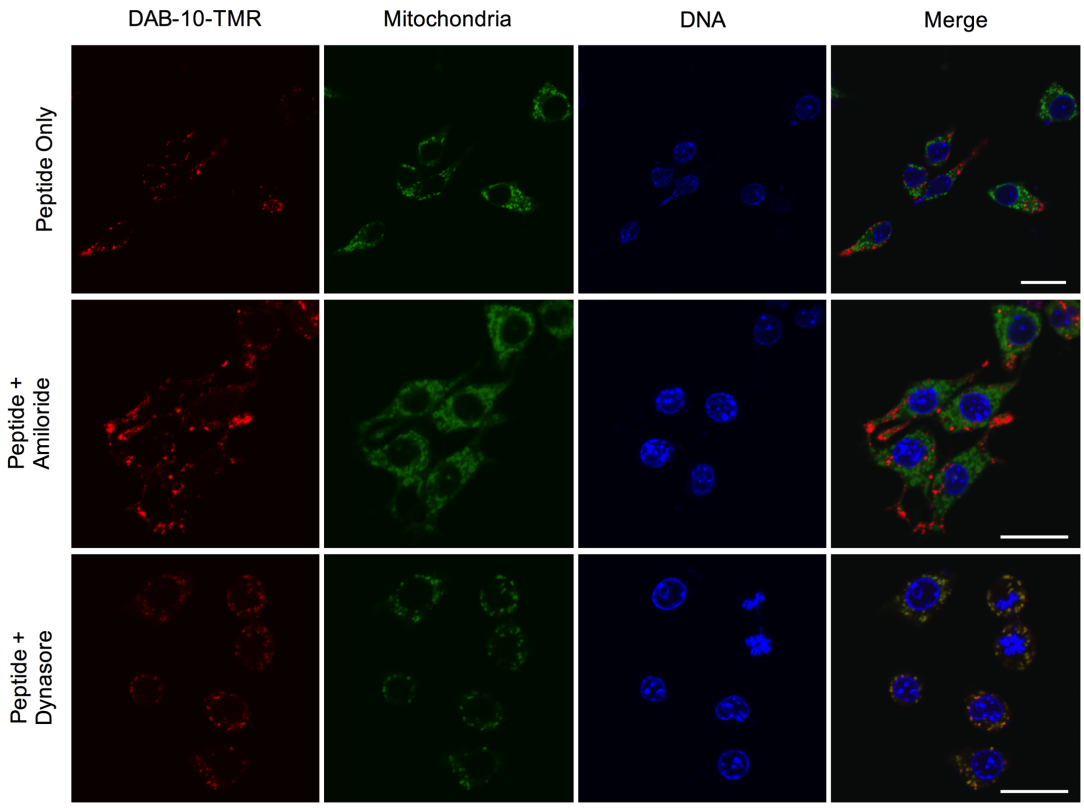

Figure 6.7. DAB-10 Internalization into Murine Macrophages. RAW264.7 cells were incubated with rhodamine-labeled DAB-10 and its localization was followed by confocal microscopy. Micrographs show cellular uptake of DAB-10 into distinct cytoplasmic vesicles dependent on COP1-mediated endocytosis. Scale bars = 10 μm.

We then infected RAW264.7 cells with Msm (multiplicity of infection, MOI 1:100) prior to incubation with 4 μM of DAB-10-TMR. We found co-localization of bacteria and DAB-10 as early as 30 mins post-exposure to the peptide (Figure 6.8). This co-localization was observed even at DAB-10 concentrations as low as 1 μM (Appendices, Figure S6.3). Figure 6.8 also shows that intracellular Msm was homogenously stained by DAB-10, indicating that DAB-10 also translocates across the mycobacterial membrane. Indeed, treatment of isolated Msm with DAB-10-TMR resulted in the same phenotype (Figure 6.9). We assume that the DAB-10-containing and Msm-containing phagosomes fuse at the stage of early to late endosomes because neither the bacteria nor the peptide co-localize with lysosomes after 30 mins (Appendices, Figure S6.4). However, because Msm cannot arrest phagosomal maturation like Mtb, both bacteria and peptide find their way to the lysosomes after 3 hours (Appendices, Figure S6.4). Overall, our data demonstrate that DAB-10 co-localizes with intracellular mycobacteria.

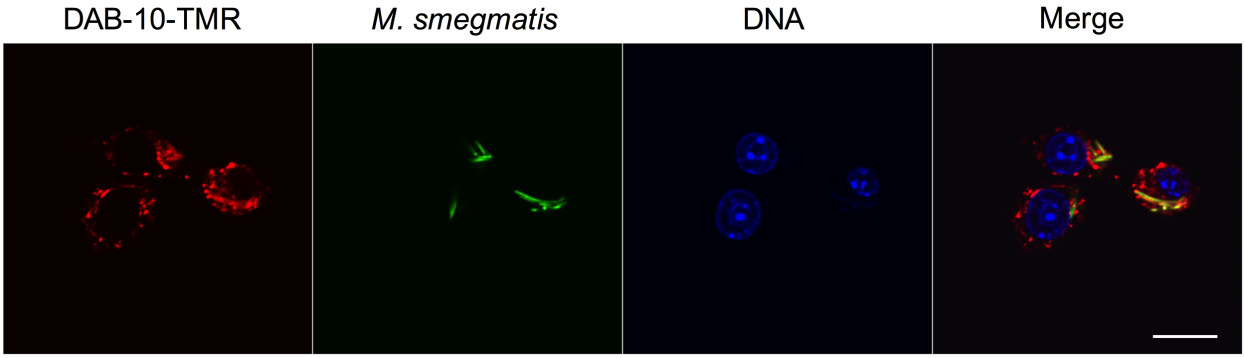

Figure 6.8. DAB-10 Colocalization with Intracellular *Mycobacteria*. GFP-expressing Msm was used to infect RAW264.7 cells (multiplicity of infection 1:100) prior to incubation with 8 μM of rhodamine-labeled-DAB-10. Images show peptidomimetic colocalizing with bacteria 30 mins post-exposure. Scale bar = 10 μm.

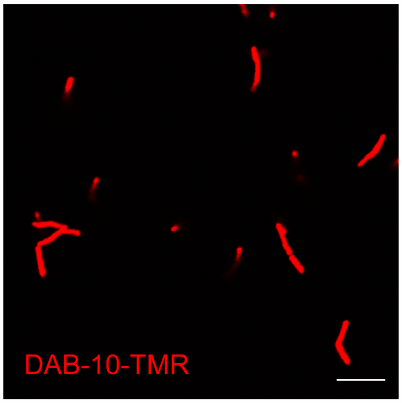

Figure 6.9. Bacterial Localization of DAB-10. Msm cells were exposed to 4 μM of rhodamine-labeled DAB-10 and imaged in a confocal microscope to follow DAB-10 localization. Micrograph shows DAB-10 intrabacterial staining. Scale bar = 5 μm.

DAB-10 binds to phagosomal copper

We next sought to determine whether DAB-10 can competitively sequester copper in the intracellular milieu. For this purpose, we synthesized CS-1 (Appendices, Figure S6.5), a copper-selective fluorescent probe[262] to determine whether DAB-10 co-localizes with the metal. Because the emission spectra of CS-1 significantly overlaps with that of TMR, we synthesized fluorescein (FL)-labeled DAB-10. Incubation of RAW264.7 cells with 8 μM DAB-10-FL and 2 μM of CS-1 showed fluorescence co-localization within distinct puncta (Figure 6.10). Activation of RAW264.7 cells with either IFN-γ or LPS resulted in overexpression of the copper transporters Ctr1 and ATP7A effectively increasing intracellular copper content.[53] When we used LPS-activated macrophages, not only did we see a stronger signal at the red channel, but also co-localization of the metal with the peptide. Our results indicate that DAB-10 and copper are within proximity of each other making metal binding possible.

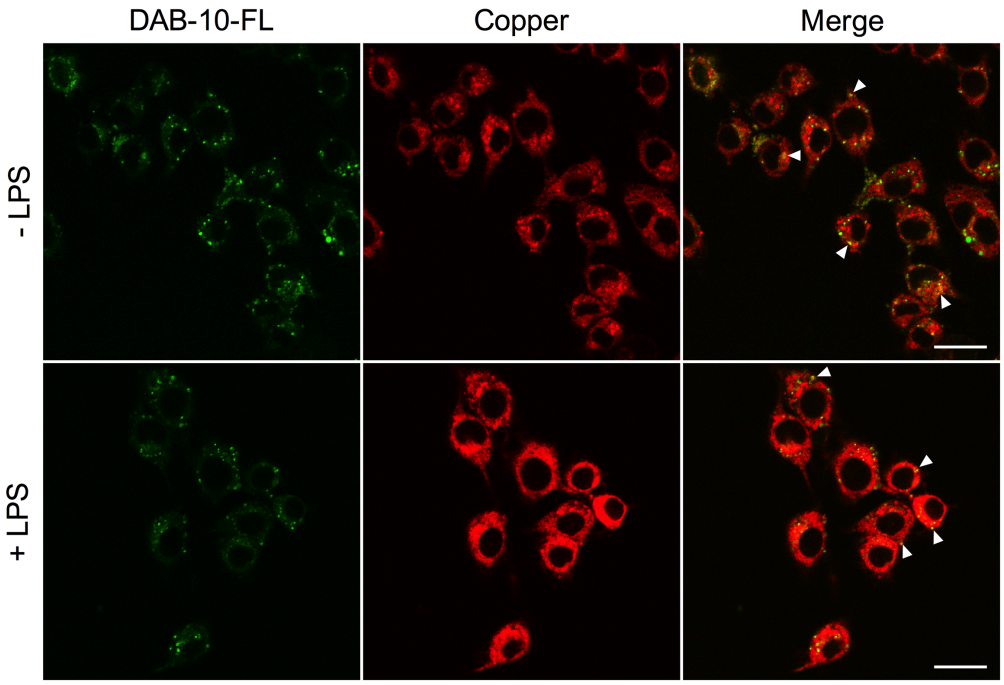

Figure 6.10. DAB-10 Colocalization with Intracellular Copper. Resting and activated RAW264.7 cells were incubated with fluorescein-labeled DAB-10 and 2 μM of the fluorescent copper sensor, CS-1. Images show co-localization of DAB-10 with intracellular copper in regions highlighted by white arrowheads. Scale bar = 10 μm.

We next examined whether direct metal binding occurs within macrophages. For this purpose, we exploited the fluorescence quenching properties of copper[262] and designed DAB-10 derivatives that differed in the position of the fluorophore with respect to the ATCUN motif. We attached TMR (a pH insensitive fluorophore) to the ε-amino group of either Lys-20 (DAB-10-K_{20}(TMR)) or an extra Lys placed immediately after the ATCUN motif (DAB-10-K_4(TMR)), and reasoned that since TMR is closer to the metal in the K_4 derivative, DAB-10-K_4(TMR) should exhibit fluorescence quenching upon copper binding. Not surprisingly, we observed ~35% decrease in emission intensity in vitro when 1 equivalent of copper was added to DAB-10-K_4(TMR) but not when added to DAB-10-

K_{20}(TMR) (Figure 6.11A). When incubated with macrophages (figure 6.11B), we observed intracellular fluorescence for DAB-10-K_{20}(TMR) with a similar intensity upon macrophage activation. On the other hand, DAB-10-K_4(TMR) exhibited minimal fluorescence (irrespective of LPS addition) which was later rescued upon addition of TTM. This result proves that quenching of the DAB-10-K_4(TMR) intracellular fluorescence is a function of copper binding.

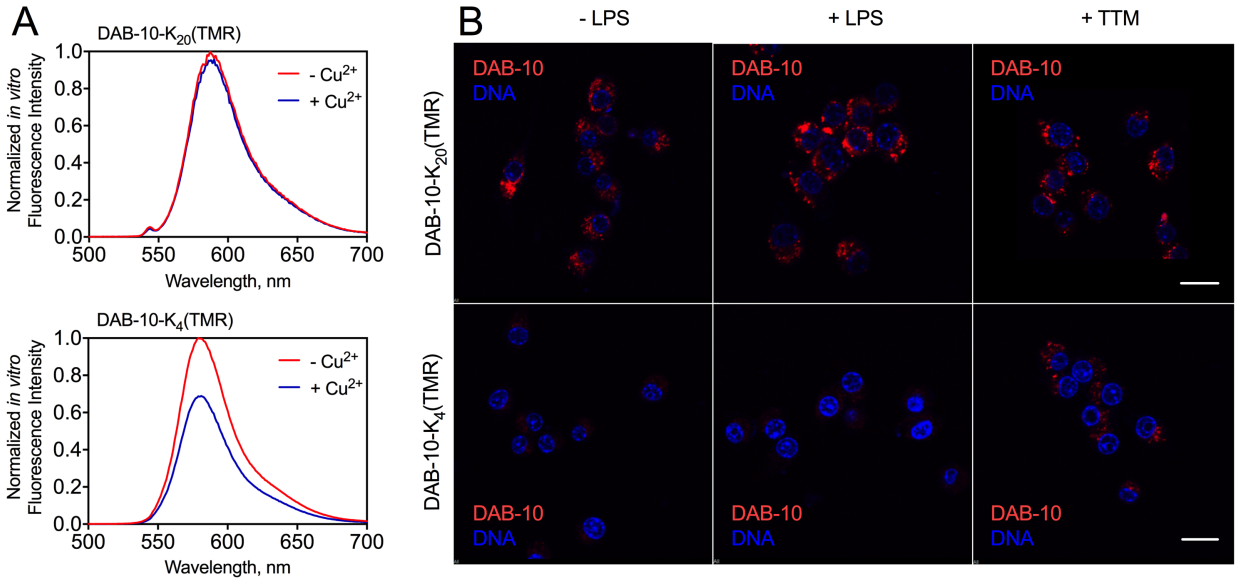

Figure 6.11. Intracellular Copper binding of DAB-10. (A) 1 eq of Cu^{2+} was added to rhodamine-labeled DAB-10 derivatives differing in the position of the fluorophore. In vitro fluorescence quenching was confirmed for the K_4 derivative. (B) 4 μM of DAB-10-TMR derivatives were added to resting or activated RAW264.7 cells in the presence or absence of TTM. Quenched fluorescence of DAB-10-K_4(TMR) suggests direct copper binding to the ATCUN motif of DAB-10. Images were acquired using the same instrument settings. Scale bars = 10 μm.

To ensure that the differences in fluorescence intensity is not a result of decreased peptide uptake, we quantified the intracellular concentration of both DAB-10 derivatives

(Figure 6.12A). We found that at 4 μM, the concentration at which the microscopy experiments were done, both DAB-10-K_{20}(TMR) and DAB-10-K_4(TMR) were taken up by RAW264.7 cells to similar extents (~0.1 nmol/mg of protein). Thus, the weaker fluorescence intensity by DAB-10-K_4(TMR) is not an experimental artifact, but rather a result of direct copper binding within the cell. Note that a similar fluorescence intensity and cell uptake profile was observed for the same set of DAB-10 derivatives labeled with fluorescein (Appendices, Figure S6.6 and S6.7), indicating that the observed phenotype is independent of the identity of the fluorophore.

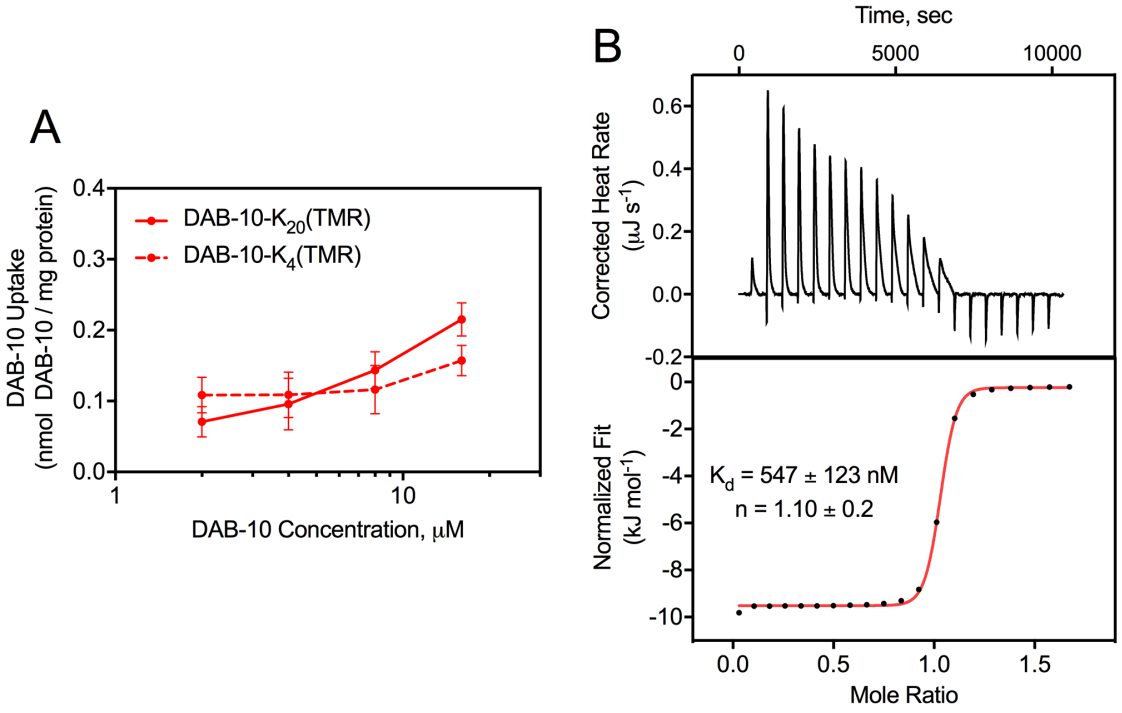

Figure 6.12. Measurement of Copper binding Constant of DAB-10. (A) Analytical quantification of cellular uptake of DAB-10 derivatives used in Figure 6.11B shows that at the concentration used in the experiment, both K_4 and K_{20} derivatives of DAB-10 had similar intracellular concentration. (B) Isothermal titration calorimetry (ITC) was used to determine binding constant of DAB-10 to Cu^{2+} at pH 6.40, resembling pH of Mycobacterium-containing phagosome.

Finally, using isothermal titration calorimetry (ITC), we found that DAB-10 binds to Cu^{2+} with a sub-micromolar affinity (K_d = 547 ± 123 nM, Figure 6.12B) under pH 6.40, simulating arrested acidification of the Mtb-containing phagosome.[263, 264] Together with the fact that following infection with Mtb, intraphagosomal copper reaches concentrations well above the observed K_d,[57] our data thus far indicates that DAB-10 is likely copper-bound inside Mtb-infected macrophages.

Phagosomal copper is essential for eradicating intracellular M. tuberculosis

Having confirmed copper-dependent oxidative activity and intracellular copper scavenging of DAB-10, we proceeded to determine whether it uses the metal for its activity against intracellular Mtb. We first examined the toxicity of DAB-10 in naïve macrophages using a standard viability assay. We found that DAB-10 has negligible toxicity against THP-1 and RAW264.7 cells up to 256 μM (Figure 6.13), in line with the reported minimal toxicity against other mammalian cell lines including HeLa and HEK293 cells (Chapter 5).

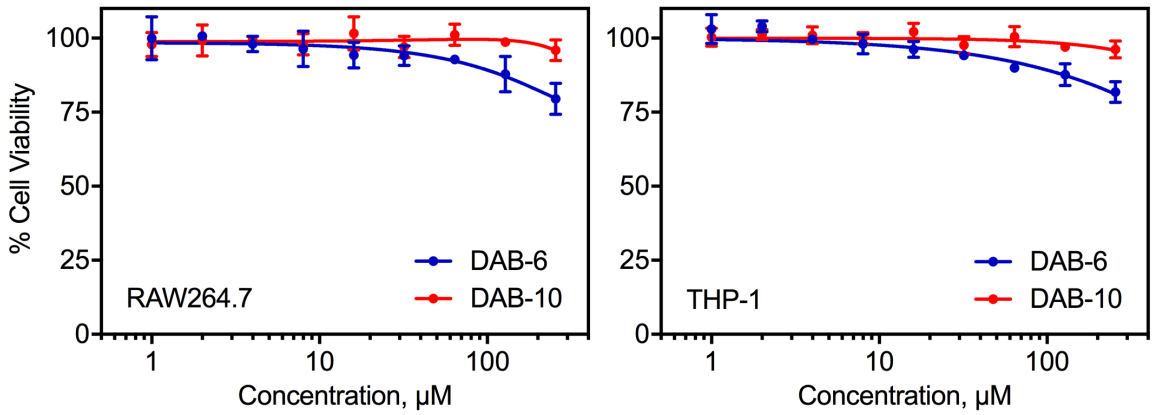

Figure 6.13. Peptidomimetic Cytotoxicity against Macrophage Cell Lines. The cytotoxicity of DAB-6 and DAB-10 against macrophages *in vitro* was assessed through the MTT assay. Data shows minimal toxicity up to 128 μM.

We next infected differentiated THP-1 cells with *M. tuberculosis* H37Rv (MOI 1:5) and measured the bacterial survival following peptide treatment (at 10X MIC) for 24 and 48 hours. We found minimal bactericidal activity after 24 hours of incubation (Appendices, Figure S6.8), however, both peptides effected ~50% bacterial killing after 48 hours (Figure 6.14B). Furthermore, we observed almost a complete sterilization of intracellular Msm after 24 hours of peptide incubation (Figure 6.14A). We conclude that DAB-10 is active against intracellular *Mycobacteria*. To unambiguously determine whether phagosomal copper is involved, we co-treated infected macrophages with DAB-10 and either TTM (cell-permeable) or BCS (bathocuproinedisulfonate, cell-impermeable). We hypothesized that by using copper chelators with varying permeability profiles, we could determine, without bias, whether intracellular or extracellular copper is utilized by DAB-10. DAB-6 activity was unaffected by the presence of the chelators indicating that it does not utilize copper for its activity. However, we observed a significant decrease in DAB-10 activity only in the presence of TTM. Taken together with the fact that DAB-10 is restricted within endosomes, our results demonstrate that it is indeed the phagosomal copper that is utilized by DAB-10. Note that at 100 μM of the chelators, neither the intracellular survival of Mtb nor the THP-1 viability is affected (Appendices, Figure S6.9). Overall, our results emphasize that DAB-10 utilizes phagosomal copper to kill intracellular *Mycobacteria*.

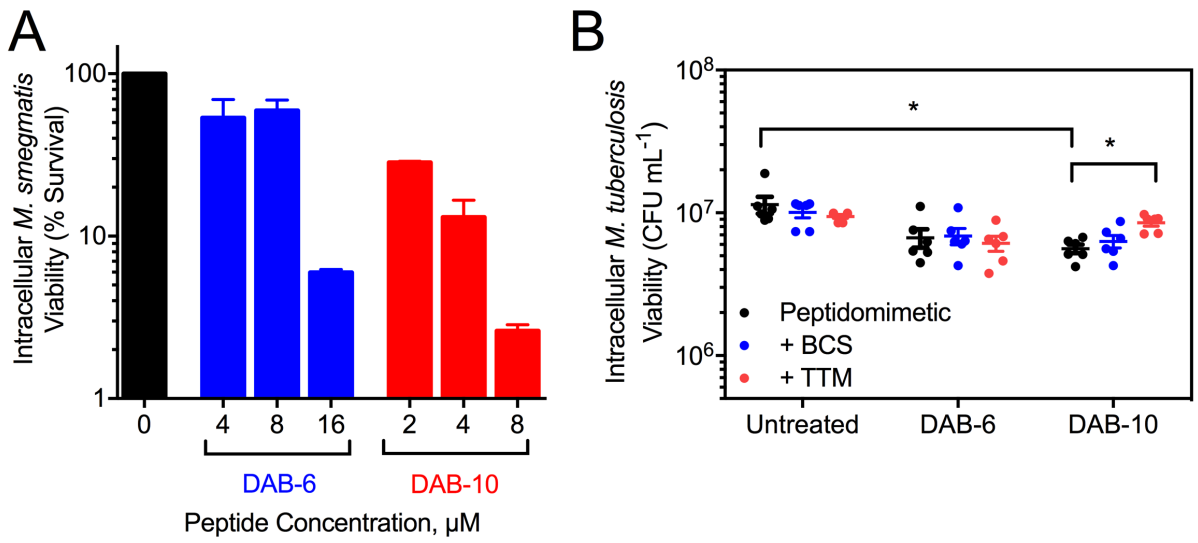

Figure 6.14. Activity of Peptidomimetics against Intracellular *Mycobacteria*. (A) Resting RAW264.7 cells were infected with Msm (MOI 1:100) and treated with peptidomimetics at the indicated concentration for 24 hrs. (B) Differentiated THP-1 cells were infected with Mtb H37Rv (MOI 1:5) prior to treatment with DAB-6 (80 μM) and DAB-10 (20 μM) corresponding to 10X the in vitro MIC for 48 hrs. Results show bactericidal activity against intracellular mycobacteria for both peptides, however, only DAB-10 efficacy was attenuated upon addition of the chelator TTM. *, $P<0.05$.

Discussion

The need to develop novel antimicrobials and understand their mechanism of attack is becoming increasingly urgent due to the rise of bacterial strains resistant to conventional antibiotics. For TB, multiple strategies involving bacterial enzyme targeting[265] and modulation of host-immune response[266, 267] were proven to be effective in proof-of-concept studies, whereas use of agents that exploit factors in the host-pathogen interface have been limited. The influx of copper ions into the mycobacterial phagosome, resulting from the concerted action of copper transporters (Ctr1 and ATP7A)

and chaperones (Atox1),[268] represents an untapped resource for novel therapeutic interventions. Agents that harness this exchangeable metal pool would circumvent the copper resistance of Mtb[246] without requiring secondary exogenous factors. Furthermore, because copper tends to accumulate during infection,[269, 270] it was suggested that compounds which turn into potent antimicrobials in the presence of copper can be used to control bacterial loads *in situ*.[253] The promise of this approach has been tested using small organic molecules that become anti-mycobacterial upon binding to copper.[251-253] However, these studies lacked evidence for a direct phagosomal copper involvement and conclusions made from *ex vivo* models of infection were reasonable yet inferential. Herein, we present explicit evidence of a peptidomimetic utilizing phagosomal copper for its anti-mycobacterial activity. Our approach combines exploitation of host-derived copper ions with susceptibility of Mtb to ROS, to generate an activatable oxidant for inhibition of intracellular Mtb.

Central to our strategy is the ATCUN motif, which performs both copper-binding and oxidative chemistry in DAB-10. When in vitro MIC measurements were done, DAB-10 was neither pre-incubated nor was the medium supplemented with copper. While most of the copper in Middlebrook 7H9 (~6.3 μM) is sequestered by albumin (which incidentally also contains an ATCUN motif), we assumed that not adding exogenous copper simulates conditions of metal competition that are relevant physiologically. Indeed, DAB-10 MICs were in the low micromolar range, below the total copper content of 7H9, rendering existence of metallated DAB-10 plausible. Furthermore, depletion of copper in 7H9 via addition of the high affinity chelator TTM[271] attenuated DAB-10 potency, signifying copper-dependence of its activity. While DAB-10 in our experiments may not be saturated

with copper, the fact that the ROS formation by the Cu-ATCUN motif is catalytic[90, 91] suggests that a small population of metallated DAB-10 can effect a similar, albeit weaker oxidative activity.

The observation that DAB-10, but not DAB-6, exhibits copper-dependent redox cycling supports the notion that addition of the ATCUN motif results in a gain-of-function phenotype that affords DAB-10 a secondary mode of attack. Indeed, DAB-6 displays a weaker potency relative to DAB-10, which we believe is stemming from its DNA binding ability, possibly resulting in inhibition of nucleic acid metabolism.[11, 114] Conversely, we propose that a major contributor to the activity of DAB-10 is its redox cycling. However, without comprehensive investigations, we cannot completely exclude the possibility that it also inhibits growth in a manner similar to DAB-6. The Msm transposon mutants we isolated were paradoxically resistant to DAB-10 but susceptible to ROS. Apart from the aforementioned neutralization of DAB-10 toxicity by the proteins that form functional associations with the products of the interrupted genes, this paradox can likely be explained by a secondary, non-oxidative mode of attack which is probably a function of the C-terminal domain of DAB-10, exclusive of the ATCUN motif. This supplementary mechanism likely involves direct binding of DAB-10 to the products of *MSMEG_6617*, *MSMEG_4041*, and *MSMEG_6091*; with the transposon insertion preventing interaction with the peptidomimetic. This suggests that not only can DAB-10 overwhelm the bacteria with ROS, but it can also elicit an inhibitory effect independent of its oxidative ability, a route it can take when surrounding copper levels are not sufficient for binding.

It has been repeatedly shown that bactericidal antibiotics – both small molecules and AMPs – induce formation of deleterious hydroxyl radicals by liberating ferrous ions

(from iron-sulfur clusters) that promote the Fenton reaction.[154, 155, 188, 272] The observation of a copper-dependent oxidative stress experienced by DAB-10-treated cells therefore suggests that instead of inducing the formation of ROS, metallated DAB-10 is directly producing it. While the exact mechanism of ROS formation by Cu-ATCUN complexes is still a matter of debate, the accepted pathway proposed by Cowan and co-workers[91] involves initial formation of a peroxo-bridged Cu-ATCUN dimer that then forms a hydroperoxide anion (technically a deprotonated H2O2). This hydroperoxide anion is then involved in the reduction of another Cu-ATCUN complex to form a copper-bound hydroxyl radical, the actual ROS in this context (Eqns 1-3 in Chapter 1). From this scheme, it can easily be seen why catalase attenuates DAB-10 activity, because in the presence of the H_2O_2 scavenging enzyme, reaction 3 cannot occur, terminating the scheme prior to formation of the active oxidant. Moreover, this scheme also supports the susceptibility of our Msm transposon mutants to superoxide, singlet oxygen and hydroxyl radicals because none of these three canonical ROS is proposed to be formed by the Cu-ATCUN complex in metallated DAB-10.

Because the oxidative activity of DAB-10 is a function of its copper co-factor, the question of where DAB-10 acquires the metal becomes relevant. As previously mentioned, we assume that DAB-10 sequesters copper from 7H9 because it contains micromolar levels of the metal, well above the measured K_d of Cu-DAB-10. Since copper is supplied as $CuSO_4$, and because of the relative instability of Cu(I) under aerobic conditions, there is likely a sufficient amount of copper in the preferred oxidation state of the ATCUN motif. Moreover, binding constants to Cu(II) previously measured for the ATCUN motif of Ctr1[273] are close to those of Human Serum Albumin (HSA)[126] indicating

that competition for the metal between ATCUN motifs of varying sequences is possible and bidirectional. Therefore, DAB-10 can competitively sequester copper from albumin in the supplement as well. In the intracellular milieu, DAB-10 co-localized and bound directly to copper regardless of whether resting or activated macrophages were used. The Cu(I) selective probe CS-1 used here was shown to have endosome-like localization (termed copper "hotspots") in primary macrophages[52] similar to DAB-10 distribution in RAW264.7 cells. Taken together with the fact that the ATCUN motif also has considerable affinity toward Cu(I) as previously described for Ctr1,[273] DAB-10 is most-likely copper bound within naïve macrophages. Moreover, endosomal Cu(I) can disproportionate, or can be oxidized to Cu(II) as the phagosome matures and the lumen becomes increasingly oxidizing. In addition, even though it is widely known that the reductive conditions in the cytoplasm favor Cu(I), the fact that endosomes are topologically equivalent to the extracellular environment[274] suggests that any copper taken up during endocytosis is likely in the +2 state. These conditions generate a transient pool of Cu(II) which can serve as metal source for DAB-10 making formation of metallated DAB-10 probable. Finally, within macrophages infected with Mtb, it is even more plausible that DAB-10 is copper-bound for the following reasons. First, naïve macrophages infected with *M. avium*, or macrophages activated with IFN-γ prior to or following infection were shown to contain 17 μM, 82 μM, and 177 μM of copper in the phagosome, respectively.[57] All of these reported concentrations are well above the measured K_d of Cu-DAB-10. Second, Mtb expresses a periplasmic multicopper oxidase (MmcO) that possibly converts Cu(I) to Cu(II).[73] Therefore, in the context of an infection, not only is there an abundant copper supply in

the phagosome, this labile pool also contains copper in the oxidation state preferred by DAB-10.

Pooling our results together, we propose a pathway through which DAB-10 oxidatively targets intracellular Mtb (Figure 6.15). Infected macrophages, regardless of activation, contain micromolar levels of copper due to transport pathways involving Ctr1, Atox1 and ATP7A. During DAB-10 treatment, the peptidomimetic is taken up via COP1-mediated endocytosis and the resulting vesicle is uncoated in the cytosol. At this stage, a fraction of DAB-10 is probably already bound to copper, but because of the depletion of reductive equivalence in a progressively maturing endosome, minimal redox cycling occurs. It was shown that intracellular Mtb acquires extracellular iron by gaining access to the transferrin recycling pathway[57, 275, 276] suggesting that the Mtb-containing phagosome can likely fuse with early endosomes. Therefore, bacteria and peptidomimetic co-localization occurs following fusion of the DAB-10-containing and Mtb-containing endosomes. Vesicular fusion affords DAB-10 access to high levels of copper upon which metal sequestration ensues. DAB-10 probably translocates across the mycobacterial membrane in the metallated form, if not, apo-DAB-10 can get metallated in the mycobacterial periplasm where Cu(II) is formed by MmcO. Finally, the biological reductants present in the mycobacterial cytosol triggers oxidative activity of DAB-10 resulting in Mtb death.

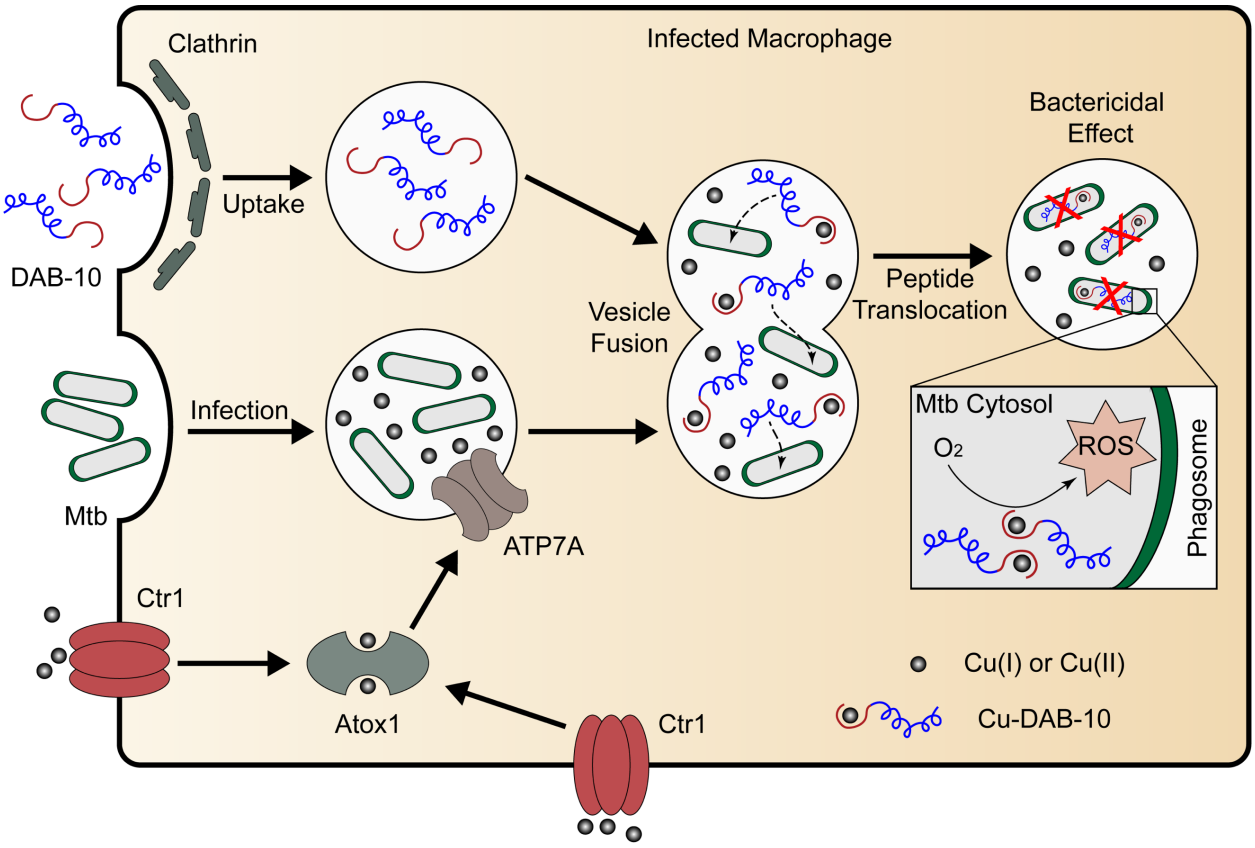

Figure 6.15. Proposed Mechanism of Action of DAB-10 against Intracellular Mycobacteria. Following intermalization to macrophages, DAB-10-containing vesicles fuse with the Mtb-containing phagosome allowing access to high levels of copper. Copper binding triggers oxidative activity of DAB-10 against Mtb resulting in bacterial death.

In conclusion, our work describes a new drug candidate which does not only target susceptible, but also drug-resistant Mtb for control of the devastating threat of TB. We build upon the proof-of-concept studies that exploit the profusion of copper ions in the host-Mtb interface by using a system that not only binds copper but also leverages the metal's redox properties to generate ROS.

Methodology

Antimicrobial Susceptibility Testing and Time Kill Kinetics. (MIC measurements against *M. tuberculosis* were performed by Dr. Kushi Anand and Dr. Amit Singh, Indian Institute of Science). Activity testing was done using the broth microdilution method as suggested by Hancock. *Mycobacteria* were grown until exponential phase in Middlebrook 7H9 broth with 10% OADC (Oleic acid, Albumin, Dextrose, Catalase) supplement and 0.05% Tween 80. For experiments without catalase, media contained 4.7 g/L of 7H9 base, 5 g/L BSA, 0.85 g/L NaCl, 2 g/L glucose, 0.4% glycerol, and 0.05% Tween-80. Peptidomimetic stock solutions were diluted in growth medium and 50 μL of a 2-fold serial dilutions were placed on separate wells of a sterile 96-well polypropylene plate (polystyrene plates were used for *M. tuberculosis* and *M. bovis*). To each well, 50 μL of bacterial suspension was added to yield a final inoculum of $5x10^5$ CFU/mL per well. Plates were incubated in seal plastic bags at 37°C for 24 hrs for *M. smegmatis*, and 7 days for *M. bovis* and *M. tuberculosis*. Following incubation, 10 μL of Alamar Blue was added and the color was allowed to develop for an additional 4 hrs for *M. smegmatis* and 24 hrs for *M. bovis* and *M. tuberculosis*. Fluorescence of the plate was read using a microplate reader and was converted into percent growth inhibition. The Minimum Inhibitory Concentration (MIC) was defined as the lowest concentration that resulted in 90% growth inhibition. Data shown was obtained from three independent trials done in duplicates. To test synergy of DAB-10 with isoniazid and rifampicin, a similar method was adopted, except that DAB-10 was added to the rows of the 96-well plate while the anti-TB drugs were added to the columns. Heat maps represent data obtained from three independent trials done in duplicates. The time kill kinetics experiments were done by mixing *M.*

smegmatis with the indicated concentration of DAB-10 with or without 100 μM tetrathiomolybdate (TTM) in a total volume of 500 μL. At each time point, a 20 μL aliquot was withdrawn and diluted 100- and 1000-fold. Then 100 μL of the dilutions were plated in 7H9 plates and incubated for three days. Colonies were enumerated manually and results show Mean ± SEM from three trials done in duplicates.

Measurement of Intramycobacterial Reduction Potentials. Calibration curves were first generated by treating *M. smegmatis* mc^2155 expressing Mrx1-roGFP2 with varying ratios of DTT_{ox} and DTT_{red} corresponding to known potential values based on the Nernst Equation with a fixed total concentration of 10 mM. Bacilli were suspended in degassed PBS and the DTT mix was added. After a 5-min treatment, cells were pelleted and immediately fixed with 4% paraformaldehyde for 15 mins. Cells were washed and resuspended in 10 μL of degassed PBS for flow cytometry measurements. For bacteria treated with DAB-10, M. smegmatis was incubated with DAB-10 at its MIC and 2X MIC in Middlebrook 7H9 at 37°C for 1 hour. Afterwards, the cells were washed and fixed with 4% paraformaldehyde for 15 mins and analysed using a BD FACSCalibur flow cytometer. The fluorescence of 100,000 cells were measured and the data analyzed using FlowJo v.10. The fluorescence intensity values at 405 nm and 488 nm was obtained and the ratio converted to EMSH values using the previously generated Calibration Curves. Data shown represent Mean ± SEM obtained from three independent trials done in duplicates.

TUNEL Assay. *M. smegmatis* mc^2155 was treated with DAB-10 at the indicated concentration in the presence or absence of 100 μM tetrathiomolybdate (TTM) for 1 hour at 37°C. Following treatment, cells were prepared for TUNEL labeling according to a procedure described in Chapter 5. The cells were then analyzed using a BD FACSCalibur

flow cytometer to which fluorescence of 100,000 cells were measured and data were analyzed using FlowJo v.10. The events were gated first for propidium iodide (PI) fluorescence to differentiate the cells from debris and then gated for green fluorescence to select for TUNEL positive cells. Total TUNEL (+) cells were divided with the total number of PI (+) cells to determine % TUNEL (+) cells. Bars represent data obtained from two independent trials done in triplicates.

Generation of M. smegmatis Transposon Mutant Library. A two-day old, 200 mL M. smegmatis culture was pelleted and washed twice with 20 mL of 7H9 base medium (no supplements, no Tween 80). Then the cells were resuspended in 10 mL of 7H9 base medium. A 1 mL aliquot of MycoMar phage was added and the suspension was mixed gently by inversion. Infection was allowed to proceed for 90 mins at 37°C without shaking. The cells were then pelleted at 4000g for 10 mins at 37°C and resuspended in 10 mL of 7H9 base medium. The suspension was triturated to minimize cell clumps. A 1 mL aliquot of the transposon mutant library was then plated onto large 7H11 plates containing 20 μg/mL of Kanamycin and either 2.5 μM, or 5 μM of DAB-6 or 1.25 μM, or 2.5 μM of DAB-10. The plates were incubated at 37°C until visible colonies appeared.

Transposon Mutant Library Screening, Rescue Cloning and ROS Susceptibility Testing. The transposon mutants isolated were expected to be resistant to DAB-10. This resistance was confirmed in liquid culture by performing a microdilution broth assay similar to the one described above. Three truly resistant mutants were isolated and propagated. The genomic DNA of the resistant clones (including that of the WT) were extracted and digested with BamH1 overnight and then treated with T4 DNA ligase to circularize the DNA fragments. The DNA was then transformed into chemically competent

E. coli Pir cells and plated onto LB agar plates containing 50 μg/mL Kanamycin. The resulting colonies were isolated and propagated in LB medium containing Kanamycin. The rescued plasmid from the transformants were extracted and sequenced using primers that recognized the transposon termini to determine the insertion site. The sequencing was supplemented with genotyping PCR using primers recognizing the termini of the WT gene to validate site of transposon insertion. The ROS susceptibility of the transposon mutants were tested using known superoxide and hydroxyl radical generating agents. Mutants were treated with 5 mM Menadione, 1 mM cumene hydroperoxide or 1 mM tert-butyl hydroperoxide for 1 hr at 37°C. Ten-fold serial dilutions were plated onto 7H11 agar plates and incubated at 37°C overnight. Colonies were enumerated manually and converted to CFU/mL. Bars represent data obtained from two independent trials done in duplicates.

Macrophage Cell Culture. RAW264.7 cells were grown in 10% FBS in DMEM with 200 U/mL each of Penicillin and Streptomycin. THP-1 cells were cultured in RPMI-1640 with 10% FBS, 200 U/mL each of Penicillin and Streptomycin, and 0.05 mM 2-mercaptoethanol. THP-1 cells were differentiated prior to infection by addition of phorbol 12-myristate 13-acetate (PMA) to a final concentration of 40 ng/mL and incubation for 72 hours. Cells were grown in a 37°C incubator with 5% CO2.

Laser Confocal Microscopy. 30,000 RAW264.7 cells were seeded into each well of a chambered cover glass and allowed to adhere overnight. For peptidomimetic localization; 1, 2, 4, and 8 μM of tetramethylrhodamine-labeled DAB-10 (TMR-DAB-10) was added to each well and peptide labeling was allowed to proceed for 30 mins at 37°C. For endocytosis inhibitor experiments, cells were pre-treated with either 50 μM Amiloride

or 80 μM Dynasore (both inhibitors were from stock solutions in DMSO and final DMSO concentration was <0.5%) for 1 hr. The cells were then washed once with growth medium and replaced with fresh media containing the inhibitors and desired concentration of DAB-10. For co-localization experiments, *M. smegmatis* constitutively expressing GFP were grown in Middlebrook 7H9 + 10% ADC with 50 μg/mL Kanamycin was washed twice with PBS, and resuspended in 10% FBS in DMEM. The bacteria were quantified via OD_{600} measurements. The RAW264.7 cells were then infected (MOI 1:100) for 1 hr, washed exhaustively with PBS and fresh growth medium was added. Infected cells were then treated with TMR-DAB-10 for 30 mins and then washed and replenished with fresh media. For copper co-localization studies, cells were simultaneously treated with 1 μM CS-1 and 4 μM TMR-DAB-10 for 30 mins. Whenever activated RAW264.7 cells were used, 100 ng/mL of Lipopolysaccharide (LPS) from *E. coli* was added 24 hours prior to cell staining. Cellular organelles were labeled with MitoTracker Deep Red and/or LysoTracker based on the manufacturer's instructions. Samples were analyzed using a Nikon A1R Laser Confocal Microscope using the appropriate filter sets.

Quantification of DAB-10 Uptake by Macrophages. 50,000 RAW264.7 cells were seeded into 24-well polystyrene plates and allowed to adhere overnight. TMR-DAB-10 or fluorescein-labeled DAB-10 (FL-DAB-10) was added at the indicated concentration and allowed to incubate for 30 mins at 37°C. After incubation, cells were washed exhaustively and lysed with 200 μL RIPA lysis buffer. The fluorescence of the lysate was measured using a Molecular Devices FlexStation 3 microplate reader via a top-read mode. The absolute quantity of fluorescent peptide in the lysate was established by using a

calibration curve generated from peptide standards dissolved in the lysis buffer. Data represent Mean ± SEM obtained from three independent trials done in duplicates.

Isothermal Titration Calorimetry. Binding constants were measured on a TA instruments NanoITC calorimeter with the peptidomimetic being titrated into a solution of Cu^{2+} at 25°C. Solutions used were 2 mM DAB-10 (in the ITC syringe) and 400 μM $Cu(NO_3)_2$ (in the ITC cell) both in 20 mM MES buffer at pH 6.40. Blank titrations were run to determine heats of dilution. Data were analyzed using TA Instruments NanoAnalyze software and represent values obtained from three independent titrations.

Mammalian Cell Viability. 10,000 RAW264.7 or THP-1 cells were seeded and differentiated (for the case of THP-1 cells) in 96-well polypropylene plates. 100 μL of media containing 2-fold serial dilutions of the test agent was added to each well and the cells were incubated for 24 hrs at 37°C. Then, the cells were washed with PBS twice and replaced with fresh media containing 5 mg/mL of MTT. The color was allowed to develop for 4 hrs in the incubator afterwhich, the cells were washed with PBS twice. 200 μL of DMSO was then added to each well to lyse the cells and quantify degree of MTT oxidation. The absorbance of each well at 595 nm was recorded and used to calculated % cell viability. Data shows Mean ± SEM obtained from three independent trials done in duplicates.

Activity against Intracellular Mycobacteria. (Experiment performed by Dr. Gopinath Krishnamoorthy, Dr. Peggy Kaiser, and Dr. Stefan H.E. Kaufmann, Max Planck Institute for Infection Biology) 50,000 THP-1 cells were seeded into 24-well plates and PMA-differentiated for 72 hrs. *M. tuberculosis* H37Rv was grown until exponential phase and was used to infect fully differentiated THP-1 cells at an MOI of 1:5. The infection was

allowed to proceed for 4 hours after which the macrophages were washed with PBS exhaustively. Then fresh medium was replaced into the cell containing either 80 μM of DAB-6 or 20 μM of DAB-10 in the presence or absence of 100 μM of either bathobuproinedisulfonate (BCS) or TTM. The cells were incubated for 24 and 48 hours after which macrophages were lysed and the lysate serially diluted and plated in 7H11 agar plates. The plates were incubated for four weeks and colonies were enumerated manually. Data shows values obtained from two trials done in duplicates.

Statistical Analysis. Data were plotted and analyzed for statistical differences using GraphPad Prism 7.0. One-way or Two-way ANOVA was used to determine statistical significance which was set at $P<0.05$.

Chapter References:

[1] World Health Organization., and Global Tuberculosis Programme. (2015) Global tuberculosis control : WHO report, p 15 volumes, Global Tuberculosis Programme, Geneva, Switzerland.

[2] Hood, M. I., and Skaar, E. P. (2012) Nutritional immunity: transition metals at the pathogen-host interface, *Nat Rev Microbiol 10*, 525-537.

[3] Schaible, U. E., and Kaufmann, S. H. (2004) Iron and microbial infection, *Nat Rev Microbiol 2*, 946-953.

[4] White, C., Lee, J., Kambe, T., Fritsche, K., and Petris, M. J. (2009) A role for the ATP7A copper-transporting ATPase in macrophage bactericidal activity, *J Biol Chem 284*, 33949-33956.

[5] Samanovic, M. I., Ding, C., Thiele, D. J., and Darwin, K. H. (2012) Copper in microbial pathogenesis: meddling with the metal, *Cell Host Microbe 11*, 106-115.

[6] Rowland, J. L., and Niederweis, M. (2012) Resistance mechanisms of Mycobacterium tuberculosis against phagosomal copper overload, *Tuberculosis (Edinb) 92*, 202-210.

[7] Wagner, D., Maser, J., Lai, B., Cai, Z., Barry, C. E., 3rd, Honer Zu Bentrup, K., Russell, D. G., and Bermudez, L. E. (2005) Elemental analysis of Mycobacterium avium-, Mycobacterium tuberculosis-, and Mycobacterium smegmatis-containing phagosomes indicates pathogen-induced microenvironments within the host cell's endosomal system, *J Immunol 174*, 1491-1500.

[8] Ward, S. K., Abomoelak, B., Hoye, E. A., Steinberg, H., and Talaat, A. M. (2010) CtpV: a putative copper exporter required for full virulence of Mycobacterium tuberculosis, *Mol Microbiol 77*, 1096-1110.

[9] Wolschendorf, F., Ackart, D., Shrestha, T. B., Hascall-Dove, L., Nolan, S., Lamichhane, G., Wang, Y., Bossmann, S. H., Basaraba, R. J., and Niederweis, M. (2011) Copper resistance is essential for virulence of Mycobacterium tuberculosis, *Proc Natl Acad Sci U S A 108*, 1621-1626.

[10] Gold, B., Deng, H., Bryk, R., Vargas, D., Eliezer, D., Roberts, J., Jiang, X., and Nathan, C. (2008) Identification of a copper-binding metallothionein in pathogenic mycobacteria, *Nat Chem Biol 4*, 609-616.

[11] Rowland, J. L., and Niederweis, M. (2013) A multicopper oxidase is required for copper resistance in Mycobacterium tuberculosis, *J Bacteriol 195*, 3724-3733.

[12] Festa, R. A., Jones, M. B., Butler-Wu, S., Sinsimer, D., Gerads, R., Bishai, W. R., Peterson, S. N., and Darwin, K. H. (2011) A novel copper-responsive regulon in Mycobacterium tuberculosis, *Mol Microbiol 79*, 133-148.

[13] Liu, T., Ramesh, A., Ma, Z., Ward, S. K., Zhang, L., George, G. N., Talaat, A. M., Sacchettini, J. C., and Giedroc, D. P. (2007) CsoR is a novel Mycobacterium tuberculosis copper-sensing transcriptional regulator, *Nat Chem Biol 3*, 60-68.

[14] Shi, X., Festa, R. A., Ioerger, T. R., Butler-Wu, S., Sacchettini, J. C., Darwin, K. H., and Samanovic, M. I. (2014) The copper-responsive RicR regulon contributes to Mycobacterium tuberculosis virulence, *MBio 5*.

[15] Speer, A., Shrestha, T. B., Bossmann, S. H., Basaraba, R. J., Harber, G. J., Michalek, S. M., Niederweis, M., Kutsch, O., and Wolschendorf, F. (2013) Copper-boosting

compounds: a novel concept for antimycobacterial drug discovery, *Antimicrob Agents Chemother 57*, 1089-1091.
[16] Dalecki, A. G., Haeili, M., Shah, S., Speer, A., Niederweis, M., Kutsch, O., and Wolschendorf, F. (2015) Disulfiram and Copper Ions Kill Mycobacterium tuberculosis in a Synergistic Manner, *Antimicrob Agents Chemother 59*, 4835-4844.
[17] Shah, S., Dalecki, A. G., Malalasekera, A. P., Crawford, C. L., Michalek, S. M., Kutsch, O., Sun, J., Bossmann, S. H., and Wolschendorf, F. (2016) 8-Hydroxyquinolines Are Boosting Agents of Copper-Related Toxicity in Mycobacterium tuberculosis, *Antimicrob Agents Chemother 60*, 5765-5776.
[18] Yu, M., Nagalingam, G., Ellis, S., Martinez, E., Sintchenko, V., Spain, M., Rutledge, P. J., Todd, M. H., and Triccas, J. A. (2016) Nontoxic Metal-Cyclam Complexes, a New Class of Compounds with Potency against Drug-Resistant Mycobacterium tuberculosis, *J Med Chem 59*, 5917-5921.
[19] Vilcheze, C., Hartman, T., Weinrick, B., and Jacobs, W. R., Jr. (2013) Mycobacterium tuberculosis is extraordinarily sensitive to killing by a vitamin C-induced Fenton reaction, *Nat Commun 4*, 1881.
[20] Grant, S. S., Kaufmann, B. B., Chand, N. S., Haseley, N., and Hung, D. T. (2012) Eradication of bacterial persisters with antibiotic-generated hydroxyl radicals, *Proc Natl Acad Sci U S A 109*, 12147-12152.
[21] Palde, P. B., Bhaskar, A., Pedro Rosa, L. E., Madoux, F., Chase, P., Gupta, V., Spicer, T., Scampavia, L., Singh, A., and Carroll, K. S. (2016) First-in-Class Inhibitors of Sulfur Metabolism with Bactericidal Activity against Non-Replicating M. tuberculosis, *ACS Chem Biol 11*, 172-184.
[22] Singh, R., Manjunatha, U., Boshoff, H. I., Ha, Y. H., Niyomrattanakit, P., Ledwidge, R., Dowd, C. S., Lee, I. Y., Kim, P., Zhang, L., Kang, S., Keller, T. H., Jiricek, J., and Barry, C. E., 3rd. (2008) PA-824 kills nonreplicating Mycobacterium tuberculosis by intracellular NO release, *Science 322*, 1392-1395.
[23] Tyagi, P., Dharmaraja, A. T., Bhaskar, A., Chakrapani, H., and Singh, A. (2015) Mycobacterium tuberculosis has diminished capacity to counteract redox stress induced by elevated levels of endogenous superoxide, *Free Radic Biol Med 84*, 344-354.
[24] Jin, Y., Lewis, M. A., Gokhale, N. H., Long, E. C., and Cowan, J. A. (2007) Influence of stereochemistry and redox potentials on the single- and double-strand DNA cleavage efficiency of Cu(II) and Ni(II) Lys-Gly-His-derived ATCUN metallopeptides, *J Am Chem Soc 129*, 8353-8361.
[25] Joyner, J. C., Hodnick, W. F., Cowan, A. S., Tamuly, D., Boyd, R., and Cowan, J. A. (2013) Antimicrobial metallopeptides with broad nuclease and ribonuclease activity, *Chem Commun (Camb) 49*, 2118-2120.
[26] Park, C. B., Yi, K. S., Matsuzaki, K., Kim, M. S., and Kim, S. C. (2000) Structure-activity analysis of buforin II, a histone H2A-derived antimicrobial peptide: the proline hinge is responsible for the cell-penetrating ability of buforin II, *Proc Natl Acad Sci U S A 97*, 8245-8250.
[27] Brewer, G. J. (2009) Zinc and tetrathiomolybdate for the treatment of Wilson's disease and the potential efficacy of anticopper therapy in a wide variety of diseases, *Metallomics 1*, 199-206.

[28] Bhaskar, A., Chawla, M., Mehta, M., Parikh, P., Chandra, P., Bhave, D., Kumar, D., Carroll, K. S., and Singh, A. (2014) Reengineering redox sensitive GFP to measure mycothiol redox potential of Mycobacterium tuberculosis during infection, *PLoS Pathog 10*, e1003902.
[29] Morones-Ramirez, J. R., Winkler, J. A., Spina, C. S., and Collins, J. J. (2013) Silver enhances antibiotic activity against gram-negative bacteria, *Sci Transl Med 5*, 190ra181.
[30] Jin, Y., and Cowan, J. A. (2005) DNA cleavage by copper-ATCUN complexes. Factors influencing cleavage mechanism and linearization of dsDNA, *J Am Chem Soc 127*, 8408-8415.
[31] Kapopoulou, A., Lew, J. M., and Cole, S. T. (2011) The MycoBrowser portal: a comprehensive and manually annotated resource for mycobacterial genomes, *Tuberculosis (Edinb) 91*, 8-13.
[32] von Mering, C., Huynen, M., Jaeggi, D., Schmidt, S., Bork, P., and Snel, B. (2003) STRING: a database of predicted functional associations between proteins, *Nucleic Acids Res 31*, 258-261.
[33] Zeng, L., Miller, E. W., Pralle, A., Isacoff, E. Y., and Chang, C. J. (2006) A selective turn-on fluorescent sensor for imaging copper in living cells, *J Am Chem Soc 128*, 10-11.
[34] Vandal, O. H., Pierini, L. M., Schnappinger, D., Nathan, C. F., and Ehrt, S. (2008) A membrane protein preserves intrabacterial pH in intraphagosomal Mycobacterium tuberculosis, *Nat Med 14*, 849-854.
[35] Sturgill-Koszycki, S., Schlesinger, P. H., Chakraborty, P., Haddix, P. L., Collins, H. L., Fok, A. K., Allen, R. D., Gluck, S. L., Heuser, J., and Russell, D. G. (1994) Lack of acidification in Mycobacterium phagosomes produced by exclusion of the vesicular proton-ATPase, *Science 263*, 678-681.
[36] Sacchettini, J. C., Rubin, E. J., and Freundlich, J. S. (2008) Drugs versus bugs: in pursuit of the persistent predator Mycobacterium tuberculosis, *Nat Rev Microbiol 6*, 41-52.
[37] Wallis, R. S., and Hafner, R. (2015) Advancing host-directed therapy for tuberculosis, *Nat Rev Immunol 15*, 255-263.
[38] Kaufmann, S. H., Lange, C., Rao, M., Balaji, K. N., Lotze, M., Schito, M., Zumla, A. I., and Maeurer, M. (2014) Progress in tuberculosis vaccine development and host-directed therapies--a state of the art review, *Lancet Respir Med 2*, 301-320.
[39] Darwin, K. H. (2015) Mycobacterium tuberculosis and Copper: A Newly Appreciated Defense against an Old Foe?, *J Biol Chem 290*, 18962-18966.
[40] Garba, I. H., Ubom, G. A., and Ejiogu, N. B. (2006) Serum copper concentration in adults with acute, uncomplicated falciparum malaria infection, *Biol Trace Elem Res 113*, 125-130.
[41] Porcheron, G., Garenaux, A., Proulx, J., Sabri, M., and Dozois, C. M. (2013) Iron, copper, zinc, and manganese transport and regulation in pathogenic Enterobacteria: correlations between strains, site of infection and the relative importance of the different metal transport systems for virulence, *Front Cell Infect Microbiol 3*, 90.

[42] Helz, G. R., and Erickson, B. E. (2011) Extraordinary stability of copper(I)-tetrathiomolybdate complexes: possible implications for aquatic ecosystems, *Environ Toxicol Chem 30*, 97-102.
[43] Park, C. B., Kim, H. S., and Kim, S. C. (1998) Mechanism of action of the antimicrobial peptide buforin II: buforin II kills microorganisms by penetrating the cell membrane and inhibiting cellular functions, *Biochem Biophys Res Commun 244*, 253-257.
[44] Dwyer, D. J., Belenky, P. A., Yang, J. H., MacDonald, I. C., Martell, J. D., Takahashi, N., Chan, C. T., Lobritz, M. A., Braff, D., Schwarz, E. G., Ye, J. D., Pati, M., Vercruysse, M., Ralifo, P. S., Allison, K. R., Khalil, A. S., Ting, A. Y., Walker, G. C., and Collins, J. J. (2014) Antibiotics induce redox-related physiological alterations as part of their lethality, *Proc Natl Acad Sci U S A 111*, E2100-2109.
[45] Dwyer, D. J., Camacho, D. M., Kohanski, M. A., Callura, J. M., and Collins, J. J. (2012) Antibiotic-induced bacterial cell death exhibits physiological and biochemical hallmarks of apoptosis, *Mol Cell 46*, 561-572.
[46] Kohanski, M. A., Dwyer, D. J., Hayete, B., Lawrence, C. A., and Collins, J. J. (2007) A common mechanism of cellular death induced by bactericidal antibiotics, *Cell 130*, 797-810.
[47] Liu, Z., Cai, Y., Young, A. W., Totsingan, F., Jiwrajka, N., Shi, Z., and Kallenbach, N. R. (2012) OH radical production stimulated by (RW)4D, a synthetic antimicrobial agent and indolicidin, *MedChemComm 3*, 1548.
[48] Haas, K. L., Putterman, A. B., White, D. R., Thiele, D. J., and Franz, K. J. (2011) Model peptides provide new insights into the role of histidine residues as potential ligands in human cellular copper acquisition via Ctr1, *J Am Chem Soc 133*, 4427-4437.
[49] Rozga, M., Sokolowska, M., Protas, A. M., and Bal, W. (2007) Human serum albumin coordinates Cu(II) at its N-terminal binding site with 1 pM affinity, *J Biol Inorg Chem 12*, 913-918.
[50] Achard, M. E., Stafford, S. L., Bokil, N. J., Chartres, J., Bernhardt, P. V., Schembri, M. A., Sweet, M. J., and McEwan, A. G. (2012) Copper redistribution in murine macrophages in response to Salmonella infection, *Biochem J 444*, 51-57.
[51] Alberts, B., Johnson, A., Lewis, J., Raff, M., Roberts, K., and Walter, P. (2008) Intracellular Compartments and Protein Sorting, In *Molecular Biology of the Cell* (Anderson, M., and Granum, S., Eds.) 5th ed., pp 695-748, Garland Science, Taylor & Francis Group, LLC, New York, NY.
[52] Sturgill-Koszycki, S., Schaible, U. E., and Russell, D. G. (1996) Mycobacterium-containing phagosomes are accessible to early endosomes and reflect a transitional state in normal phagosome biogenesis, *EMBO J 15*, 6960-6968.
[53] Olakanmi, O., Schlesinger, L. S., Ahmed, A., and Britigan, B. E. (2002) Intraphagosomal Mycobacterium tuberculosis acquires iron from both extracellular transferrin and intracellular iron pools. Impact of interferon-gamma and hemochromatosis, *J Biol Chem 277*, 49727-49734.

Chapter 7

Concluding Remarks

The Bigger Picture, Outstanding Questions, and What Lies Ahead

"The task is…not so much to see what no one has yet seen; but to think what nobody has yet thought, about that which everybody sees."

– Erwin Schrödinger

Looking Back and Connecting the Dots

The host immune system employs a plethora of antimicrobial factors that act in concert either amongst themselves or with other chemical components present to eradicate invading microbes. The competition for essential metal micronutrients between microbes and host-derived factors represent a long-standing battle in the host-pathogen interface.[1, 2] While several intervention strategies involving metal ions at sites of infection are currently being explored, most, if not all focus on interfering or overriding the bacterial metal acquisition mechanisms.[3-6] Unlike iron, zinc, and manganese that are depleted during microbial challenge, copper is deliberately trafficked into regions containing bacteria.[7, 8] While it may be advantageous to boost the copper concentration during infection due to its inherent antimicrobial properties, bacteria have developed clever ways to evade the toxic effects of copper. Be that as it may, spending cellular currency to redistribute copper during infection must be auspicious, otherwise, evolution would have selected against it.

To address this conundrum, we looked at what else is present in the site of infection: cells, proteins, etc. Professional phagocytes flood the region containing bacteria. These cells contain or secrete several antimicrobial effectors which include host-defense peptides (some of which are known to bind metals) and reactive intermediates. We postulated that copper exhibits a dynamic interplay with the subset of HDPs that contain an ATCUN motif to elicit synergistic effects. That way, copper can exert direct bactericidal effects that circumvent bacterial resistance mechanisms. We set out to study the subset of HDPs that contain an ATCUN motif and asked the question: how is copper binding beneficial to the bioactivity of these peptides? More importantly, we wondered

how copper-mediated bacterial targeting is leveraged or exploited by other antimicrobial effectors. Finally, in an effort to contribute to the development of novel intervention strategies against resistant strains of bacteria, we also wondered whether the ATCUN motif can be used to improve the potency of other peptides.

The results described in this dissertation span four aspects that when taken together allow us to define the biological significance and advantage of the ATCUN motif.

First, the ATCUN motif is necessary for the oxidative mechanism of naturally occurring AMPs. We demonstrated in Chapter 2 that whereas a His-to-Ala substitution or an ATCUN deletion generated derivatives that were equally as potent, those mutants lack the oxidative capability of the WT peptide. This suggests that the inherent oxidative capacity of the resulting Cu-ATCUN complex is used by these AMPs to effect oxidative stress into their targets. Biomolecular oxidation is largely dictated by the affinity of these peptides toward different structures in bacteria. For instance, ixosin has a great affinity towards the bacterial membrane and thus can cause membrane lipid peroxidation and piscidin 3 binds nucleotides and can therefore oxidatively cleave DNA. Ultimately, what this implies is that ATCUN-containing AMPs and HDPs can covalently damage their targets, instead of just relying on electrostatic and steric contributions. Covalently damaging the target generates new functionalities that either has to be degraded and recycled, or can be toxic on its own.

Second, we observed direct target oxidation in Chapters 2 and 3 without pre-loading the peptides with copper. Because oxidative capacity is a phenotype expected only if the peptides are metallated, these observations suggest a competitive ability of the ATCUN-containing peptides to scavenge copper ions and utilize it for their oxidative

mechanism. Copper can come from extracellular sources or from the endogenous pool of labile copper inside bacteria. Together with the fact that the ATCUN motif has a high affinity towards copper ions, it doesn't seem surprising that these peptides actually sequester copper. In chapter 3, we dissected where the copper can come from, and found that both extracellular and intracellular copper reserves can supply piscidins with copper. Moreover, because a significant level of oxidation was observed, it seemed like the soup of chemical effectors in the cellular milieu is sufficient in promoting the redox cycling to the metal center. This generates a catalytic oxidant that is likely the major driving force for bacterial death.

Third, copper-binding and the subsequent target oxidation paves the way for synergistic interactions between homologous and/or co-expressed peptides to occur. In chapter 2 we showed that the oxidized phospholipids generated by Cu-Ixosin-mediated membrane oxidation is a target for ixosin B. This phospholipid targeting by ixosin B likely involves imine group formation between the amine groups of the peptide and the carbonyl groups of the oxidized lipids, effectively anchoring the peptide into the membrane. Therefore, in the presence of ixosin, a smaller amount of ixosin B is required for bacterial killing. In chapter 3, we discussed how the homologous peptides p1 and p3, who both have considerable yet contrasting activity towards the bacterial membrane and DNA exhibit synergistic interactions with each other in the absence of a robust DNA repair pathway. More importantly, their synergy is likely more relevant in terms of their functional complementarity. Taken together, these results suggest that ATCUN-containing peptides sensitize bacteria toward the effects of other AMPs, leading to a cooperative interaction. This represents a case where expression of ATCUN-AMPs may be selected for because

it offers a pathway not only for direct protection against microbes but also for boosting the activity of other effectors *in situ*.

Finally, the redox cycling is a function of the ATCUN moiety alone and is therefore a transferrable trait. In Chapters 4, 5, and 6, we were able to integrate the oxidative capability of the ATCUN motif to peptides that normally would not have it. While the tripeptide alone is not a sufficient antimicrobial, exogenously adding this sequence to other AMPs affords the latter a secondary mode of attack resulting in a gain-of-function phenotype. We were able to observe a similar nucleotide or membrane targeting in the conjugates. More importantly, we developed an *in situ* activatable peptidomimetic which can exploit the transition metal trafficking in macrophages to target intracellular *M. tuberculosis*. Apart from its oxidative capabilities, the small size of the ATCUN motif lends itself amenable for bioconjugations – one gets an entirely new mode of attack from these peptides at the small expense of adding three extra amino acids. The pharmaceutical industry is dominated by molecules that target one specific protein or pathway in the cell, with the hope of minimizing side-effects arising from off-target toxicity. However, this seems to ignore the question of what happens when mutations in these proteins or pathways occur? Resistance mechanisms oftentimes abolishes target recognition step, effectively rendering antibiotics ineffective. While combination therapy gets around this problem, treating bacteria with two single-acting drugs which may have varying serum half-lives leads to the slow emergence of multidrug resistant strains. One has to wonder whether a new paradigm – one that is based on developing multiple modes of inhibition by a single agent is more advantageous. After all, it seems to be the method of choice by our immune systems.

The Bigger Picture

The results presented in this dissertation shed light on the small and ubiquitous ATCUN motif, a tripeptide sequence whose chemistry has long been established but whose biology is largely unexplored. Although we initially set out to study a specific subset of HDPs and AMPs, the results we obtained through the years lead us to paint a bigger picture of the interface between bioinorganic chemistry and immunology – one which expands the catalog of mechanisms by which AMPs and HDPs utilize metal ions for their activity. The underlying theme to every chapter in this dissertation is the demonstration of copper-binding and oxidative damage by ATCUN-containing peptides. Our data show that these peptides leverage the chemical reactivity of the Cu-ATCUN complex in their biological activity. Therefore, it is clear that HDPs – apart from sequestering metal ions from bacteria or using metals as structural scaffolds – also utilize transition metals as direct chemical co-factors. This suggests that copper trafficking into sites of infection likely is advantageous because it generates a pool of exchangeable copper for some of these HDPs to exploit. We show here that ATCUN-containing peptides likely utilize a generalized mechanism of attack – one that directly generates oxidative stress in their target. Moreover, since ATCUN-AMPs have been isolated from diverse sources, it represents a common defense mechanism by seemingly unrelated organisms.

Which Questions Remain Unanswered?

While most of the AMPs studied in this dissertation come from non-mammalian sources, there are a number of human HDPs that contain the ATCUN motif and can therefore utilize a similar mechanism of attack. First, the histatin family of salivary AMPs

consists of three ribosomally-synthesized parent peptides and nine proteolytic degradation products, all of which have antifungal activity.[9, 10] Of this 12-member family, eight of which contain the ATCUN motif.[9] One has to wonder why there is a need for such a large number of antifungal peptides in a region where bacterial invaders pose a greater threat. Moreover, histatins have always been screened for antibacterial activity alone and never in combination with other members of their family. It is therefore a likely possibility that the narrow-spectrum activity reported doesn't take into consideration the possibility that histatins act in concert when they target bacteria. From their narrow-spectrum activity and the sheer number of members in this family, it seems reasonable to question whether these peptides exhibit synergistic interactions among them.[11]

Further support to the notion of ATCUN-AMPs boosting the antimicrobial effects of other peptides in its family have been alluded to by reports published a decade ago. For instance, antimicrobial peptide expression in *Drosophila* is differentially induced by specific microbes. Infection with Gram-negative bacteria induces expression of metchnikowin, diptericin, cecropin A, and drosocin; whereas Gram-positive infections leads to expression of metchnikowin and drosomycin. Fungal infections cause metchnikowin, diptericin, attacin, and drosomycin to be expressed.[12] From these expression profiles, one can see that regardless of the pathogen, the AMP metchnikowin is always expressed. Metchnikowin contains His-Arg-His (HRH) in its N-terminal, and does not exhibit any antimicrobial activity up to 512 μM (data not included in this dissertation). Because of the ATCUN-mediated synergy between Ixosin and Ixosin B (which were isolated from insects as well) presented in Chapter 2, it seems logical to propose that metchnikowin might be acting as an adjuvant AMP to other AMPs in

Drosophila eliciting synergistic interactions from other AMPs which are differentially induced. This is likely because the ROS formed by the ATCUN motif is non-specific and can therefore be used to sensitize any microbe to the attack of other AMPs.

Some peptides that exists within mammalian (phagocytic) cells also contain the ATCUN motif. In particular, ubiquicidin, an AMP derived from proteolytic degradation of ubiquitin contains a Lys-Phe-His (KFH) in its N-terminal.[13, 14] Given the abundance of copper ions in the *Mycobacteria*-containing phagosome and the trafficking of ubiquitin derived fragments into the phagosome, one has to wonder whether there is involvement by the ATCUN motif in the killing of Mtb. Indeed, the ubiquitin pathway has been shown to play a role in the mycobactericidal activity of activated macrophages.[15, 16] Moreover, hepcidin, an ATCUN-AMP that partakes in iron homeostasis also plays a role in mycobacterial eradication in macrophages.[17]

Indeed, even though the peptides studied here are not derived from humans, the fact that copper-binding and oxidative capacity is less-sequence independent than it is donor-atom-dependent, suggests that human-derived ATCUN-HDPs can also deliver a mode of attack similar to the ones described in this dissertation. That is, the properties that make the Cu-ATCUN complex antimicrobial is the three-dimensional arrangement of nitrogen atoms around the copper center that are able to support the metal's trivalent state. Therefore, it seems reasonable to posit that all ATCUN-AMPs likely have an oxidative mode of attack.

The Future of Metalloimmunology

While this dissertation focused on how host-derived AMPs utilize copper for their activity, differential trafficking during infection is not unique to copper. For instance, two

paradigms exist for zinc in the host-pathogen interface – sequestration and intoxication.[18] We know which antimicrobial effectors are involved in each mechanism, but the reason why contrasting zinc regulation exist during infection is not clear. The Zn^{2+} ion, owing to its small size and high-position in the Irving-Williams series can also effect metal co-factor replacement. However, the ion is redox-silent unlike Fe^{2+} and Cu^{+}. Considering its inability to form ROS, the question of what other toxic effects does Zn^{2+} have remains unanswered.

The concept of nutritional immunity dictates that metals are sequestered away from pathogens to inhibit their growth. However, what happens after the bacteria dies? Do the metals get recycled? If so, what mechanisms exists to remove the metal out of the high-affinity S100 proteins?[19] Moreover, does the host leverage the sudden surge in extracellular metals to recruit other immune effectors given the emerging role of transition metals in cell signaling?

Finally, a model of the immune response that focuses on late first-row transition metals biases against their lighter congeners, which are also abundant in other organisms. In particular, Vanadium is highly enriched in tunicate hemocytes, immune cells that also express AMPs.[20-22] Does V have a role in the immune system of invertebrates? If so, how is the metal utilized? These questions, among many others, promise to make keep the field of metalloimmunology dynamic. Answering these questions will bring us one step closer to an understanding of the metallobiology of the immune system, and help us build a detailed narrative of its bactericidal activity.

References (Chapter 7):

[1] Hood, M. I., and Skaar, E. P. (2012) Nutritional immunity: transition metals at the pathogen-host interface, *Nat Rev Microbiol 10*, 525-537.

[2] Skaar, E. P., and Raffatellu, M. (2015) Metals in infectious diseases and nutritional immunity, *Metallomics 7*, 926-928.

[3] Roush, R. F., Nolan, E. M., Lohr, F., and Walsh, C. T. (2008) Maturation of an Escherichia coli ribosomal peptide antibiotic by ATP-consuming N-P bond formation in microcin C7, *J Am Chem Soc 130*, 3603-3609.

[4] Sassone-Corsi, M., Chairatana, P., Zheng, T., Perez-Lopez, A., Edwards, R. A., George, M. D., Nolan, E. M., and Raffatellu, M. (2016) Siderophore-based immunization strategy to inhibit growth of enteric pathogens, *Proc Natl Acad Sci U S A 113*, 13462-13467.

[5] Zheng, T., Bullock, J. L., and Nolan, E. M. (2012) Siderophore-mediated cargo delivery to the cytoplasm of Escherichia coli and Pseudomonas aeruginosa: syntheses of monofunctionalized enterobactin scaffolds and evaluation of enterobactin-cargo conjugate uptake, *J Am Chem Soc 134*, 18388-18400.

[6] Zheng, T., and Nolan, E. M. (2014) Enterobactin-mediated delivery of beta-lactam antibiotics enhances antibacterial activity against pathogenic Escherichia coli, *J Am Chem Soc 136*, 9677-9691.

[7] Besold, A. N., Culbertson, E. M., and Culotta, V. C. (2016) The Yin and Yang of copper during infection, *J Biol Inorg Chem 21*, 137-144.

[8] Samanovic, M. I., Ding, C., Thiele, D. J., and Darwin, K. H. (2012) Copper in microbial pathogenesis: meddling with the metal, *Cell Host Microbe 11*, 106-115.

[9] Melino, S., Santone, C., Di Nardo, P., and Sarkar, B. (2014) Histatins: salivary peptides with copper(II)- and zinc(II)-binding motifs: perspectives for biomedical applications, *FEBS J 281*, 657-672.

[10] Oppenheim, F. G., Xu, T., McMillian, F. M., Levitz, S. M., Diamond, R. D., Offner, G. D., and Troxler, R. F. (1988) Histatins, a novel family of histidine-rich proteins in human parotid secretion. Isolation, characterization, primary structure, and fungistatic effects on Candida albicans, *J Biol Chem 263*, 7472-7477.

[11] Puri, S., and Edgerton, M. (2014) How does it kill?: understanding the candidacidal mechanism of salivary histatin 5, *Eukaryot Cell 13*, 958-964.

[12] Lemaitre, B., Reichhart, J. M., and Hoffmann, J. A. (1997) Drosophila host defense: differential induction of antimicrobial peptide genes after infection by various classes of microorganisms, *Proc Natl Acad Sci U S A 94*, 14614-14619.

[13] Brouwer, C. P., Bogaards, S. J., Wulferink, M., Velders, M. P., and Welling, M. M. (2006) Synthetic peptides derived from human antimicrobial peptide ubiquicidin accumulate at sites of infections and eradicate (multi-drug resistant) Staphylococcus aureus in mice, *Peptides 27*, 2585-2591.

[14] Hiemstra, P. S., van den Barselaar, M. T., Roest, M., Nibbering, P. H., and van Furth, R. (1999) Ubiquicidin, a novel murine microbicidal protein present in the cytosolic fraction of macrophages, *J Leukoc Biol 66*, 423-428.

[15] Alonso, S., Pethe, K., Russell, D. G., and Purdy, G. E. (2007) Lysosomal killing of Mycobacterium mediated by ubiquitin-derived peptides is enhanced by autophagy, *Proc Natl Acad Sci U S A 104*, 6031-6036.

[16] Pearce, M. J., Mintseris, J., Ferreyra, J., Gygi, S. P., and Darwin, K. H. (2008) Ubiquitin-like protein involved in the proteasome pathway of Mycobacterium tuberculosis, *Science 322*, 1104-1107.
[17] Sow, F. B., Nandakumar, S., Velu, V., Kellar, K. L., Schlesinger, L. S., Amara, R. R., Lafuse, W. P., Shinnick, T. M., and Sable, S. B. (2011) Mycobacterium tuberculosis components stimulate production of the antimicrobial peptide hepcidin, *Tuberculosis (Edinb) 91*, 314-321.
[18] Lemire, J. A., Harrison, J. J., and Turner, R. J. (2013) Antimicrobial activity of metals: mechanisms, molecular targets and applications, *Nat Rev Microbiol 11*, 371-384.
[19] Zackular, J. P., Chazin, W. J., and Skaar, E. P. (2015) Nutritional Immunity: S100 Proteins at the Host-Pathogen Interface, *J Biol Chem 290*, 18991-18998.
[20] Macara, I. G., and McLeod, G. C. (1979) Tunichromes and metal ion accumulation in tunicate blood cells, *Comp Biochem Physiol B 63*, 299-302.
[21] Smith, M. J., Ryan, D. E., Nakanishi, K., Frank, P., and Hodgson, K. O. (1995) Vanadium in ascidians and the chemistry of tunichromes, *Met Ions Biol Syst 31*, 423-490.
[22] Taylor, S. W., Kammerer, B., and Bayer, E. (1997) New Perspectives in the Chemistry and Biochemistry of the Tunichromes and Related Compounds, *Chem Rev 97*, 333-346.

Chapter 8

Appendices

Supplementary Figures and Tables

"Simple ingredients can be used to make elegant dishes with just a little extra attention to detail."

– Marcus Samuelsson

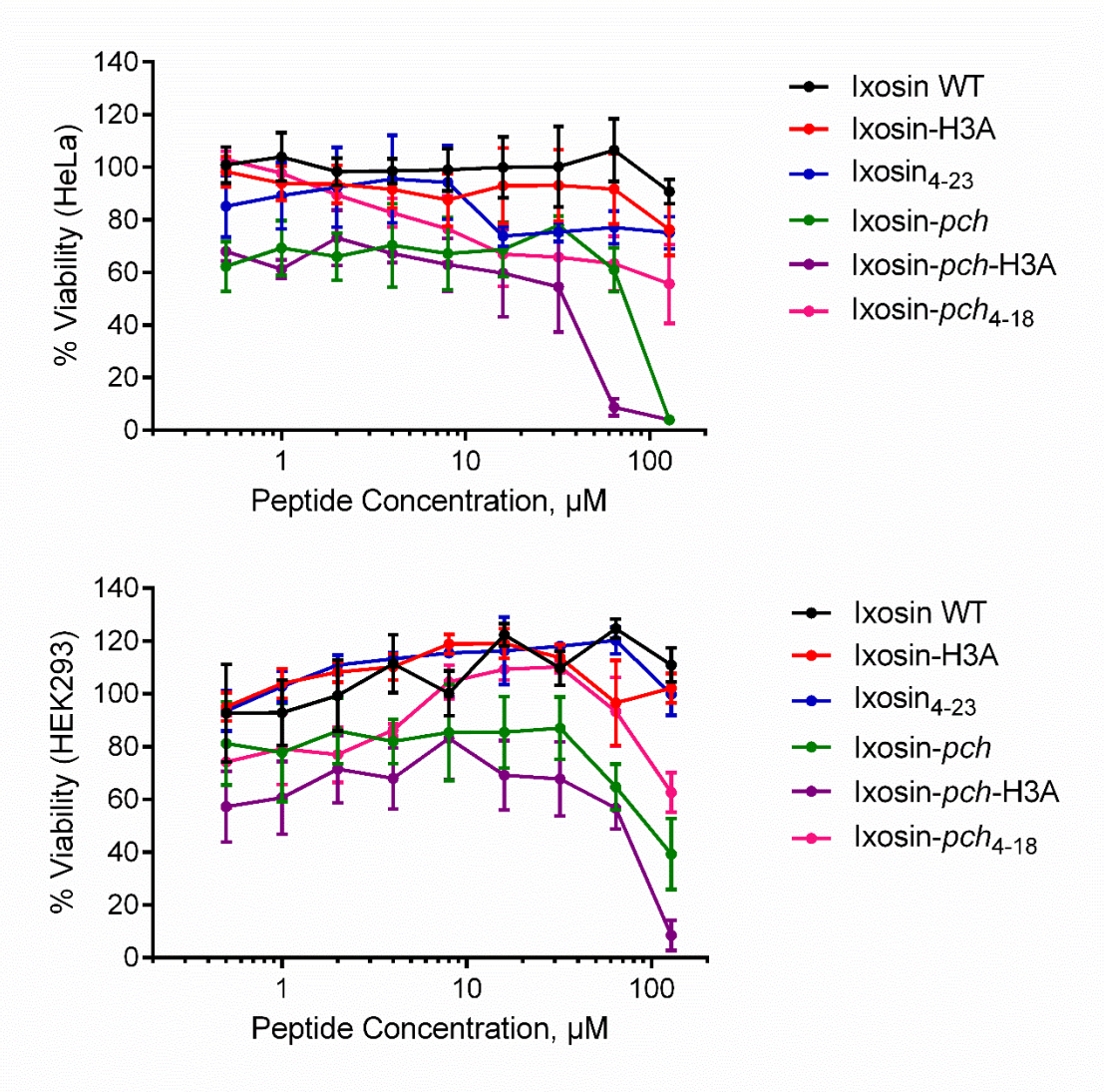

Figure S2.1. Cytotoxicity of Peptides under study. MTT Assay was used to determine extent of Mammalian cell toxicity of peptides. IC_{50} could not be determined with confidence since at the concentration range used for the experiment, complete inhibition and complete growth was not seen.

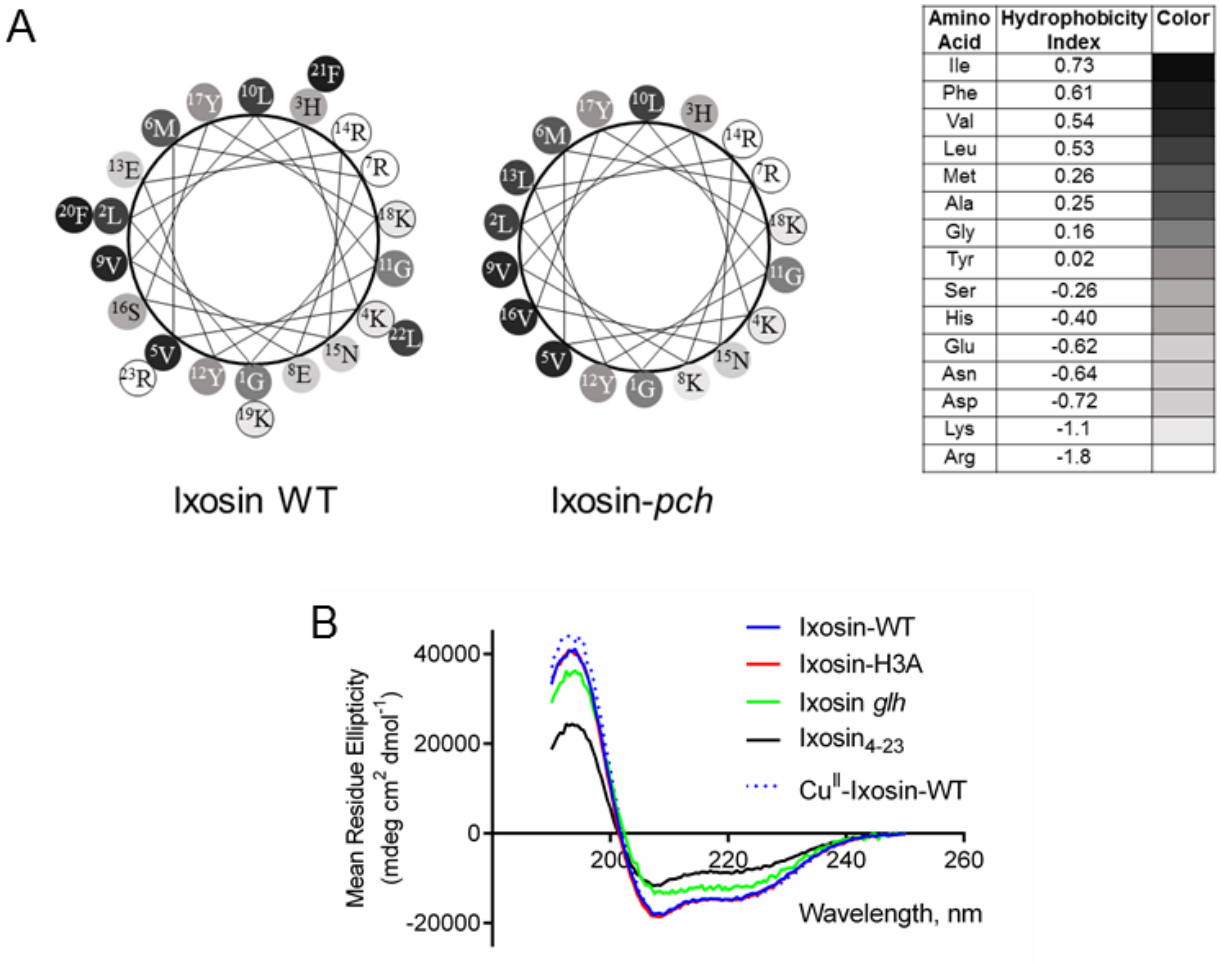

Figure S2.2. Helical Wheel Projection and CD Specta of Ixosin in TFE. (A) Helical wheel diagram of ixosin WT and Ixosin-*pch* using the Eisenberg consensus hydrophobicity scale. (B) The CD spectra of the peptides were obtained in 50% TFE in sodium phosphate buffer. Ixosin *glh* refers to a derivative (not included in main text) containing D-Leu, and D-His.

A

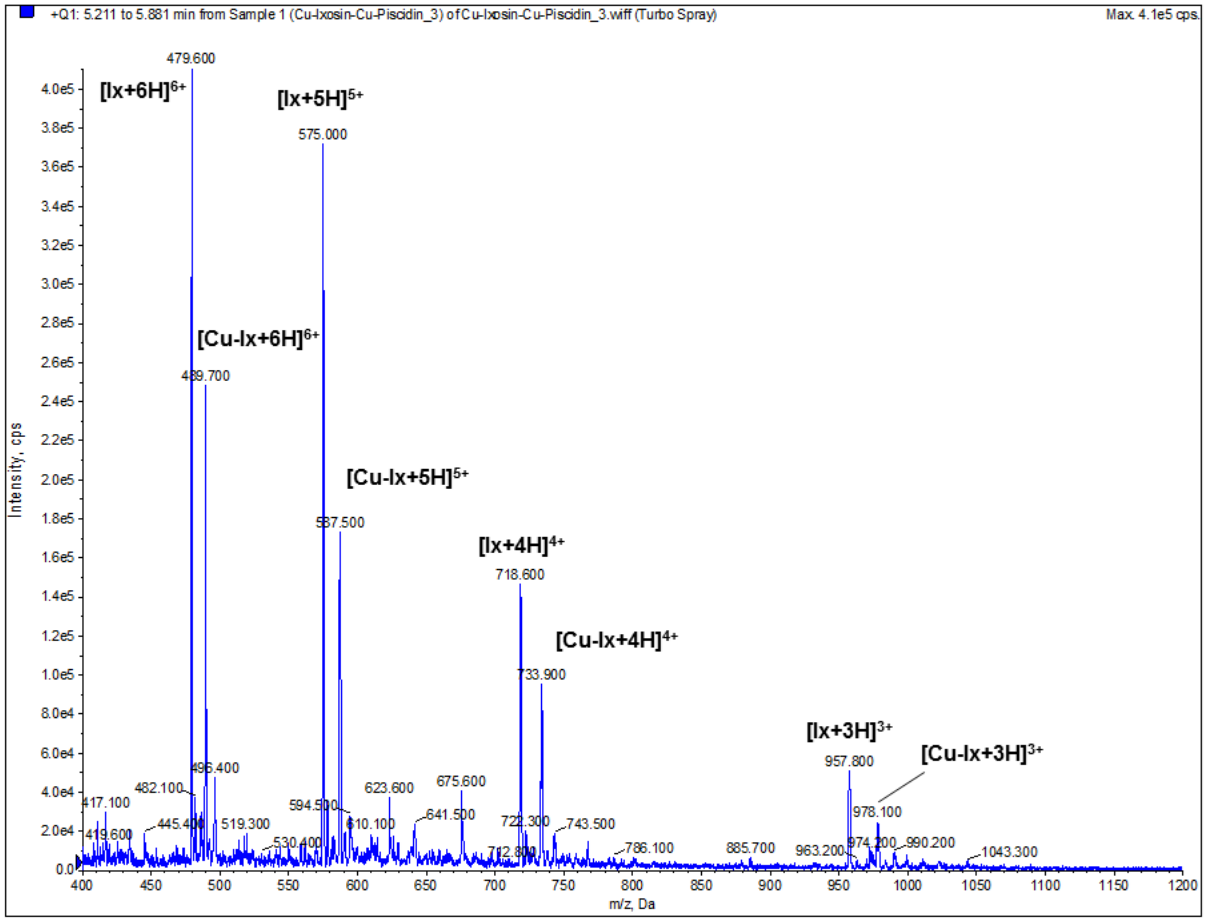
+Q1: 5.211 to 5.881 min from Sample 1 (Cu-Ixosin-Cu-Piscidin_3) of Cu-Ixosin-Cu-Piscidin_3.wiff (Turbo Spray)
Max. 4.1e5 cps.
[Ix+6H]6+
[Ix+5H]5+
[Cu-Ix+6H]6+
[Cu-Ix+5H]5+
[Ix+4H]4+
[Cu-Ix+4H]4+
[Ix+3H]3+
[Cu-Ix+3H]3+
Intensity, cps
m/z, Da

B

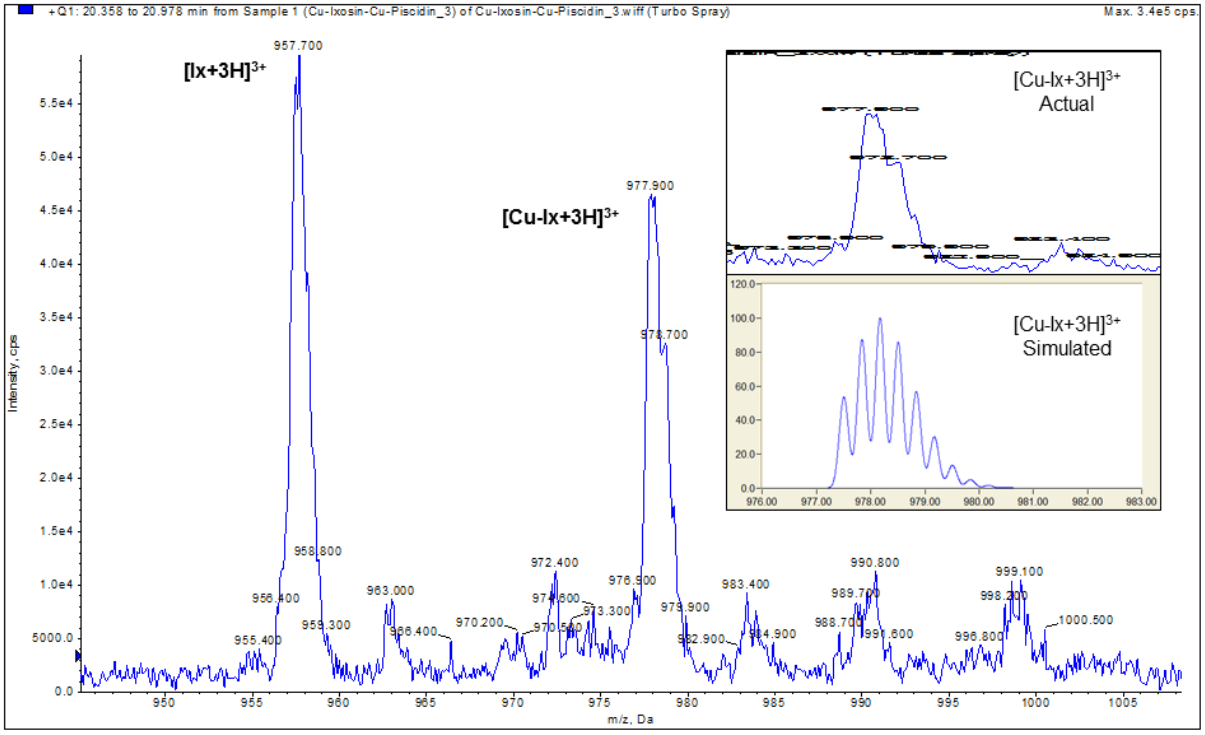
+Q1: 20.358 to 20.978 min from Sample 1 (Cu-Ixosin-Cu-Piscidin_3) of Cu-Ixosin-Cu-Piscidin_3.wiff (Turbo Spray)
Max. 3.4e5 cps.
[Ix+3H]3+
[Cu-Ix+3H]3+
[Cu-Ix+3H]3+ Actual
[Cu-Ix+3H]3+ Simulated
Intensity, cps
m/z, Da

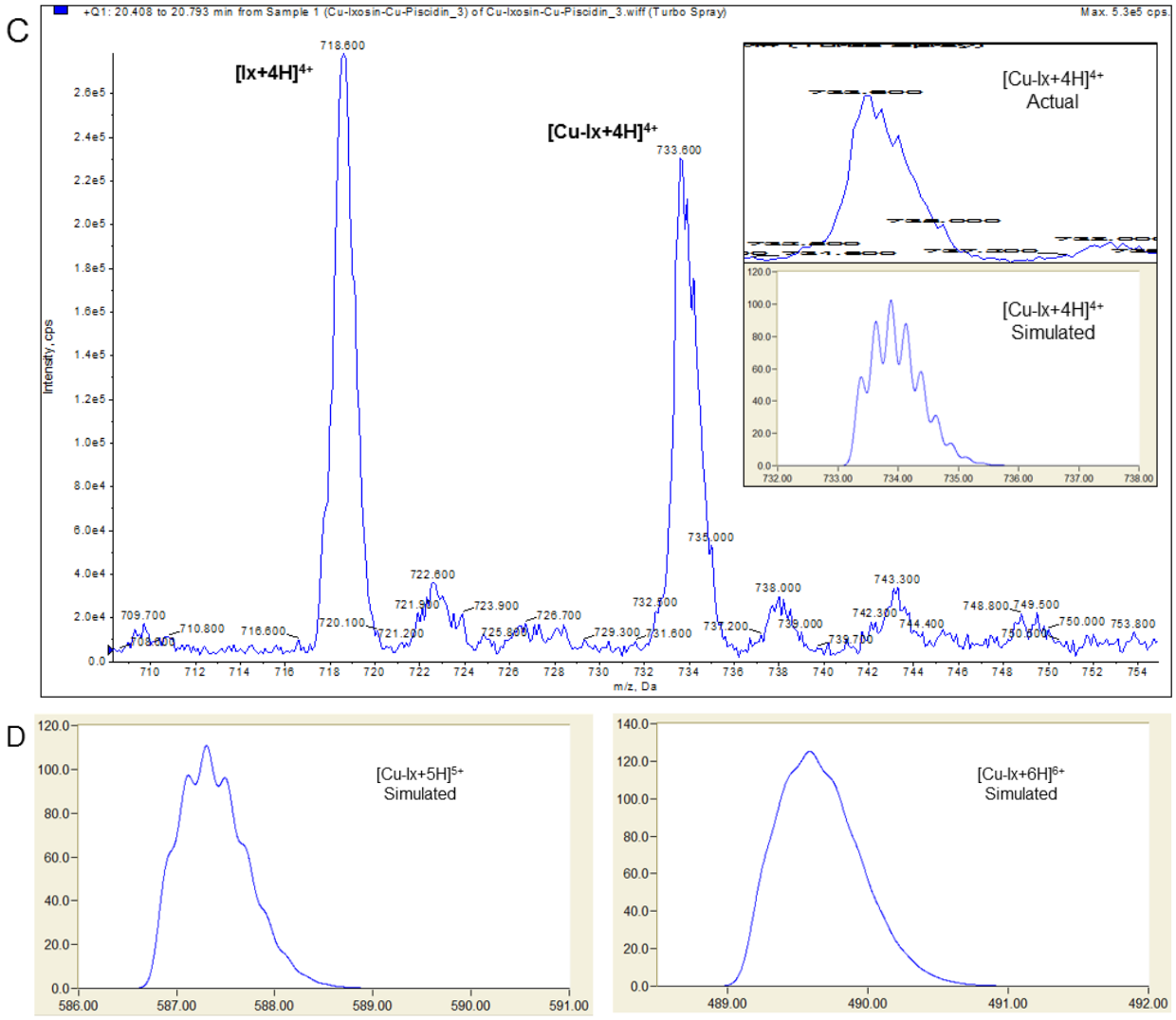

Figure S2.3. Mass Spectra of Ixosin copper complexes. (A) ESI-MS unreconstrcuted Spectra of Ixosin and its copper complex showing multiply charged species +3 through +6. (B-C) Unreconstructed ESI-MS Spectra of Cu-Ixosin focusing on the +3 and +4 charged states. Insets show peaks for the corresponding Cu-Ixosin zoomed in and stretched out to highlight similarity of actual peaks with simulated peaks. (D) Simulated isotopic distribution pattern for the +5 and +6 charged states for Cu-Ixosin showing that peaks converge into one broad peak making it difficult to resolve given the resolution of the mass spectrometer used.

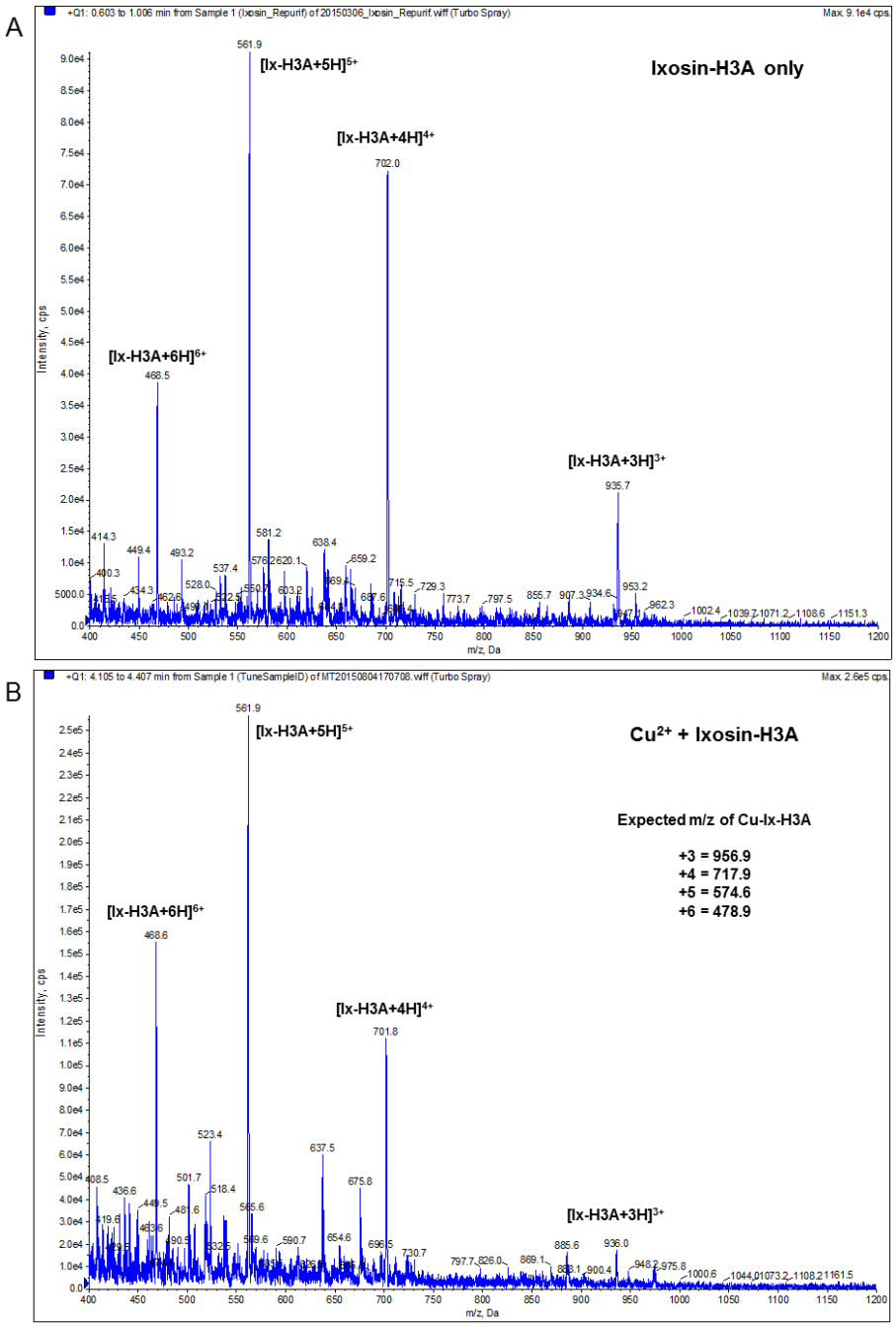

Figure S2.4. Mass Spectra of Ixosin-H3A with and without Cu^{2+}. (A) Ixosin-H3A and (B) Ixosin-H3A pre-incubated with Cu^{2+} were injected in an ESI-MS. Both spectra show that No apparent 1:1 copper complex is formed, suggesting the H3A mutation effectively abolishes Cu^{2+} binding.

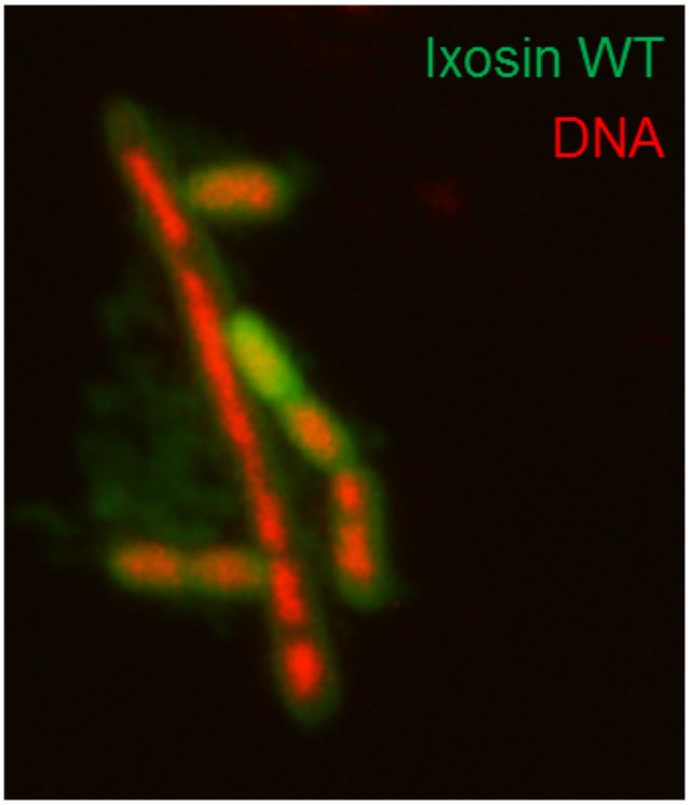

Figure S2.5. Localization of Ixosin WT with respect to DNA. Laser Confocal Micrograph of Ixosin WT (green channel) and DNA (false colored red to enhance contrast). Ixosin WT accumulate in the bacterial membrane. *E. coli* cell in the middle is filamentous probably showing a defect in cell division most likely a downstream effect of Ixosin WT treatment.

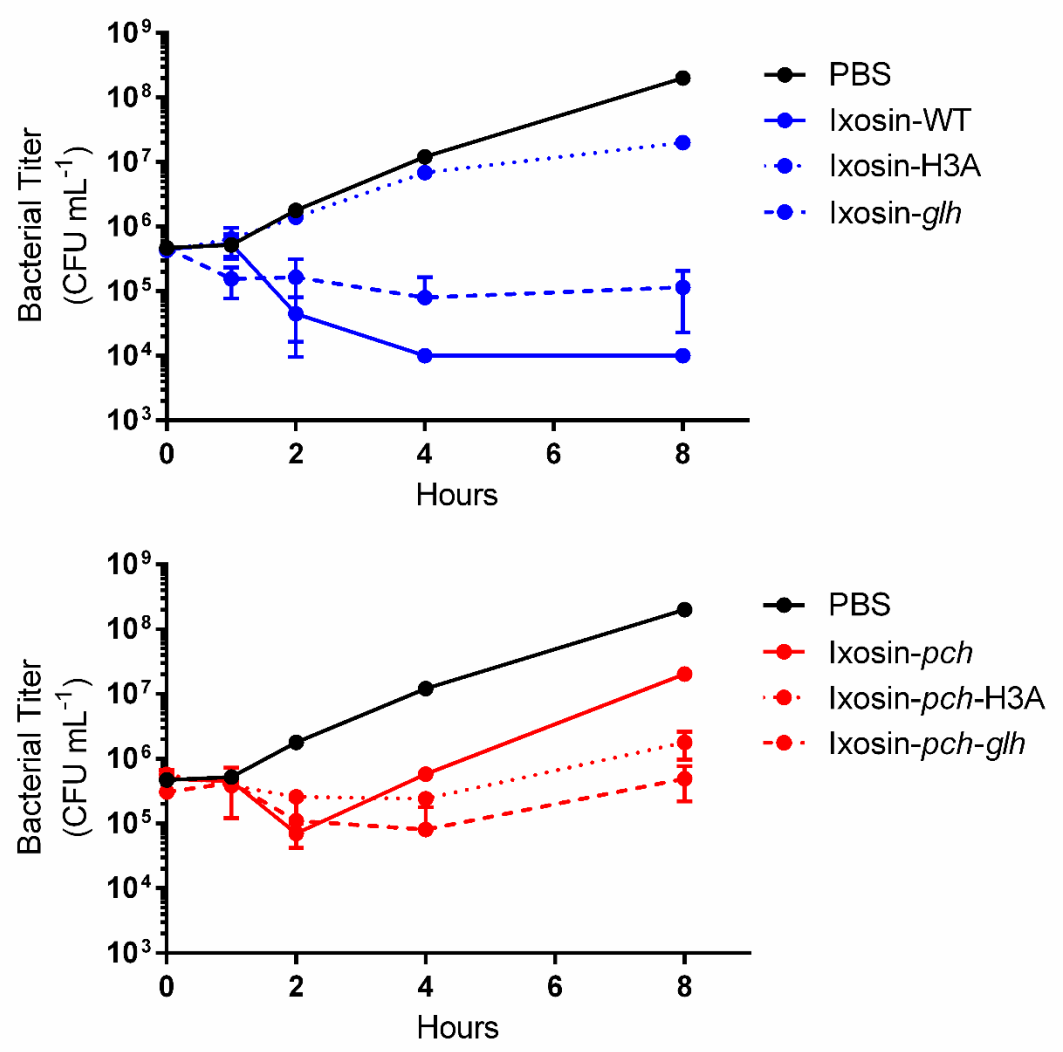

Figure S2.6. Time-Kill Curves of D-amino acid containing derivates. Dynamics of bacterial growth inhibition caused by Ixosin-*glh* and Ixosin-*pch-glh* (containing D-Leu and D-His instead of the L-stereoisomer).

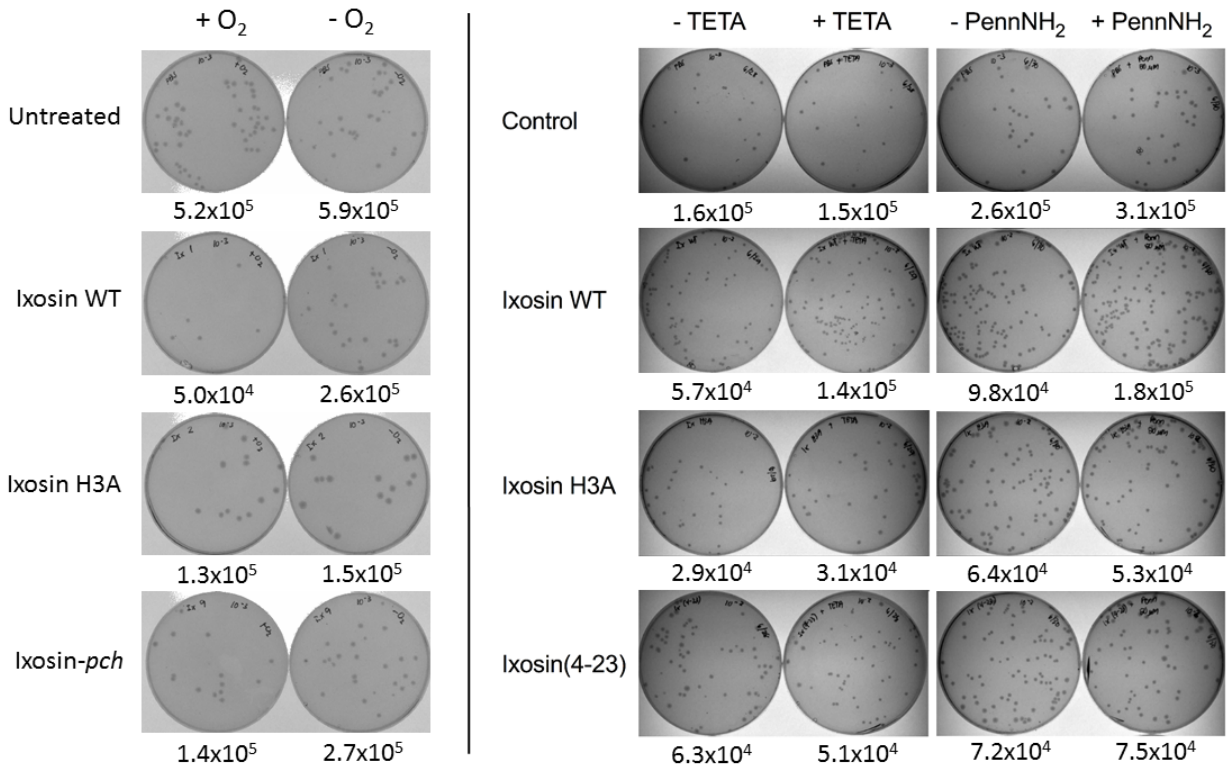

Figure S2.7. Bacterial Survival on media depleted of O_2 or Cu^{2+}. Colonies survival after treatment with Ixosin and derivatives in oxygen- and copper-starved conditions. Each colony was counted and done over three trials. For TETA and $PennNH_2$ treatment, 10^{-3} dilution was used for Control whereas 10^{-2} dilution was used for treated cells. Numbers shown below each plate image corresponds to Bacterial Titer in CFU/mL obtained from the specific trial shown (which may or may not represent the average).

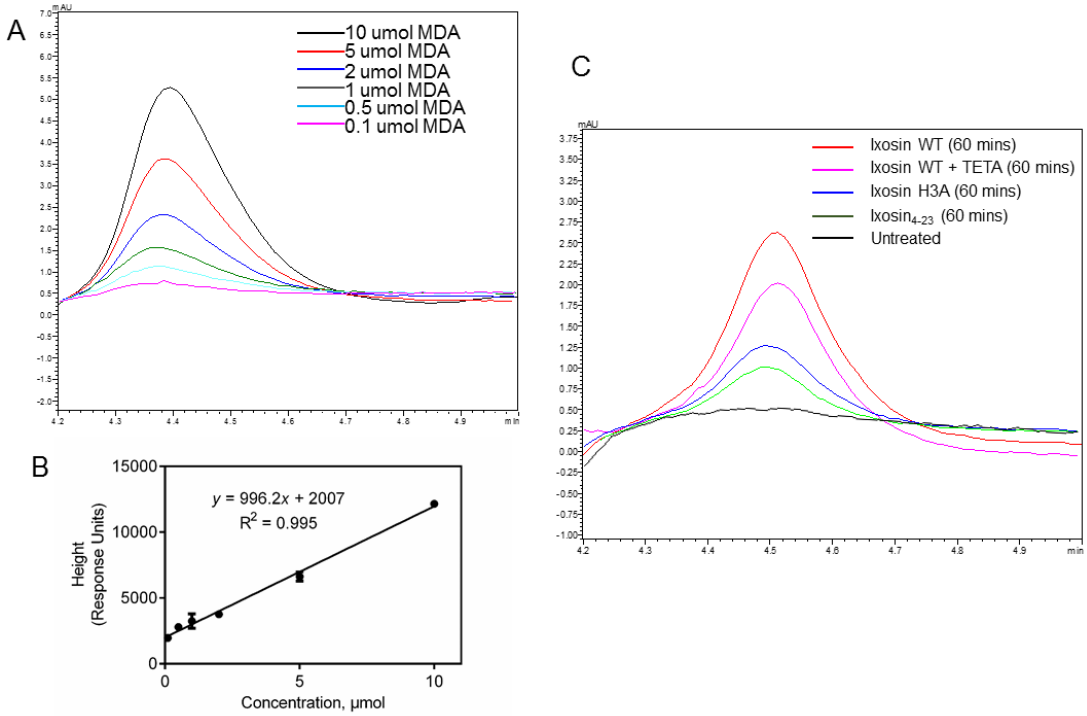

Figure S2.8. Lipid Peroxidation of Ixosin and Derivatives. (A) Analytical HPLC traces of MDA external standards used to quantify thiobarbituric acid reactive substances (TBARS). (B) Calibration Curve for lipid peroxidation experiments. Peak Height from HPLC was used to quantify TBARS. (C) HPLC traces of TBARS obtained from Ixosin-treated cells.

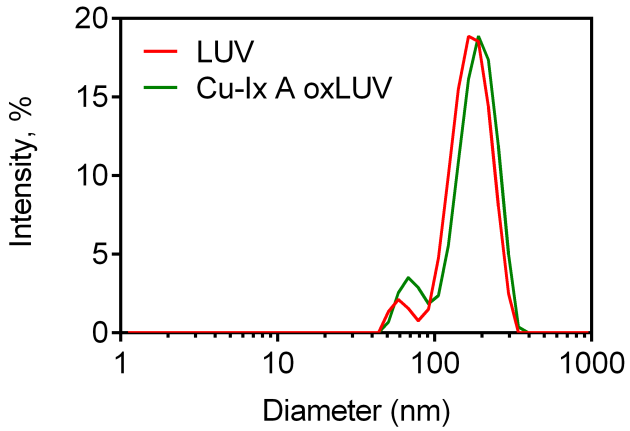

Figure S2.9. Size distribution of native and oxidized LUVs. Dynamic Light Scattering of native and oxidized LUVs showing no significant change in diameter is observed upon lipid oxidation. Cu-Ix A oxLUV = native LUVs pre-oxidized using copper complex of Ixosin A before using in quenching experiments.

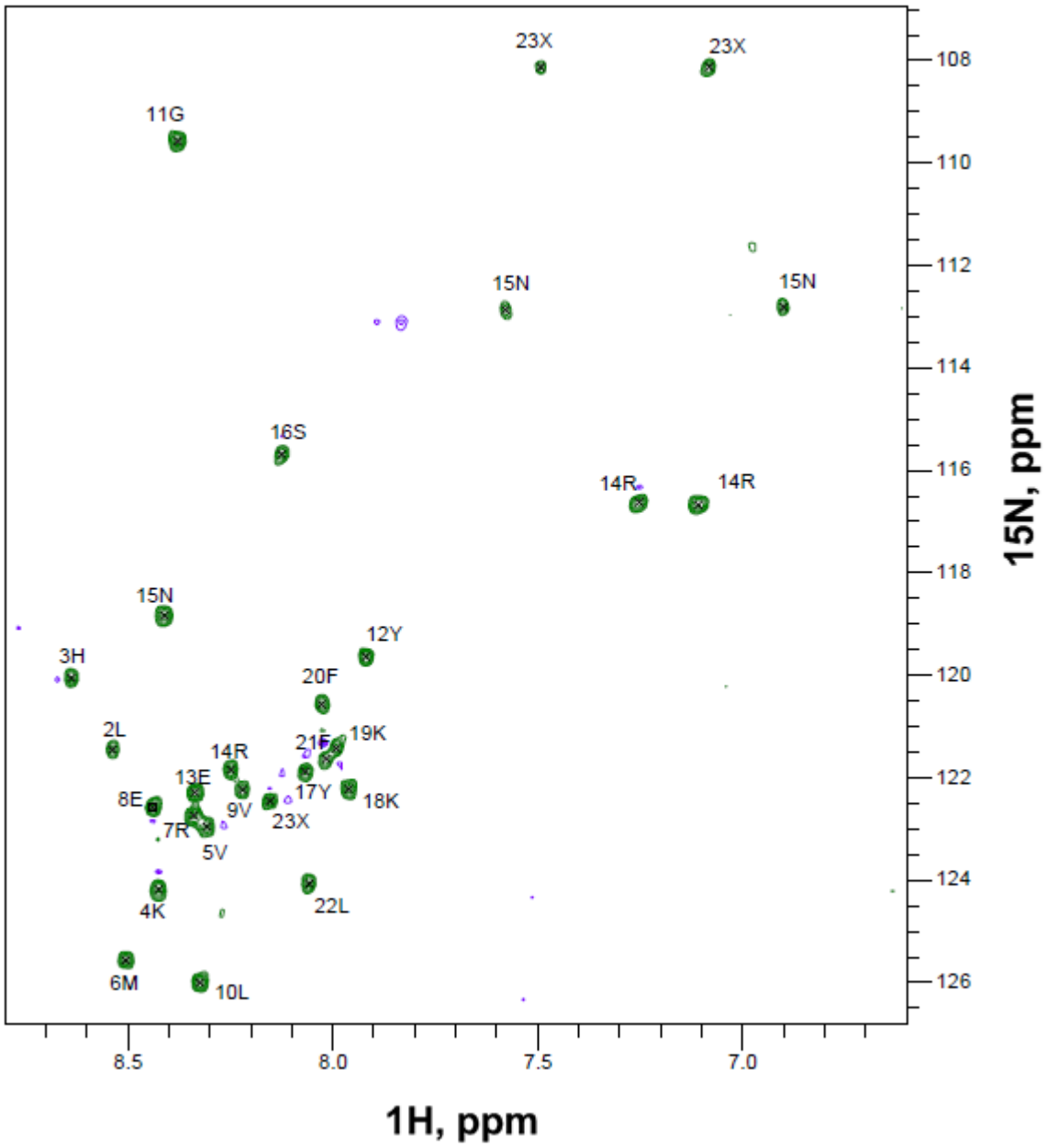

Figure S2.10. Complete assignments of 1H-15N Correlations in Ixosin. H-N correlations and crosspeak assignment of Ixosin WT. 23X refers to Arg-23. Spectra was collected in 20 mM acetate buffer pH 7.4 with 7% D2O using a 600 MHz Varian Spectrometer.

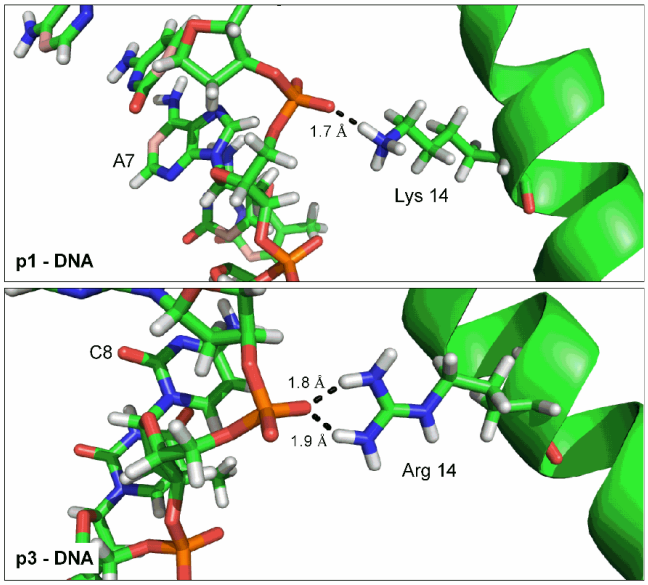

Figure S3.1. Atomic Resolution of Piscidin-DNA Interaction. Molecular Dynamics simulations reveal Arg14 in p3 forms two hydrogen bonds with the phosphate backbone of the DNA whereas Lys14 forms only one.

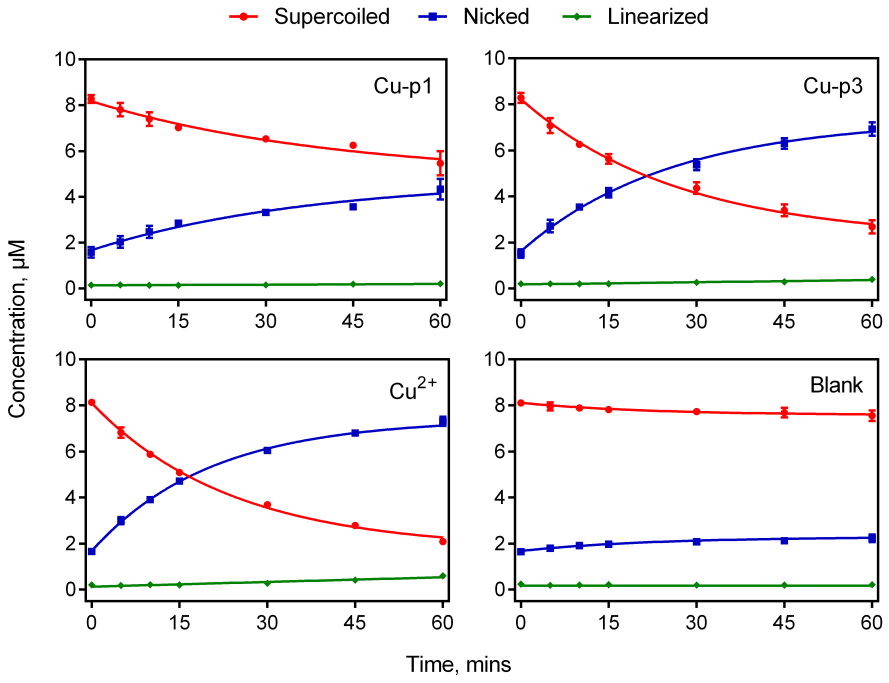

Figure S3.2. in vitro DNA Cleavage Promoted by Cu-p1 and Cu-p3. Agarose Gel Electrophoresis was used to monitor time-dependent cleavage of the plasmid pUC19 in response to ROS formation by Cu-p1 or Cu-p3. Loss of the supercoiled form is accompanied by a concomitant increase in the nicked and linearized form.

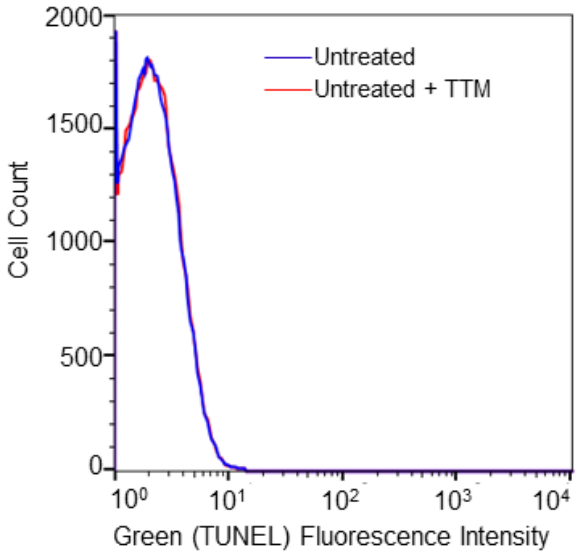

Figure S3.3. TUNEL Assay Tetrathiomolybdate Control. *In cella* DNA damage promoted by piscidin was studied using the TUNEL Assay (Terminal deoxynucleotidyl transferase (TdT)-mediated dUTP Nicked End Labeling). Figure above shows that addition of tetrathiomolybdate (TTM) to the bacteria had negligible effect in the TUNEL fluorescence, indicating that observed decrease in TUNEL (+) cells upon cotreatment with piscidin and TTM is a result of decreased copper bioavailability.

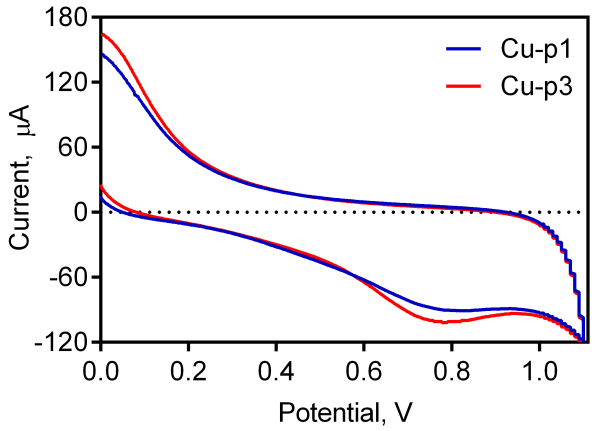

Figure S3.4. Cyclic Voltammetry of Piscidin Copper Complexes. To ensure no free Cu^{2+} was left in solution, we mixed piscidin and Cu^{2+} in a 1.1:1.0 molar ratio. Our voltammogram showed a cathodic peak current (~100 μA) at potentials (vs an Ag/AgCl reference electrode) of 0.796 V (for Cu-p1) and 0.778 V (for Cu-p3) characteristic of a $Cu^{3+/2+}$ couple.

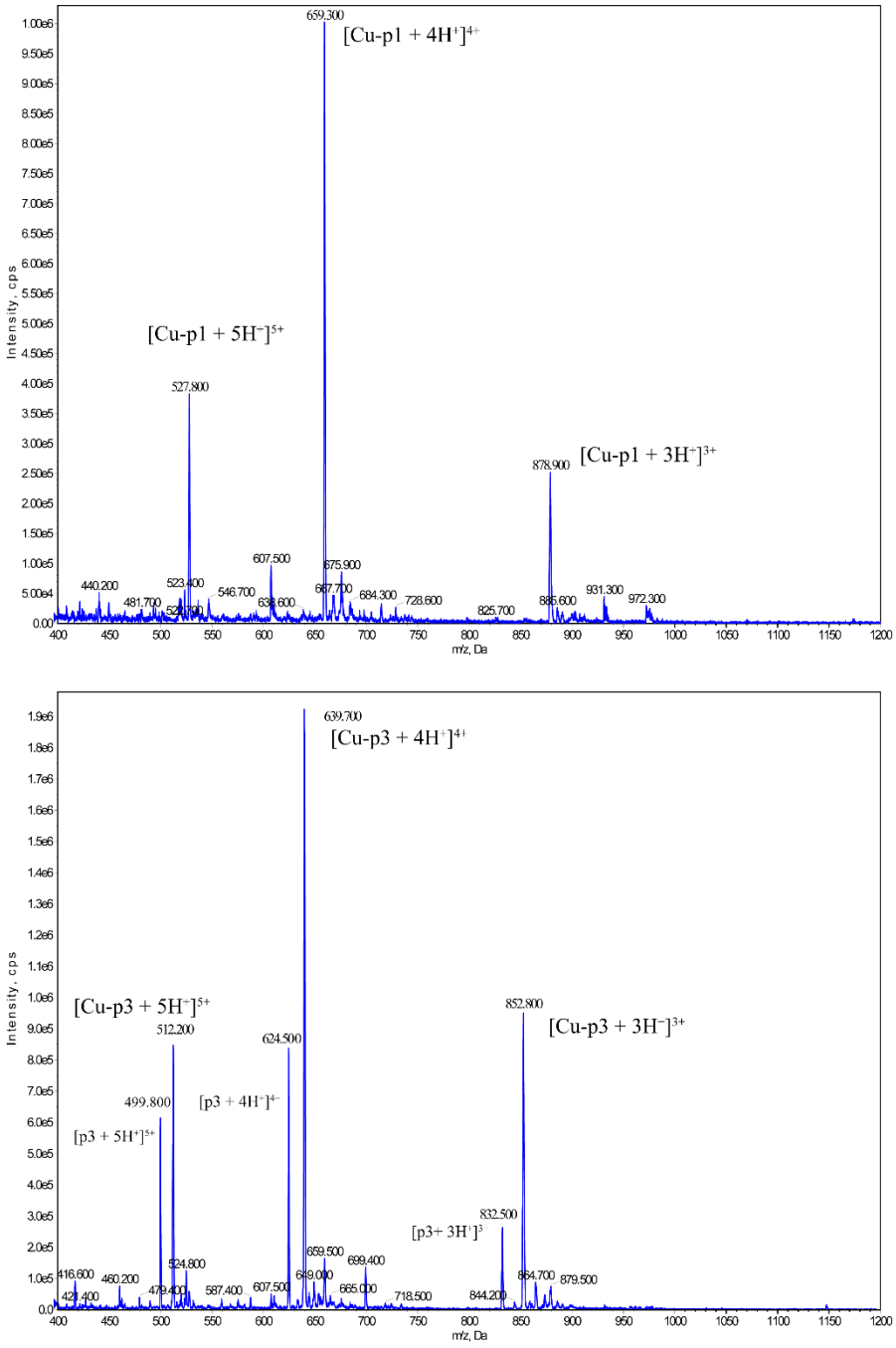

Figure S3.5. ESI-MS Spectra of Copper-Piscidin Complexes. Cu^{2+} and piscidin were mixed in a 1:1.2 molar ratio and subsequently injected to an electrospray ionization MS. Peaks corresponding to a 1:1 stoichiometry of binding appear in the mass spectra. Peaks at m/z 499.8, 624.5, and 832.5 in the bottom panel corresponds to the +5, +4, and +3 charged states of non-metallated p3.

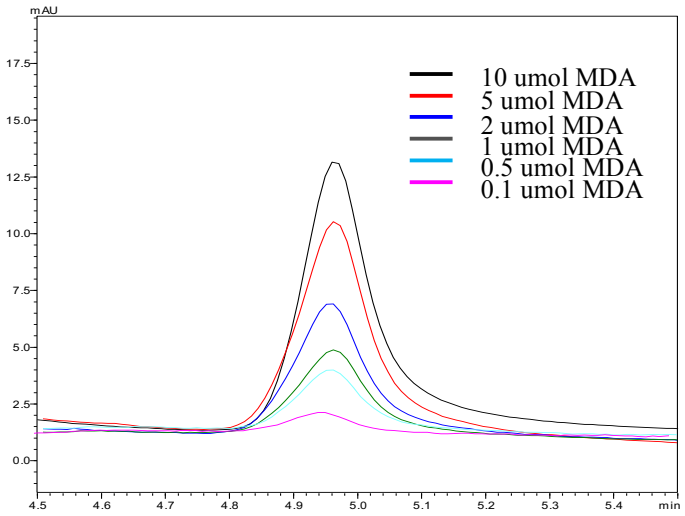

Figure S3.6. Piscidin-Induced Lipid Peroxidation. Calibration peaks of lipid peroxidation-derived products via RP-HPLC using the external standard tetraethoxypropane. The product malonyldialdehyde (MDA) was detected at 512 nm. The peak heights were used to generate a calibration equation for the analysis of piscidin-treated bacteria.

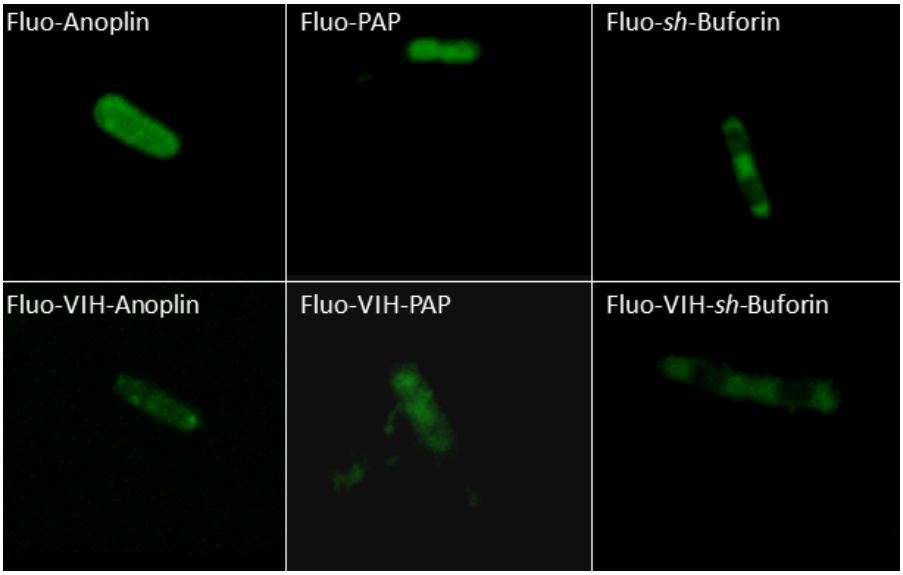

Figure S4.1. Localization of labeled ATCUN-AMPs. Fluorescence images of live *E.coli* cells exposed to 5(6)-carboxyfluorescein-labeled Anoplin (4 μM), VIH-Anoplin (0.5 μM), PAP (0.25 μM), VIH-PAP (0.06 μM), sh-Buforin (8 μM) and VIH-sh-Buforin (2 μM) for 60 min.

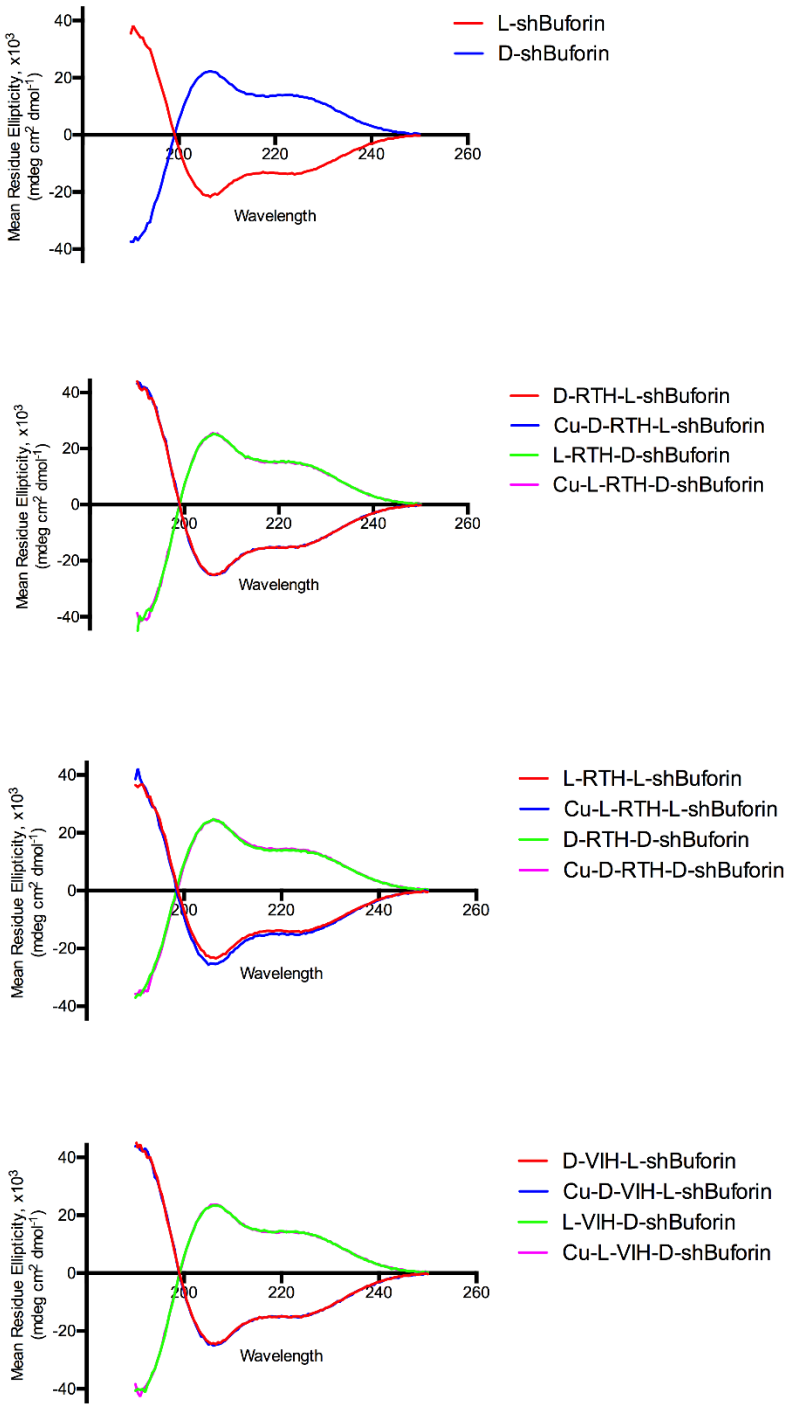

Figure S5.1. Circular Dichroism Spectra of *sh*-Buforin and ATCUN-*sh*-Buforin conjugates showing characteristic alpha helical curves. Addition of ATCUN motif and Cu^{2+} do not induce a significant change in helical content.

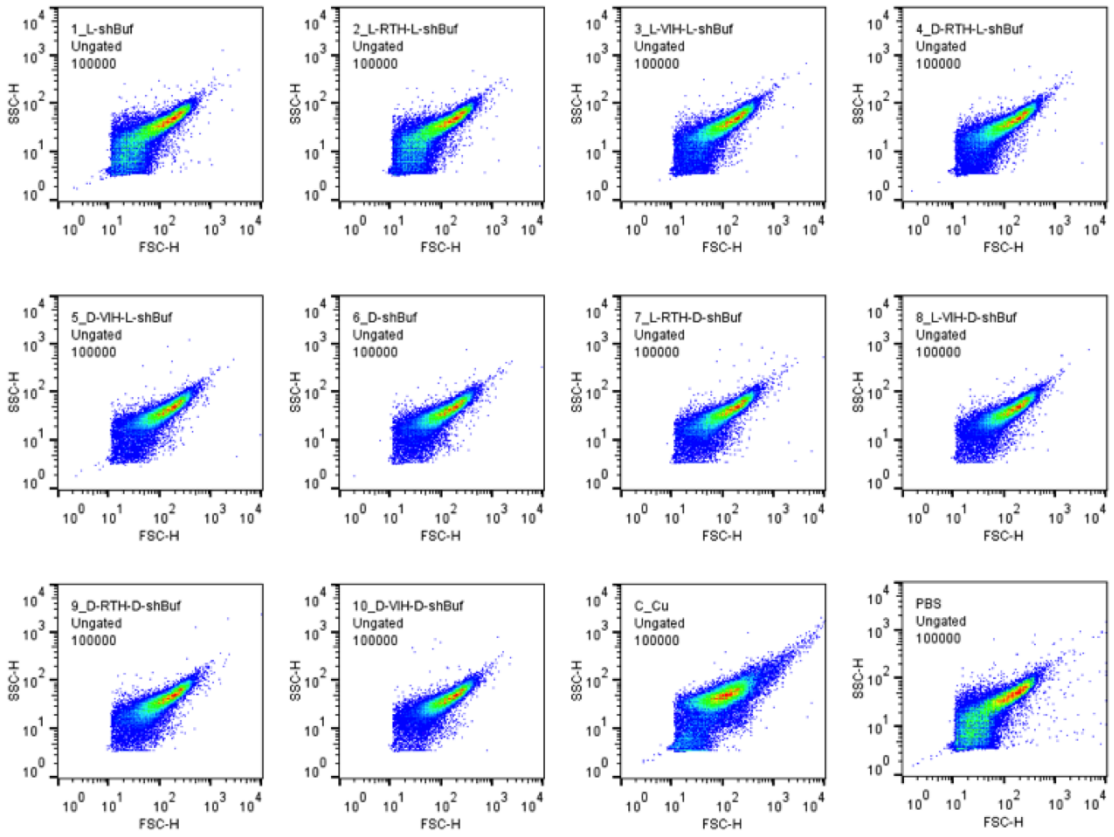

Figure S5.2. Scatter plots obtained from flow cytometry experiments. Data reveal no significant morphological changes in the cells when treated with all the synthesized peptides.

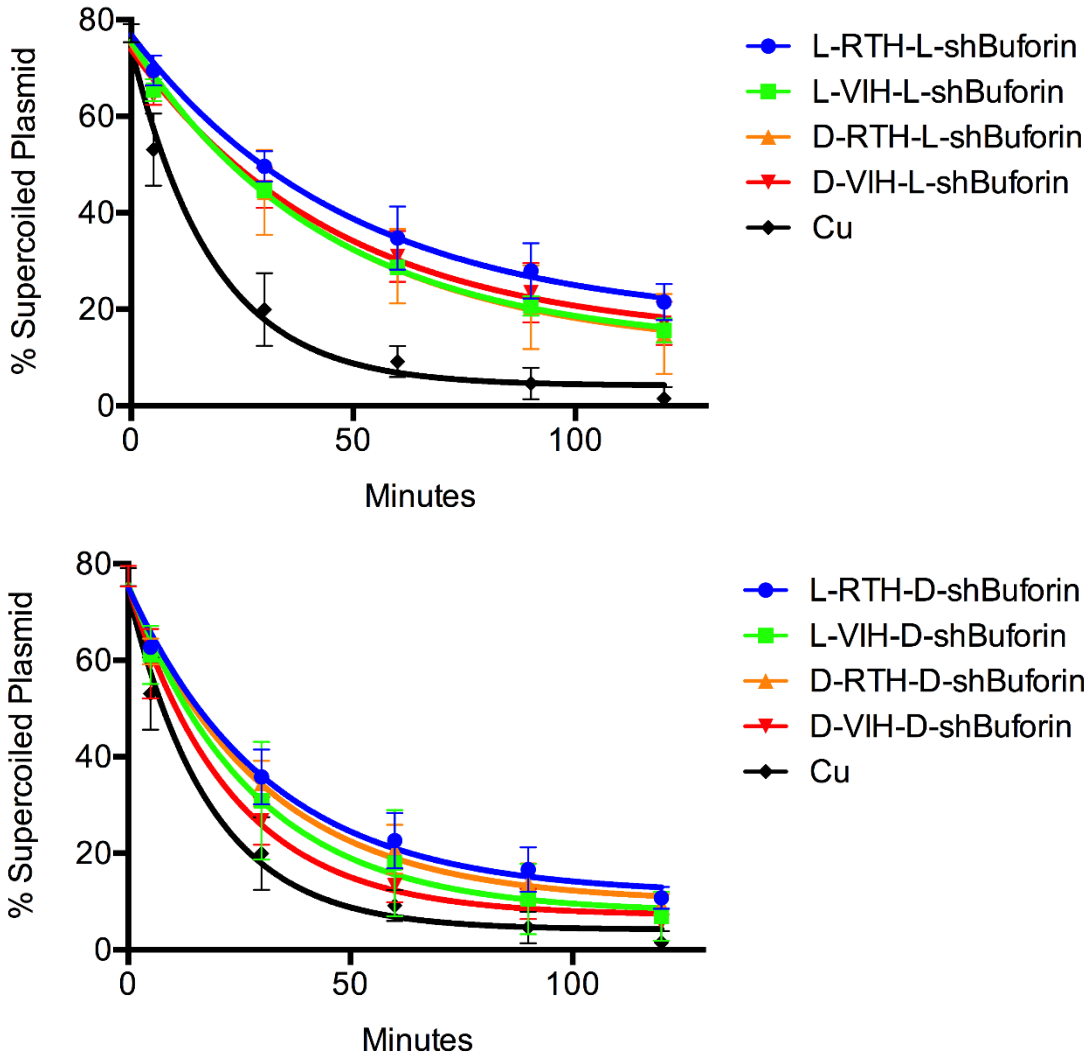

Figure S5.3. Kinetic curves of pUC19 cleavage. The exponential decrease in the amount of supercoiled pUC19 when incubated with CuII-ATCUN-sh-Buforin is due to oxidative DNA cleavage. The black curve is the same for both graphs.

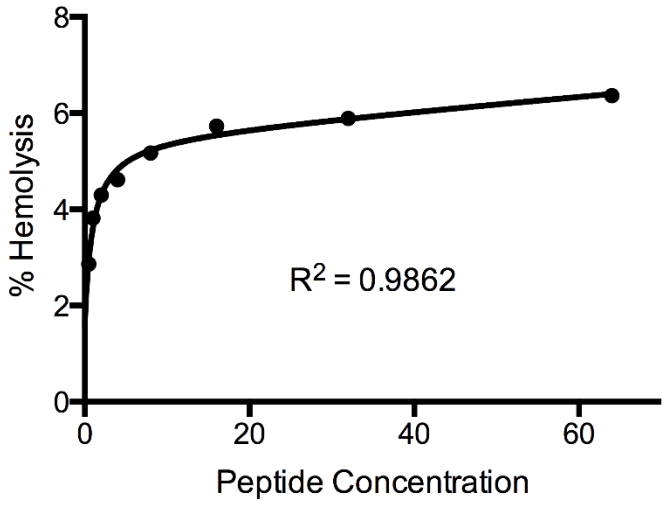

Figure S5.4. Concentration-dependence of RBS Hemolysis. A hyperbolic relationship exists between RBC hemolysis and L-sh-Buforin concentration. The equation of the best-fit line was used to calculate HD5, which is defined, as concentration causing hemolysis of 5% of RBCs.

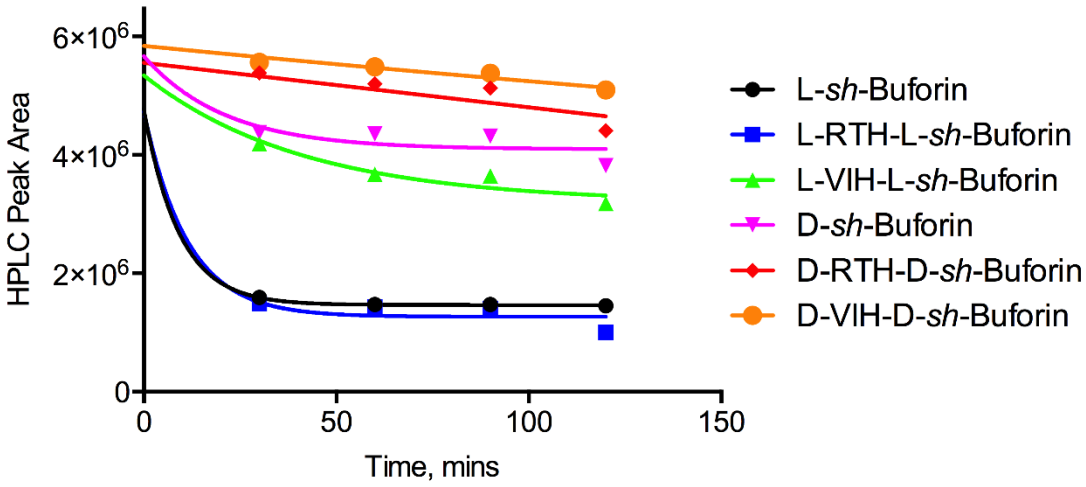

Figure S5.6. Proteolytic Stability of tested peptides. Equal volumes of 256 uM purified peptides (in PBS) and 0.2 ug of trypsin were mixed in a sterile microcentrifuge tube. At each time point, a 10 uL aliquot was withdrawn and the reaction was stopped using 10 uL of 20% TFA. A 15 uL aliquot was then injected in an analytical C18 HPLC column. The products of degradation were monitored at 214 nm, and relative concentrations were obtained from peak areas arising from respective chromatograms.

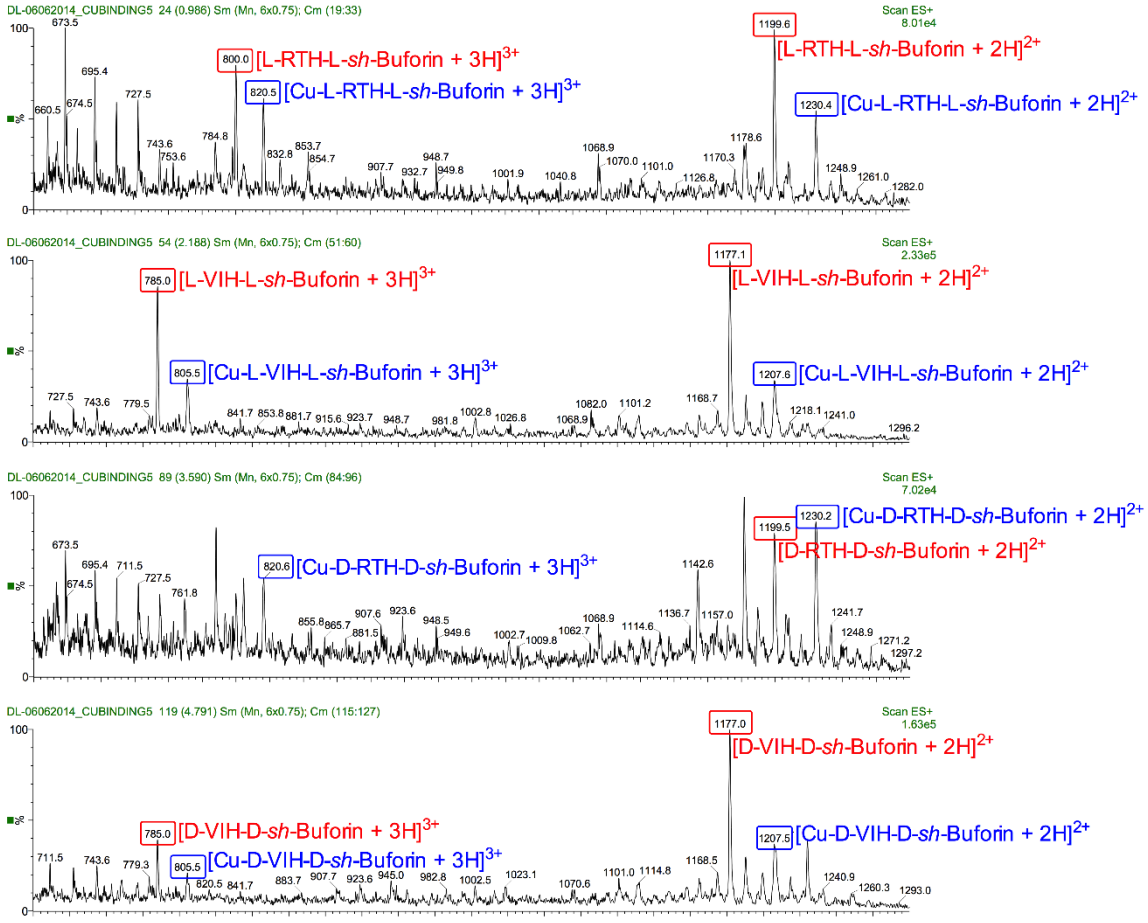

Figure S5.7. ESI-MS Spectrum of a 1.0:0.8 mixture of Cu^{2+} and ATCUN-*sh*-Buforin. We observed a 1:1 stoichiometry of binding evidenced by the doubly and triply charged species.

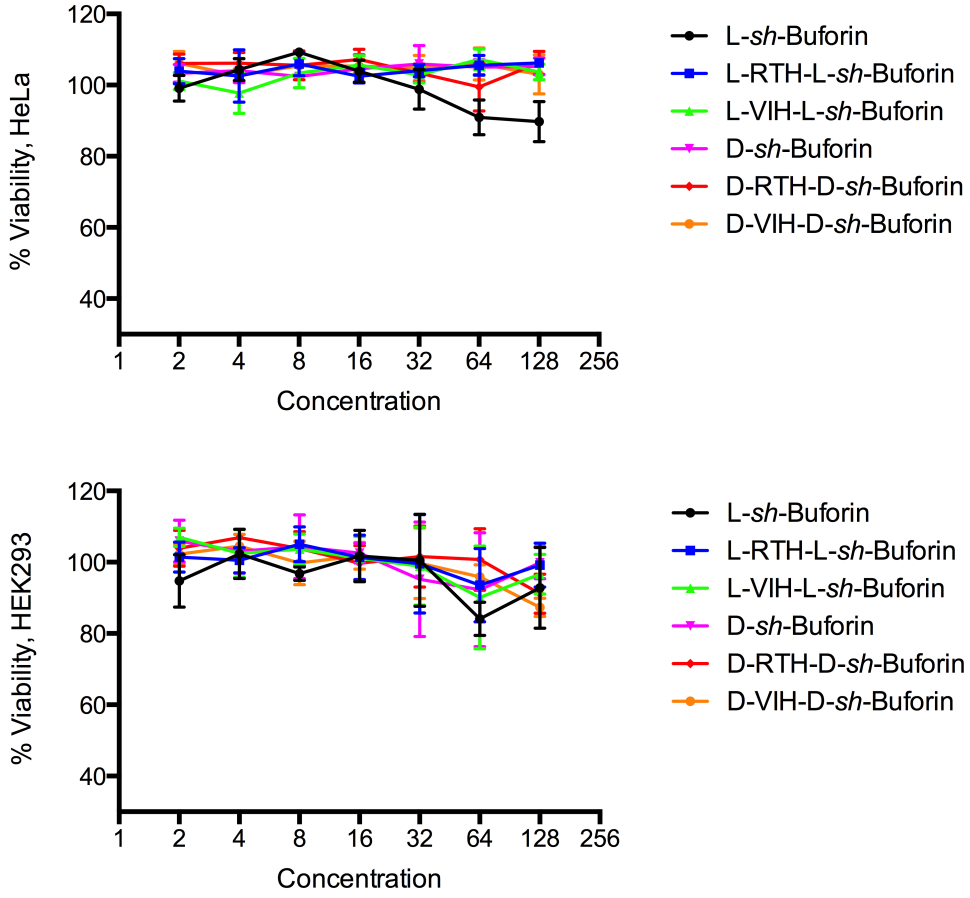

Figure S5.8. Cytotoxicity of synthesized peptide was assessed using the MTT Assay. Cells treated with the peptide were incubated for 24 hours and viability was determined by quantification of the insoluble formazan product. All tested peptides exhibited minimal cytotoxicity even at the highest tested concentration, 128 uM.

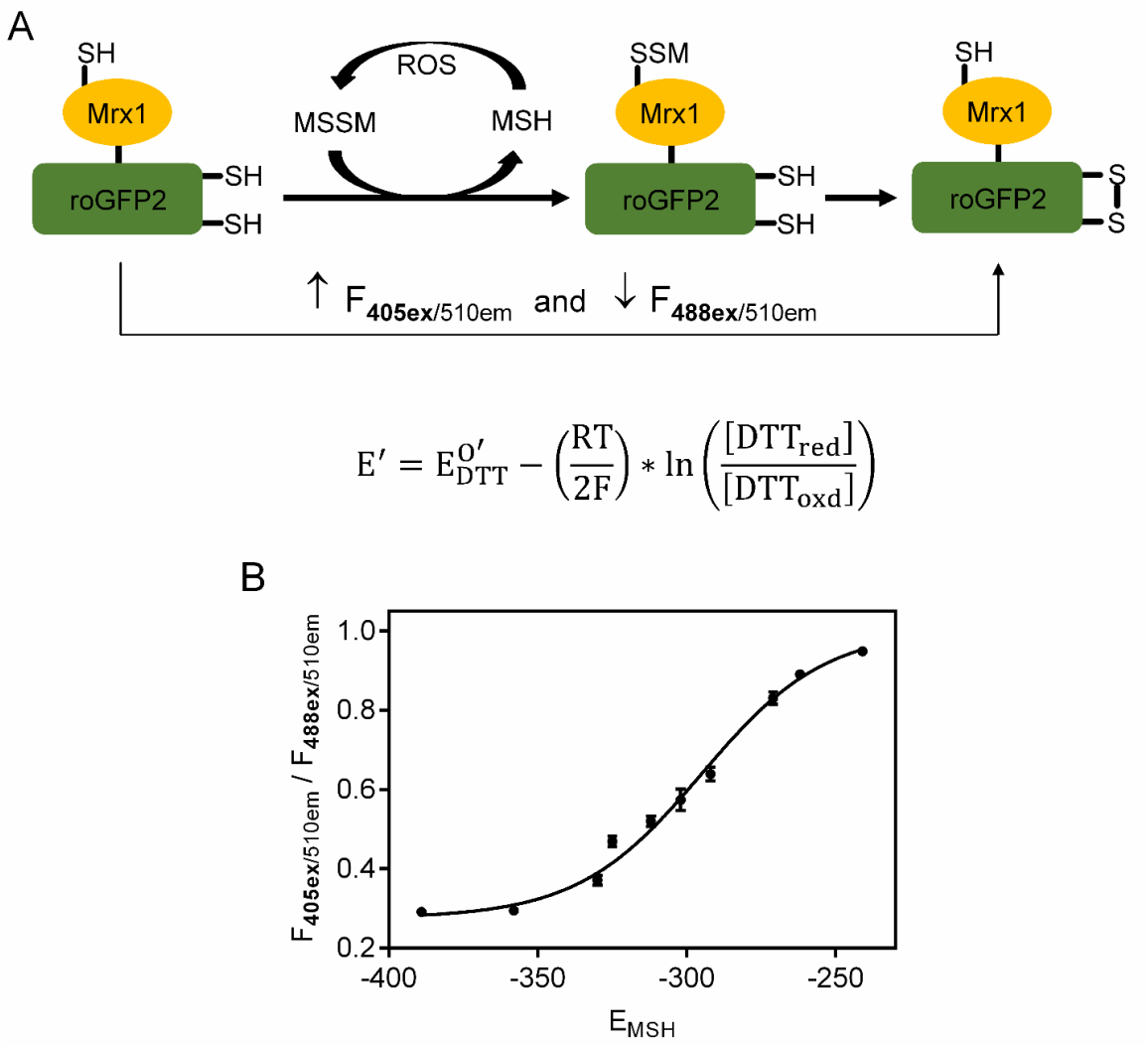

Figure S6.1. Real-Time Measurement of Oxidative Stress in Msm. (A) top, schematic representation of changes occurring in the Mrx1-roGFP2 sensor as a result of oxidation by intracellular ROS; bottom, Nernst Equation used to convert concentrations of oxidized and reduced forms of DTT to EMSH values. (B) Calibration curve for EMSH determinations. Msm were treated with varying ratios of DTTred and DTToxd corresponding to calculated EMSH values (in mV) using the Nernst equation. These EMSH values were plotted against 405/488 fluorescence ratios obtained from flow cytometry. Plot represents data obtained from three independent experiments and shown as Mean ± SEM.

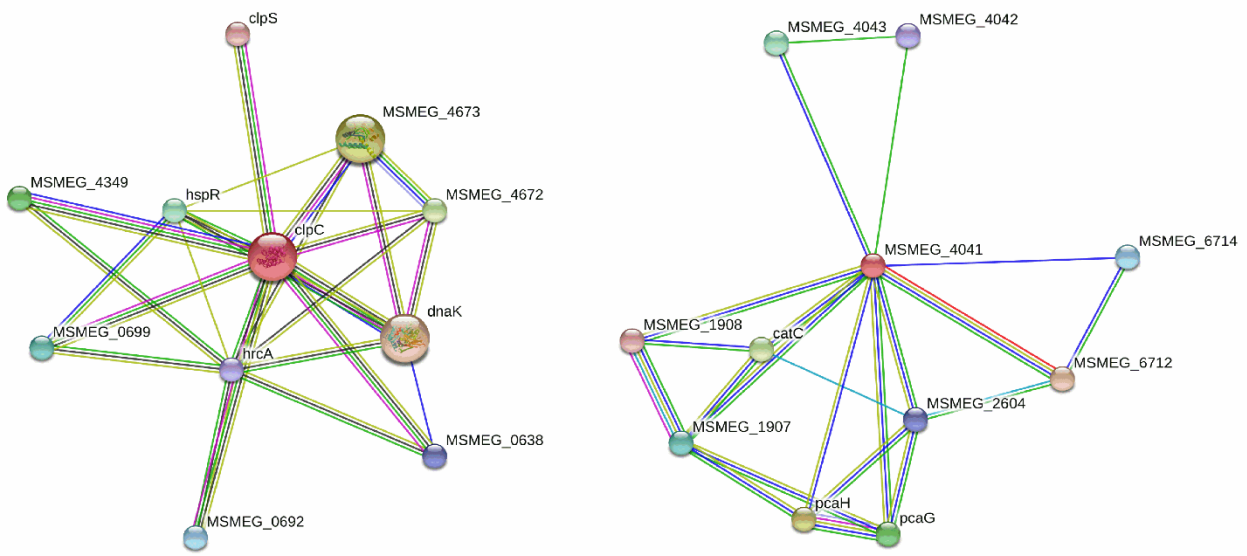

MSMEG_6091 (clpC)				*MSMEG_4041*		
Functional Partner	**Gene Product**	**STRING Score**		**Functional Partner**	**Gene Product**	**STRING Score**
dnaK	Molecular chaperone	0.980		*MSMEG_6712*	Maleylacetate reductase	0.840
MSMEG_4673	Clp protease subunit	0.976		*MSMEG_4043*	amidohydrolase	0.573
MSMEG_4672	Clp protease subunit	0.973				
clpS	Clp protease adaptor protein	0.904				

Figure S6.2. STRING Analysis for Functional Associations of Interrupted Genes Identified from Msm Tn Screen. Top, the network of functional associations predicted for *MSMEG_6091* (*clpC*) and *MSMEG_4041*. Nodes of the network represent proteins; colored nodes are proteins within the first shell of interaction whereas white nodes are within secondary shell of interactions; large nodes mean that some 3D structure is known or predicted. Green lines indicate gene neighborhood, red line for gene fusions, blue lines for gene co-occurrence, black lines for co-expression, and purple lines for protein homology. Bottom, names of proteins to whom *MSMEG_6091* and *MSMEG_4041* form functional associations with. STRING scores closer to 1.0 mean a better quality prediction.

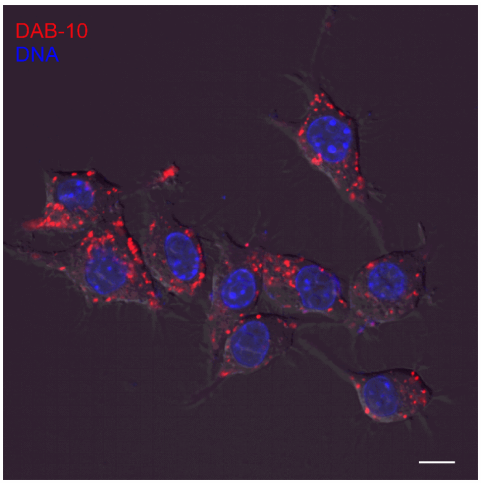

Figure S6.3. DAB-10 Intracellular Localization. 1 μM of DAB-10-TMR was incubated with RAW264.7 cells for 1 hr at 37°C and localization was followed using laser confocal microscopy. Localization observed here is similar to localization when 4 μM of DAB-10-TMR was used. Image is a composite of the red, blue and DIC channels. Scale bar = 5 μm.

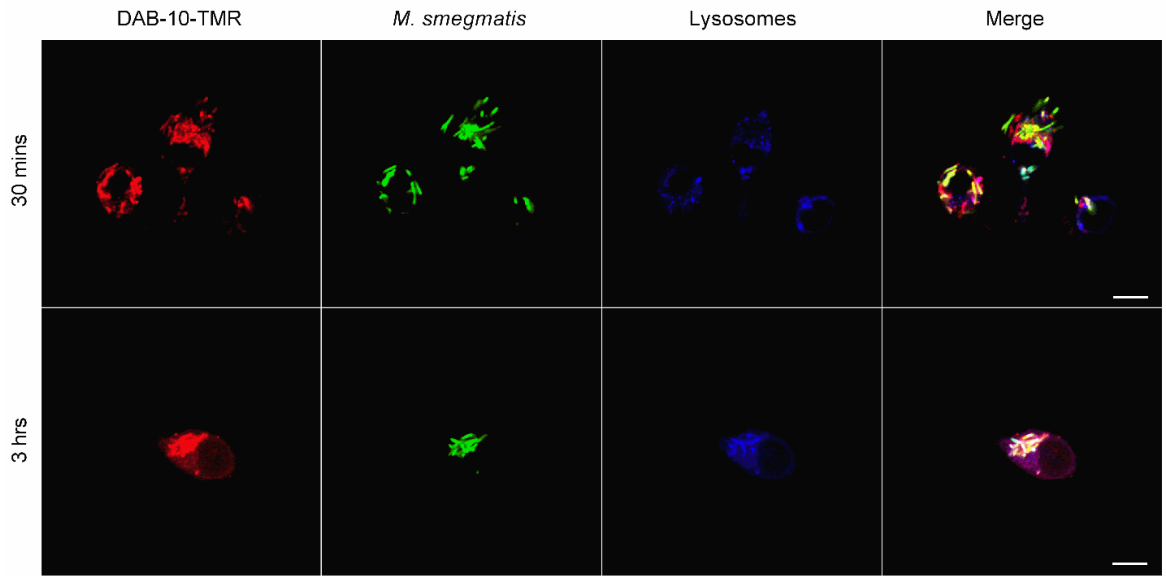

Figure S6.4. Co-localization of Msm and DAB-10 with Lysosomes. RAW264.7 cells were infected with Msm (MOI 1:100) for 2 hours and extracellular Msm were washed away with PBS. The macrophages were then incubated with media containing DAB-10 and LysoTracker for 30 mins in the dark. The cells were washed and fresh media was added. The peptidomimetic, bacteria and lysosomes were tracked using confocal microscopy. Results show that DAB-10 co-localization with bacteria occurs prior to fusion with lysosomes. Scale bars = 5 μm.

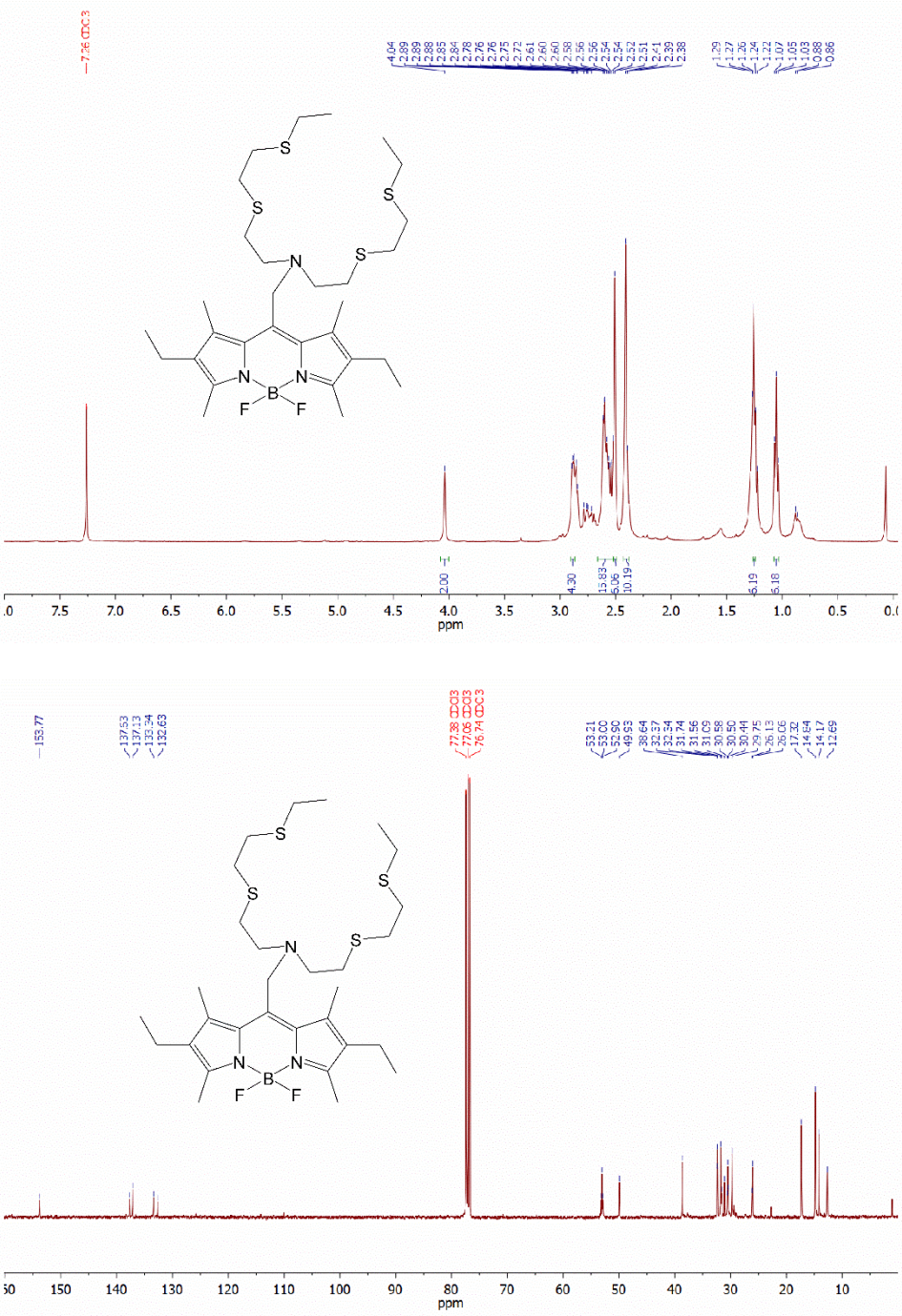

Figure S6.5. Synthesis of the Fluorescent Copper Probe, CS-1. Chemical structure of CS-1 is shown. 1H NMR (top) and 13C NMR (bottom) spectra of synthesized CS-1. All peaks are accounted for based on literature procedure.

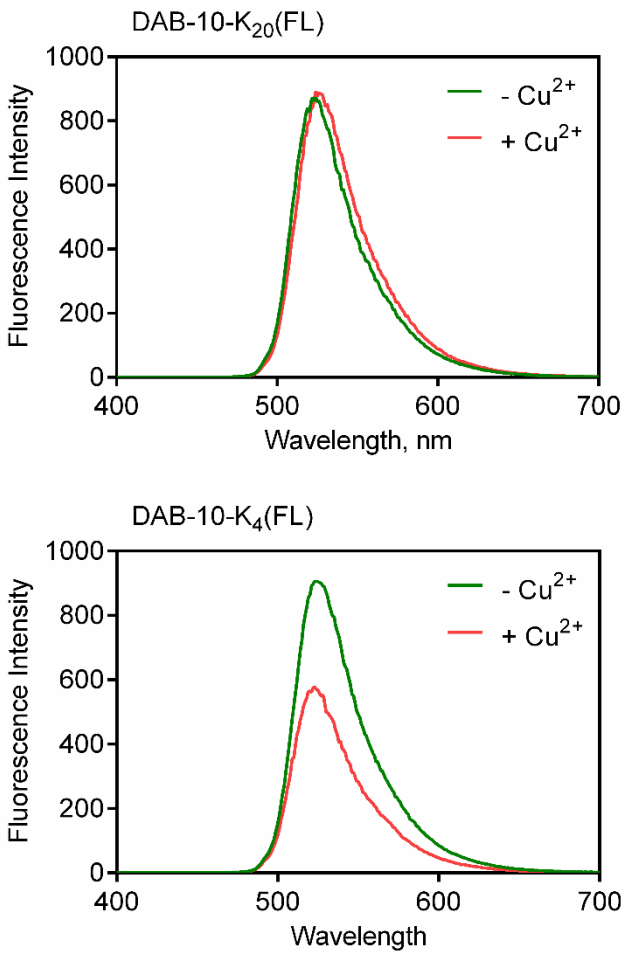

Figure S6.6. Probing the in vitro Copper binding of DAB-10-FL derivatives. The same experimental conditions as in Fig S9 was used but with excitation wavelength set at 495 nm. Quenching of fluorescein (FL) fluorescence in the K4 and not in the K20 derivative suggests direct copper binding to the ATCUN motif. Both S9 and S10 shows that emission suppression phenotype is independent of the identity of the fluorophore and is only a function of its position relative to the copper-binding site.

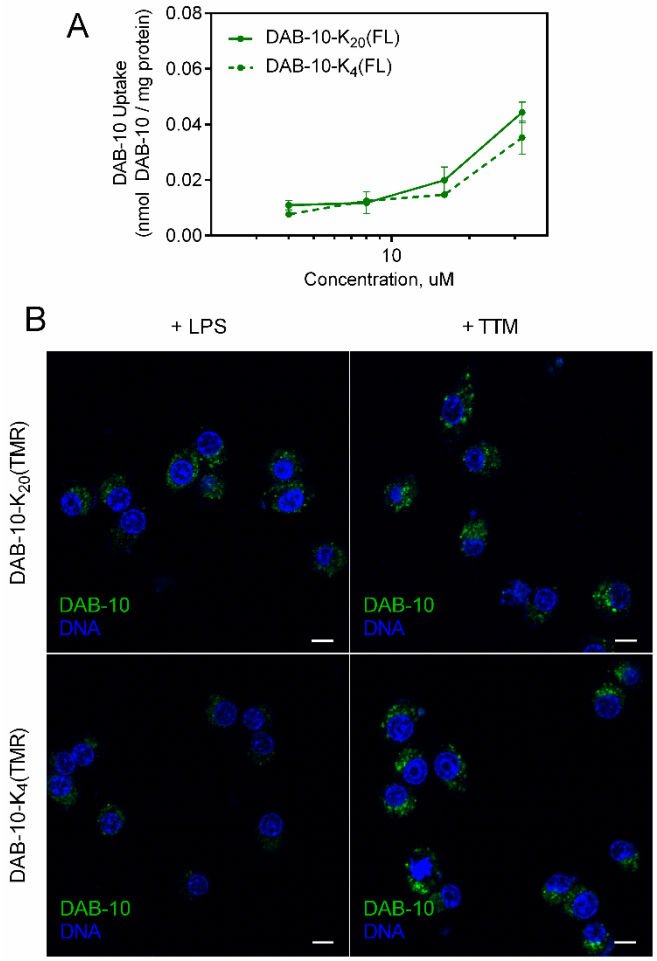

Figure S6.7. Probing Intracellular Copper Binding of DAB-10. (A) Analytical quantification of DAB-10-FL uptake in RAW264.7 cells. Results show that across all concentrations (from 4 – 32 μM) both DAB-10-K_4(FL) and DAB-10-K_{20}(TMR) was taken up to the same extent. Comparison with Fig 4C (in the main text) shows a lower uptake of fluorescein-labeled DAB-10 relative to rhodamine-labeled version. Data represent Mean ± SEM (n = 3 duplicates) (B) Fluorescence quenching phenotype similar to that observed *in vitro* (Fig S6.6) for DAB-10-K_4(FL) but not for DAB-10-K_{20}(FL) upon incubation with LPS-activated RAW264.7 cells suggests that DAB-10 directly binds to copper within the cell. The fluorescence of the K_4 derivative was rescued via addition of the high affinity copper chelator, TTM; suggesting that lower fluorescence was not a result of impaired peptidomimetic uptake. Scale bar = 5 μm.

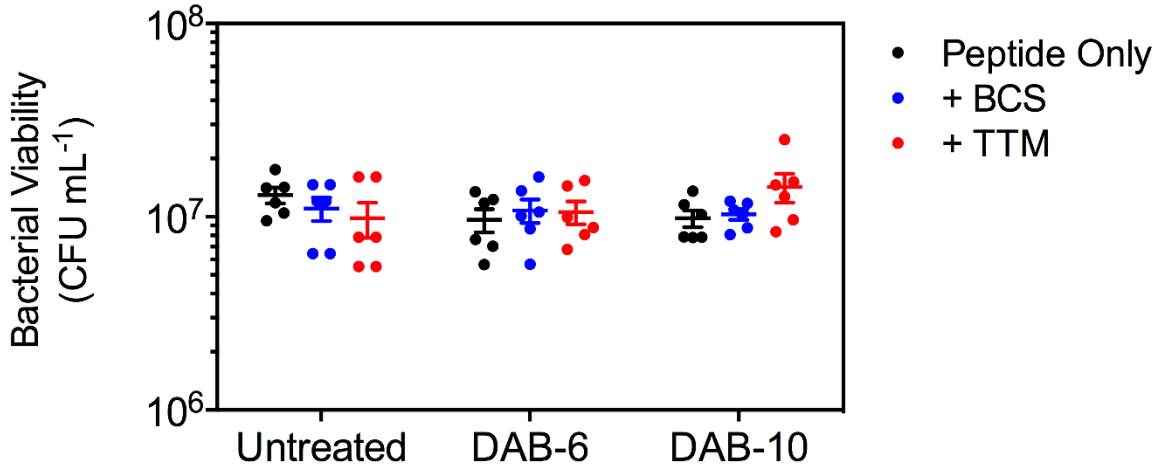

Figure S6.8. Activity of DAB-10 against Intracellular Mtb. Differentiated THP-1 cells were infected with Mtb (MOI 1:5) for 1 hour and extracellular bacteria were washed off via extensive PBS rinsing. DAB-6 (80 μM) and DAB-10 (20 μM) was added to the cells in the presence or absence of 100 μM BCS (cell impermeable) or TTM (cell permeable). Peptidomimetic treatment was allowed to proceed for 24 hour prior to CFU enumeration. Data represent Mean ± SEM (n = 3 duplicates).

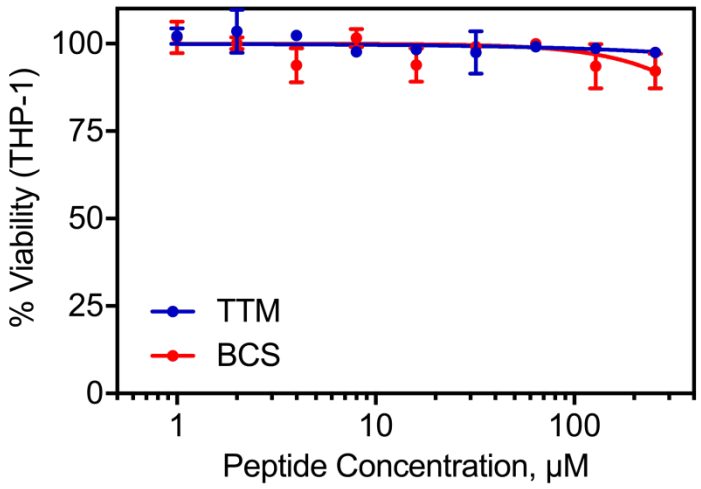

Figure S6.9. Cytotoxicity of Copper Chelators towards Macrophages. Differentiated THP-1 cells were incubated with the indicated concentration of tetrathiomolybdate (TTM) or bathocuproinedisulfonate (BCS) for 24 hrs. Cellular viability was determined using the MTT assay.

Table S2.1. Sequence and physicochemical properties of the designed peptides.

Peptide Name	Sequence	<H>[a]	<μH>[b]
ixosin	GLHKVMREVLGYERNSYKKFFLR	0.282	0.382
ixosin$_{4-23}$	GLHKVMREVLGYERNSYKKFFLR	0.232	0.36
ixosin-H3A	GLAKVMREVLGYERNSYKKFFLR	0.290	0.383
ixosin$_{1-12}$	GLHKVMREVLGYERNSYKKFFLR	0.460	0.573
ixosin$_{12-23}$	GLHKVMREVLGYERNSYKKFFLR	0.160	0.199
ixosin$_{1-18}$	GLHKVMREVLGYERNSYKKFFLR	0.178	0.478
ixosin$_{4-18}$	GLHKVMREVLGYERNSYKKFFLR	0.091	0.462
ixosin$_{7-18}$	GLHKVMREVLGYERNSYKKFFLR	-0.008	0.370
ixosin$_{1-18}$ E8K, E13L, S16V / ixosin-*pch*	GLHKVMRKVLGYLRNVYK	0.358	0.664
ixosin$_{1-18}$ H3A, E8K, E13L, S16V / ixosin-*pch*-H3A	GLAKVMRKVLGYLRNVYK	0.368	0.663
ixosin$_{4-18}$ E8K, E13L, S16V / ixosin-*pch*$_{4-18}$	GLHKVMRKVLGYLRNVYK	0.308	0.685

[a] Hydrophobicity and [b] Hydrophobic Moment were calculated using HeliQuest [2] (an online resource tool available from www.expasy.org) using α-helix as conformation.

Table S2.2. Antimicrobial and cytotoxic activity of other peptides under study.

Peptide	Minimum Inhibitory Concentration, μM				% Cell Viability (@ MIC vs *E. coli*)	
	Bacterium			Fungus		
	S. aureus	*E. coli*	*P. aeruginosa*	*C. albicans*	HeLa	HEK293
ixosin$_{1-12}$	>128	>128	>128	>128	73 ± 11	97 ± 10
ixosin$_{12-23}$	>128	>128	>128	>128	72 ± 6	90 ± 5
ixosin$_{1-18}$	>128	>128	>128	>128	87 ± 6	94 ± 10
ixosin$_{4-18}$	>128	>128	>128	>128	97 ± 5	86 ± 14
ixosin$_{7-18}$	>128	>128	>128	>128	85 ± 3	82 ± 14

Table S5.1. MIC of synthesized peptides against Pre-logarithmic phase bacteria.

Peptide	Minimum Inhibitor Concentration, μM	
	E. coli MG1655 (WT)	*E. coli* TD172 (*ΔrecA*)
L-*sh*-Buforin	64	32
L-RTH-L-*sh*-Buforin	32	16
L-VIH-L-*sh*-Buforin	64	32
D-RTH-L-*sh*-Buforin	32	16
D-VIH-L-*sh*-Buforin	64	16
D-*sh*-Buforin	8	4
L-RTH-D-*sh*-Buforin	2	1
L-VIH-D-*sh*-Buforin	2	1
D-RTH-D-*sh*-Buforin	2	2
D-VIH-D-*sh*-Buforin	2	1
Ampicillin	2	2
Kanamycin	0.125	0.125

Table S6.1. Activity of DAB-10 pre-incubated with Cu(II).

Mycobacterial Species	Minimum Inhibitory Concentration[a] (MIC), μM	
	DAB-10	**Cu-DAB-10**
M. smegmatis mc^2155	0.125 – 0.25	0.25
M. bovis BCG (SSI 1331)	1 – 4	2 – 4

[a]Results obtained from three independent trials done in duplicates.

Curriculum Vitae

Mark Daben Javate Libardo, Ph.D.

EDUCATION

2012 – 2017 *PhD*, Chemistry, **University of Connecticut**, Storrs, CT, USA

2007 – 2011 *B.S.*, Chemistry, *Cum Laude*, **University of the Philippines**, Diliman,
Quezon City, Philippines

RESEARCH EXPERIENCE

08/2016 – 09/2016 *Research Intern*, Department of Immunology
Max Planck Institute for Infection Biology, Berlin, Germany
PI: Stefan H. E. Kaufmann, M.D., Ph.D

2012 – 2017 *Graduate Research Assistant*, Department of Chemistry
University of Connecticut, Storrs, CT, USA
PI: Alfredo M. Angeles-Boza, Ph.D
Dissertation Title: Copper-Binding Antimicrobial Peptides: Microbial Elimination through Lipid and DNA Oxidation

2010 – 2011 *Undergraduate Research Assistant*, Institute of Chemistry
University of the Philippines – Diliman, Quezon City, Philippines
PI: Portia Mahal G. Sabido, Ph.D
Thesis Title: Synthesis and Evaluation of the Antimicrobial Activity of Truncated Anoplin Lipopeptide Derivatives.

PUBLICATIONS

Libardo, M.D.J., Wang, T.Y., Pellois, J.-P., and Angeles-Boza, A.M. How Does Membrane Oxidation Affect Cell Delivery and Cell Killing? *Trends in Biotechnol* **2017**, *in press*, DOI: 10.1016/j.tibtech.2017.03.015

Wang, T.Y., **Libardo, M.D.J.**, Angeles-Boza, A.M., and Pellois, J.-P. Membrane Oxidation in Cell Delivery and Cell Killing Applications. *ACS Chem Biol* **2017**, 12, 1170-1182.

Libardo, M.D.J., Gorbatyuk, V.Y., and Angeles-Boza, A.M. Central Role of the Copper-Binding Motif in the Complex Mechanism of Action of Ixosin: Enhancing Oxidative Damage and Promoting Synergy with Ixosin B. *ACS Infectious Diseases* **2016**, 2 (1), 71-81. (*Featured in the Cover of the January 2016 Issue*)

Hayden, R.M., Goldberg, G.K., Ferguson, B.M., Schoeneck, M.W., **Libardo, M.D.J.**, Mayeux, S.E., Shresta, A., Bogardus, K.A., Hammer, J., Pryschep, S., Lehman, H.K., McCormick, M.L., Blazyk, J., Angeles-Boza, A.M., Fu, R., and Cotten, M.L. Complementary effects of Host Defense Peptides Piscidin 1 and Piscidin 3 on DNA and Lipid Membranes: Biophysical Insights into Contrasting Biological Activities. *J. Physical Chemistry B* **2015**, 119 (49), 15235-15246.

Libardo, M.D.J., Paul, T.J., Prabhakar, R., and Angeles-Boza, A.M. Hybrid Peptide ATCUN-*sh*-Buforin: Influence of the ATCUN charge and stereochemistry on antimicrobial activity. *Biochimie* **2015**, 113, 143-155.

Libardo, M.D.J., Nagella, S., Lugo, A., Pierce, S., and Angeles-Boza, A.M. Copper-Binding Tripeptide Motif Increases Activity of the Antimicrobial Peptide Anoplin via Reactive Oxygen Species Generation. *Biochemical and Biophysical Research Communications* **2015**, 456, 446-451.

Libardo, M.D.J., and Angeles-Boza, A.M. Bioinorganic Chemistry of Antimicrobial and Host-Defense Peptides. *Comments on Inorganic Chemistry* **2014**, 34, 42-58.

Libardo, M.D.J., Cervantes, J.L., Salazar, J.C., and Angeles-Boza, A.M. Improved Bioactivity of Antimicrobial Peptides by Addition of the Amino-Terminal Copper and Nickel (ATCUN) Binding Motifs. *ChemMedChem* **2014**, 9, 1892-1901.

PENDING MANUSCRIPTS

Libardo, M.D.J., Anand, K., Krishnamoorthy, G., Kaiser, P., Dietz, C., Smith, M., Kaufmann, S.H.E., Singh, A., and Angeles-Boza, A.M. Phagosomal Copper Triggers a Peptidomimetic's Oxidative Activtity and Enables Eradication of Intracellular *M. tuberculosis*. *Manuscript in Preparation*.

Libardo, M.D.J., Bahar, A.A., Ma, B., Fu, R., Zhao, J., Nussinov, R., Ren, D., Angeles-Boza, A.M., and Cotten, M.L. Piscidins 1 and 3 as Antimicrobial Metallopeptides: Nuclease Activity Reveals New Insights into Vertebrate Innate Immune Response. *Submitted*.

CONFERENCE PRESENTATIONS

Poster Presentations

Potent Anti-*Mycobacterial* Peptidomimetic Activated by Copper Ion Binding. **Gordon Research Conference: Metals in Medicine**. Andover, NH. June 26-July 1, 2016. (*Poster Slam Presenter*, among the few students selected to present their poster orally within 2.5 mins)

Central Role of the Copper Binding Motif in the Complex Mechanism of Action of Ixosin: Enhancing Oxidative Damage and Promoting Synergy with Ixosin B. **ASBMB 2016 Annual Meeting**. San Diego, CA. April 1-6, 2016. (*Graduate Student Travel Award Recipient*)

Copper-Binding Sequence in the Antimicrobial Peptide Ixosin is Essential for its Bactericidal and Oxidative Activity. **250th ACS National Meeting**. Boston, MA. Aug 16-20, 2015.

Copper-Binding Sequence in the Antimicrobial Peptide Ixosin is Essential for its Bactericidal and Oxidative Activity. **Gordon Research Seminar & Gordon Research Conference: Antimicrobial Peptides**. Lucca, Barga, Italy. May 2-3, 2015.

Oral Presentations

L-to-D Amino Acid Substitution Positively Affects the Antimicrobial Activity of ATCUN-*sh*-Buforin. **32nd Graduate Student Symposium**. Buffalo, NY. May 19-21, 2014.

Improved Bioactivity of Antimicrobial Peptides by Conjugation to the Amino Terminal Copper and Nickel (ATCUN) Binding Motifs. **39th ACS Northeast Regional Meeting**. New Haven, CT. Oct 23-26, 2013.

HONORS AND ACHIEVEMENTS

2016 **2017 University of Connecticut Outstanding Graduate Teaching Award.** *Nominee.*

2015 **Bobbit-Chou Fellowship**. Award given to the "most promising" third-year graduate student. Department of Chemistry, University of Connecticut

2015 **Masterton Teaching Award**. Award recognizing the best teaching assistant in the department. Department of Chemistry, University of Connecticut

2013 **Charles E. Waring Award**. Award given to the student who garnered the highest GPA. Department of Chemistry, University of Connecticut

2011 **2nd Placer, Philippine Chemists' Licensure Examination**
Manuel L. Quezon University, Quiapo, Manila, Philippines.

2010 **Champion, PACSiklaban 2010**. An Inter-University Chemistry Quiz Bee.
University of the Philippines, Quezon City, Philippines

PROFESSIONAL MEMBERSHIPS

2016 American Society for Biochemistry and Molecular Biology, Graduate Student Member

2015 American Chemical Society, Graduate Student Member

2011 Integrated Chemists of the Philippines, Member

TEACHING AND WORK EXPERIENCE

2012 – 2017 **Graduate Teaching Assistant**, Department of Chemistry, University of Connecticut

2011 – 2012 **Instructor III**, Institute of Chemistry, University of the Philippines

04/2011 – 06/2011 **Research Intern**, Petron Corporation (Petrochemical)